



SCUOLA DOTTORALE IN GEOLOGIA DELL'AMBIENTE E DELLE
RISORSE

XXIII CICLO

Implementation of groundwater numerical models in geological
contexts of urban areas.

Cristina Di Salvo

A.A. 2010/2011

Tutor: Prof. Giuseppe Capelli

Coordinatore: Prof. Domenico Cosentino

Implementation of groundwater numerical models in geological contexts of urban areas.



Tutor: prof. Giuseppe Capelli*

Dottoranda: dott. Cristina Di Salvo

Co-tutors: dott. Giampaolo Cavinato **

prof. Daniel Feinstein**

**Laboratorio di Idrogeologia Numerica e Quantitativa, Dipartimento Scienze Geologiche, Università Roma Tre*

*** IGAG-CNR*

****USGS, U.S. Geological Survey and UWM, University of Wisconsin, Milwaukee*

Index

1.	Introduction.....	4
2.	Conceptual model.....	6
2.1	Geological framework	6
2.2	Aquifer system.....	12
2.2.1	General hydrogeological framework.....	12
2.2.2	Hydrogeological complexes.....	16
2.2.3	Hydrogeological database	21
2.2.4	Building main hydrogeological surfaces	24
2.3	Hydraulic properties	35
2.3.1	Volcanic complexes	36
2.3.2	PGT Formation complex	36
2.3.3	Plio-Pleistocene units	38
2.3.4	Alluvium complexes.....	38
2.4	Aquifer system inflows and outflows	46
2.4.1	Climate feature.....	46
2.4.2	Hydrologic boundaries.....	53
2.4.4	Piezometry of the study area	63
2.4.5	Withdrawals.....	67
2.5	Estimated water budget	72
3	Ground-water flow model construction.....	75
3.1	Hydrogeological modeling in urban areas; the case of Rome.....	75
3.2	Code selection	76
3.3	Model grid	79
3.4	Hydraulic parameters	84
3.5	Boundary conditions.....	87
3.5.1	Recharge	87
3.5.2	Specified flux boundary conditions	90
3.6	Withdrawals.....	96
4	Model calibration	101

4.1	Calibration strategy	101
4.2	Selection of calibration targets.....	102
4.3	Nature and sources of uncertainty.....	104
4.4	Performing calibration.....	105
5	Model results.....	121
6	Summary and discussion	141
7	References	147

1. Introduction

This study is part of the UrbiSit research project (Informative System for Geological Hazards in Urban Areas), led by the CNR-IGAG (Institute for Environmental Geology and Geoengineering) in collaboration with other CNR institutes and University of Rome Roma Tre; the project was promoted and funded by the National Civil Protection in order to realize an integrated geological model of the subsoil beneath the city of Rome for risk evaluation, urban planning and projecting. The core project is the construction of a geodatabase containing surface and subsurface data as thematic maps, well lithological and stratigraphic logs, geotechnical and hydrogeological data. By extracting geological information from the database, a geological model of the area was built as a base for a hydrogeological analysis. Under this perspective the geological units were roughly interpreted as hydrogeological complexes, grouping together sedimentary and volcanic terrains with similar lithological properties.

The study (**fig. 1.2 and 2.3**) area is a rectangle which extends for 237 km² between the 16th kilometer of Salaria road (close to Traversa del Grillo) and the Testaccio bridge, including the northernmost part of the City and the country area at the north of Rome; lateral boundaries are the alignments S. Cornelia-La Giustiniana-Città del Vaticano-Villa Pamphili to the west and Bufalotta-Ponte Mammolo-Tor Pignattara to the east. Within the area the Tiber River flows in a North-South direction and it receives several tributary streams included the Aniene River on its left bank; around the river path the old city center has been developing since the last 3000. The study of this area is crucial to understand the main features of groundwater circulation and the hydraulic relationships between aquifers in the subsoil of the city. This aspects are fundamental to evaluate the water resource condition and to identify areas prone to differentiated settlement due to water level variation.

So far the UrbiSit project has collected well data within the entire Rome municipality and surrounding areas. For the geological modeling, we used 326 wells selected among 2950 in the study area. Each well was analyzed and codified assigning the different layers to the identified geological unit. The volcanic terrains were considered as a geological multilayer including coeval sedimentary terrains. The sedimentary complexes confining the Tiber valley have been distinguished as aquifers or aquicludes depending on their textural characteristics and internal organization. A hydrogeological characterization of the Tiber Valley alluvium was performed; finally, within the Tiber valley we considered apart a basal gravel level underlying the clayey and sandy terrains within the Pleistocene-Holocene alluvial deposits. Such a basal coarse-grained level, could be considered as a buried aquifer. The study is therefore focused on its potential hydrogeological exchange with the surrounding hydrogeological complexes.

Afterwards, well data were used to realize structural maps by means of gridding algorithms. We used the ESRI ArcGis® software to manage the geological information and to build a 3D geological model of the area, focusing on the spatial relationships between aquifers and aquiclude. This modeling software allows to evaluate volumes of the main aquifers and the potential recharge of the basal alluvial aquifer. Then, the geological model's surfaces and the hydrogeological conceptual model were used to build a hydrogeological numerical model by using the code MODFLOW2000 (Harbaugh and McDonald, 1996) and the graphical interface Groundwater Vistas®. In **fig. 1.1** is shown the flux diagram which was followed in this study. Setting up the numerical model and reviewing critically the model result could implies also a review of the conceptual modeling.

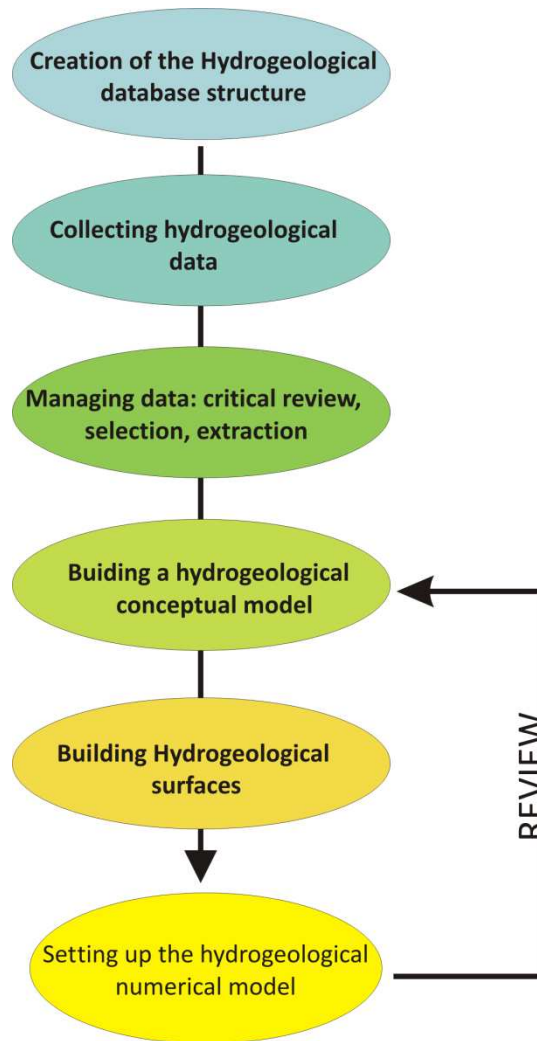


Fig. 1.1: flux diagram for the work presented in this thesis

It is important to remark that this is the first attempt of modeling the hydrogeological system of Rome at wide scale. The reason of such a delay in investigating numerically the groundwater system could be partially due to the big water supply that the City enjoys since the ancient times: the big aqueducts network had provided Roman inhabitants for drinkable water (which is still used also for all the domestic uses) and only in recent times Romans started to use groundwater for gardens irrigation and other “typically urban” uses. Besides that, in the last years, the interest for groundwater as a resource had rose with the expansion of the systems for cooling and refrigerating by “geothermal” exchange; actually, there are several project in the City involving the use of groundwater to produce geoexchange (“open-loop systems”). The aim of a numerical modeling in this context should be to answer to some questions about that:

- Which are the most transmissive aquifers in the City? And what is the balance inflow/outflow for those aquifers?
- What is the amount of water resource that can be used without significantly alter the aquifer system?

- What can be the response of the ground to a scenario of increasing withdrawal, in terms of soil subsidence (which is acting in alluvial context (see Campolunghi et alii, 2007))?

Since the model presented in this study is still in progress, it can't answer to all those questions; anyway, this is a first step that can make clearer what can be done in terms of research to reach this aim.

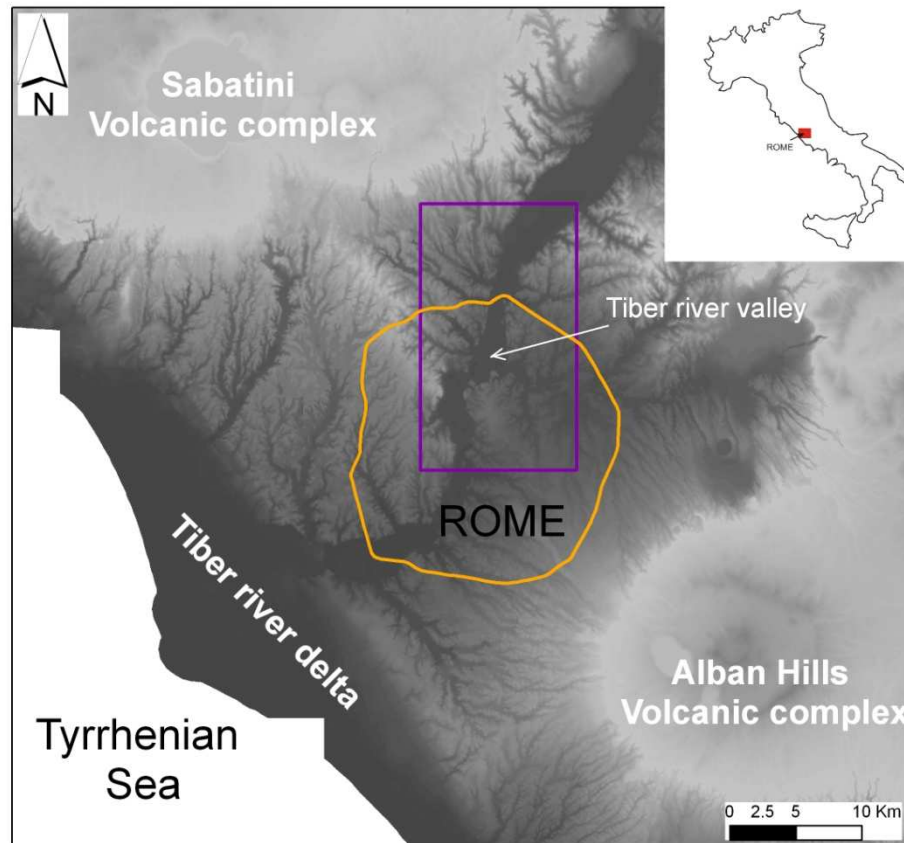


Figure 1.2 : Digital Elevation Map of the Roman are; the red circle shows the G.R.A.(City Ring Road), while the yellow square indicate the study area.

2. Conceptual model

2.1 Geological framework

The geological framework of the investigated area is the result of sedimentary and volcanic processes featuring the Plio-Pleistocene evolution of the drowned western margin of the Central Appennine.

The oldest terrains were deposited in a marine platform environment during the late Pliocene; the clay and sandy clay of the “*Monte Vaticano Formation*”, (Conato et alii 1980, Marra et alii 1995, Marra & Rosa 1995, Milli 1997, Funicello & Giordano 2005, 2008) are considered as a continuous and homogeneous bedrock of the whole Rome municipality.

The Plio-Pleistocene time-boundary was characterized by widespread uplift and erosion due to Appennine geodynamics. Marine depositional environment reestablished in the lower Pleistocene with the sedimentation of littoral facies.

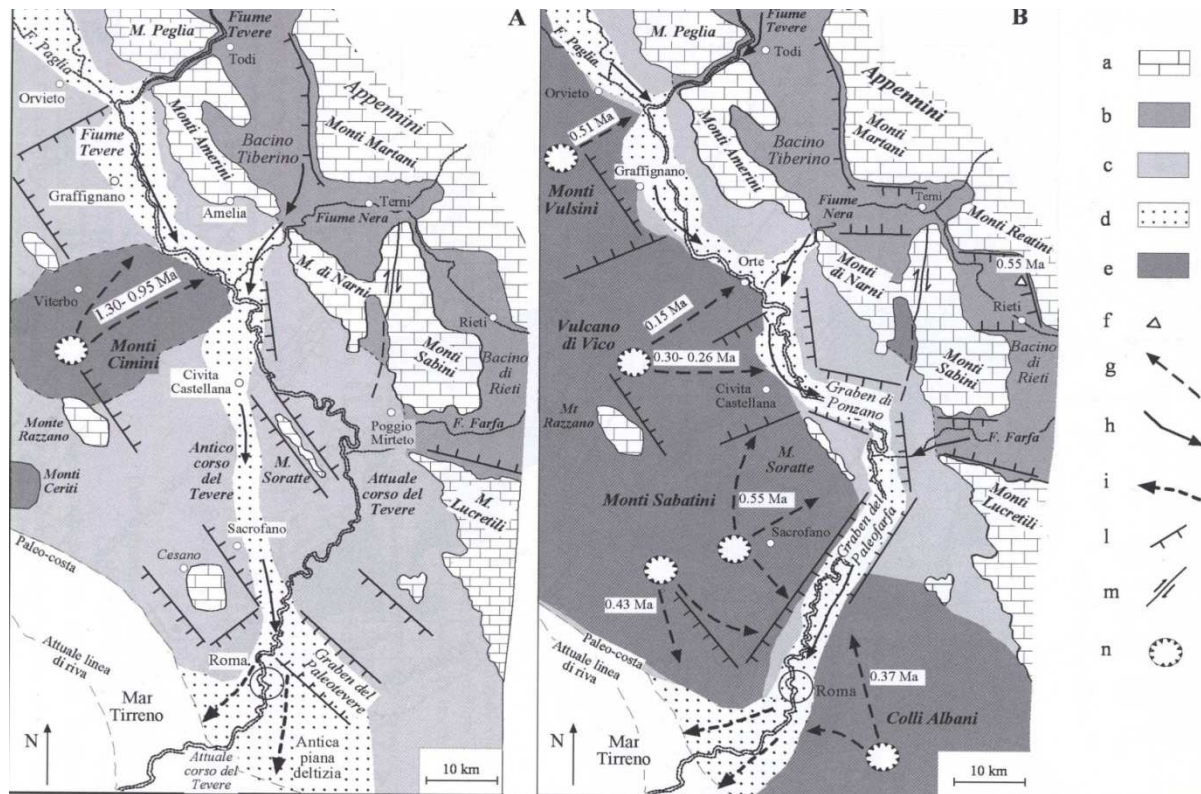


Fig 2.1: Paleogeography of the Latium region during: A) Lower Pleistocene; B) Medium Pleistocene (modified from Mancini & Cavinato, 2004). Legend: a) meso-cenozoic substratum; b) valleys continental deposits subjected to fluvial incision; c) marine deposits emerged and subjected to incision; d) fluvial deposits; e) volcanic complexes; f) lavas; g) main pyroclastic flows or lava flows; h) direction of flows for ancient rivers and streams; i) delta prograding direction; l) normal fault; m) strike slip fault; n) crater or caldera.

The sand and clay of the *Monte Mario Formation* (Conato et alii 1980, Marra et alii 1995, Marra & Rosa 1995, Milli 1997, Funicello & Giordano 2005, 2008) unconformably covered the Pliocene substratum, this last dismembered in NW-SE and NE-SW oriented tilted blocks (Marra & Rosa, 1995; Faccenna et alii, 1993) as a consequence of normal faulting. A transition to a continental environment occurred at the end of the lower Pleistocene with the sedimentation of fluvial-deltaic-coastal deposits belonging to the *Ponte Galeria Formation*, that was controlled by eustatism and persistent tectonic.

The *Ponte Galeria Formation* (PGT) we refer in this paper includes space and time separated sedimentary cycles lying above the Pliocene-lower Pleistocene marine substratum and underlying the volcanic terrains (formation “d” in fig 2.1).

A first cycle (*"Paleotiber1"* sensu Marra e Rosa 1993, Marra et alii 1998) was deposited during the end of the lower Pleistocene and the beginning of the middle Pleistocene in the western part of the city (Ponte Galeria area), where it was established a fluvial-deltaic depositional environment feed by waters streaming eastern of the Monte Mario hill. Sediment supply was guaranteed from the uplifting and the erosion of the Apenninic chain.

In the central part of the City this sequence was almost completely eroded. A younger fluvial sequence aggraded in a NW-SE oriented, subsident tectonic structure known as *"Paleo-Tiber Graben"*, located in the north-east of the urban area.

The Tiber River was diverted from its previous path, canalized within the graben and flew in the eastern part of the city reaching its delta in a southernmost position along the coast. The related sedimentary sequence (corresponding to the *"Paleotiber2"* by Marra & Rosa 1993, Marra et alii 1998 and recently named *Fosso della Crescenza Formation* by Funicello & Giordano, 2008) is featured by a multi-layer made by fluvial gravels, sands and clays filling the tectonic depression. Deposits of the *"Paleotiber2"* are found also beneath the city center featured by basal gravel intervals. The uppermost part of the *"Paleotiber2"* sequence contains volcanoclastic material indicating the beginning of the volcanic activity (0.6 Ma).

Table 2.0 Stratigraphic reference frame used in this work.

<i>Syntetic Urbisit geological reference frame</i>	<i>Stratigraphic reference from Foglio 374 "Roma" 1:50.000 (Funicello & Giordano, 2008)</i>
RP	Anthropic landfill formation
AR	Recent alluvium formation
AT	Terraced alluvium formation
AA	Ancient alluvium formation
VTA	volcanic formations: pyroclastic and fallout deposits
VTB	volcanic formation: phreatomagmatic tuffs (<i>"Peperino di Albano"</i> , <i>"Unità di Valle Marciana"</i> , <i>"Unità di via Nomentana"</i> auct.)
VTC	volcanic formations: cineritic and grained lahar deposits (<i>"Tavolato Formation"</i> auct.)
VTAs	volcano-sedimentary formations: syn-eruptive lahar and fluvial reworked deposits
VTAl	lava formations
PGT	<i>"Ponte Galeria"</i> formation (includes facies from Paleotiber1 and Paleotiber2-FCZ)
MM	<i>"Monte Mario"</i> formation
MV	<i>"Monte Vaticano"</i> formation

The explosive volcanism from the Sabatini Mountains and Alban Hills districts produced big volumes of both fall deposits (enveloping the preexisting topography) and ignimbritic pyroclastic flow deposits thickening within morphological depression and locally inverting and flattening the preexistent topography (Barberi et alii, 1994). The deposition of volcanic units determined a further modification of the hydrographic network: the main course of *Paleotiber2* was diverted by the coming up of the volcanic blankets and remains definitely confined to the actual course of the Tiber River, constrained between the slopes of the Plio-Pleistocene Monte Mario-Gianicolo ridge and the ignimbritic plateau of the Alban Hills.

Contemporaneously to the middle-late Pleistocene volcanic activity the deposition of alluvial sedimentary units was controlled by glacial eustatism, determining complexes stratigraphic relationships.

During the last Würmian glacial period, from 116.000 to 20.000 years ago, the strong regression of the sea level determined the erosion of the present Tiber valley whose bed in the city of Rome reaches -50 m a.s.l. carved within the Plio-Pleistocene sedimentary bedrock.

The deposition of the recent alluvium, which began since the further sea level rising, continues until the actual age. Alluvial deposits filling the paleo-valleys reach a thickness of more than 60 meters.

Late Pleistocene-Holocene alluvium are featured by a basal level of polygenic gravels, with thickness ranging from 10 meters in the center of the main valleys, to few meters along the valley borders.

The main part of alluvium is represented by silty-clayey and silty-sandy sediments bearing volcanic minerals and by intercalations of peat and vegetable remains.

Starting from the geologic reference frame from Funicello & Giordano (2008) we adopted a simplified stratigraphic framework for the volcano-sedimentary multilayer of the Roman basin (**Tab. 2.0**) recognizing few geological complexes bounded by unconformity regional surfaces. This geological grouping operation is the same we used for geological modeling.

By considering the lithological characterization and assuming correspondent hydrogeological properties, geological units of table **2.0** were grouped together in four main geological complexes bounded by main unconformity surfaces.

- a- The Pliocene - Lower Pleistocene geological complex made by the marine deposits of the "*Monte Vaticano*" and "*Monte Mario*" Formations (MV+MM), which can be considered the geological bedrock of the study area and that acts as basal aquiclude.
- b- The Middle-Pleistocene pre-volcanic sedimentary multy-layer featured by the continental fluvial and alluvial deposits of the *Ponte Galeria Formation* (PGT) (featured by the two sequences *Paleotiber 1* and *Paleotiber2*)
- c- The Middle-Late Pleistocene volcanic deposits, including sin-volcanic sedimentary deposits (VTA+VTAs+AA+AT)
- d- The Uppermost Pleistocene - Holocene Tiber alluvial deposits (AR) in which we distinguished the basal gravel bed.

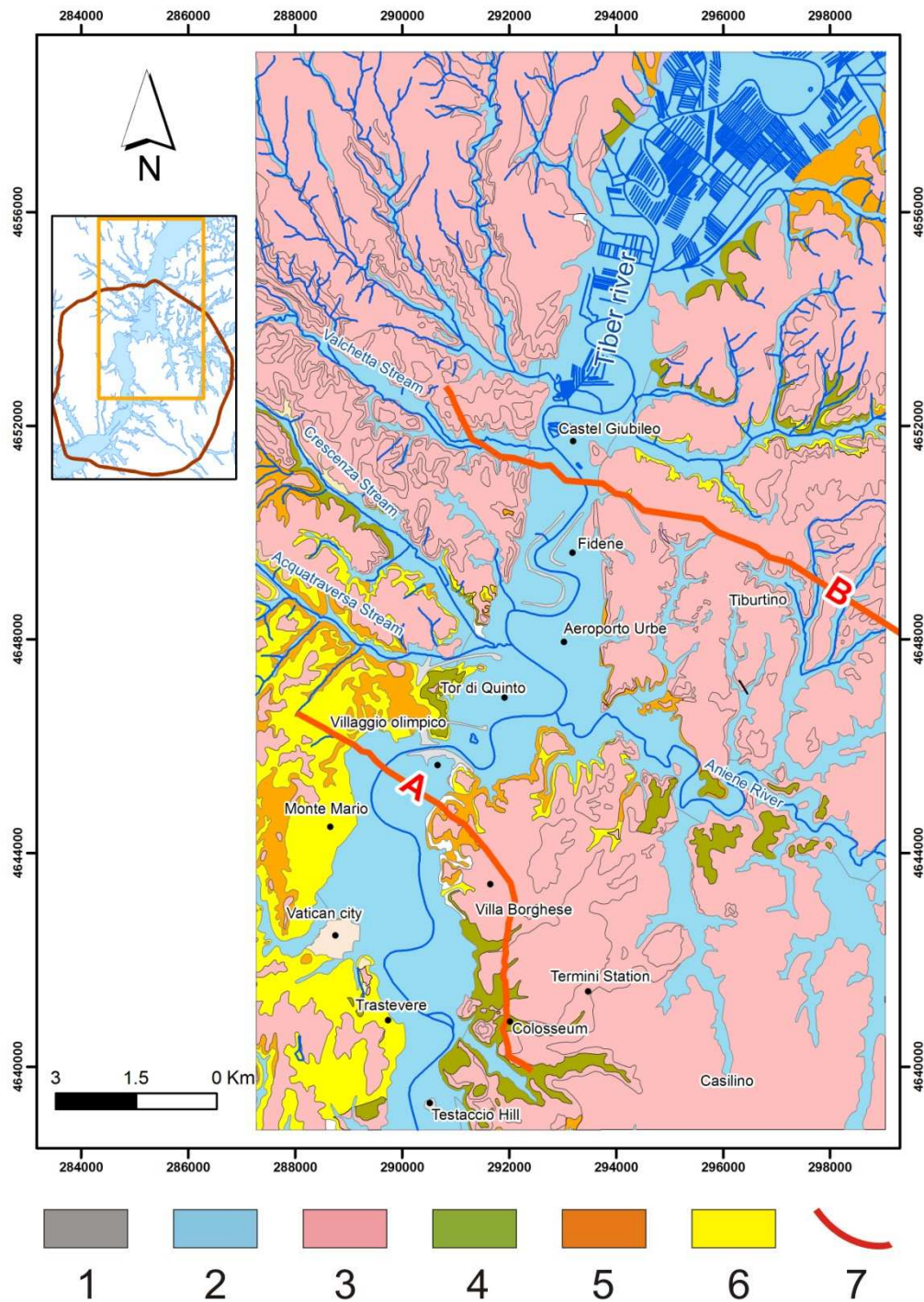


Figure 2.3: Principal geological complexes outcropping in the study area. Legend: 1: anthropic Holocene deposits; 2: Holocene alluvial complex; 3: Volcanic complexes; 4: Aurelia and Valle Giulia sedimentary complexes 5: Fluvial sin-volcanic deposits ("*Ponte Galeria*" Formation); 6: Plio-Pleistocene marine clayey and sandy complex ("*Monte Vaticano*" and "*Monte Mario*" Formations); 7: Cross section.

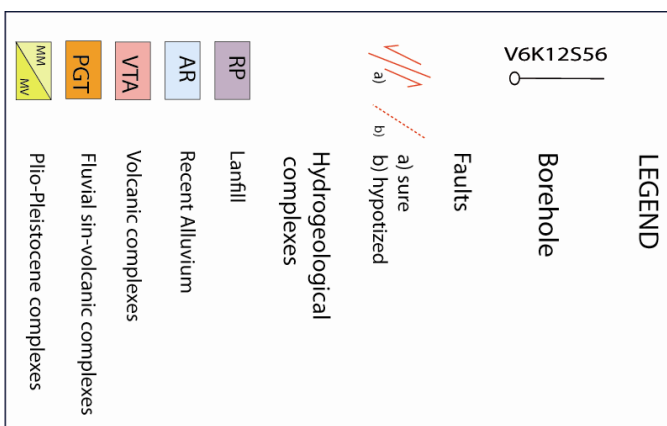
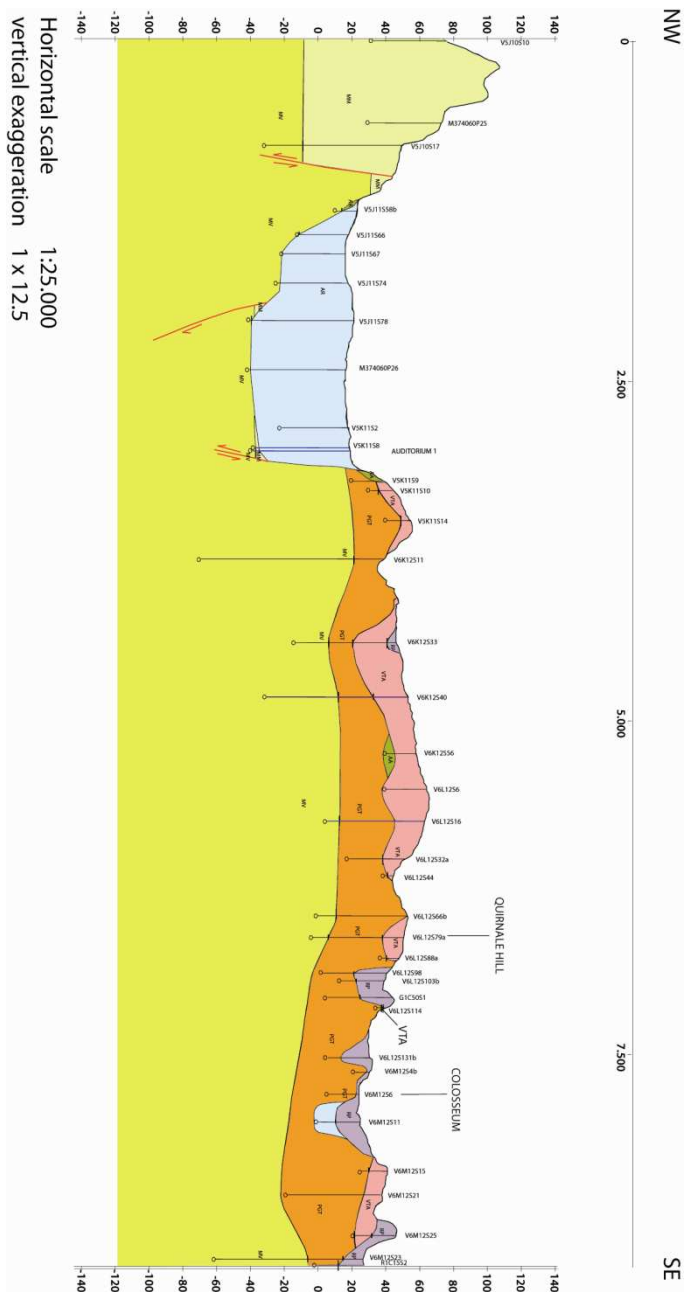
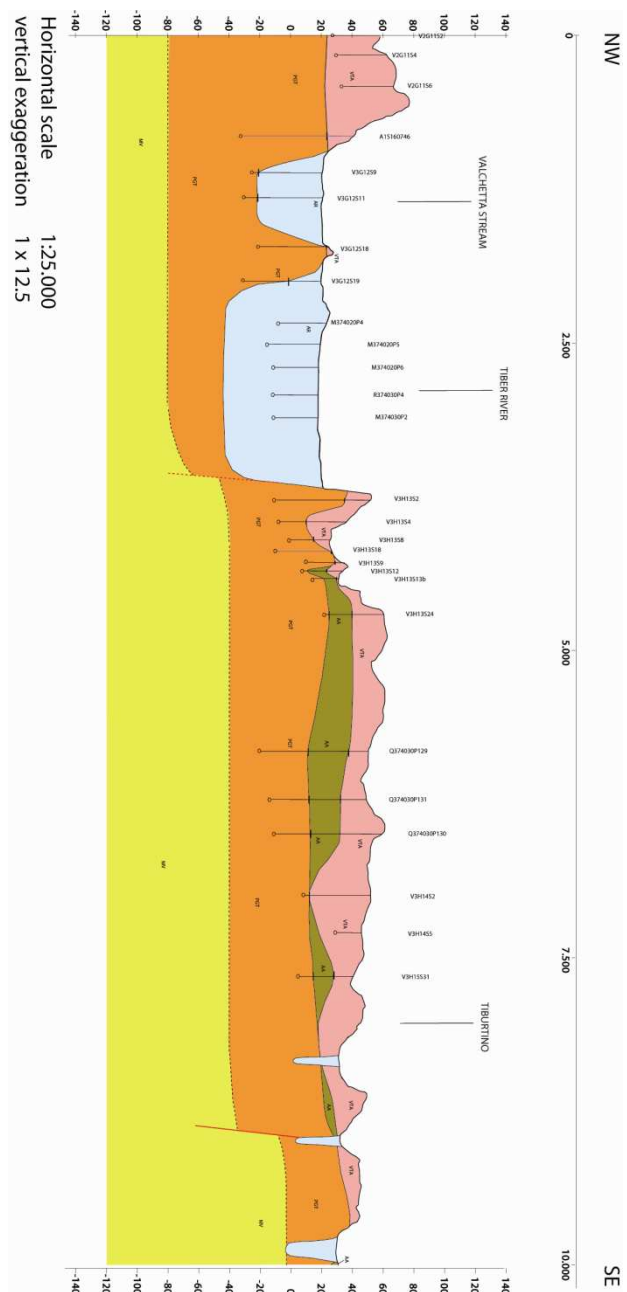


Figure 2.4: Cross section A (left) and B (right); traces are in Fig 2.3; Cross section B shows how the Tiber River Valley is engraved in the north area inside the “PGT” complex filling the Paleo-Tiber graben. .attached n.2 contains all the four cross section table drawn in this study.

2.2 Aquifer system

2.2.1 General hydrogeological framework

In the study area, ground-water flows from piezometric highs, located on the Sabatini Mountains and Alban Hills volcanic reliefs, towards the Tiber alluvial valley, where the water table reaches the lowest elevations, ranging from 20 to 3 m a.s.l.; ground-water flows inside the volcanic and prevolcanic sedimentary units (*"Ponte Galeria" formation*), to the Tiber Valley; the alluvial complex then drains groundwater toward the Tyrrhenian sea. Field head measurements show that the volcanic and sedimentary aquifers have different saturation levels; the uppermost unconfined aquifer occurs in the volcanic complexes and in the topmost sandy layers of the sedimentary complex (*PaleoTiber2*). The *PaleoTiber2* formation hosts different sandy-gravelly aquifers confined by clayey layers; the circulation is sustained by the impermeable Pliocene clayey *Monte Vaticano formation* (Conato et alii 1980, Marra et alii 1995, Marra & Rosa 1995, Milli 1997, Funiciello & Giordano 2005, 2008); due to the lack of data on the deepest saturation levels, in this study the conceptual model is simplified by considering the volcanic and the *"Ponte Galeria" formation* complexes as one single aquifer.

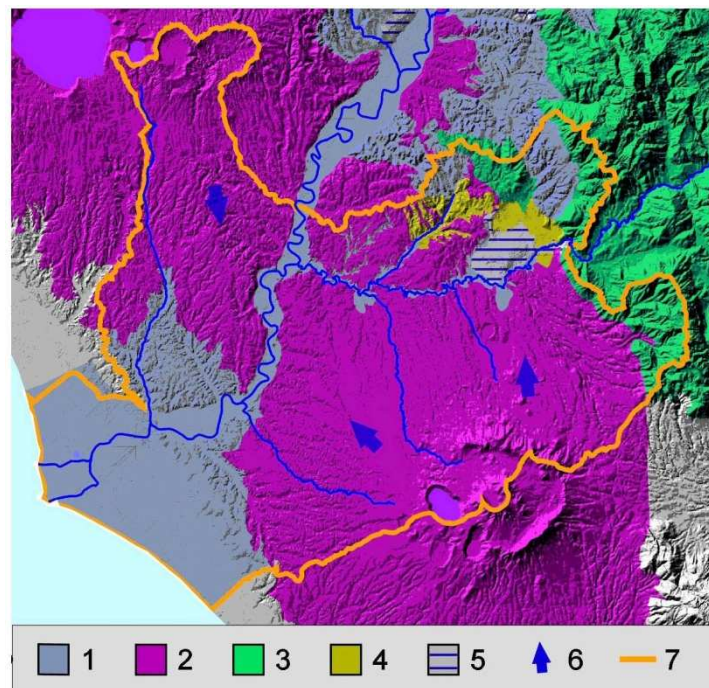


Fig 2.5 Hydrostructures and main ground-water flux directions; from “Piano Stralcio per l’assetto idrogeologico del fiume Tevere-tratto Castel Giubileo-Foce”, Autorità di Bacino del fiume Tevere, 2004. Aquifer systems: 1= alluvionale e costiero; 2=vulcanici; 3= carbonatici; 4= Flysch; 5= travertini; 6= direzione di deflusso sotterraneo; 7= area di piano.

It can be hypothesized that the main groundwater inflow from the volcanic-sedimentary aquifer toward the alluvial valley occurs in the area of the Paleo-Tiber Graben (**figg 2.6 and 2.7**), where the Tiber valley is engraved in the high trasmissivity sedimentary complexes filling the graben (*Paleotiber 2 or Fosso Crescenza* lithofacies, FCZ) of the *PGT Formation*. On contrary, in the other sectors, which is northern and southern then the Paleo-Tiber Graben, the valley is excavated in the Plio-Pleistocene complexes *Monte Vaticano and Monte Mario formations*, which is mainly made by clay and sandy clay; here, the groundwater exchange with the surrounding aquifers is supposed to be very small.

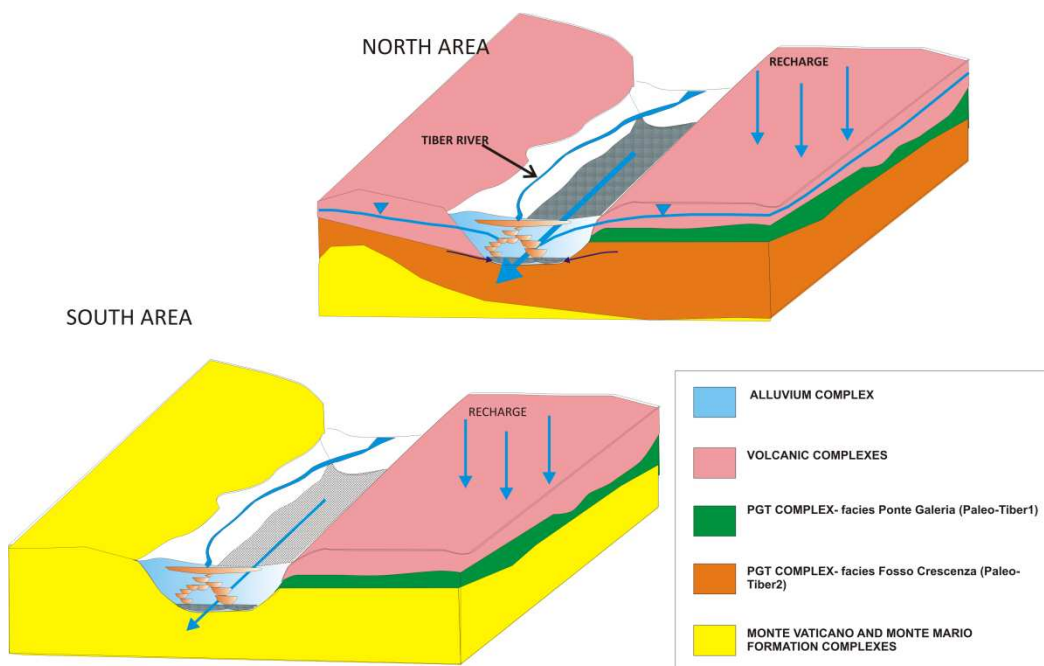


Fig 2.6: Conceptual scheme of inflows in the alluvium complex; the upper picture shows the alluvium inflows in the area of the Paleo-Tiber sedimentary graben, while the lower one shows inflows in the other areas.

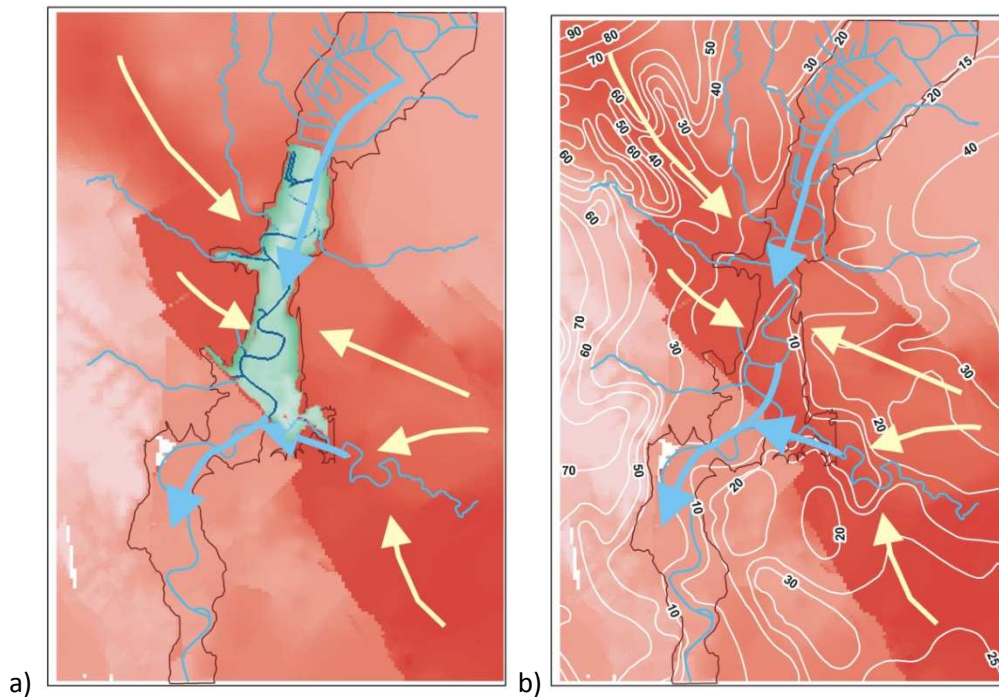


Figure 2.7: a) Visualization of inflows in the portion of Tiber River valley excavated inside the Paleo-Tiber Graben. White arrows indicate the groundwater flux from volcanic and pre-volcanic aquifers toward the Aniene and Tiber alluvial valleys. The blue arrows indicate the flux direction of groundwater within the recent alluvium complex. b) The isolines of the top of water table (from Capelli et alii 2008) confirm the main direction of groundwater.

In the Tiber valley alluvial complex, the wide range of hydraulic conductivity values, related to different depositional facies (see geotechnical characterization on chapter 2.3.4), influences the groundwater circulation; technical reports for “Metro C” subway line works (Lanzini M., 1995-2000 a and b) describe that groundwater flow is absent in areas with high percent of pelitic fraction and organic matter, as between Largo Torre Argentina and Piazza Venezia,; where the sandy and silty-sand fraction increases, as in the area between Piazza Argentina e Viale Mazzini, an aquifer can be recognized, hosted by the sandy and coarse-sandy facies, and having variable transmissivity and hydraulic gradient. As a general scheme, it can be observed that the sandy and coarse sandy lens and levels constitutes unconfined or semi-confined aquifers depending on the presence of confining clayey levels (which act as *aquiclude*) (see **fig. 2.11**). The hydraulic gradient measured inside the sands lens in the hystorical center of the City is very low ($i=0.002$) (Lanzini M., 1995-2000 a and b).

The alluvial basal sandy-gravels host a confined aquifer which head is often higher than the Tiber River stage and, thus, higher than the sandy alluvial aquifer’s stage.

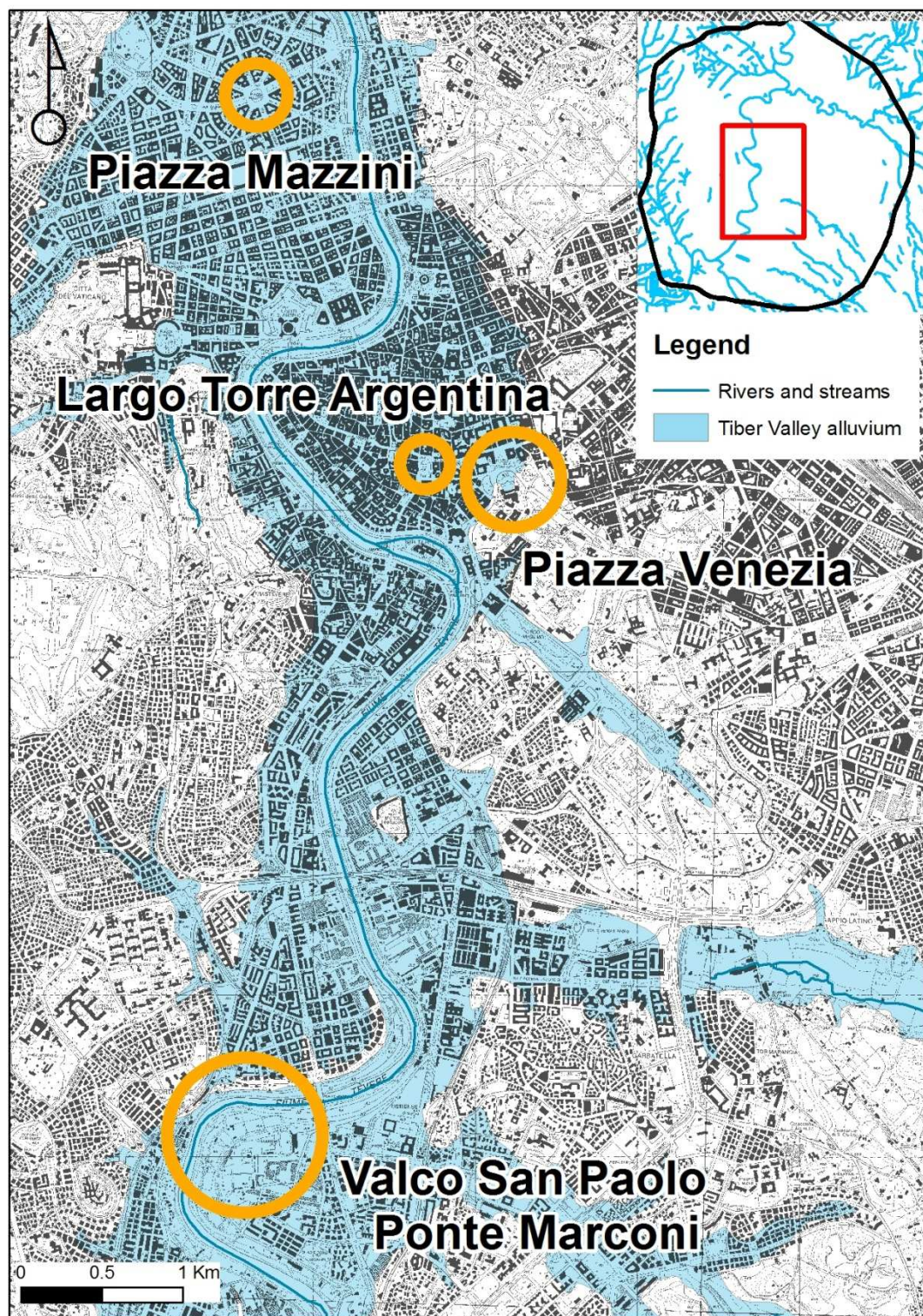


Fig 2.8: location of areas of Piazza Mazzini, Largo di Torre Argentina, Piazza Venezia and Ponte Marconi

Head measurement in the historical center (technical reports, works for “C” subway line, Metro C” Geostudi, 2007-2009), show, with some exceptions, equal or higher head level for gravel aquifer respect to the sand. Southernmost, in the Valco San Paolo area, the gravels mean head is 50 cm higher than the sand head, as measured by the Roma Tre *LinQ* (*Laboratorio di Idrogeologia*

Numerica e Quantitativa, Università Roma Tre) piezometers and hydrometric station Tiber -“Ponte Marconi” since september 2009 (**fig. 2.9**).

By those data, it can be assessed that the aquifers hosted by the sand lens and in the gravel bed can have different hydraulic relationships, that are function of the stratigraphy; where several meters of clay separate sands and gravels the two aquifers show different head, while where sands and gravels are not isolated each other by clay, a similar head can be observed in both aquifers.

The alluvial aquifer is strongly connected to the river, as observed in monitoring wells and hydrometers at “Ponte Marconi” –Valco San Paolo (**fig. 2.9**).

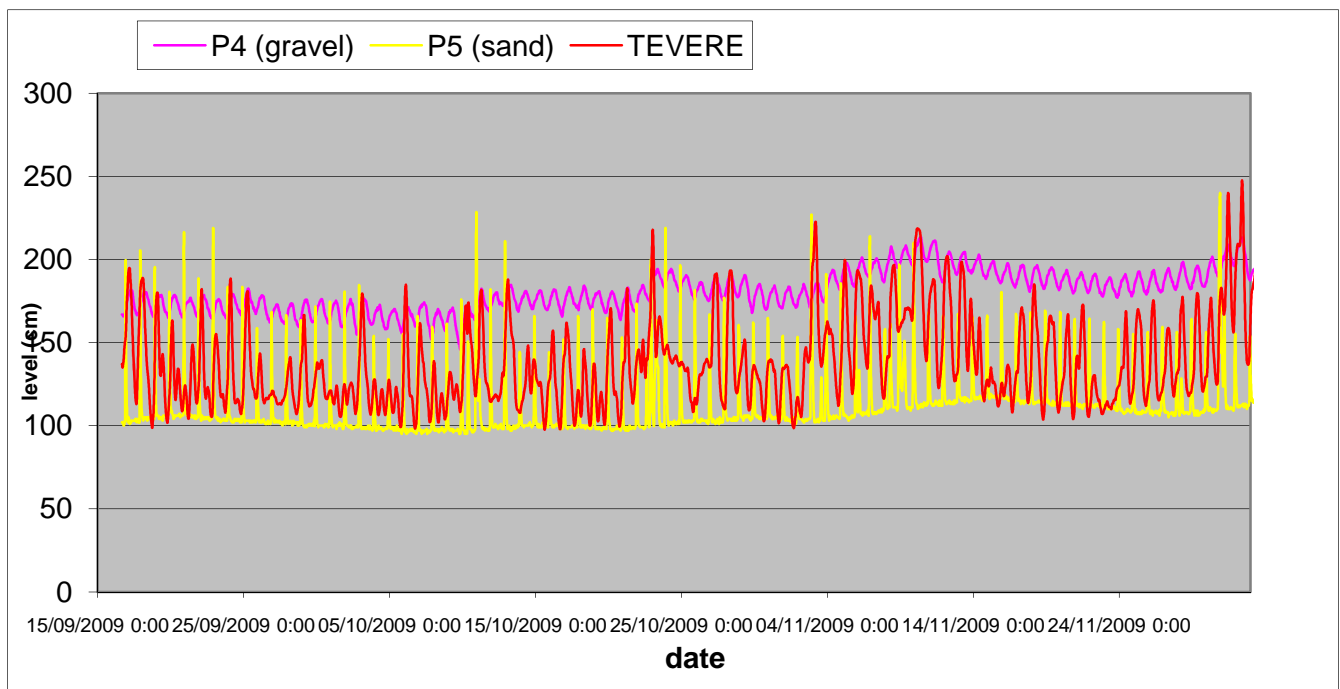


Figure 2.9: field measurements in the Valco San Paolo area (Roma Tre *LinQ* gauging station at Ponte Marconi and piezometers); the sands head is lower that the gravels head; also, the strong connection between the Tiber River and the aquifer can be observed.

2.2.2 Hydrogeological complexes

Here is a description of the main hydrogeological complexes from Capelli et alii, 2008; authors recognized complexes starting from the geological complexes by Funicello & Giordano 2008 (Carg Project, 2008); terrains and rocks having homogeneous hydrogeological features were grouped together, so that a single hydrogeological complex can include facies from different geological formations; this is because of the lithological and, thus, hydrogeological heterogeneity of the geological units. Synthetically, **table 2.1** shows how the complexes described above were grouped together according with their hydrogeological rule in the Rome’s groundwater system.

Tab. 2.1: list of hydrogeological complexes a coded in Funiciello & Giordano, 2008 and this study

Reference code (from Funiciello & Giordano, 2008)	Simplified code (this study)	HYDROGEOLOGICAL COMPLEX
VGU	AA	Valle Giulia Formation complex
AEL	AA	Aurelia Formation complex
a1	AR	Lacustrine deposits and alluvium Holocene –clay- complex
a2	AR	Lacustrine deposits and alluvium Holocene –sand - complex
I	AR	Lacustrine deposits and alluvium Holocene –gravel- complex
FTR e FTR1	AT	Fosso del Torrino Formation complex
MVA	MV	Monte Vaticano Formation complex
MTM1, PGL4b e PGL3b	MV	Sandy clay, sandy silt and sand complex
FCZ	PGT	Complex of gravels and calcareous and siliceous clasts of Fosso della Crescenza Formation complex
MDP e PGL2	PGT	Complex of sandy clay of Monte delle Picche and Ponte Galeria formation
PGL4a, PGL1 e PGL3a	PGT	Complex of gravel and sands of Ponte Galeria formation complex
VTN e SKP	PGT	Complex of gravel and sand of Vitinia e dell'Unità di Saccopastore formation
MTM2 e PGL3c	PGT	Complex of coarse sand of Monte Mario and Ponte Galeria formations
CIL	PGT	Fluvial- palustrine S. Cecilia complex
h	RP	Holoceneantropic landfill complex
h1c	RP	Quarry waste deposit complex
TDC, PTI e KKA	VTA	Alban Hills “Pisolithic Tuffs” complex
VSN2 e VSN3	VTA	Alban Hills “Pozzolanelle” complex
SLV e VSN1	VTA	Alban Hills “Lionato” Tuff complex
RED e PNR	VTA	Alban Hills “Red and black Pozzolane” complex
TIB, PPT, SKF, RNR, LLT e NMT	VTA	Sabatini volcanic complex
LLL, FKBB e FKBA	VTAl	Alban Hills Lava complex
MAK, MNN e TAL	VTC	Complex of Alban Hills “Peperino di Albano”, “Valle Marciana” units and “Tavolato” formation

In the following complexes description, the first code, written in italic, is referred to the classification used in this study, while the second one represents the code from by Funiciello & Giordano 2008.

A) Complex of *Monte Vaticano* Formation (MV - MVA). Gray clay and blue stratified clay. Since this complex reaches very high thickness and very low permeability values, it works as an aquiclude for the entire aquifer system. Recent boreholes drilled in this complex shown that there's a not negligible fraction of silty sand (LinQ, 2010).

B) Complex of the alternance of sandy clay, sandy silt and sands (PGT - MTM1 and PGL3b). This complex includes the sandy-clayey facies of *Monte Mario* Formation (“Farneto” member,

MTM1) and *Ponte Galeria Formation* (“Monte Ciocchi” and “Pisana” members). Since the hydraulic conductivity of this complex is very low, represents the aquiclude of the groundwater system.

- C) Complex of coarse sands (PGT - MTMb & PGTb).** Includes the coarse sand terms of *Monte Mario* and *Ponte Galeria* Formations. The complex has a very heterogeneous permeability, which can globally be considered medium high.
- D) Complex of gravels and sands (PGT - PGTc).** Includes gravels from *Ponte Galeria* Formation. This complex has a very high hydraulic conductivity and hosts an high-potential aquifer. In the hydrogeological model, this complex is included in the complex “C”
- E) Complex of gravels of Crescenza Formation (PGT - FCZ).** Mostly made by Fluvial gravel in a sandy matrix, sands and clays; clay layers become more frequent in the uppermost portion of the sedimentary sequence, that means from -10 m a.s.l. upward. The complex, belongs to the “*Paleotiber2*” lithofacies; drilling shown that the thickness of this complex is higher than 100 meters. This deposit has got a very high permeability, and can host confined aquifers. In the hydrogeological model, this complex is included in the complex “C”.
- F) Fluvial-palustrine complex “Santa Cecilia” (PGT - CIL).** The complex is made by heterogeneous lithotypes (from gravel to silt), with volcanic material; it has a low permeability. It is able to exchange water with the volcanic plateau and the recent fluvial alluvium. In the hydrogeological model, this complex is included in the complex “C”
- G) Complexes belonging to the Alban Hills Volcanic district (VTA).** Here is an overview of the main complexes belonging to the Alban Hills Volcanic district. In the hydrogeological model, the Alban Hills Volcanic formations constitute one single complex.
- *Pisolitic Tuffs (PTI)*: pyroclastic flow deposit with very low permeability, also due to the high number of paleosols.
 - *Red and Black Pozzolane (RED, PNR)*: pyroclastic flow deposit with massive and chaotic fabric; the permeability is medium-high and it is both for porosity and fracturation. The high transmissivity and continuity of this deposits makes it one of the most important aquifer in Rome.
 - *Lionato Tuff (VSN1)*: pyroclastic flow, with massive and chaotic fabric, very lithoid for effect of zeolithization, which is responsible also of the medium-low hydraulic conductivity; it works as an aquitard, isolating the surface circulation from the deeper one.
 - *Villa Senni Tuff (VSN2)*: massive and chaotic deposit, sometime with high consistence. Generally this pyroclastic unit has got a coarse matrix. The medium high permeability values, the large thickness and areal extension makes it able to host a medium transmissive aquifer.
 - *Lavas*: this facies is referred to Vallerano Lavas (LLL), Capo di Bove Formation Lavas (FKB); the permeability is high due to the fracturation.

H) Sabatini Mt. Volcanic Complex (VTA - TIB, PPT, SKF, RNR, LLT, NMT)

This complex groups mostly pyroclastic flows, and undifferentiated fall deposits, outcropping either in the right and in the left bank of Tiber River, and they are referred to the following units (from Mattias & Ventriglia, 1970): “Red tuff with black scoria”, “La Storta stratified tuffs”, “Sacrofano Varicolori stratified tuffs”. The granulometry is the one of a fine sand, with abundance of silty matrix. The whole permeability of the complex ranges from medium to medium –low, but it can be affected by local variations of the hydraulic coefficient due to the presence of several argillified paleosoils.

I) Holocene alluvium (AR)

The complex includes the alluvium of the main rivers and streams and the alluvium still in evolution inside the embankment of Aniene and Tiber rivers.

Due to the fluvial depositional mechanisms, the alluvium is made by a wide range of depositional facies; coarse sediments are related to high energy-channel areas, while silty and clayey sediments are related to areas of low energy such as alluvial plain or fluvial-palustrine environment.

The general setting of the sedimentary alluvium valley is sketched in **figg 2.10 and 2.11**.

F.a The uppermost unit is the A, the “historical” alluvium unit, silty clay covering homogeneously all the area. This unit has an high consistence testifying a subaereal exposition and relative oxidation of the uppermost brown colored level, and several water level fluctuations.

F.b1: Below the A unit, there are silty sand and fine sands belonging to B1 unit

F.b2: The coarse sand of unit B2 covers the unit C in the Tiber right bank, while in other parts unit B2 and unit C are in etheropy. On the left bank, unit B2 covers directly unit D1.

F.c: the unit C is gray clay with peat; the deposition of this unit occurs contemporary to the unit D1 in the Tiber right bank, while in the left bank unit C is mostly missing. During the deposition of unit C, also starts the deposition of the alluvium of Cremera-Valchetta stram(Castel Giubileo - north city ring road area) with deposition of coarse-sandy sediments fining-upward until fine sands. Those sediments are partially interfingered to main river alluvium.

F.d: immediately above the basal gravel bed, there are coarse sands (D2 unit), sedimented in a medium energy- braided plain environment and sandy silts (D1 unit), sedimented in low energy environment.

F.g: discontinuous bed of basal gravel which thickness ranges between 0 and 10 meters. This deposit represents the first-high energy fluvial environment during the first phase of sea level rising at the end of the Wurmian glacial period.

J) Landfill (RP): This complex includes heterogeneous anthropic deposits. It can constitute a relevant aquifer complex when it occurs with large thickness, since its permeability is medium, and it can give local diversion of the main drainage. In the hydrogeological model, this complex is included in the complex uppermost Layer 1, representing volcanic formations.

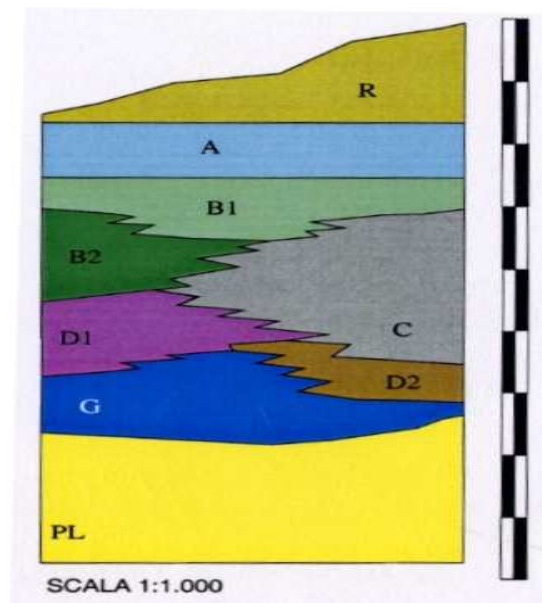


Fig 2.10: stratigraphic relationship scheme of the Tiber alluvium; R= landfill; PL= plio-pleistocene complex.

Geologic and hydrogeologic data from LINQ and Igag-CNR were integrated in a database, which structure has been built for geologic modeling. The data archiving permits to easily extract geological features (as complexes top and bottom elevation) and hydrogeological parameters measurements.

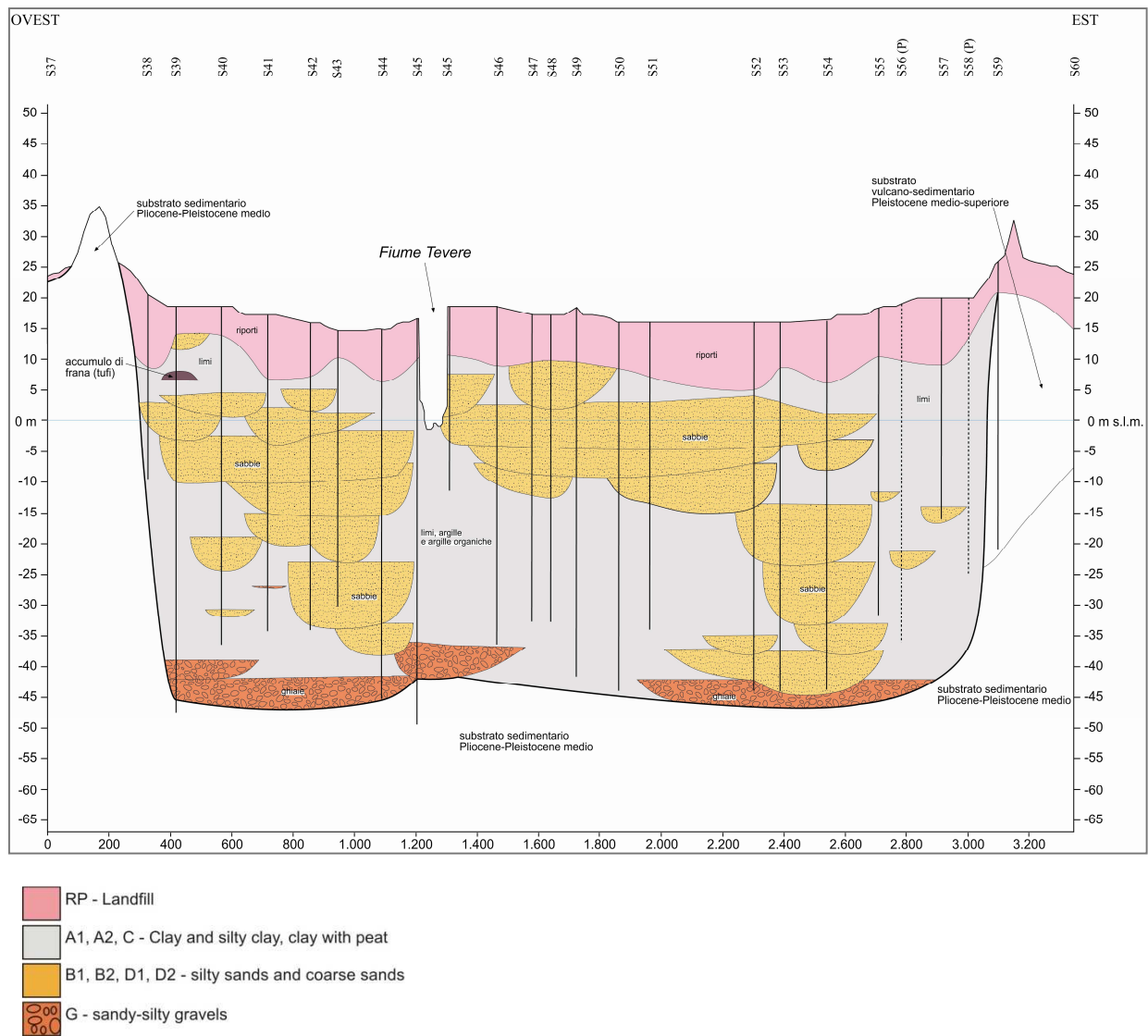


Fig 2.11: Cross section of the Tiber River alluvial valley, drawn through the Historical center (from Igag-CNR Urbisit informal meeting, 2008)

2.2.3 Hydrogeological database

The UrbiSit-LINQ database was built to collect geological, geotechnical and hydrogeological data. The hydrogeological section has been created to collect wells and springs data. The main inputs for the roman area are data from Ventriglia (1971 and 2002), public agencies (ISPRA-Istituto Superiore per la Protezione e la Ricerca Ambientale) and private companies reports (as works for “B1”, “C” and “D” subway lines, parkings, railway roads, etc.). Those elements are inserted as record in the main table “**DATO PUNTUALE**”, in which all the spatial information and identity characteristics of every object can be specified:

-*identifying code*(which is the primary key for the entire database)

-*source of the information (idfonte)*

- old code owned by the object (*idoldato*)
- coordinates
- topographic elevation above the sea level as reported in the original data.
- topographic elevation of data extracted by the Digital Terrain Model.
- place (City, municipality) and address;
- notes

The “DATO PUNTUALE” table is connected to the two tables “perforazione” and “sorgente”, in which are specified characteristics of the two main types of hydrogeological data that can be inserted: wells and springs.

In the table “**PERFORAZIONE**” characteristics of wells are carried:

- use of the well (which is: for irrigation, drinkable water, piezometer, etc.)
- type of the piezometer (“tubo aperto” o “Casagrande”), in case the use of the well is as piezometer;
- dynamic discharge of the well (liter/sec);
- Transmissivity and storage coefficient which are calculated from pumping tests;
- presence of gas in the water of the well;

The table “**FALDA**” is connected to the table “PERFORAZIONE” by a relationship “one-to-many”; in this table there are informations about aquifers which were encountered during the drilling; here there can be specified:

- depth of aquifer top and bottom respect to the surface;
- depth of aquifer top and bottom above the sea level as reported in the original data;
- depth of aquifer top and bottom above the sea level as in the Digital terrain model;
- notes related to encountered aquifers.

The table “**FILTRO**” is connected to the table “PERFORAZIONE” by a relationship “one-to-many”; in this table there are informations about the well screen:

- depth of screen top and bottom respect to the surface;
- depth of screen top and bottom above the sea level as reported in the original data;
- depth of screen top and bottom above the sea level as in the Digital terrain model;
- notes related to screen.

The table “PERFORAZIONE” is connected to the table “**MISURA PARAMIDRO**”, in which there are informations about static and dynamic head measurements and the chemical and physical characteristics of water. The connection is by a relationship “one-to-many”, so that it is possible to insert more than one measure for the same well; issues in this table are:

- static and dynamic head respect to the surface;
- static and dynamic head above the sea level as reported in the original data;
- static and dynamic head above the sea level as in the Digital terrain model;
- well dynamic discharge, from which hydrogeological parameters can be known
- chemical and physical characteristics of water in the well, as: temperature, electric conductivity, presence of gas.

The table “PERFORAZIONE” is connected to the table “STRATIGRAFIAPERF”, in which are inserted informations about top and bottom elevation of each drilled layer, plus the related description. The table “STRATIGRAFIAPERF” is related by the primary key “ididro” to the table “**IDROGEOLOGIA**” by a relationship “one-to-one”; in this table, data about hydraulic conductivity can be inserted for the considered layer. This is what can be inserted:

- Hydraulic conductivity (k) in m/s;
- Type of (k) measurement; k can be measured in the field by slug and pumping tests or in laboratory (i.e. edometric prove);
- Derived Hydraulic conductivity, which is k deducted by literature, or from geotechnical data or from granulometric curves.

The table “**IDROGEOLOGIA**” is connected to the table “INTERPIDROGEOLOGIA”, in which k values can be associated to a hydrogeological code. This table makes easier the geological interpretation because layers with very similar k values can be assimilated in the database, with the same hydrostratigraphic code; indeed, the relationship connecting “IDROGEOLOGIA” and “INTERPIDROGEOLOGIA” is a “many to one” relationship. Fields in this table are:

- “Idintstratidro”, where can be inserted the code assigned to the hydrogeological layer, which are the codes listed in **table 2.1, chapter 2.2.2**, “Hydrogeological complexes”
- “Descrizione”, where is reported the description of the hydrogeological layer;
- the field “IDROSTRAT IGRAF” contains the code used for the stratigraphic interpretation;
- For each recognized hydrostratigraphic unit is reported the corresponding cartographic code, referred to the geological map of Rome in scale 1:50.000 (Funicello & Giordano, 2008).
- it is reported also the code corresponding to the UrbiSit 2008 project, which can be considered a simplified version of the cartography.
- the hydrogeological complex description fields comes from Capelli et alii (2008).

-finally, the table contains a qualitative k classification for each hydrostratigraphic unit.

The scheme of the relationships between the database tables is in attached n1

2.2.4 Building main hydrogeological surfaces

The geological modeling process in this study is aimed to reconstruct the hydrogeological properties of geological complexes featuring the subsoil of the central and northern part of Rome, around the path of the Tiber River. The study is focused on the geological framework around the valley and the hydrogeological relationships between the Plio-Pleistocene substratum and the alluvial deposits. Besides the top of the basal gravel alluvial deposits has been reconstructed, that can be considered as a semi-confined aquifer, to understand its hydrogeological potential. Geological formations of which we reconstructed surfaces were engraved during Holocene by the erosion of Tiber and minor rivers flowing into Tiber, and this produced the need to reconstruct also the morphology of the alluvial valley, meaning the morphology containing the recent alluvium. This was possible thanks to drilling data on effective depth of alluvium and according to extrapolations reasonings on fluvial dynamics mechanisms. The reconstruction involved, in addition to the Tiber and Aniene rivers valleys, confluence zones of Crescenza stream and Valchetta stream in Tiber valley, because they have an high thickness of permeable deposits in contact with Tiber basal gravel and so they can give an important contribution to the hydric recharge of these deposits. The modeling process includes both well data and GIS analysis. At first we managed the large number of well data to derive the backbone of the geological model by coding operations. Then, using Arcgis® tools we integrated the main surface information given by the Geological map 1:50.000 of Rome municipality (Funicello R., Giordano G., 2008) and also local data derived by cross sections obtaining a complete data set of the main boundary surfaces as recognized in the reference stratigraphic frame.

managing well data

In the study area there are 2950 point data belonging to the Urbisit database, among which 938 drillings and 1219 point of measurement of groundwater level were selected.

To better constrain the coding operation for the geological modeling, a quality ranking was established, basing on the following criteria:

- Well Depth;
- Ratio well depth/number of geological levels described in the well log ;
- Nearness to a stratigraphic limit in the geological map 1:50.000 of Rome municipality (Funicello R., Giordano G., 2008)

According to this criteria, a score was assigned to each well and three ranking classes were distinguished (A,B,C); wells which are considered more reliable for geological reconstruction belong to the highest score class (**fig 2.12**).

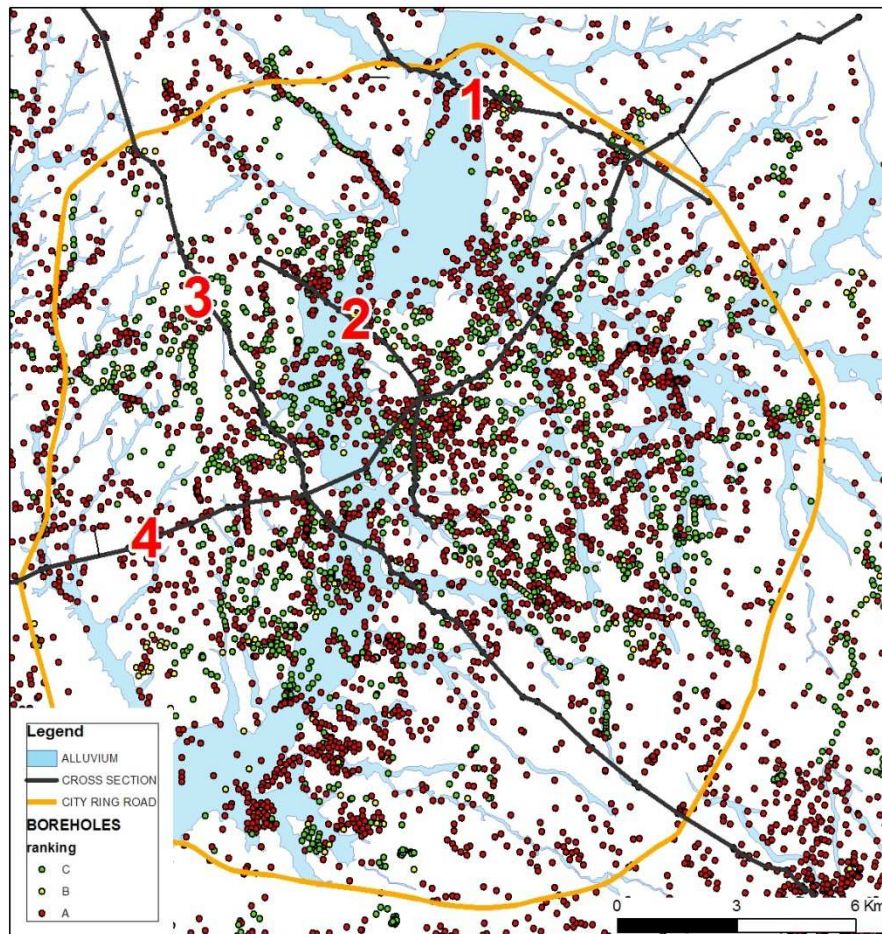


Figure 2.12: distribution of boreholes in the whole urban area of Rome.

All boreholes belonging to the class (A) in the study area (326 drillings) were analyzed and coded according to the stratigraphic reference frame of **tab.2.1**. Boreholes with highest ranking class (A) were used to draw two geological cross sections by means of stratigraphic correlations between similar multilayer. The geological framework as reconstructed in cross sections was used to analyze and codify also medium and low quality wells (B and C classes) which are placed close to their traces of cross sections. Cross sections are in **fig 2.4** and in **attached n2**.

A multiple step procedure has been followed to build the main geological surfaces taking into account all the available data; the flux diagram of tools that have been used is in **figure 2.13**.

- A) Each well data having the same code (for instance PGT) and therefore belonging to the same geological unit was extracted from the database. In the case of more than one level

of the same unit in a single well, the one with the highest elevation that was identified as the top surface was pinpoint;

- B) By using an Arcgis® tool developed by Igag-Cnr, cross sections (see **fig. 2.4** and **attached n. 2**) were digitized; moreover, for building surfaces were used also cross sections drawn in the Urbisit project 2008. For every top surface drawn on each section, points were extracted with z value, and added to the datasets extracted from the well data;
- C) In order to include in the geological reconstruction the limits of each main surface as drawn in the vector geological map, the *feature to point* Arcgis® tool in *data management toolbox* was used to obtain a point dataset featuring the limits. Therefore, the *extract values to point* Arcgis® tool in *spatial analyst/extraction* was used in order to assign the corresponding Digital Model Terrain (with resolution 20 x 20 meters) elevation value;
- D) To better shape the geological surface, not only the limits of outcropping polygons were considered, but a network of points was added within each polygon of the geology shape file; point network was derived by a sequence of GIS operations. The geology polygons were converted in raster format through the *polygon to raster* Arcgis® tool in the *conversion toolbox* and then each raster was converted in a point shape file by the *raster to point* tool in the *conversion toolbox*. Finally, by using the tool *extract values to point* in the *spatial analyst toolbox*, elevation values from the DTM were extracted and added to each point. The point network was added to the points dataset obtained by well data and cross sections.
- E) The definitive points dataset was interpolated using the IDW (inverse distance weighted) algorithm in the Arcgis® *Geostatistical Wizard tool*; fault shape files have been used as barrier polyline.

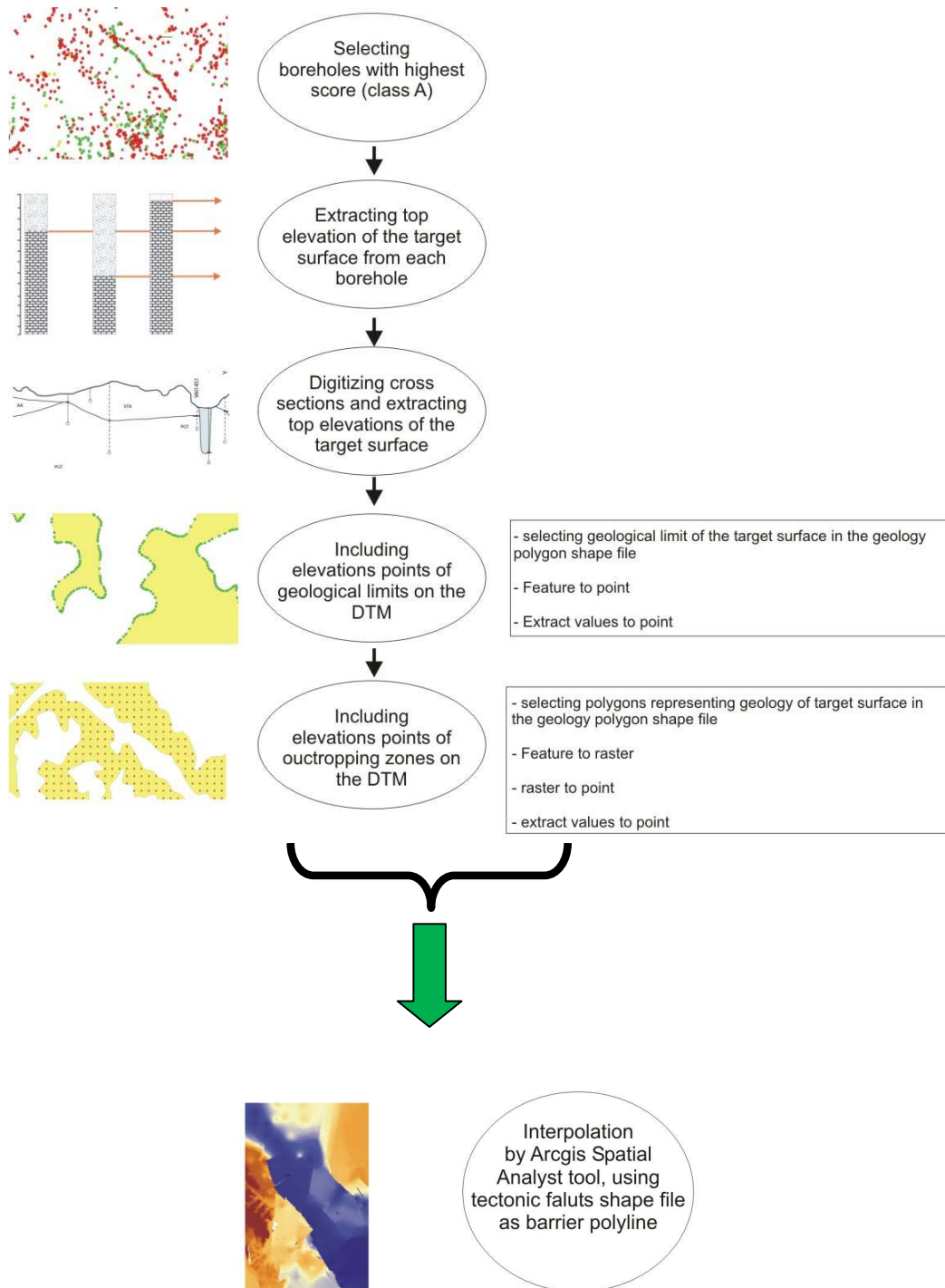


Figure 2.13: Flux diagram showing Gis tools used to build hydrogeological surfaces.

Top surfaces of the geological units featuring the subsoil of the central-northern part of the city of Rome surrounding the Tiber River were reconstructed; then, the maximum erosion surface of the Tiber River and main tributary streams were also built, and the top surface of the basal gravel level inside the alluvial filling.

The bedrock of the Tiber alluvial deposit is featured by three main geological complexes: the late Pliocene-early Pleistocene marine clayey and sandy-clayey of the Monte Vaticano-Monte Mario units; the lower-middle Pleistocene “Ponte Galeria” unit; the middle-late Pleistocene volcanic complex, including coeval sedimentary deposits.

The Monte Vaticano-Monte Mario (MV-MM) units as a whole, has been considered as an aquiclude. In the western part of the study area, along the right bank of Tiber River, the top surface of such hydrogeological complex (**Figure 2.14a and 2.14b**) reaches the highest elevations, outcropping at 130 m a.s.l. in the Monte Mario structural high. This last is bordered on the Eastern side by N-S and NW-SE trending normal faults dipping towards the East and North-East that rise the Plio-Pleistocene sedimentary complexes on their footwall.

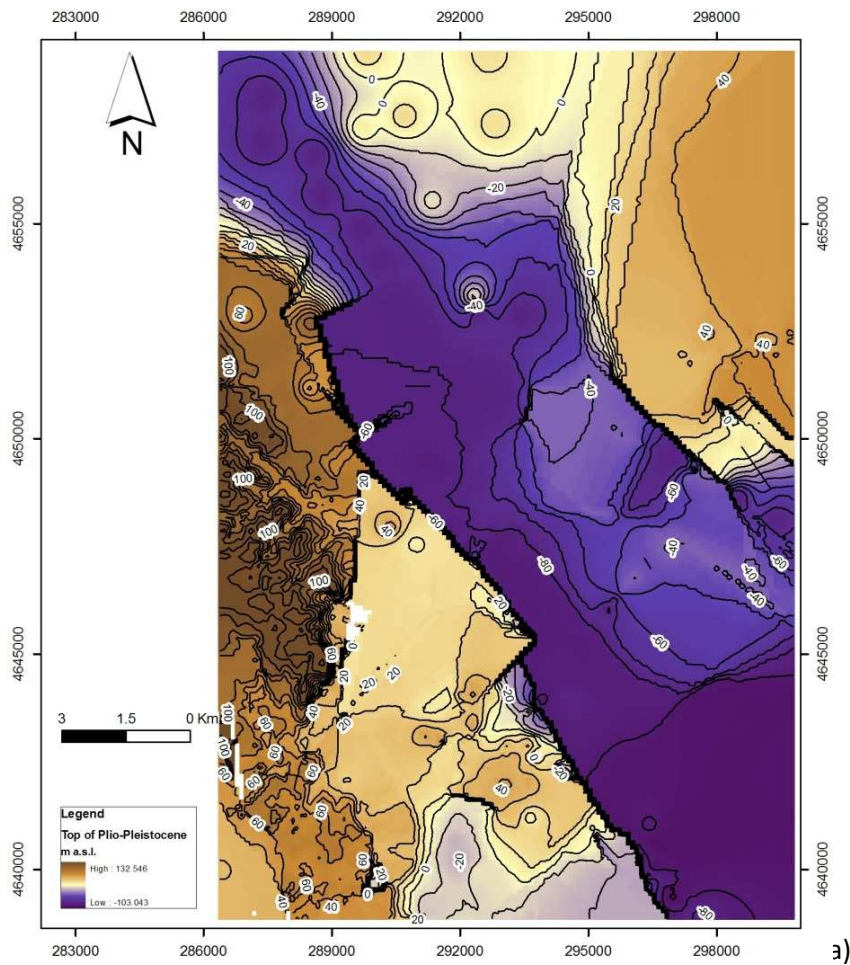
The central and eastern zones of the study area are characterized by lower elevations; the MV-MM top surface is downthrown by main tectonic lineaments and lowered up to 90 m b.s.l. at the base of a NW-SE oriented tectonic depression known as to *Paleo-Tiber Graben* (Funicello et alii, 2008 and reference therein). Between the Monte Mario structural high and the Paleo-Tiber graben, the MV-MM top surface evidences erosional features as secondary streams flowing into the main graben and isolated morphological reliefs, as for example beneath the actual position of Termini station (40 m a.s.l.).

Above the MV-MM top surface, we distinguished the boundary erosive surface between the Ponte Galeria sedimentary unit and the overlying volcanic multilayer (PGT top formation, **Figg 2.15a and 2.15b**). The absolute elevations show a decreasing trend of the PGT top surface from the North-Western sector along the right bank of Tiber River, (100 m a.s.l.), towards South-East, (up to -40 m a.s.l.).

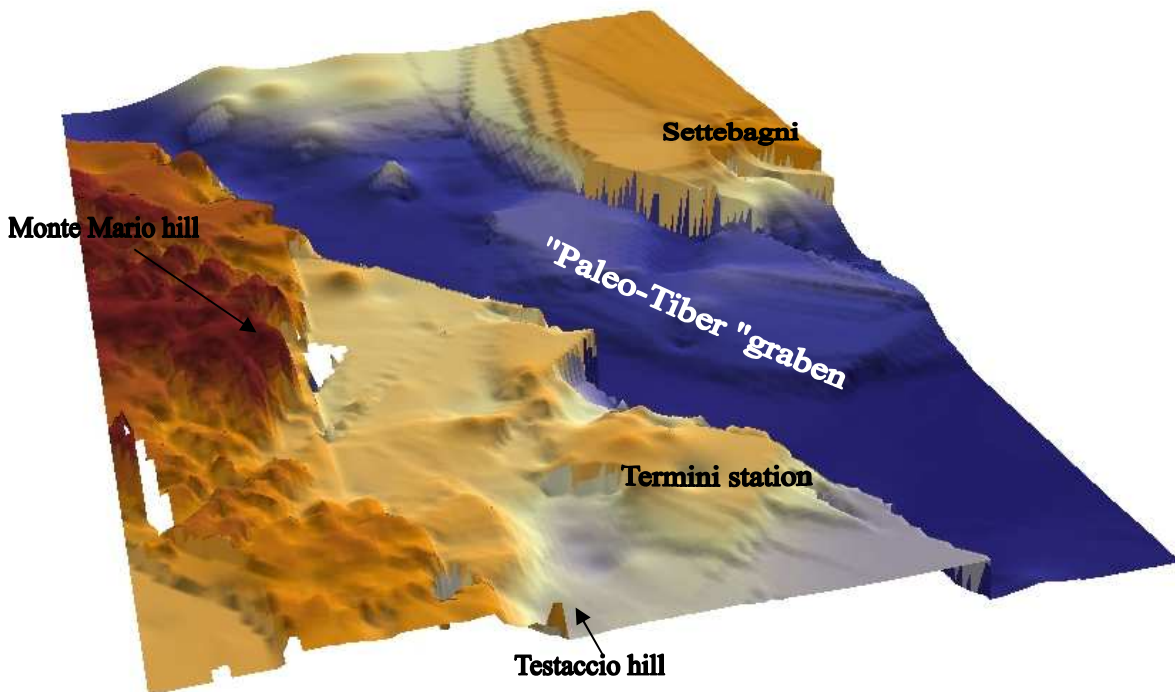
There's a nearly-complete filling of the *Paleo-Tiber Graben*: from drillings and literature (Florindo et alii, 2007) is indeed well-known that in the graben area the thickness of fluvial-deltaic sediments deposited since lower Pleistocene onwards exceeds 100 meters. The lowest elevation in the south-east sector can be related to the NE-SW trending fault linked to the volcano-tectonic activity of Alban Hills.

The surface of maximum erosion of the fluvial deposits (**figures 2.16a and 2.16b**) shows the local morphology precedent to the last depositional cycle, which occurred since the Holocene, of the alluvial complexes of Tiber River and his main tributary: the Aniene river, Crescenza e Valchetta streams.

The main valley (Tiber River Valley) has a quite regular flat floor with variable width ranging from 200 meters to 2 Km; the alluvial valley narrows at the Villaggio Olimpico zone, between Ponte Flaminio and Villa Glori, and widens at the confluence with Aniene tributary. The lowest elevation at the center of the valley is about 52 m b.s.l..



a)



b)

Figure 2.14: a) reconstruction of the bottom of Ponte Galeria Formation (equivalent to the top of Plio-Pleistocene). b) Contour map resulting from the grid interpolated with kriging method and corresponding surface. The coordinate grid is referred to ED50 N33 projected system.

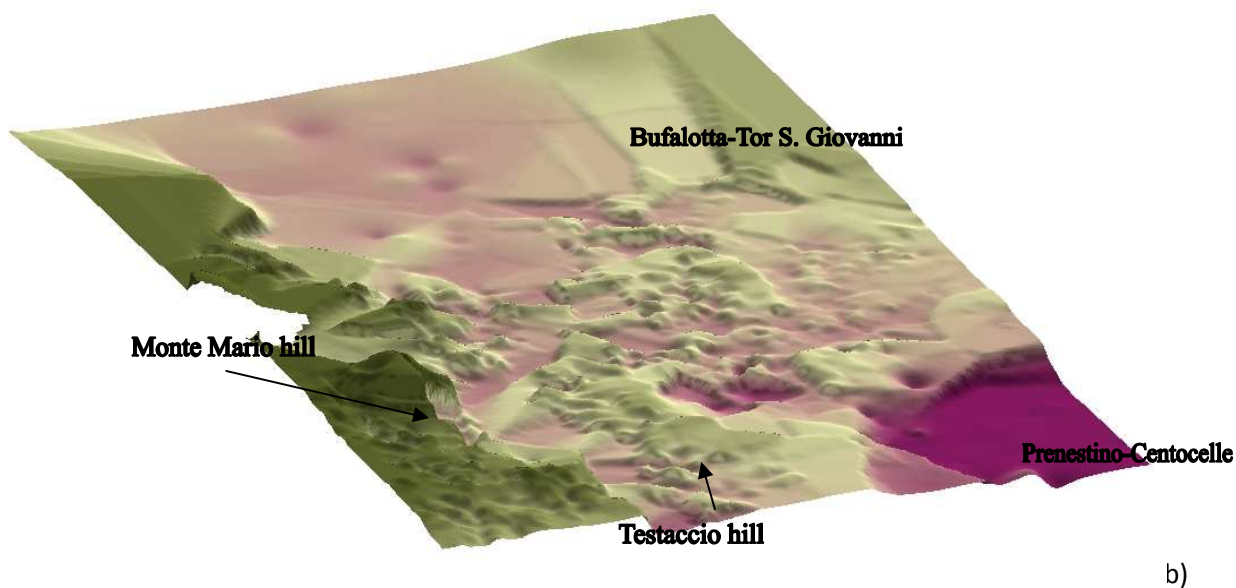
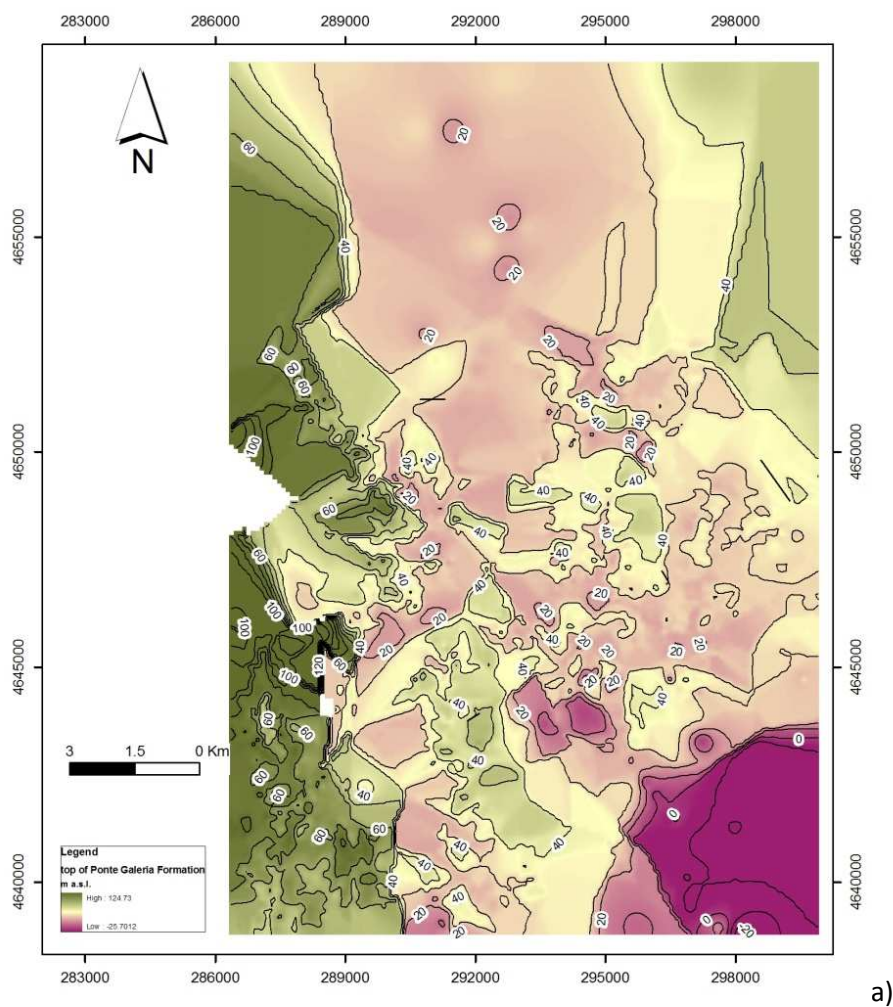


Figure 2.15: a)reconstruction of the bottom of volcanic formations (equivalent to the top of Ponte Galeria Formation). b)Contour map resulting from the grid interpolated with Inverse distance weighted algorithm and corresponding surface. The coordinate grid is referred to ED50 N33 projected system.

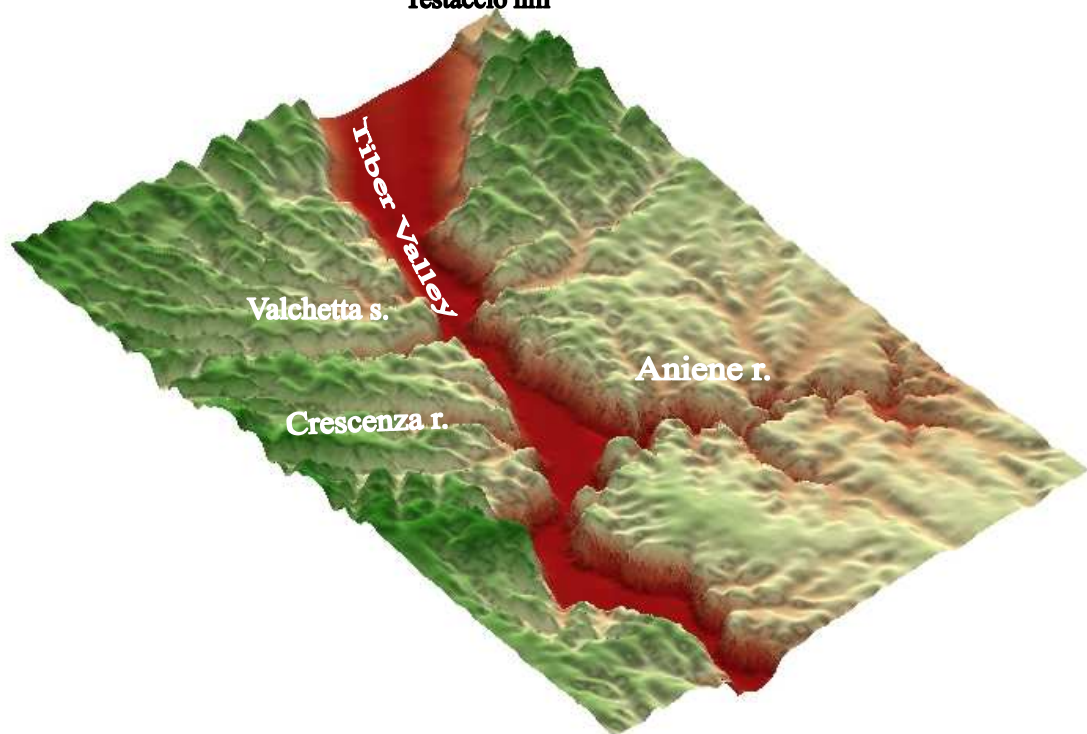
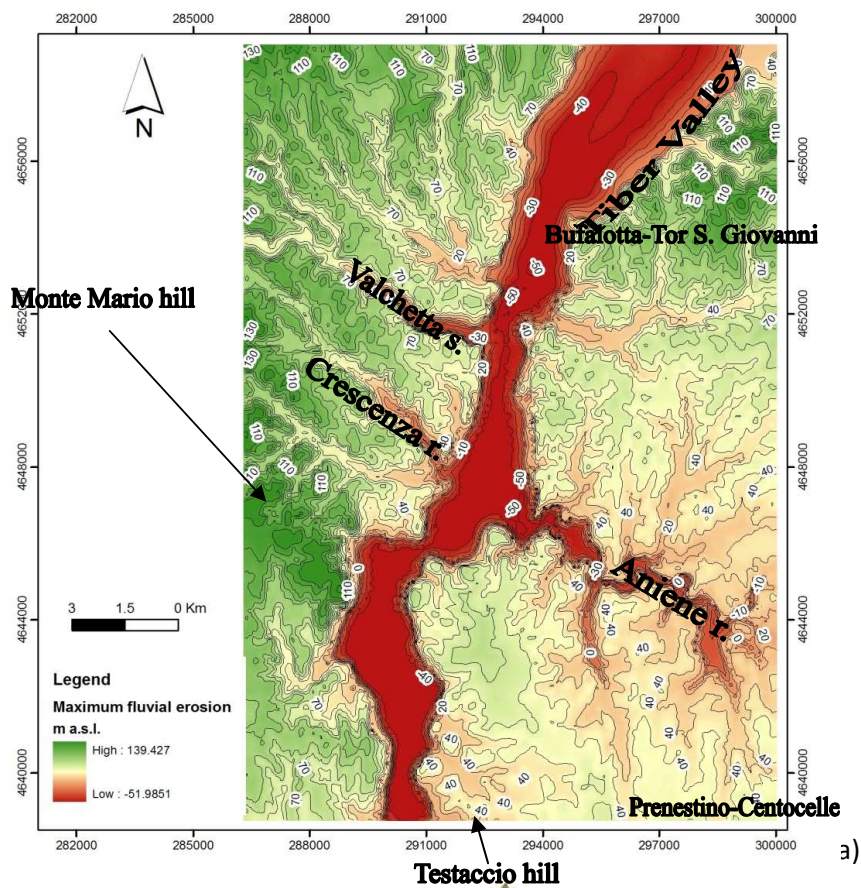


Figura 2.16: a)reconstruction of maximum erosion of alluvial Tiber Valley **b)**Contour map resulting from the grid interpolated with IDW method and corresponding surface. The coordinate grid is referred to ED50 N33 projected system.

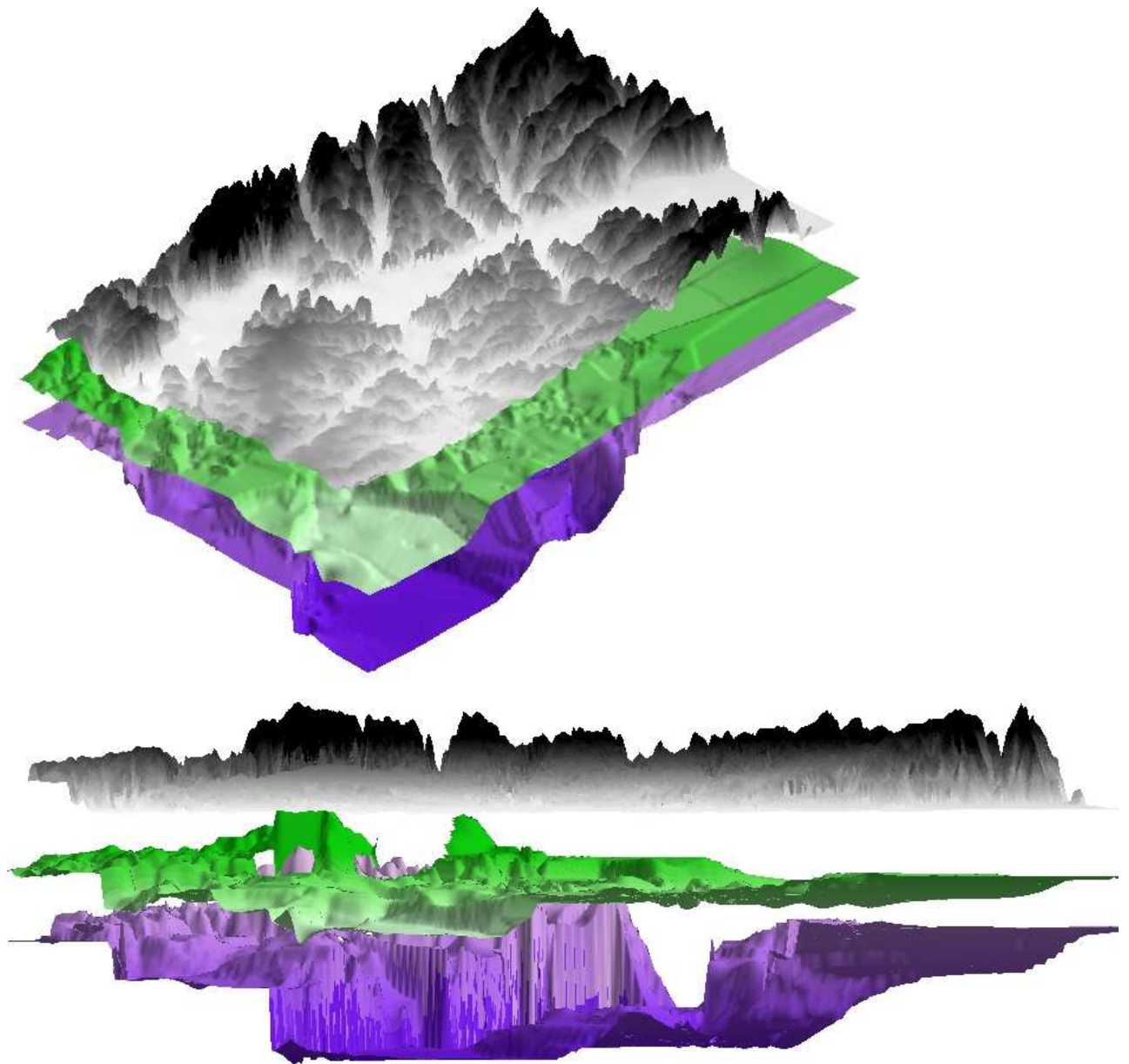


Fig 2.17: Geological model built in this study: the exaggeration is to better show the stratigraphic relationships. The black surface is the DTM; the green surface is the bottom of volcanic complexes and the blue surface is the bottom of the Ponte Galeria Formation.

The top surface of alluvial **basal gravels** was built by selecting 107 boreholes, drilled for the whole length of the alluvial valley. This complex includes the basal gravel beds of Tiber and Aniene rivers and the gravel, sandy gravel and coarse sands of minor tributary Crescenza and Valchetta streams. Tributary streams alluvium have been assimilated to the oldest Tiber basal gravel bed in the first level reconstruction, because they're made by sediments very similar in hydraulic conductivity and,

moreover, they're in stratigraphic contact; tributary alluvium give an important groundwater recharge to the Tiber alluvium.

The top of basal gravel has been built only in area with a reasonable amount of stratigraphic data, which is from the Northern part of the city ring road till the south border of the study area.

The distribution of stratigraphic data is discontinuous; in the areas of Fidene station, Urbe airport and Tor di Quinto hippodrome there are no data, while in the area from Olympic Stadium to Testaccio Hill there's a great number of data.

The Isobaths of top of basal gravel were built manually; then, with the TOPO TO RASTER Arcgis® tool, the corresponding interpolated raster was built.

The top of basal gravel surface ranges from 0 to -68 m a.s.l.; this surface's general trend shows absolute top heights decreasing from the borders of the valley (where the top of gravels is on average at around -20 m a.s.l. towards the center (where the top reaches heights till -47 m a.s.l.)

In general, top heights at the center of the valley show a general decrease from the Northern zone (Castel Giubileo) where they are found at -30 m a.s.l. towards South (Tiberina Island-Testaccio), where top heights are the highest of study area (-47 m a.s.l.).

In tributaries confluence areas, the top of this surface is considered high because of the thickness of tributary's sediments.

The thickness of the "basal gravel" complex ranges from 0 to 40 meters. The thinnest parts are those close to the border of the valley; the thickest are in the confluence areas.

In particular can be noticed the elevated thickness in the confluence zone of Valchetta stream, where sediments with high permeability are found from the height of 0 m a.s.l..

In the area Monte Mario - Olympic Stadium there's a zone where the top of basal gravel ranges from 12 to 16 meters b.s.l., higher than the immediately eastern area, where the top is at around 30 meters b.s.l.. The origin of this discrepancy could be due to tectonic, as a fault segment trending NE-SW.

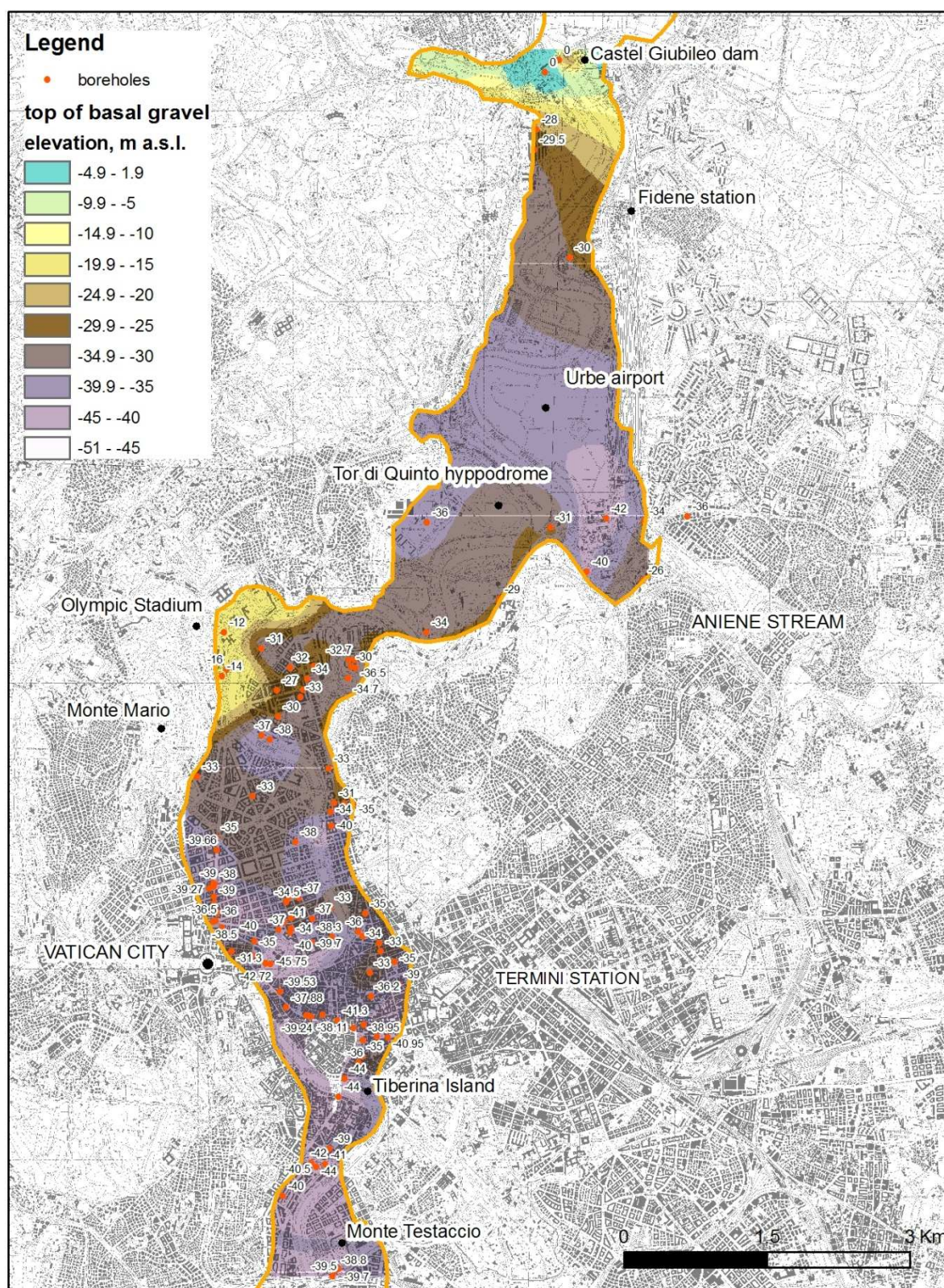


Fig. 2.18: reconstruction of the top surface of the silty-gravel bed in the Tiber alluvium.

2.3 Hydraulic properties

Hydraulic conductivity (k) values come from field measurements and from geotechnical laboratory tests (see chapter 2.3). Field data include slug tests (Lefranc permeability tests) and pumping tests, distributed in the study area as shown in **fig. 2.19**. Proves have been performed over all the types of alluvial terrains. Regarding the volcanic complexes, in the study area (considering a 3 km buffer around the boundary) there are 17 tests. Due to the high k heterogeneity of volcanic rocks, those tests are retained insufficient to represent volcanic hydraulic conductivity for the whole study area. Four pumping tests concern the sedimentary PGT complex, located along the path of Crescenza stream.

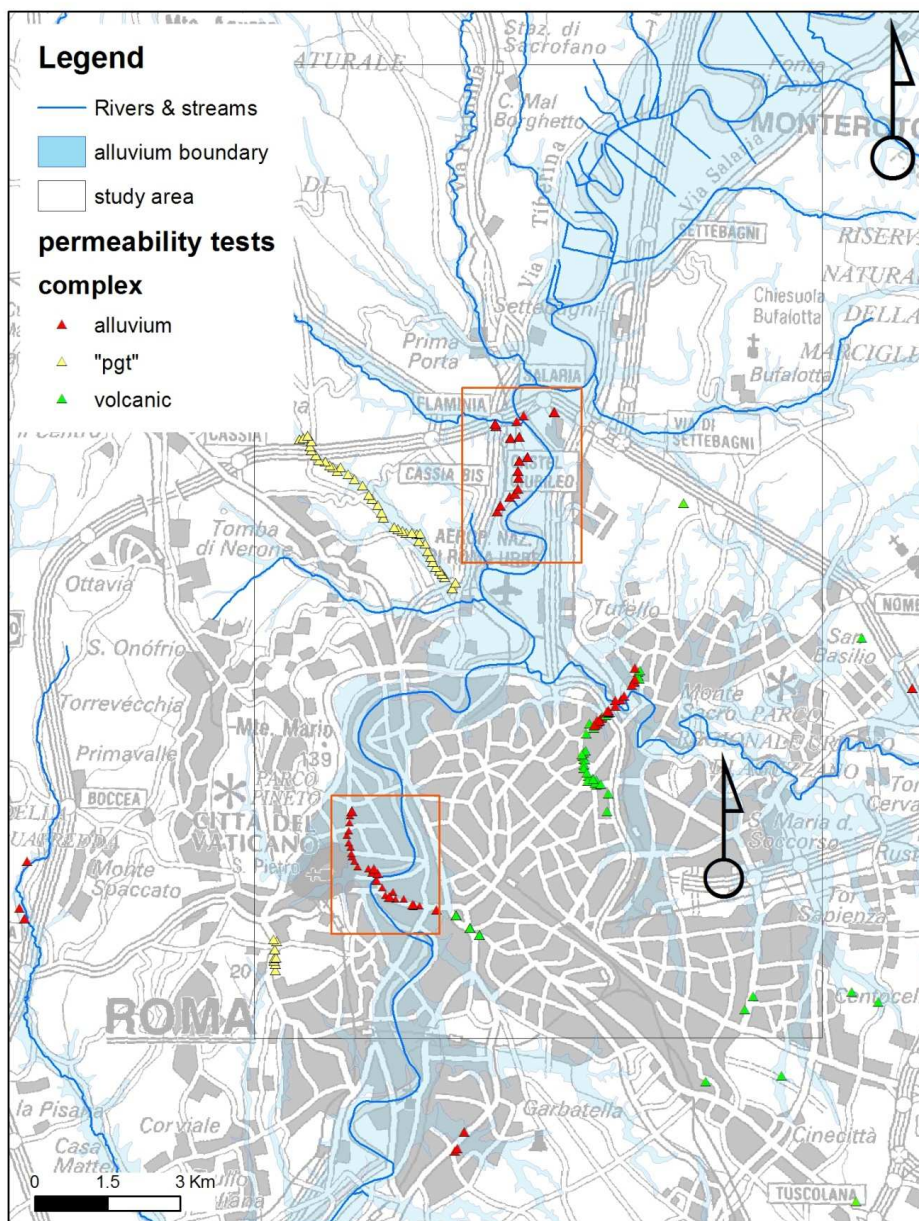


Fig 2.19: distribution of pumping and slug tests over the study area. Red rectangles are areas zoomed in **fig 2.34**),

Due to the small number of test and to the wide range of measured k values for each complex, values assigned to complexes also derive from literature data and from regional numerical models developed by the LINQ; in some case, the knowledge about granulometry and possible transmissivity has been used to derive an initial value.

2.3.1 Volcanic complexes

Two volcanic complexes are present in the study area: the Sabatini Volcanic complex and the Alban Hills volcanic complex. The Sabatini Volcanic complex includes mostly stratified tuffs, and, according to regional hydrogeological models developed in the Laboratory of Hydrogeology of Roma Tre University (LINQ) in the Sabatini Mts. area, one single hydraulic conductivity value was assigned to the whole complex. The value for k_x - k_y (2.13 m/d) is the calibrated value for regional model (see **tab 2.2**), while the k_z value was kept fixed in the Sabatini model as $1E-6$ m/s, which is 0.0864 m/d.

For the Alban Hills volcanic complexes, in the study area are present “Red and Black pozzolana” and the “Villa Senni” Formation (Funiciello & Giordano, 2008), with the two lithofacies “Villa Senni tuff” and “Lionato Tuff”; Villa Senni formation hydraulic conductivity is lower than units “Red Pozzolane” and “Black Pozzolane” due to the zeolithization and presence of cineritic interbeds. As in Sabatini complexes, in the Alban Hills volcanic products the presence of argillified paleosoils is the reason for the reduced vertical hydraulic conductivity (k_z) respect to the horizontal one (k_x , k_y).

Tab 2.2: average values for volcanic complexes (LINQ, 2010)

unit	K_x (m/d)	K_z (m/d)	notes
Sabatini stratified tuffs	2.13	0.0864	Sabatini complex volcanic units
“Villa Senni” Formation	0.1728	0.015552	Alban Hills volcanic complex
Red and Black Pozzolane	6.048	2.592	Alban Hills volcanic complex

2.3.2 PGT Formation complex

The sedimentary prevolcanic complex (which we refer to as *PGT Formation* complex) is mostly present as the Fosso Crescenza-FCZ facies; in order to assign a transmissivity value to the FCZ formation, it was considered as a homogeneous multilayer sequence of gravel-sand and clay, where gravel and sandy terms are more transmissive while clay layers are mostly aquitards; because of the low number of deep boreholes drilled in the FCZ formation, a reconstruction of different facies inside the FCZ is not possible; in fact, the extreme spatial variability of the sedimentary formation and the lack of deep well makes hard to distinguish the different facies which are in contact with sediments in the valley. The multilayer conformation derives from data

on deep boreholes in the Bufalotta-Talenti area. These 90 meters-deep continuous coring boreholes show a stratigraphy for FCZ sequence made by three sandy-gravel layers separated by three clay aquitards (**fig 2.20**). It can be assumed this stratigraphy as continuous for all the FCZ deposit inside the graben, and from this assumption an average transmissivity can be calculated.

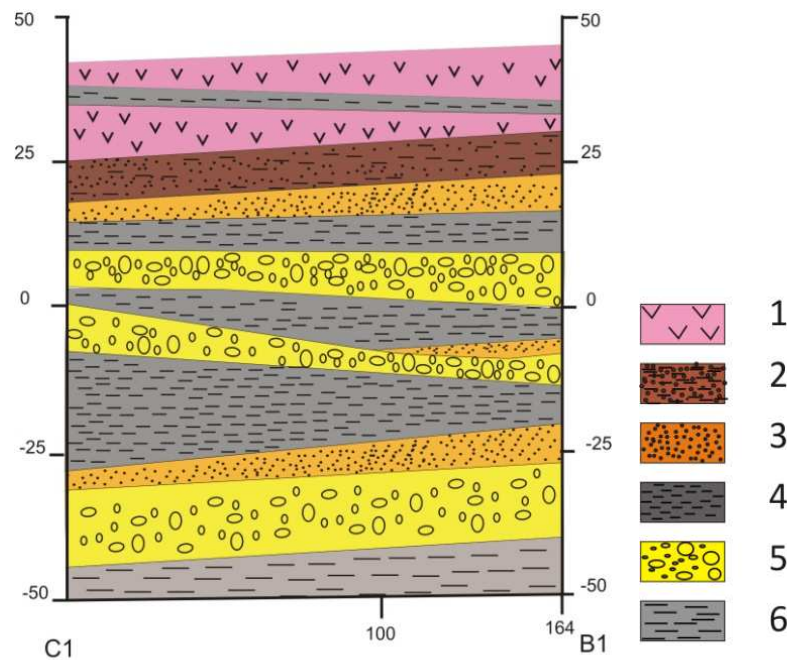


Figure 2.20: sketch of the multilayer FCZ Formation (from drillings in Bufalotta-Talenti area, LINQ 2010). Height scale: 1:500. LENGTH SCALE: 1:1000. 1) Volcanic complex; 2) PGT, silty-sand facies; 3) PGT, sand facies; 4) PGT, clay facies; 5) PGT, sandy-gravel facies; 6) Plio-Pleistocene overconsolidated clay.

The average transmissivity for each layer is computed by multiplying the average k values (from literature data) times the thickness; the total transmissivity of the multilayer as a whole is calculated by adding together the transmissivity of every single layer.

The clay part is silty clay with thin peat layers; the average k value that can be reasonably assigned is 0.000397 m/d according with the slug tests in the clay layers close to the Crescenza Stream. The average thickness is about 26 meters. The sandy-gravel unit is made by clasts having centimetric and decimetric diameter in a sandy-clayey matrix, not consolidated; the average k value that can be reasonably assigned is 0.292 m/d according with the slug tests in the sand-gravel layers close to the Crescenza Stream; the thickness is 30 meters. The computed transmissivity for the whole FCZ deposit is then calculated as 8.77 m²/d. The average hydraulic conductivity that can be deduced is 0.14 m/d for horizontal hydraulic conductivity, and 0.014 for vertical hydraulic conductivity.

2.3.3 Plio-Pleistocene units

Since the “bedrock” aquiclude formation (Marne di Monte Vaticano, MAV) is not hydrogeologically productive, there are no slug or pumping tests. Initial hydraulic conductivity was chosen in order to give a very low permeability to layers 3-8 external to the Tiber Valley. The initial assigned k value was $K_x=K_y=0.1\text{m/d}$, $k_z=0.01$.

2.3.4 Alluvium complexes

Alluvium complex is featured by a huge heterogeneity; authors recognized many lithofacies composing the complex, which are listed in **table 2.3**. The following tables and histograms briefly show the main geotechnical characteristics of Holocene Tiber River alluvium (data from laboratory geotechnical proves made by LINQ in 2002 and from geotechnical reports for “C” subway line works by Lanzini M., 1995-2000a and Geostudi, 2007-2009).

Tab 2.3: classification of Tber alluvium as recognized by from laboratory geotechnical proves made by LINQ in 2002 (LINQ, 2003)

Alluvium unit
<i>A1 - hystorical silty clay</i>
<i>A2 - hystorical silty clay with green sands</i>
<i>B1 - sand and silt</i>
<i>B2 - coarse sand (upper)</i>
<i>C - clay with peat</i>
<i>D1 - silty sand</i>
<i>D2 - coarse sand (lower)</i>
<i>G -basal gravel</i>

Parametri	Valore minimo	Valore massimo	Valore medio
γ_s (kN/m ³)	19.5	19.9	19.8
W (%)	24.2	28.6	26
LL (%)	43.2	57.6	47
LP (%)	21.3	37	28
I _c	0.87	1.64	1.14
e	0.631	0.798	0.68
p.p. (kPa)	160	240	216
c (kPa)	27	40	34
ϕ (°)	21	30	25
c _u (kPa)	31	38	36
C _c	0.13	0.25	0.21
E (kPa)	5.600	8.000	7.300

Fig 2.21: measured parameters for geotechnical group A1

Parametri	Valore minimo	Valore massimo	Valore medio
γ_s (kN/m ³)	18.3	20.2	18.85
W (%)	22	38	28
LL (%)	35	71	47
LP (%)	14	42	27
I _c	0.63	1.63	0.98
e	0.610	0.983	0.77
p.p. (kPa)	40	290	124
c (kPa)	12	30	19
ϕ (°)	20	27	25
c _u (kPa)	18	18	18
C _c	0.16	0.28	0.24
E (kPa)	3.500	9.400	4.900

Fig 2.22: measured parameters for geotechnical group A2

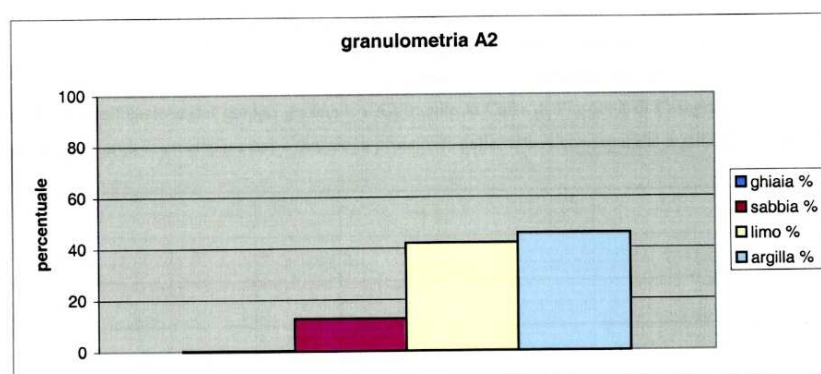


Fig 2.23: histogram of granulometric fraction for group A2. The large fraction of clay can be observed.

Parametri	Valore minimo	Valore massimo	Valore medio
γ_n (kN/m ³)	18.6	20.0	19.0
W (%)	26	33	31
LL (%)	26	48	34
LP (%)	12	31	18
I _c	0.49	0.55	0.4
e	0.780	0.976	0.83
p.p. (kPa)	0	22	7
c (kPa)	27	40	34
ϕ (°)	32	39	34
C _c	0.13	0.26	0.2
E (kPa)	5.700	6.900	5.450

Fig 2.24: measured parameters for geotechnical group B1

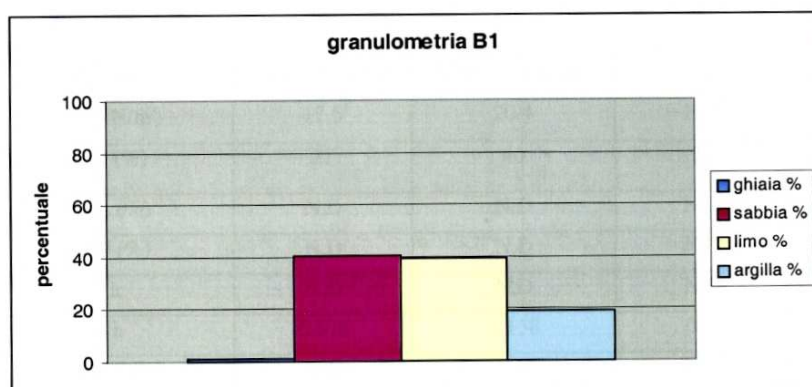


Fig 2.25: histogram of granulometric fraction for group B1. The large fraction of sand and silt can be observed.

Parametri	Valore minimo	Valore massimo	Valore medio
γ_n (kN/m ³)	17.6	20.4	19.3
W (%)	21	40	29
LL (%)	N.D	N.D	N.D
LP (%)	N.D	N.D	N.D
I _c	N.D	N.D	N.D
e	0.574	1.158	0.8
p.p. (kPa)	N.D	N.D	N.D
c(kPa)	0	11	3
ϕ (°)	36	40	39

Fig 2.26: measured parameters for geotechnical group B2

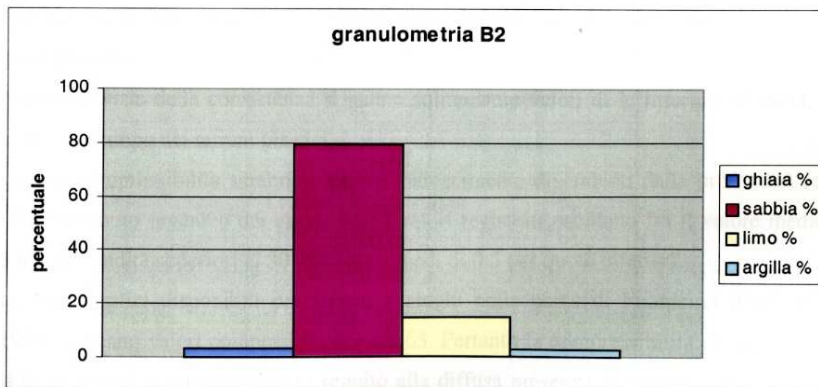


Fig 2.27: histogram of granulometry for group B1. The sand fraction is prevalent; a small amount of gravel can be noticed.

Parametri	Valore minimo	Valore massimo	Valore medio
γ_s (kN/m ³)	15.9	19.6	18.3
W (%)	25	66	37
LL (%)	42	83	61
LP (%)	19	51	31
Ic	0.43	1.04	0.92
e	0.66	1.66	0.92
p.p. (kPa)	30	170	83
c (kPa)	2	22	10
ϕ (°)	14	29	19
Cc	0.22	0.65	0.42

Fig 2.28: measured parameters for geotechnical group C

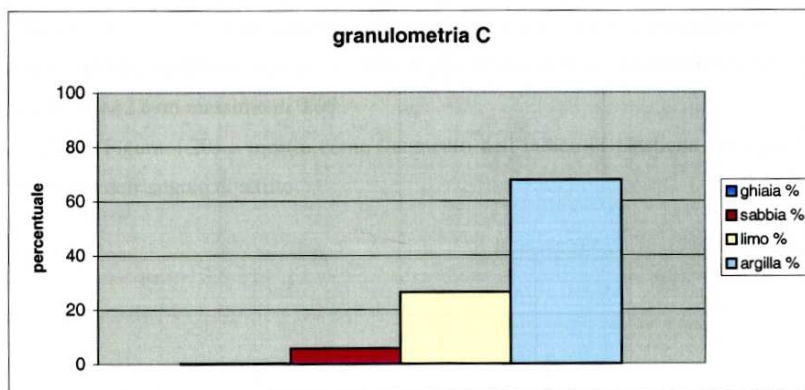


Fig 2.29: histogram of granulometry for group C. The clay fraction is prevalent.

Parametri	Valore minimo	Valore massimo	Valore medio
γ_n (kN/m ³)	18.6	20.2	19.7
W (%)	26	33	31
LL (%)	23	39	34
LP (%)	16	27	22
I _c	0.78	1.03	0.83
e	0.589	0.99	0.73
p.p. (kPa)	90	180	118
c (kPa)	9	14	11
ϕ (°)	23	33	29
C _c	0.14	0.40	0.26

Fig 2.30: measured parameters for geotechnical group D1

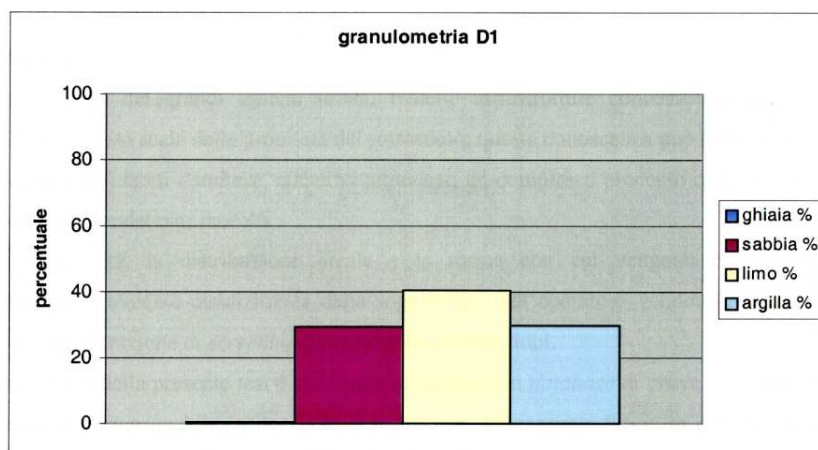


Fig 2.31: histogram of granulometry for group D1. All the granulometric fraction, except the gravel one, are represented.

We don't have geotechnical characterization for group D2, since it's made by gray coarse sands.

For the "basal" sandy gravel is reported the granulometric fraction histogram (technical reports, "Metro C" subway line, Lanzini M., 1995-2000a)

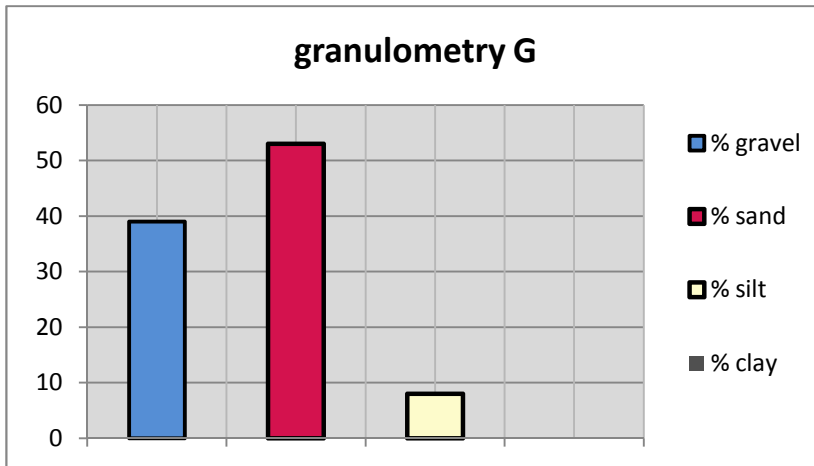


Fig 2.32: granulometric fraction histogram for group G. The sand fraction is prevalent; the fraction of gravel is around 39% (Lanzini M., 1995-2000 a and b, modified).

The histogram **Fig 2.32** refers to gravel samples coming from the hystorical center; due to its wide textural heterogeneity, the sandy-gravel complex shows different percentage of matrix and different matrix granulometry (from silty to sandy) depending on the sample-sites. (**fig 2.33**).



Fig 2.33: Pictures of cores drilled in three different sites along the path of “C” subway line (“Metro C”)

In this study’s hydrogeological modeling, alluvium units were simplified and a total number of **5 units** are distinguished (**Table 2.4**): the same “coded” unit can have different percentage of clay and sand, and this brings a wide range of possible hydraulic conductivities to be assigned.

Moreover, many authors observed an increasing of k values measured in pumping tests with the increasing of discharge (Shulze-Makuch & Chekauer, 1995), and they also observed that the increase occurs in different rates depending on the heterogeneity degree of the formation. In this study, K values for each alluvial *facies* come from slug tests, pumping tests, edhometric laboratory tests, and indirectly derived from granulometric curves; data come from public works in the city of Rome or in areas close to the city, as “Metro C” and “Metro B1” subway works, the Castel Sant’ Angelo underpass, San Pietro railway station, Nazzano Dam, Foro Italico-Trionfale street axis. We also considered published and unpublished literature as Bozzano (2000) or master degree’s thesis which analyze Tiber alluvium (LINQ 2003 and 2009). **Figure 2.34** shows permeability tests distribution in two sample areas, both located in the Tiber alluvial valley. In **Table 2.4** k for each unit are listed; both ranges and average k are taken from literature and pumping tests.

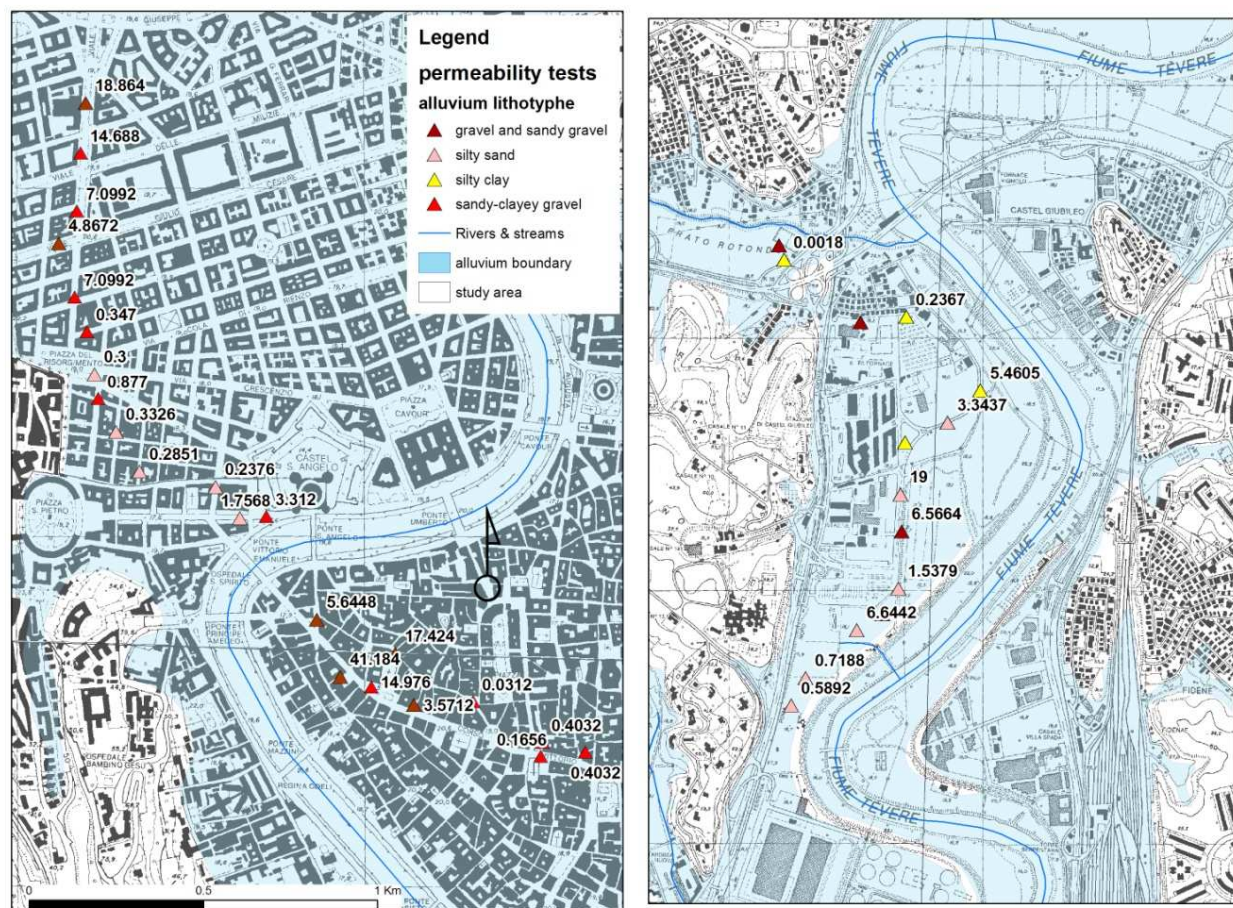


Fig 2.34: permeability tests values in two areas of the Tiber valley; areas location is **fig. 2.19**

Tab 2.4: the table lists the 5 alluvium units considered in this study and corresponding k value range (From Bozzano 2008, LINQ 2003 and Lanzini M., 1995-2000 a and b)

Alluvium unit	Corresponding unit (Bozzano 2008, LINQ 2003, Lanzini, 1995-2000 a and b)	Min k (m/d)	Max k (m/d)	Average k (m/d)
<i>Landfill</i>	RP	0.1	0.01	0.055
<i>Clay and silty clay</i>	A,	0.00003456	2.59	1.03421376
<i>Sand</i>	B1, B2, D1, D2	0.03222	43.2	8.8527312
<i>Clay with peat</i>	C	0.00001728	0.01728	0.5214312
<i>Gravel</i>	G	0.003	6.5	1

One of the purpose of Roma model is to find a k value which reproduces the effective hydraulic conductivity of the hydrogeological unit at a regional scale, despite of small scale heterogeneities that can locally change the measured hydraulic conductivity. In **table 2.5** the k values chosen as initial k values for the model are resumed; in some case values are far differ from data listed in **Tab 2.4**. K values will be subjected to calibration in the numerical model phase.

Tab 2.5: Initial k values assigned to complexes

K zone	lithotype	Kx, Ky (m/d)	Kz
1	Volcanic complex- Alban Hills	6.04	2.5
2	Volcanic complex- Sabatini Hills	2.13	0.0864
3	PGT complex (Paleo-Tiber)	0.14	0.014
5	Alluvium- clay and silty clay (A)	0.1	0.01
6	Alluvium- sand (B1,B2,D1,D2)	2	0.2
7	Alluvium- clay with peat (C)	0.1	0.01
8	Alluvium- gravel (G)	4.2	0.42
8	Alluvium- clay, also bedrock	0.01	0.001
9	Alluvium- landfill (RP)	0.1	0.01

2.4 Aquifer system inflows and outflows

2.4.1 Climate feature

Precipitations in the study area occurs with an average of 650 mm/y (Fig 2.35) and are concentrated in a restricted time comprised between autumn and spring, often occurring in intervals of more consecutive days. Data come from the SIMN- Istituto Idrografico e Mareografico Nazionale.

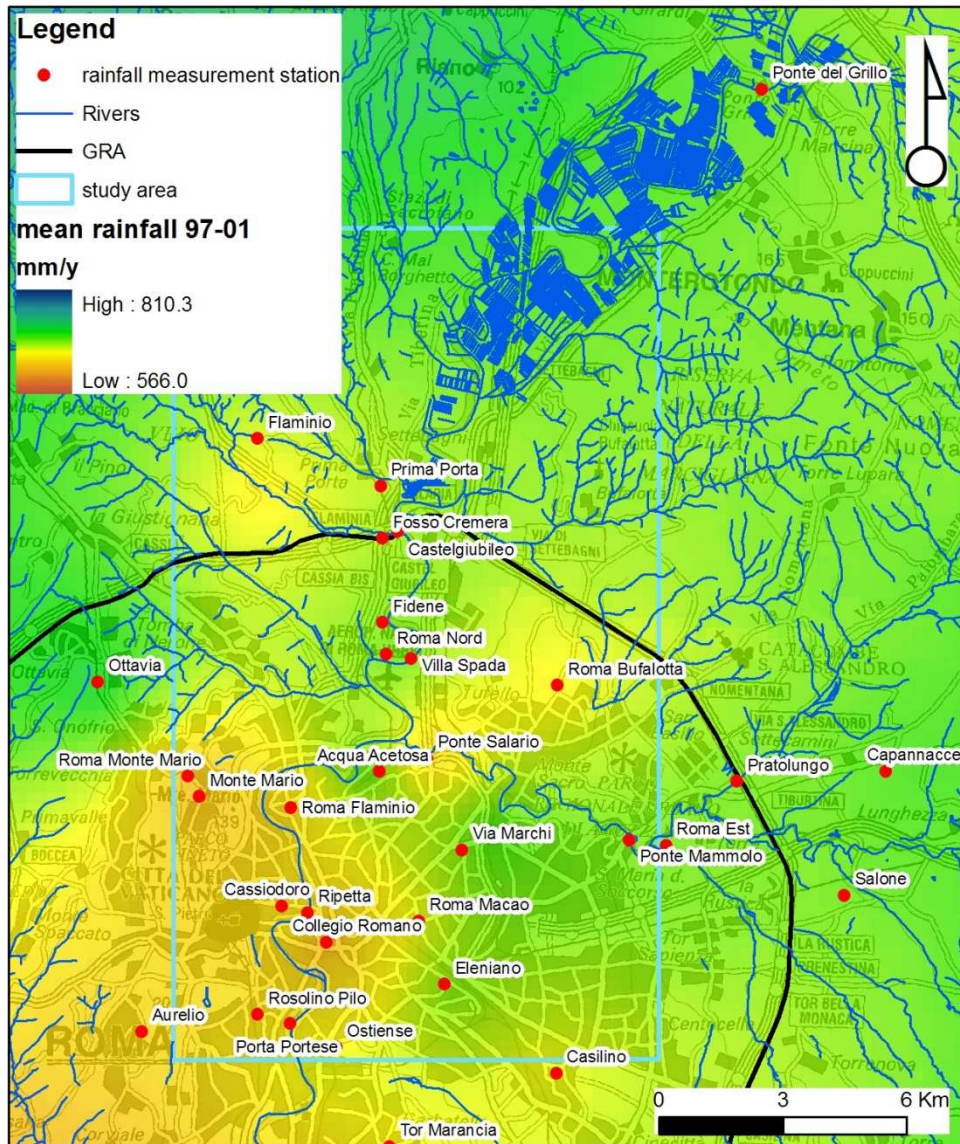


Fig 2.35: statistic interpolation of rainfall data (1997-2001) and location of SIMN measurement sites. The average rainfall in the study area (for the period 1997-2001) is 650 mm/year. (from Capelli et alii, 2005)

Temperature and rainfall data recorded by SIMN stations used for the study of volcanic aquifers show, during the period between 1980 and 2000, an increasing trend in the average annual temperature and a decrease of annual precipitation (150-200 mm in 20 years) (Capelli et al.,

2005), that, consequentially produces a decrease of effective infiltration. See **Tab. 2.6** for the process that has been followed to elaborate climate data.

The recharge has been calculated by the distribute balance method as reported in *Capelli et alii, 2005*; the annual recharge is calculated in each cell as the difference between precipitation, runoff and real evapotranspiration. The effective infiltration is the portion of rain that contributes to aquifer recharge considered. In the case of aquifers where contributions of surface water and groundwater from adjacent areas can be considered negligible, the effective infiltration corresponds to the amount of renewable resource, and thus available for the maintenance of underground and surface **outflow/inflow** basis of the waterways and the many uses associated with human activities.

In different areas of the hydrological basin, the recharge takes different values depending on:

- The spatial and temporal distribution of weather-climatic factors (temperature, rainfall, solar radiation, wind speed, humidity);
- The area's topography (slope, exposure, presence of drains areas and / or semi-Endor);
- The nature of the aquifer lithology (rock's permeability);
- The characteristics of soils (AWC, effective porosity etc.);
- Plant cover;
- Land use.

The maximum size of computational cells must be comparable with the minimum size considered cartographic element (land use, lithological associations, morphology, etc. AWC). The timescale should allow to take into account seasonal variability and, ultimately, distribution and intensity of meteorological events. The experimental data currently available would make it the approach to scale monthly and in some cases, daily scale. Note that it is always advisable to obtain the recharge by the sum of contributions monthly or daily. This makes possible to take account of variability in several years of regional factors (variables of site) and climate (weather and climate variables). In **table 2.6** is represented a scheme of the process of calculation of the recharge; the estimation of the main items (temperatures, rainfalls, runoff) is discussed below.

tab 2.6 : resume of parameters for distributed balance as computed in Capelli et alii, 2005

starting data	kind of aggregation/other informations	data processing	unit of measurement and maximum and minimum value	output	time variable
Daily precipitations	monthly cumulate precipitation	kriging, FAI-k	mm	P distributed value of monthly precipitation (grid)	yes
Maximum daily temperatures	Tmax monthly mean of the maximum daily temperatures	kriging FAI-k, with external drift	°C	Tmax distributed value of the monthly mean of the maximum daily temperatures (grid)	yes
Minimum daily temperatures	Tmin monthly mean of the minimum daily temperatures	kriging FAI-k, with external drift	°C	Tmin distributed value of the monthly mean of the minimum daily temperatures (grid)	yes
Mean daily temperatures (obtained by the mean of the minimum and maximum daily temperature values)	Tmean monthly mean of the medium daily temperatures	kriging FAI-k, with external drift	°C	Tmean distributed value of the monthly mean of the medium daily temperatures (grid)	yes
Corine land cover (shape polygon)		building a specific legend correlate to fotointerpretation areas		UTI (Unit of Territory Hydro exigency) mapping units with homogeneous need of water (shape polygon)	yes
colors ortophotos - scale 1:10.000 of the Regione Lazio flight of year 2000		fotointerpretation of colors ortophotos			
topographic map 1:10.000		draw perimeters of the UTI			
H=thickness of soil (m) -from geology map (1:25.000) shape polygon P= gradient of stone (%) I20=mean unitary value of the reference AWC for the considered soils (mm/y) F=correction factor for volcanic soils	Value necessary in the estimation of the Evapotraspiration	AWC= $H*(1-P)*120$ F Available water capacity	mm, from 0 to 235	distributed value of the AWC (grid)	no
UTI		a monthly value of kc is associated to every UTI class	from 0 to 1,1	Kc -distributed monthly value of the crop coefficients (grid)	yes
hydraulic conductivity (geology)		assigning a percent value to each component	from 0 to 1	Ck -distributed value of the Kennessey coefficient (grid)	almost no
topography slope (DEM)					
vegetal covering (UTI)					
RA solar radiation, it has an unic monthly value for the entire area	EVR (evapotraspiration)	EVR= ETR (if there isn't deficit)	if $P+U_i > ETR$	ETP= $0,0023 (T_{mean}+17,8) (T_{max}-T_{min})^{0,5} RA$	
			ETR= ETP*kc		
DF deficit		EVR= $P+U_i$ (if there is deficit)	if $P+U_i < ETR$		
$U_{im} = (P - ETR + U_i)m - 1$; if $U_{im} > AWC \Rightarrow U_{im} = AWC$; if $U_{im} < AWC \Rightarrow U_{im} = U_{im}$ and $DF = (U_i - ETR + P)m$					
Surface Runoff	SR(year) = $\Sigma (P_{month} - EVR_{month}) * C_k$				
Recharge	R (year) = $\Sigma (P_{month} - EVR_{month} - SR_{month} + Endo_{month})$				

- **Temperature and rainfall:** The hydric balance has been analyzed on a monthly scale starting from daily values, by that taking into account the annual variability. The recharge is calculated starting from the monthly estimate on cells 250x250 meters on a five-years period, from 1997 to 2001, of the following parameters:
- Rainfall;
- Maximum temperatures;
- Mean temperatures;
- Minimum temperatures.

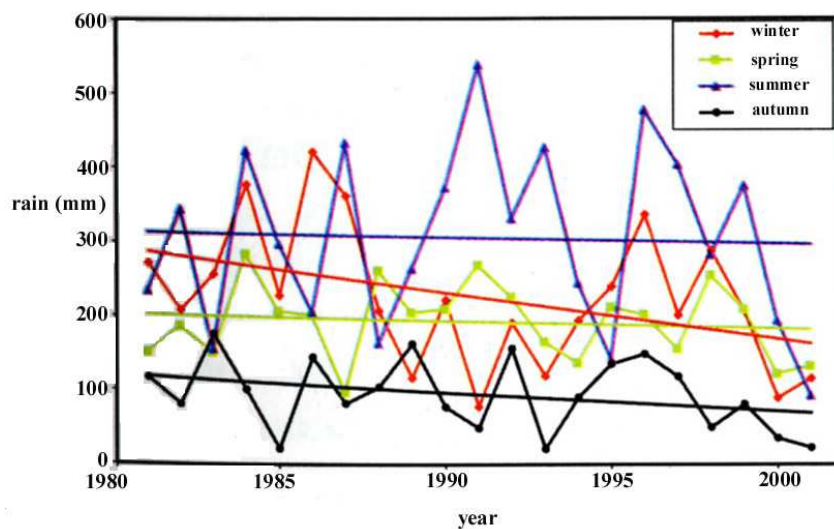


Fig. 2.36: seasonal rainfall trend recorded in the Latium SIMN stations between 1980 and 2000 and related regression curves.

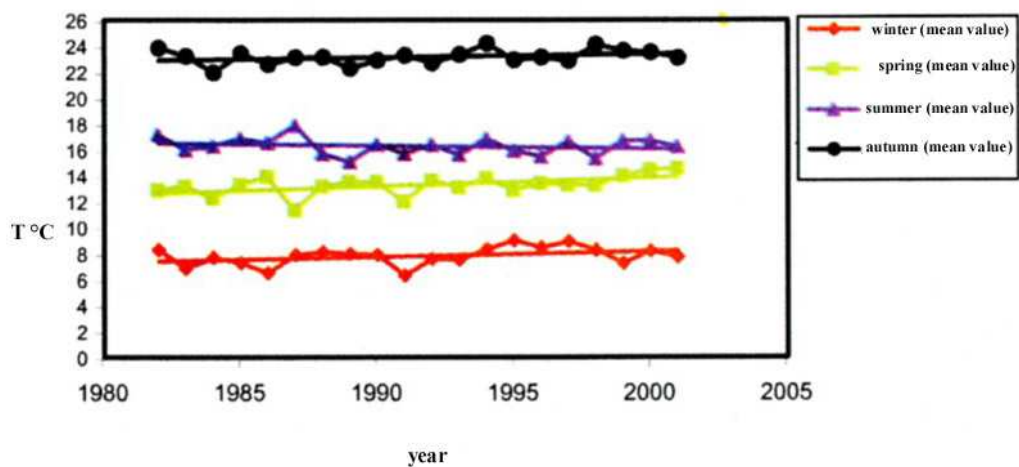


Fig. 2.37: Seasonal trend of temperatures recorded in the SIMN's stations between 1980 and 2000 and related regression curves.

The result is a set of maps of the parameters distribution; the geostatistical method that has been used is the kriging in FAI-k (Chilès & Delfiner, 1999; Wakernagel, 1995; Bruno e Raspa, 1994; Matheron, 1973), which is valid in not-steady conditions.

The accuracy of the estimation is based on processes and data statistics derived from cross-validation, which is the estimation of the variable in the measured points. The Cross-validation has been performed for each observation point, for each of the 60 months (12 months for 5 years) and for each of the four parameters; once the cross-validation is finished, also the variance of the related errors has been calculated. This last is considered a quality index of the monthly maps.

The variance of **rainfalls** is lower in the period 2000-2001 then in 1997-99 (**fig 2.38**). **Figure 2.39** indicates the frequency distribution of the relative standard deviation of the cross-validation errors; the value is lower than 0.5 for more than the 80% of the months and it is lower than 0.3 for a half of the months.

The comparison observed-simulated values can be done also for each station over 60 months. In **figure 2.41** graphs of observed vs simulated rainfalls are shown for three sample gauging stations (n° 1866 Roma Eleniana, n° 1760 Tivoli and n° 50 Talentano) and the related correlation clouds. The relative standard deviation of cross-validation in the three stations is 0.12, 0.31 and 0.52. The value shows a higher accuracy for the station located in Rome.

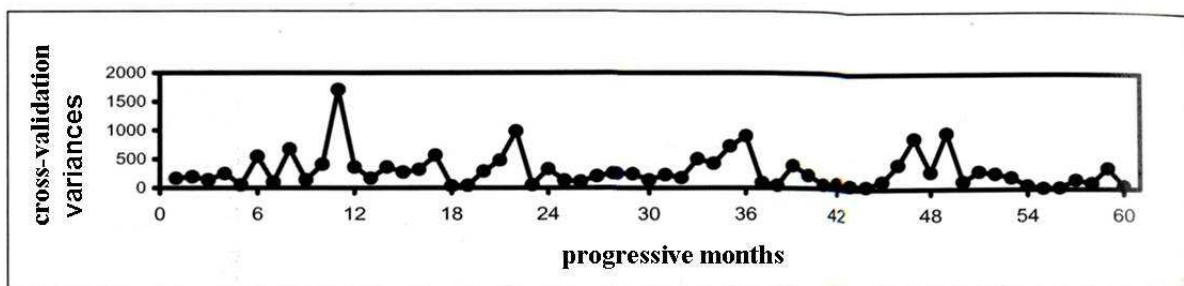


Fig. 2.38. Temporal trend of cross-validation variances for monthly rainfalls in the time window 1997-2001.

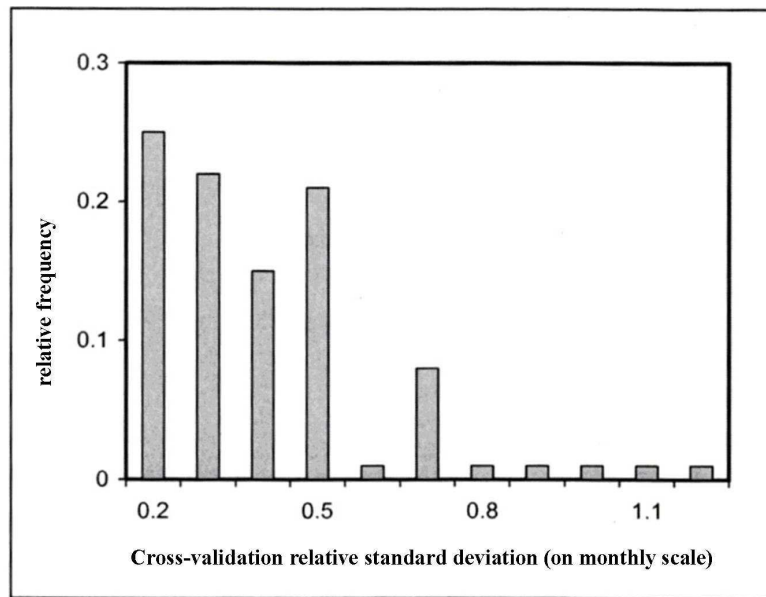


Fig 2.39: Histogram of cross-validation relative standard deviation (on monthly scale) of monthly precipitations in the time window 1997-2001

For temperature values, the cross-validation variance oscillates between 1 and 2 °C. The frequency distribution of the relative standard deviation of cross-validation (**fig 2.42**) shows values ranging between 0.01 and 0.12. the 50% of values is lower than 0.05 and the 83% is lower than 0.08.

The cross-validation has been performed taking into account the elevation above the sea level of the estimation point; this permits to delete a systematic error that could be introduced without considering the elevation.

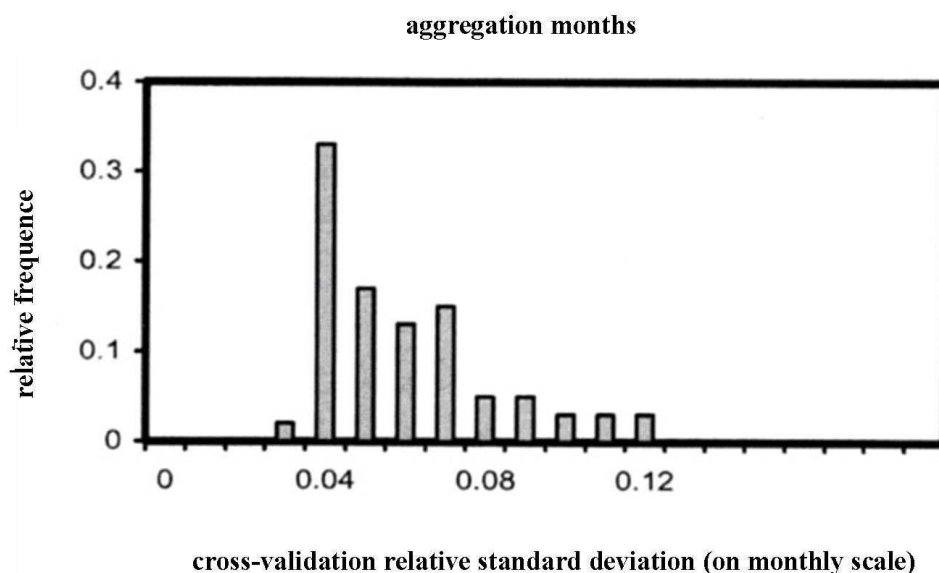


Fig 2.40: Histogram of cross-validation relative standard deviation (on monthly scale) of monthly maximum temperatures in the time window 1997-2001

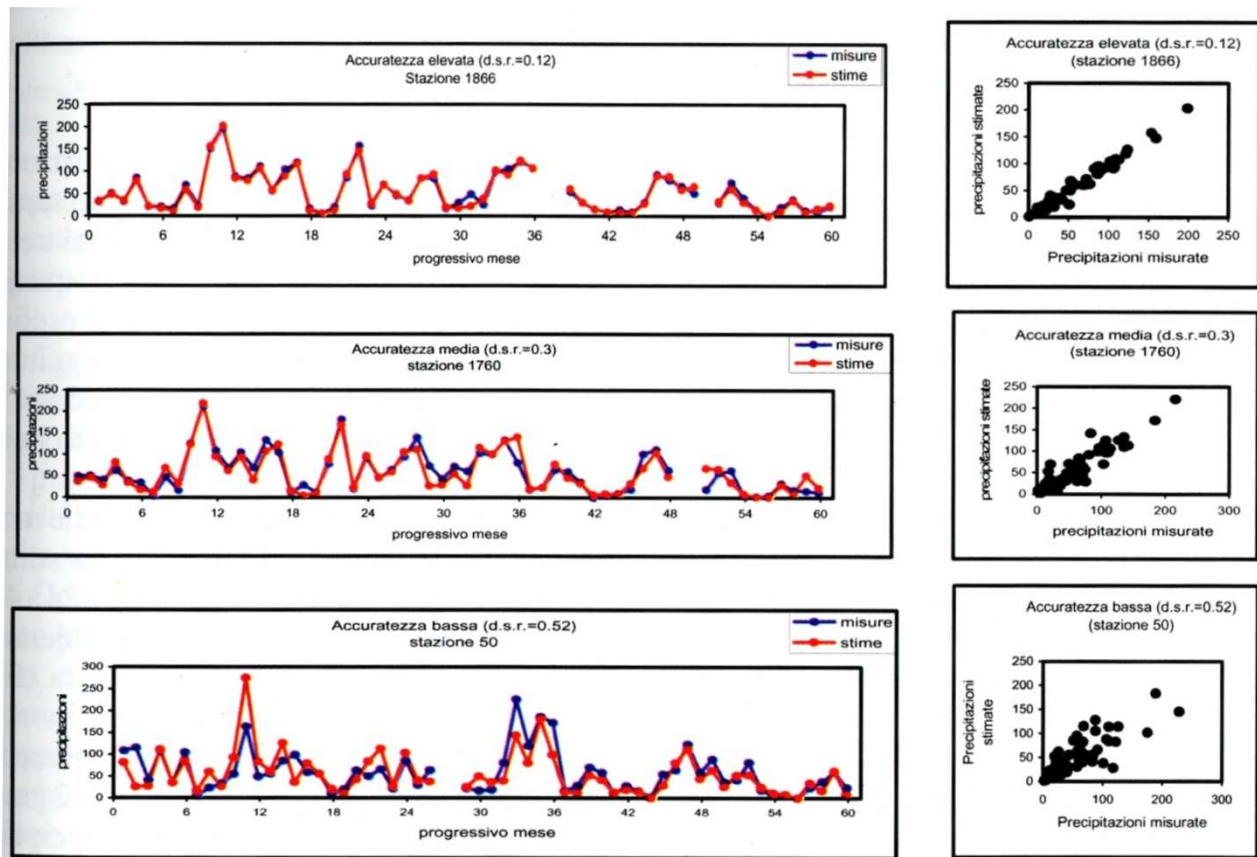


Fig. 2.41: temporal trend measurements versus cross-validation estimates and related scatterplots of monthly precipitations in the time window 1997-2001 at three different accuracy levels.

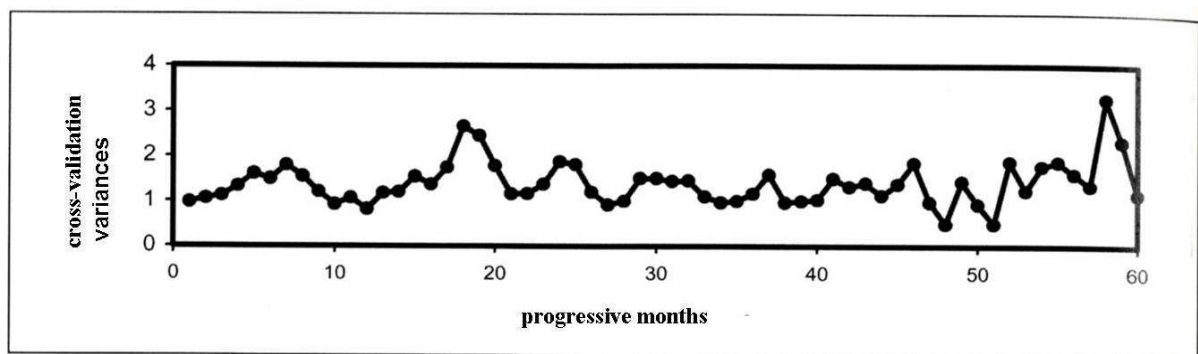


Fig 2.42: Temporal trend of cross-validation variances of maximum monthly temperatures in the time window 1997-2001.

Surface run-off: the distributed balance calculated for a defined area an annual-average run-off coefficient (Kennessey coefficient, C_k); the coefficient is the sum of three factors which changes

depending on the permeability of the outcropping rocks, the vegetable cover and the surface slope. The coefficient is calculated also taking into account an aridity index (**Ia**), which relates the annual averaged temperature and rainfall to the temperature and rainfall of the most dry month. The validity of C_k is for an annual scale, and for this reason in the hydric balance is considered the annual values sum and not the monthly value; for this reason, C_k doesn't take into account the rainfall intensity distribution, introducing in that way an error of value estimation. In fact, in case of very intense rainfall, the run-off is prevalent respect to the evapotranspiration and the infiltration but, being the daily precipitation averaged on the entire month, the C_k value is underestimated.

In urban areas, the surface run-off is increased respect to the not-urbanized areas, and are calculated as higher than 270 mm/y. For the run-off model calibration, the calculated run-off has been compared on monthly and annual scale, with the field data collected in measurement stations of the SIMN of Rome; the gauging stations are on a limited number of streams and river, and there are relevant lacks of data. However, the difference between simulated and observed values underlines errors around 5% of rainfall value on a single hydrographical basin.

The recharge as calculated in Capelli et alii 2005 was referred to years 1997-2001; in order to extend the recharge across the time-window 1997-2007 and match those data with head and rivers stage measurements, the rainfall and temperatures data for years 2002-2007 were added to the averaged data; no changes are assumed for land use, AWC and U_{ti} . The calculated recharge for years 02-07 is increased of a **61%** respect to years 97-01, and this is due to an increase in the annual average precipitation. The final recharge rate is the average of years 97-07 and it is 118540 m³/d (or 324.7 m³/y) over the entire model area; it is represented by a raster with cells with spatial resolution 250x250 m. Since, in the cited study, urban areas were considered as totally sealed, recharge in urban cells is assumed equal to zero; this value will be changed in the calibration phase (see **chapter 4**).

2.4.2 Hydrologic boundaries

In the study area the drainage pattern is generally directed from north to south; tributary streams are directed toward the main rivers, the Tiber and Aniene, which are the main sink; in **fig 2.42** the main hydrological basins are shown. In **Tab. 2.7** basins and their main features are listed.

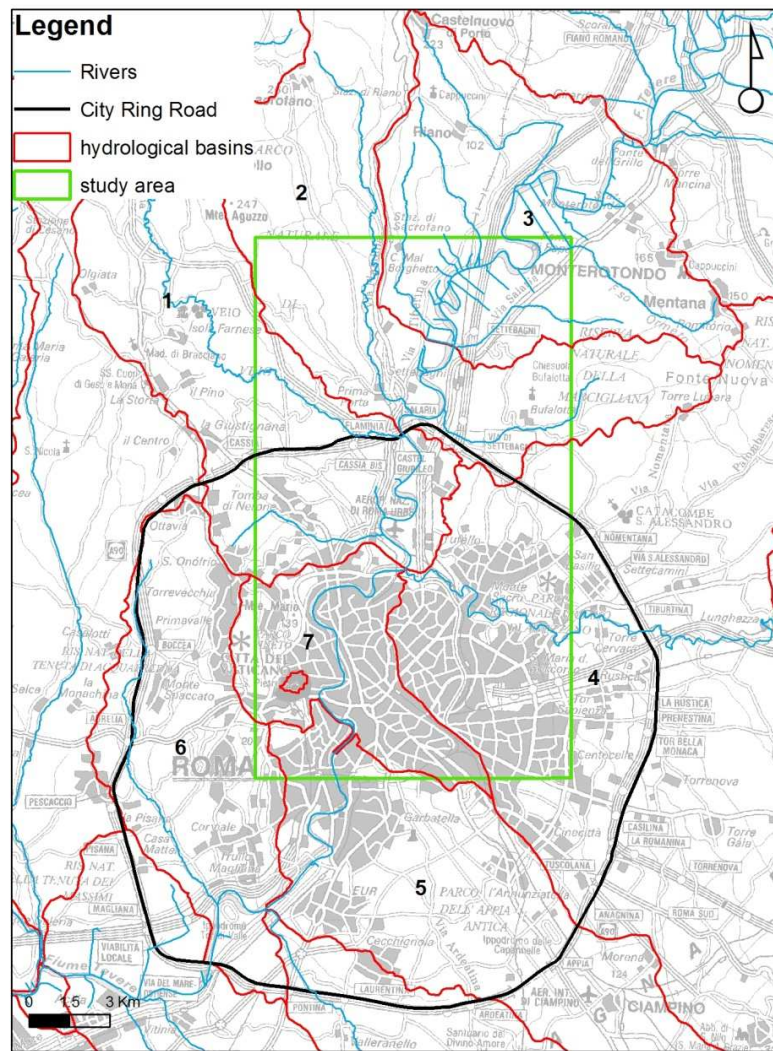


Fig 2.42: Hydrological basins; surface flow is directed from streams towards the Tiber and Aniene rivers. 1= Basin of Valchetta, Crescenza and Acquatraversa streams; 2= Basin of Mole and Malviata and Settebagni streams; 3= Basin of Tiber River-a; 4= Basin of Aniene river; 5= basin of Grottaperfetta and Vallerano streams; 6= Basin of Magliana stream; 7= Basin of Tiber River.

Tab. 2.7

basin	area km2	draining streams:	flux toward main river	main river bank
1	151.243	Valchetta, Crescenza, Acquatraversa	Tiber	right
2	119.703	Mole, Malviata		right
3	108.843	Drago, Regina		left
4	333.77	Cinquina, Cesarina, Settebagni	Aniene	right, left
5	115.725	Grottaperfetta, Vallerano	Tiber	left
6	78.605	Magliana	Tiber	right
7	43.852		Tiber	right, left

2.4.3 Rivers and streams

Figure 2.43 shows the rivers and streams network; all streams are Tiber River's tributaries. Table 2.8 lists some stream flow measurements (from LINQ database).

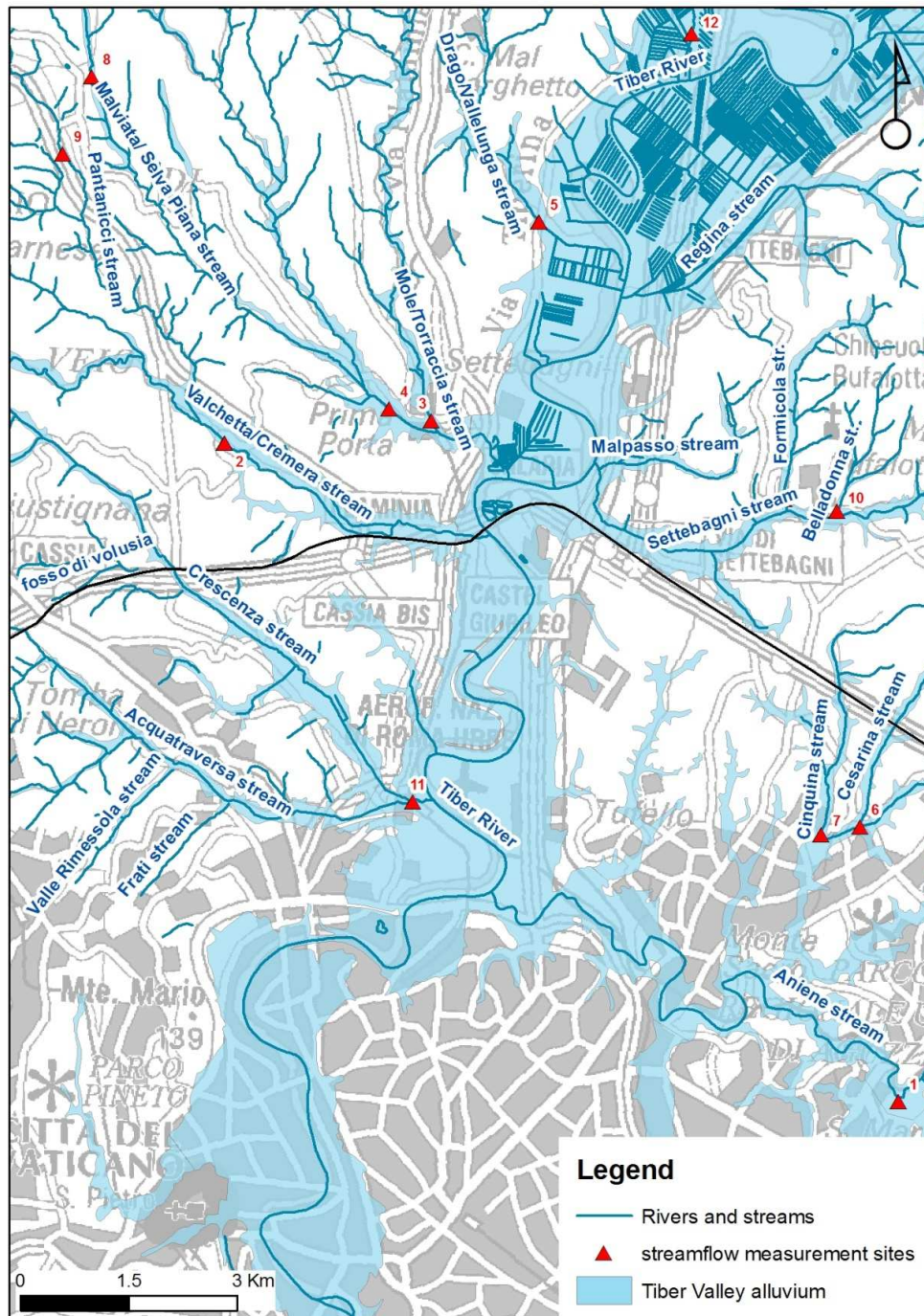


Fig 2.43: River and streams network

Tab. 2.8: stream flow measurements (from LINQ database).

Station ID	River/stream name	Q min (l/s)	Q max (l/s)	Q average (l/s)	time window for averaged Q or single measure date
1	Quarticciolo	0	950	159.00	january 78-july 81
2	Valchetta/Cremera/La Mola	320	905	657.7	january 81-january 82
3	Torraccia/le Mole	0	200	82	january 81-january 83
4	Fontanile	0	40	11.37	january 81-january 84
5	Drago/Vallelunga	5	20	3	january 81-january 85
6	Cesarina	0	20	13.9	march-october 2003
7	Cinquina		0		9/22/2003
8	Malviata/Selva piana		0		8/19/2002
9	Pantanicci		3.5		8/21/2002
10	Bella Donna		0		8/20/2002
11	Acquatraversa		10		8/1/1981
12	n.d.		11		9/1/1981
13	Formicola		2.5		8/20/2002

Tiber River's average discharge from 1921 to 2008 is $230\text{m}^3/\text{s}$ (Ripetta gauging station, Istituto Idrografico e Mareografico Regione Lazio, **figg. 2.44 and 2.45**). The negative trend of discharge from 1930's to the last decade is due to the large amount of pumping for irrigation . Actually, the Tiber stage is controlled by several dams that were built along its course; in the urban area the stage is strictly controlled by the Castel Giubileo dam, close to the northern part of the City ring road, which works for the production of electric energy.

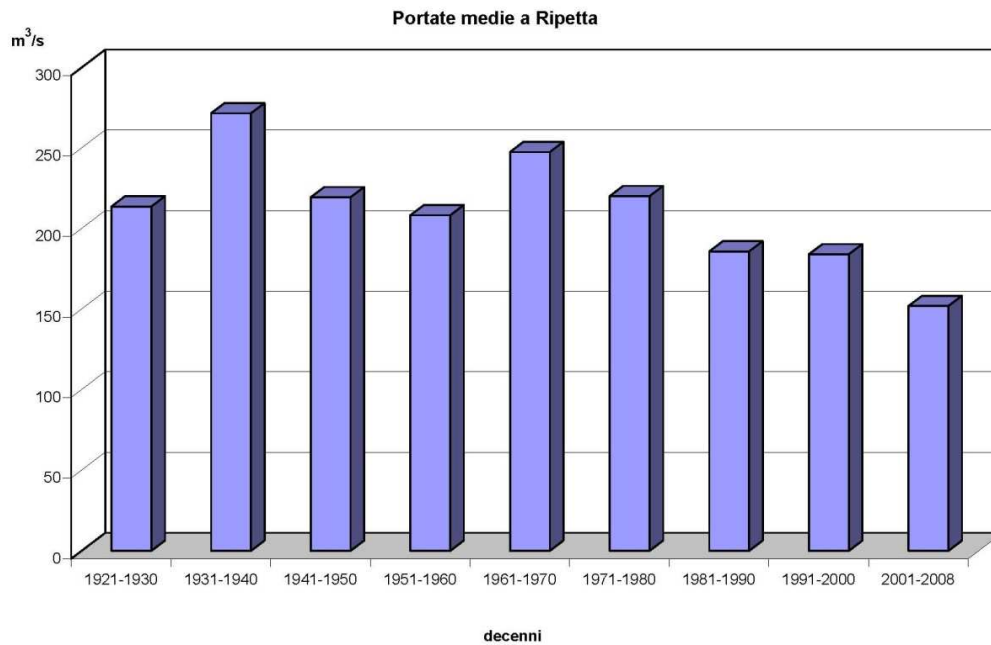


Fig 2.44: the graph shows the medium discharge of Tiber River in m^3/s from 1921 to 2008.

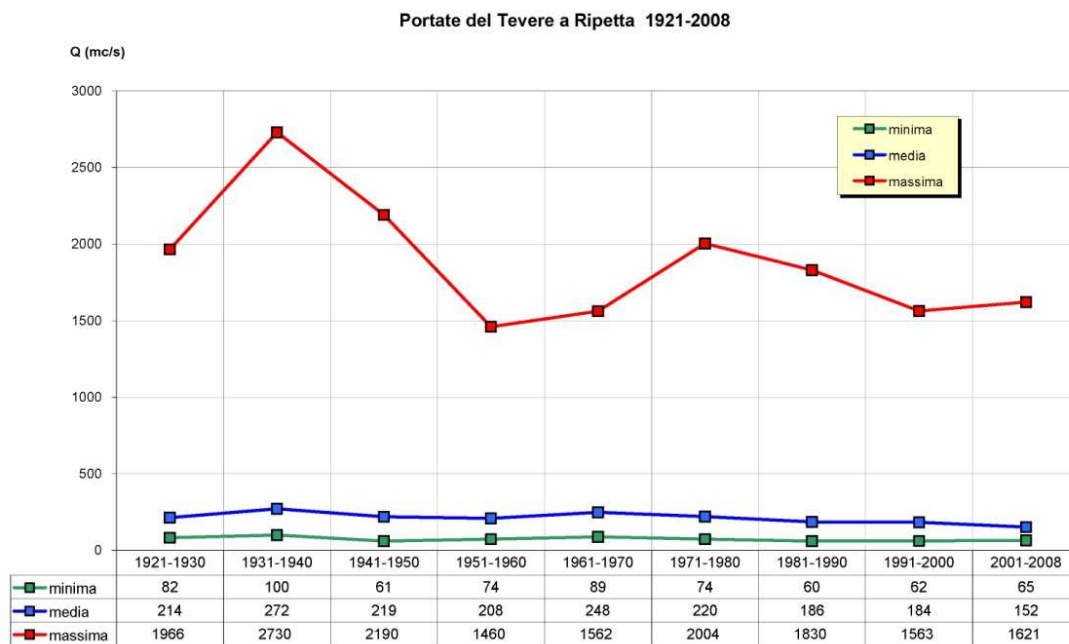


Fig 2.45: the graph shows the minimum, maximum and medium discharge of Tiber River in m^3/s through the years 1921 to 2008.

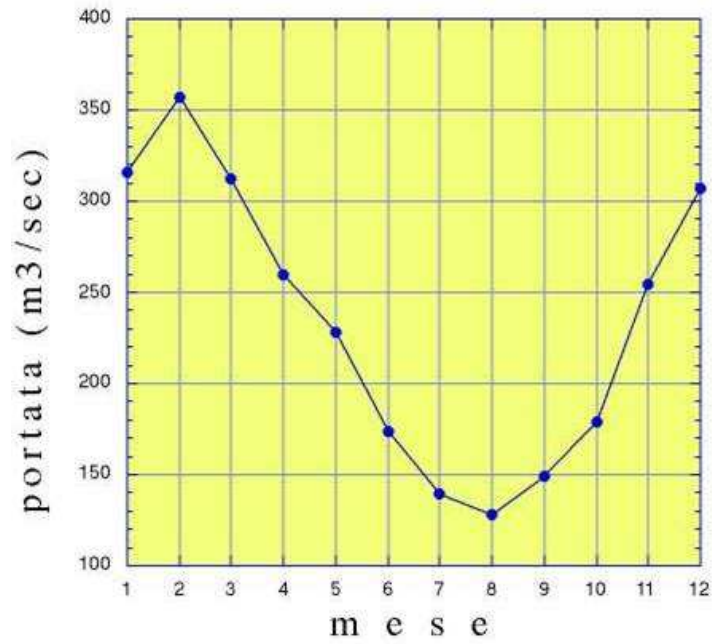


Fig 2.46: the graph shows the averaged monthly discharge of Tiber River in m^3/s .

Rivers stages used as input in the numerical model are data from SIMN hydrometric stations; stages are averaged over variable time windows depending on the data availability; where data are present (as for Ripetta and Ponte del Grillo gauging stations), stage is computed as the average over years 1994-2007, while for other stations the time window is shorter (see **fig 2.47**, and table **2.8**)

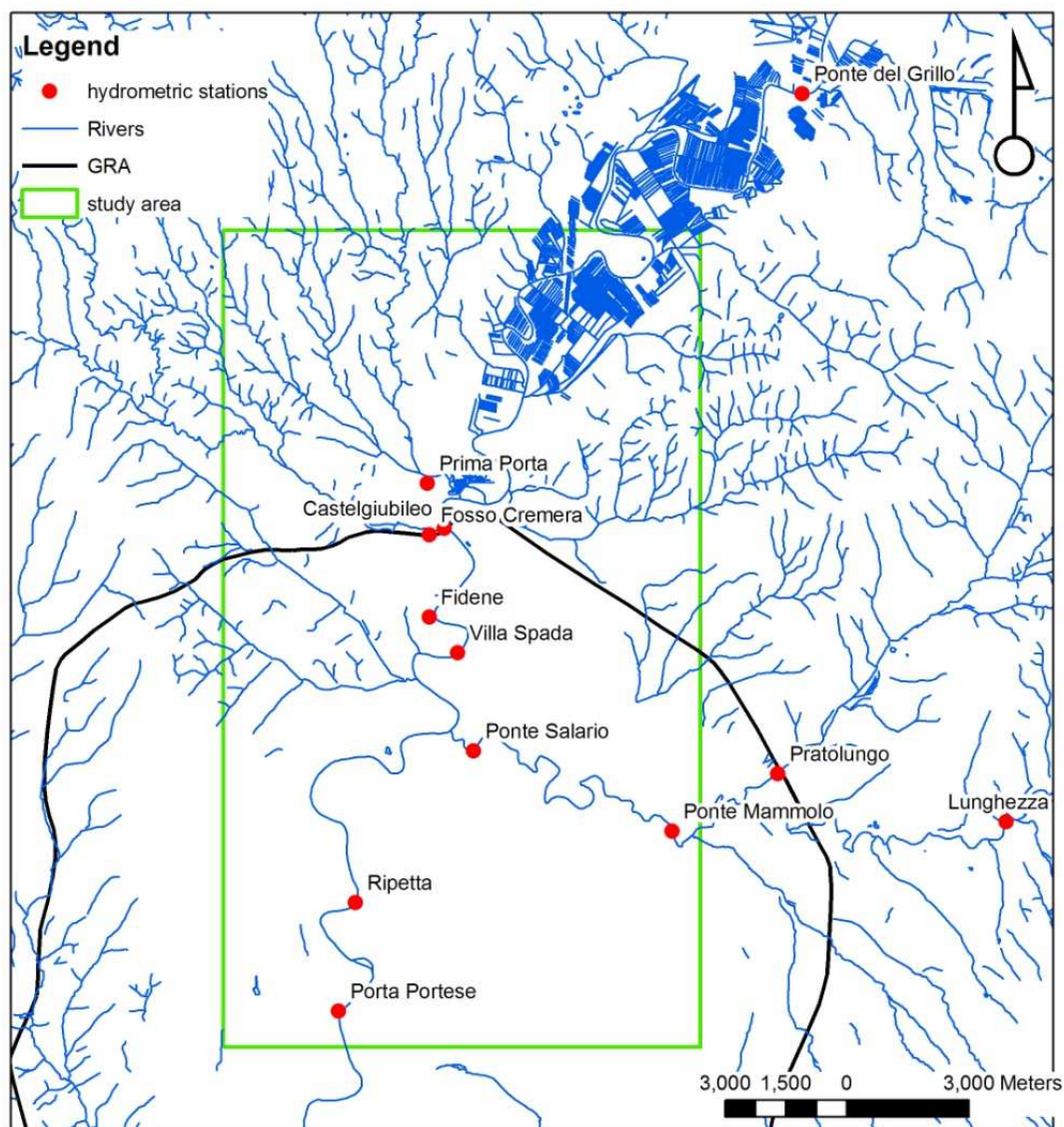


Fig 2.47: Hydrometric SIMN stations, monitoring Tiber and Aniene rivers, Prima Porta and Valchetta streams.

Tab. 2.8: average rivers and streams stages (SIMN)

TIBER RIVER gauging station	Average stage m s.l.m.	Average on years
Ponte del Grillo	16.73	1994-2007
Ripetta	6.01	1994-2007
Porta Portese	2.96	2004-2007

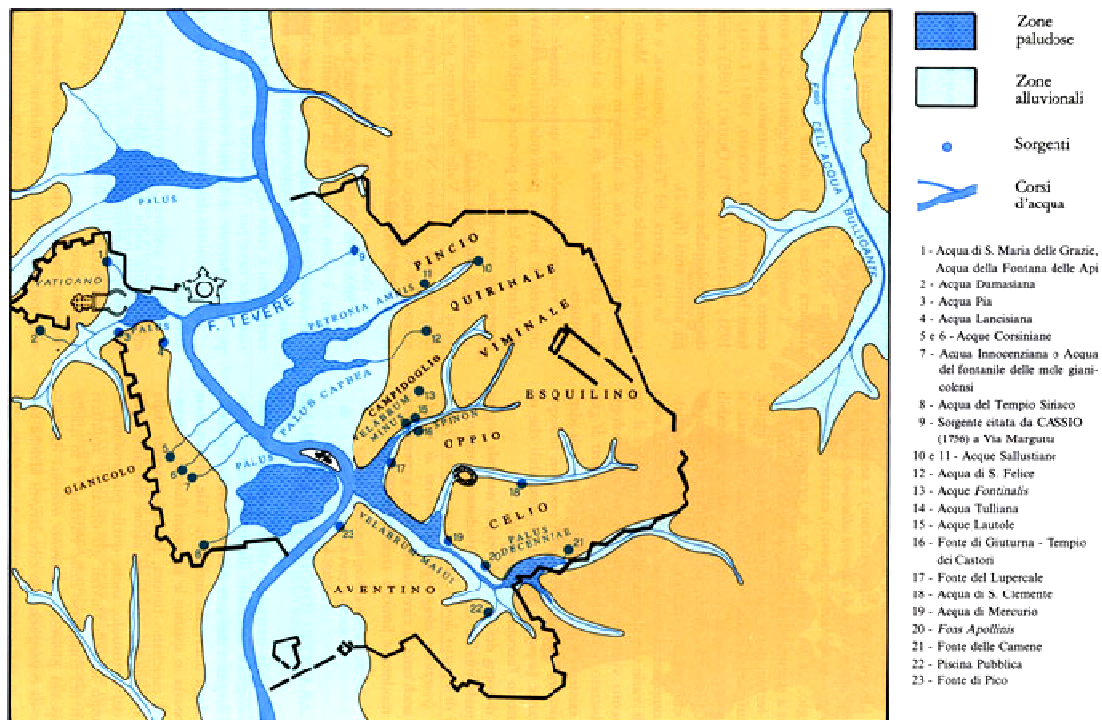
ANIENE RIVER gauging station	Average stage m s.l.m.	Average on years
Ponte Salario	8.92	1994-2007
Ponte Mammolo	13.28	1994-2007

STREAM gauging station	Average stage m s.l.m.	Average on years
Prima Porta (confluence of Malviata and Mole streams)	16.8	1994-1999
Fosso Cremera/Valchetta	13.06	1996-2004

The hydrogeological setting has been strongly modified during the centuries; in ancient times, several springs were located at the footwall of the reliefs bounding the alluvial valley; the alluvial plan was a frequently flooded area, with many wetlands (**Fig. 2.48 and 2.49**). Ancient Romans started building drainage systems to avoid flooding and divert water for water battles and fountains, often substituting the natural streams network with sewers and Cloacae. As shown in the “*Piano di Assetto idrogeologico, Autorità di Bacino Fiume Tevere, 2003*” (**fig 2.49**) the hystorical center’s natural drainage network disappeared, being substitute by water mains (**Fig 2.50**)



Fig 2.48: Sewers and drains system in ancient Rome (Source: Katherine W. Rinne NGM Maps)



Caratteri idrografici originari del centro storico (disegno: Anna Jori).

Fig. 2.49: Springs and wetlands in ancient Rome (from Corazza and Lombardi, 1995)

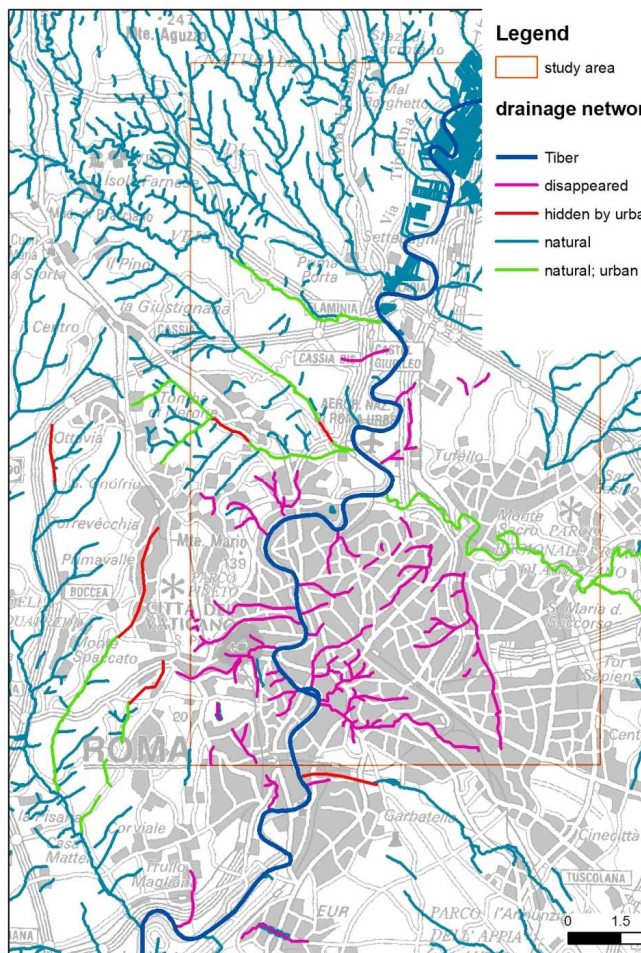


Fig 2.50: map showing the anthropic modification of natural drainage. (from Autorità di Bacino Fiume Tevere, PAI 2003)

Today, water mains receive both wastewaters from urban uses, and surface flow from streams entering in the mains where the urbanization becomes dense. **Figure 2.51** also shows some of the 30 stream entrances into water mains. Water from mains are collected in the 39 wastewater treatment plants; the main plants are Roma Nord, Roma Sud, Roma Est and Ostia. The treatment plants average discharge (from ACEA-ATO2 2009 reports) are in **tab 2.9**; calculated discharge includes surface flow from canalized streams plus wastewater coming from civil and industrial uses, which is supplied from a source external to the system (aqueducts); thus, the total stream flow entering in treatment plants is not correctly computable.

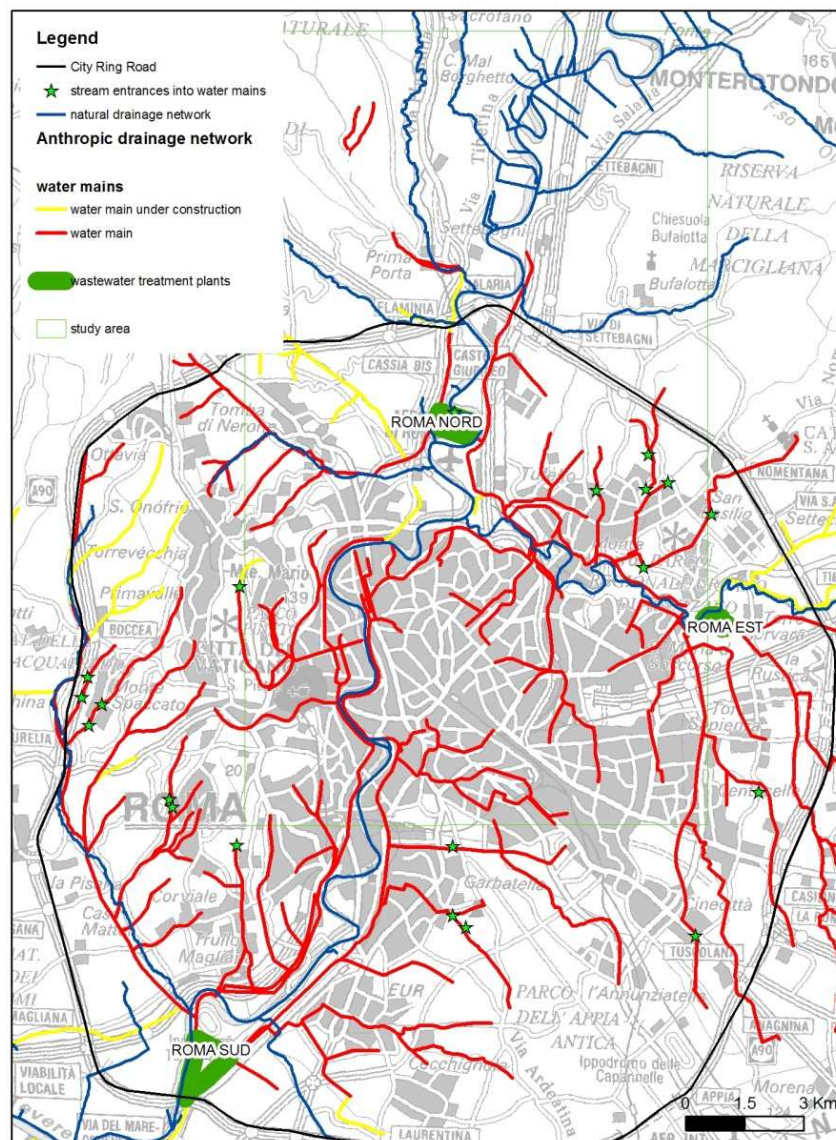


Fig. 2.51: Water mains network in the City.

Tab 2.9: Wastewater treatment plants average discharge (from ACEA-ATO2 2009 reports)

WASTEWATER TREATMENT PLANT	discharge mc/s (2009)
ROMA NORD	3.07
ROMA EST	2.82
ROMA SUD	8.21
ROMA OSTIA	0.68
average total daily discharge	16
max treated water during rainfall	33
total treated water (Mmc/y)	490

2.4.4 Piezometry of the study area

We refer to Ventriglia (2002) as the first piezometry of the Rome Municipality (**fig. 2.52**); the second one is from Capelli et alii (2008), **fig. 2.53**. As assessed in chapter 2.2.1, since the availability of head data of the deepest confined sedimentary aquifers is very small, the water table drawn in **figg. 2.52 and 2.53** is referred to the uppermost aquifer, hosted in the volcanic complexes and in the uppermost portion of the sedimentary PGT complex.

The two maps show similar water table elevations; ground-water flows from boundaries towards the Tiber alluvial valley, where it reaches the lowest elevations, ranging from 15 to 3 m a.s.l.. The highest piezometric levels are located along the western border; the absolute highest heads are in the area of Monte Mario-Gianicolo ridge; a relative piezometric high is in the area of Termini train station (30 m a.s.l.). When the groundwater reaches the Tiber, it is drained by the alluvial deposits; in normal flow conditions the groundwater feeds the rivers, while in condition of high flow, the aquifer receives water from the river (Lanzini M., 1995-2000 a and b, Bozzano 2000); the groundwater then flows southwards in direction of Tyrrhenian sea. No accurate literature piezometry is drawn inside the Tiber Alluvium. In this study, the measured head in the portion of the Tiber Valley between Castel Giubileo and Tiberina Island is presented (**fig 2.54**); the head ranges from 20 meters a.s.l.at the valley's borders, to 3 meters a.s.l. close to the Tiber. The piezometry is strongly perturbed by pumping and diversions due to the subservices.

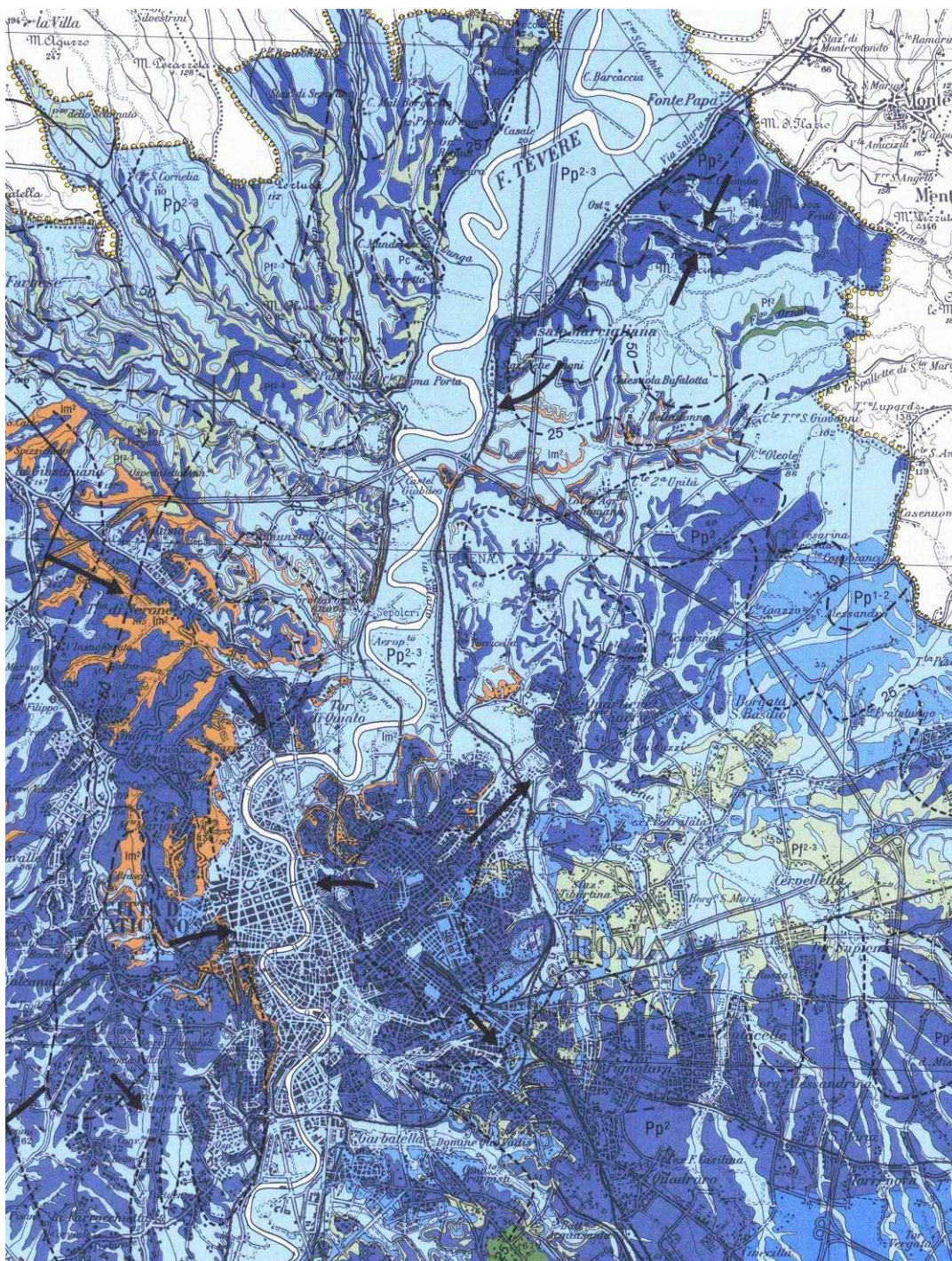


Fig. 2.52: Rome Municipality Water table (Ventriglia, 2002)

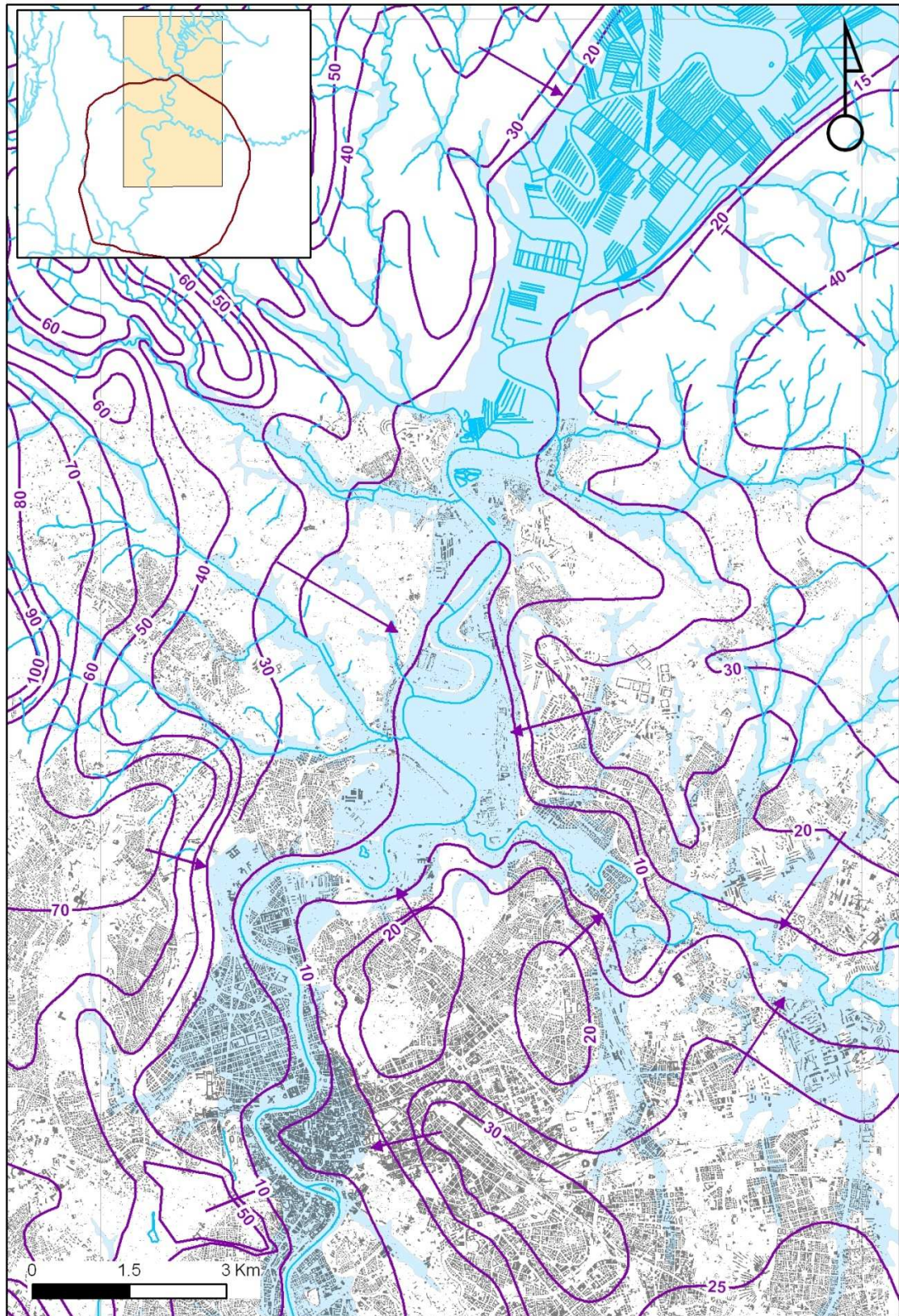


Fig. 2.53: Mean water table elevation in m a.s.l. and groundwater flow direction in the study area (from Capelli et alii, 2008, modified)

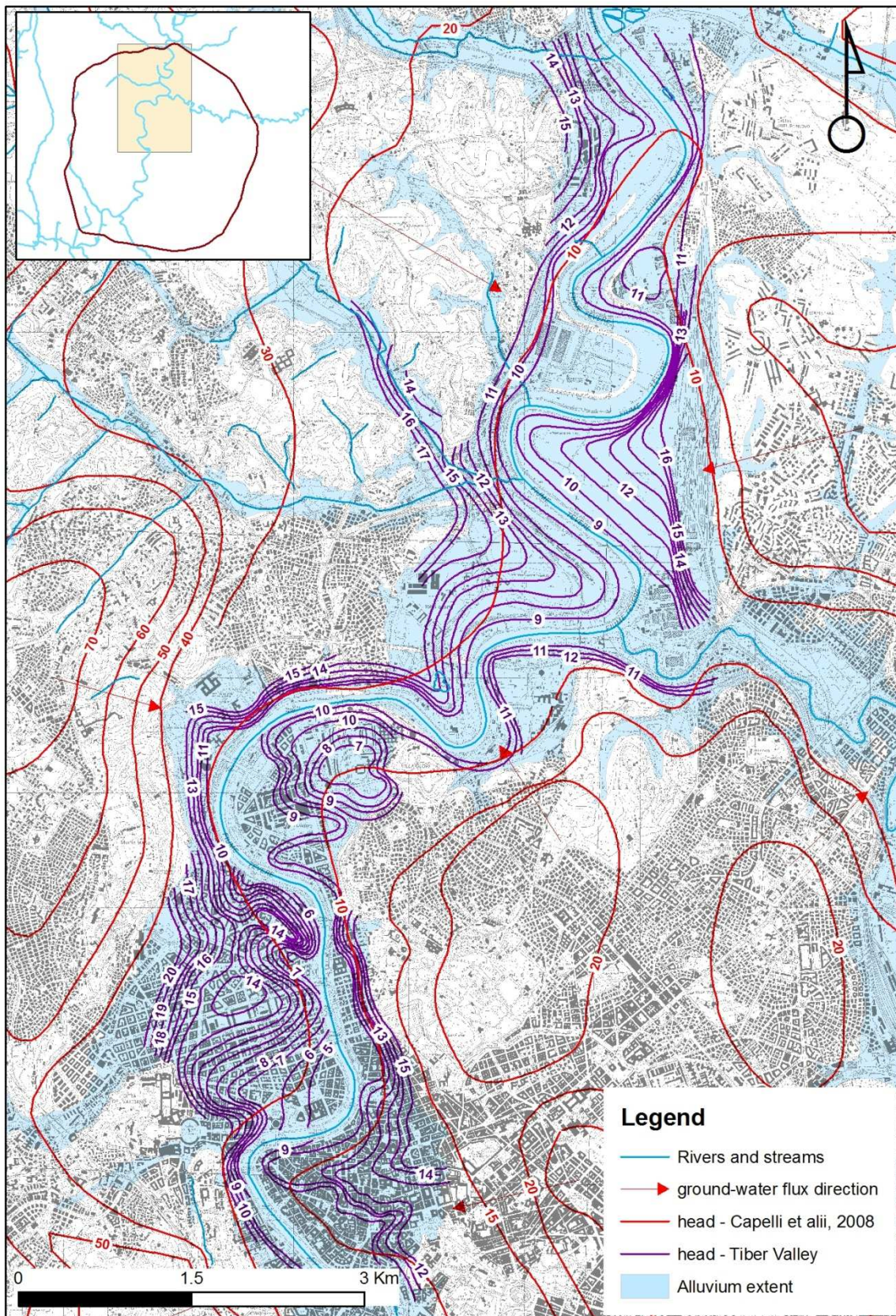


Fig 2.54: Mean water table elevation in m a.s.l. and groundwater flow direction in the Tiber valley (LINQ, 2010)

2.4.5 Withdrawals

Since ancient times, the water supply in the City was guaranteed starting from the fourth century B.C.; the aqueducts used to brought a big amount of water, necessary to provide crowded urban population with relatively safe, potable water and also for other aquatic uses as thermal bath, water battles, fountains. Ancient Rome had 11 aqueducts; built between the fourth century B.C. and the first century A.D. Aqueducts were built because the springs, wells, and Tiber River were no longer providing the safe water that was needed for the swelling urban population.



Fig. 2.55: The network of eight aqueducts built in ancient Rome is show; at the end of II century, they used to bring to the City around 10 m³/s.

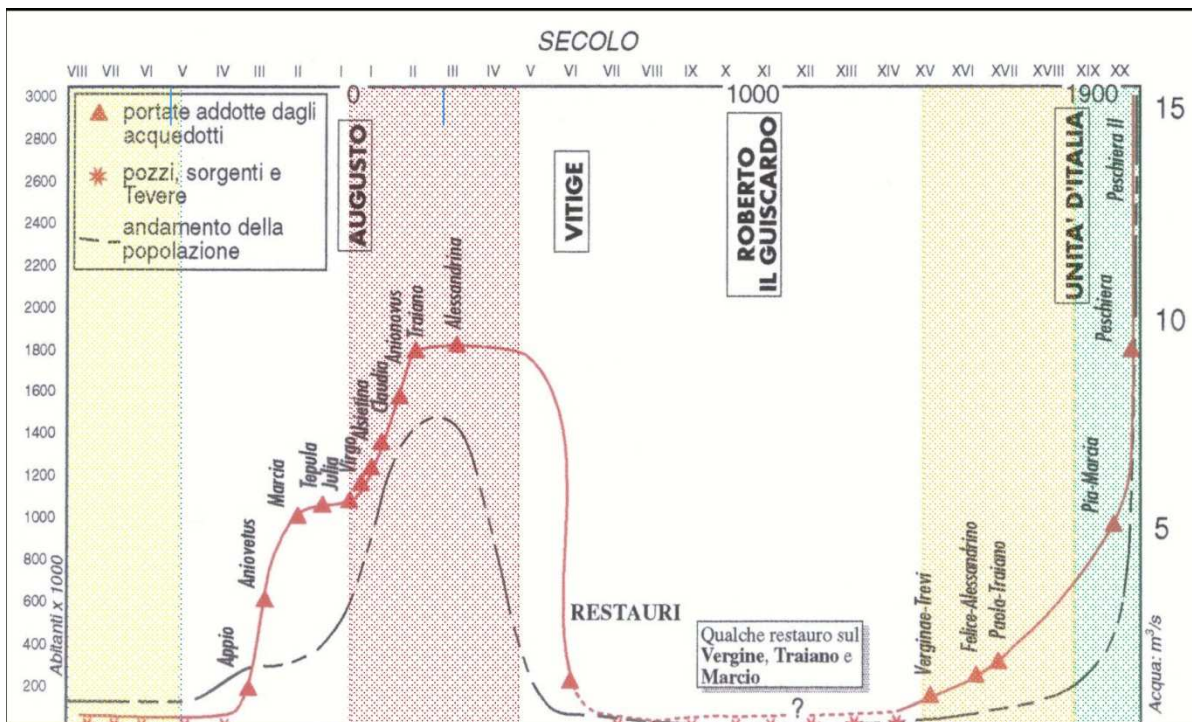


Fig 2.56: The graph shows the increasing of water supply with the population and, thus, water demand. After the peak of III-IV century, the aqueduct destruction by the barbaric invasions, together with the decrease of inhabitants number, caused a drastic decrease of water supply.

For this reason, wells drilling for water supply in the City has developed only in recent times; today pumping wells are used for:

- irrigation of municipal gardens;
- car washing centers;
- industrial uses;
- domestic supply in not-strongly urbanized portions of the City;

In order to quantify withdrawals, three database were acquired, which collects data from Rome Municipality, Province and Latium Region istitutional offices:

- 1) 275_Dom: private wells, drilled and registered to the municipal offices, which are used for domestic purposes;
- 2) 275_nonDom: private wells, drilled and registered to the municipal offices, which are used for no domestic purposes
- 3) RM_Conc: water yielding; the amount of water requested from a private.

Wells use can be domestic, industrial, garden irrigation, zoothechnical, fire hydrant, sport plant of not declared used (**figure 2.56**)

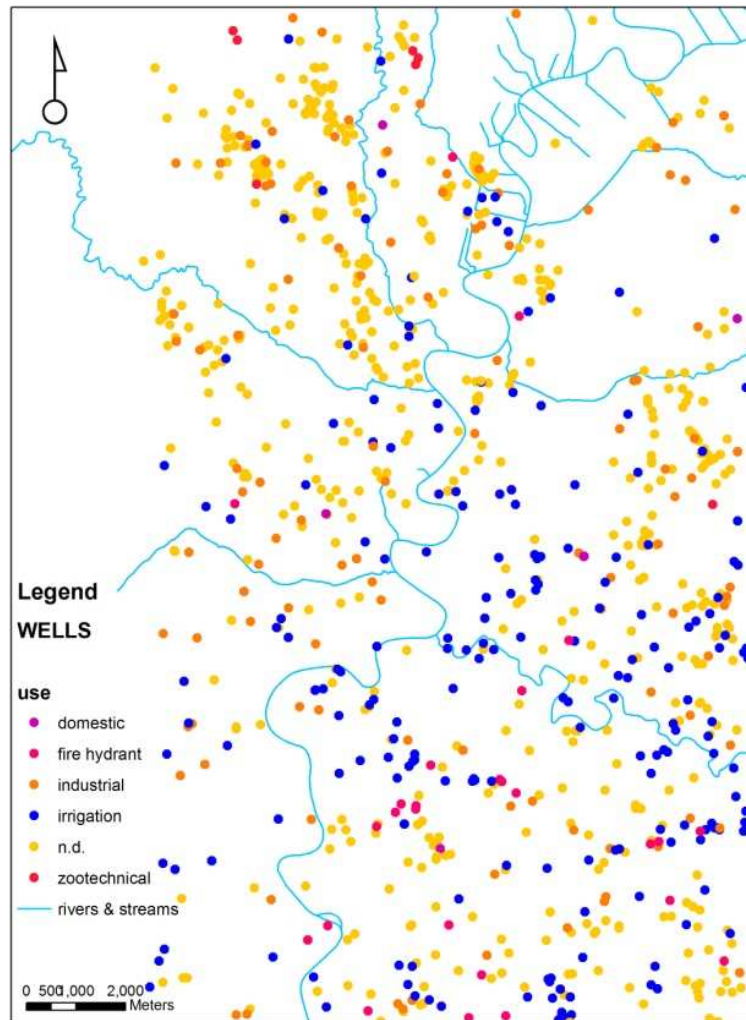


Fig 2.56: distribution of pumping wells.

Withdrawals were calculated as follows:

- Where present, the annual pumping rate for each well is considered, transformed in m^3/d ; thus, the withdrawal is averaged over the entire year, and no dry-wet periods are considered. We retain that this assumption can be valid since the model is steady-state, and also the river stage and recharge are put as the annual average of a total period of 5 years.
- Where in the database are indicated both the annual discharge (m^3/y), and the distributed daily-scale discharge (that means the water concession (l/s), the annual regime (days/year) and the hour regime (hours/day)), an attempt of data validation was made, comparing the two discharge values. Unfortunately, no correspondence was found; this error is probably

due to a lacking of data quality check. For this reason, the pumping rate was assumed equal to the annual volume, re-calculated in m/d;

- Where no annual volume is reported, the discharge was calculated depending on the stated well use as explained below:
 - **Irrigation wells:** the water concession (l/s) was considered active for 4 months and three hours per day; these pumping times are retained compatible with the average irrigation needs for municipal gardens in the Roman climatic regime. The type of irrigated vegetation is not taken into account, so a certain approximation has been introduced;
 - **Domestic use wells:** where the only available information was the granted discharge in l/s, a pumping time of 2 hours for 365 days/year was considered.
 - **Domestic use wells:** where no other data were available, the pumping rate was considered equal to the average pumping rate of domestic use pumping wells in the database 275_Dom (that is 300 m³/y).
 - **Wells for car washing:** a pumping rate of 8 hours for 365 days/year was used; we consider that those type of commercial activities is 24-h open, so that even not always full-working, they collect a big number of pumping hours.
 - **Wells for different uses:** where no pumping rate and no destination use are reported, the well is not considered; this action introduces an underestimation of the total withdrawals.

The calculated pumping rate is 29097.5 mc/d

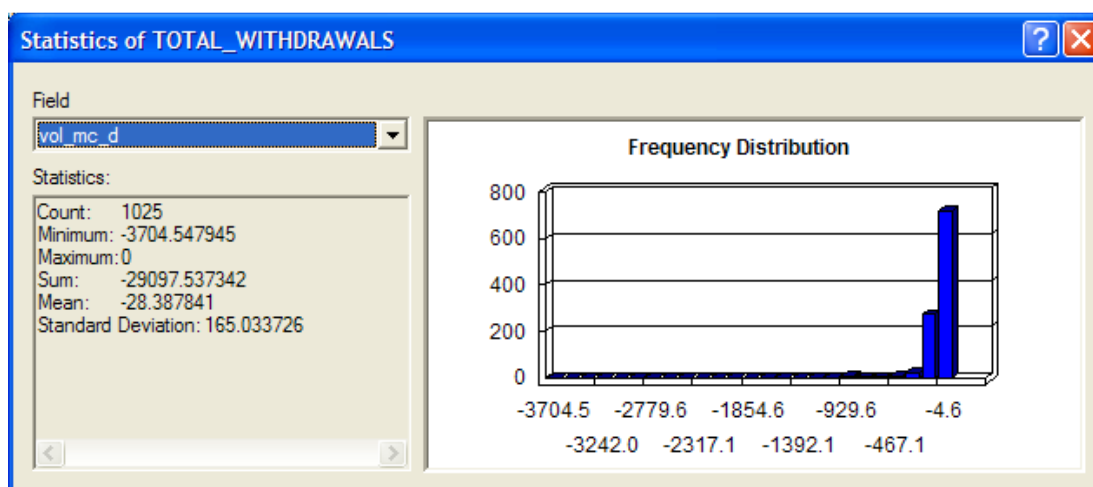


Fig. 2.57: Frequency distribution of well pumping rates in m³/d.

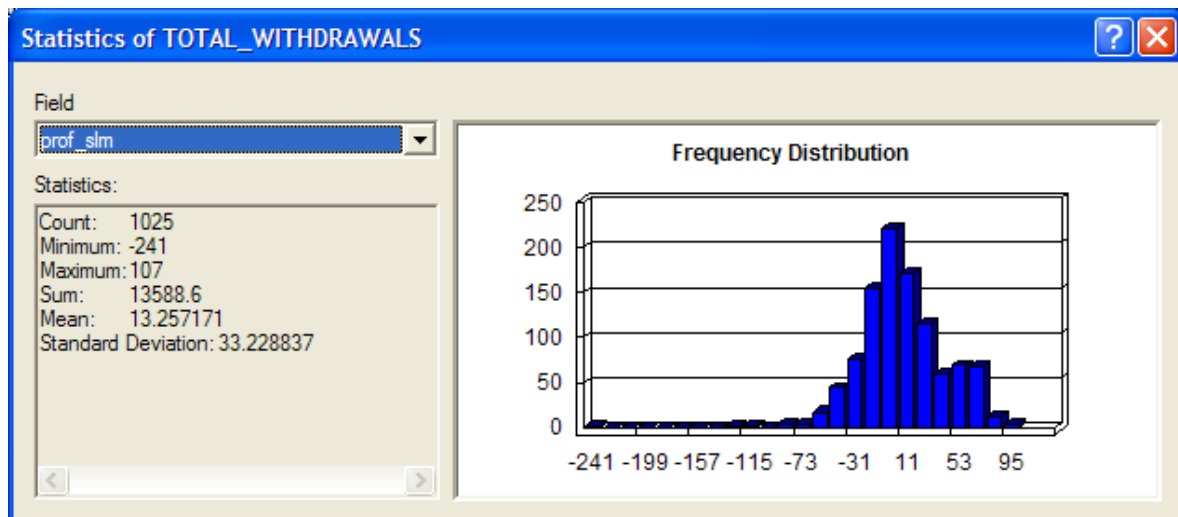


Fig2.58: Frequency distribution of well depth in meters a.s.l..

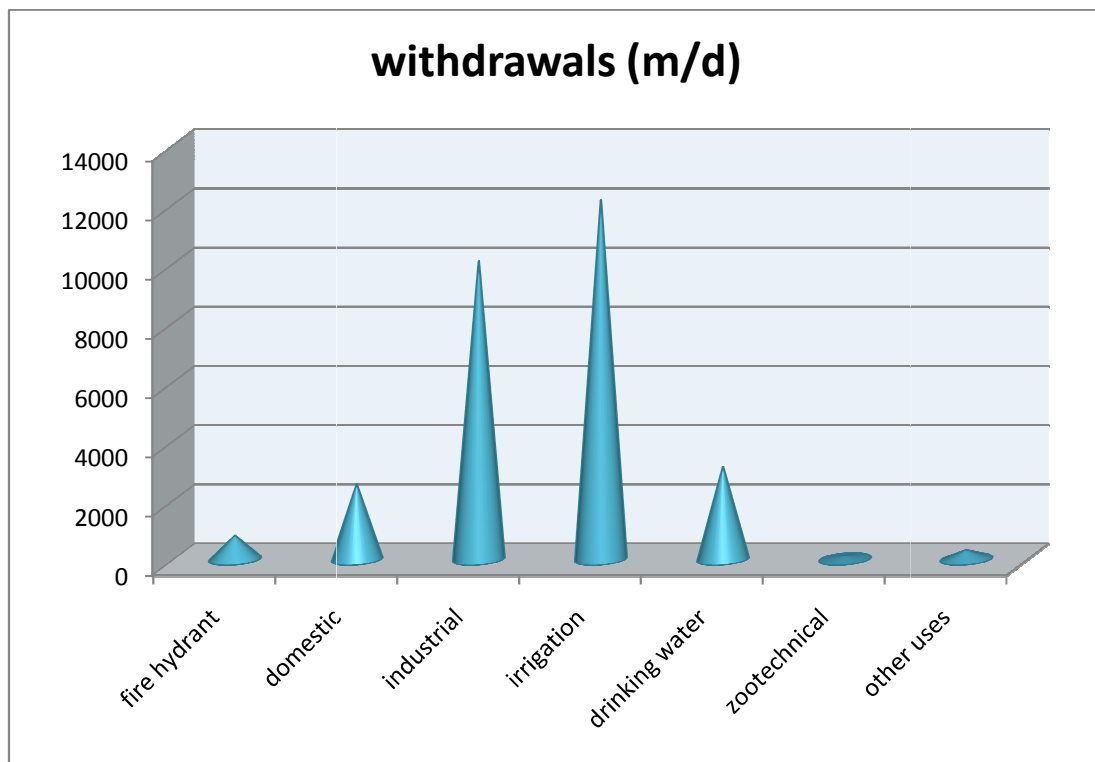


Fig2.59: histogram of withdrawals for different uses

% of total withdrawal

■ fire hydrant ■ domestic ■ industrial ■ irrigation
■ drinking water ■ zootechnical ■ other uses

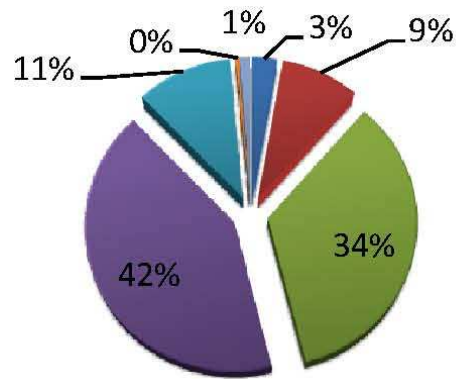


Fig 2.60: percentage of withdrawals for different uses

2.5 Estimated water budget

Figure 2.61 shows the hydrogeological basins drawn on the base of observed water table (chapter 2.4.4); **table 2.10** lists basins inflows and outflows, calculated in Capelli et alii, 2005 (see chapter 2.4.1). Only basins which flow is directed into the model area are considered; for basin 2, because of its prevalent clayey lithology, no effective infiltration is considered, and the total flow is considered to be all surface flow. No calculation are given in the cited study for basin 6, Tiber River alluvium.

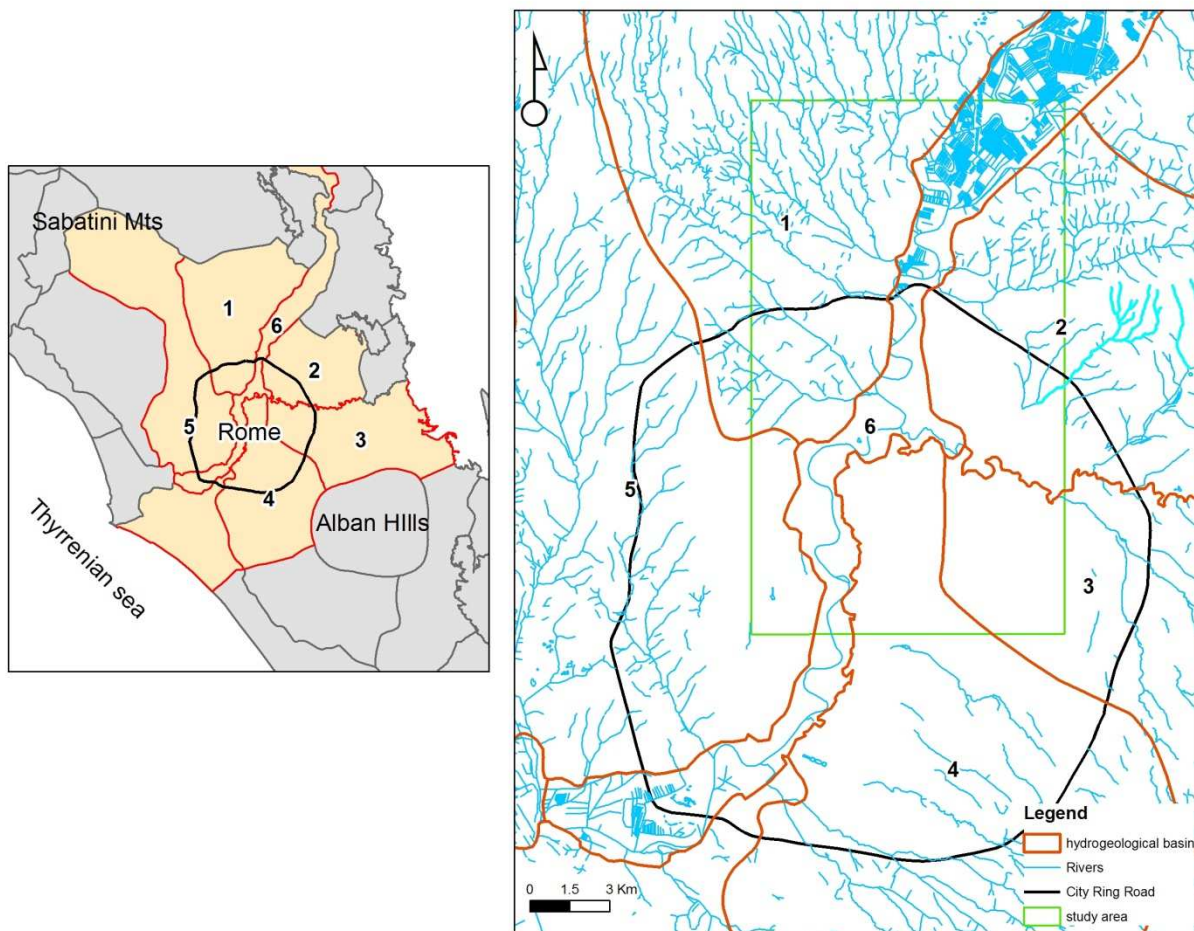


Fig 2.61: Main hydrogeological basins, (Latium Region, 2009)

In basin 2, because of its lithology, no infiltration is considered, and the total flow is considered to be all surface flow. No calculation are given for basin 6, Tiber River alluvium. Values in **tab 2.10** are referred to basins as a whole; on contrary, **Tab 2.11** accounts inflows and outflows only for the basins or part of basins draining water to the study area. Basins 1 and 3 drain all the groundwater and surface water into the model area; basins 2 groundwater flow contribute is very low due to the small aquifer's thickness; the contribute of basin 4 is only due to a small percentage of its surface. Basin 5 is considered to not contribute to the water balance in the model area, because the outcropping impermeable substratum baffles the basin flow diverting it southernwards. For basins 2 and 5 the only flow contribute to the model is the surface flow. Withdrawals are calculated in this study.

The total basins infiltration term includes the infiltration occurring inside the model's area, and also includes groundwater infiltrating and then flowing toward the Tiber and Aniene rivers outside the model's area; this water budget will be compared with model's Mass Balance after calibrations (see chapter 5)

Tab. 2.10: total flows and inflows for hydrogeological basins in fig. 3.4 as calculated in Capelli et alii, 2005.

number	Basin	area km2	rainfall Mm3/y	evapotraspiration Mm3/y	runoff Mm3/y	effective infiltrato n Mm3/y	stream base flow Mm3/y	tot withdrawals Mm3/y
1	basin of streams flowing from eastern Sabatini Mountains	271.00	183.90	99.80	23.80	61.30	18.20	21.40
2	basin of streams flowing on the Marne Vaticane formation complexes	171.00	nd	nd	n.d.	nd	0.08	nd
3	basin of streams flowing from the north-eastern Alban Hills	409.00	292.90	130.80	65.90	94.40	14.20	
4	basin of streams flowing from the north-western Alban Hills	577.00	381.70	170.90	91.50	114.20	34.60	58.60
5	basin of streams flowing from Sabatini Mts (southern Tolfa Mts.)	1109.00	736.90	348.50	118.20	226.50	10.80	94.90
6	Basin of Tiber River alluvium	n.d.	n.d.	n.d.	n.d.	n.d.	n.d.	n.d.

Tab. 2.11: water budget for the study area; the budget is calculated by data from Capelli et alii, 2005 in the time window 1997-2001.

parameter	m3/d	m3/y	Mm3/y
Total basins precipitation	1363911.959	497827865	497.8279
Total basins evapotraspiration	657575.0311	240014886.4	240.0149
Total basins runoff	259563.6654	94740737.87	94.74074
streams base flow	89847.12329	32794200	32.7942
Total hydrogeological basins infiltration	443808.2192	161990000	161.99
withdrawals	28146.5	10273472.5	10.27347

3 Ground-water flow model construction

3.1 Hydrogeological modeling in urban areas; the case of Rome

A numerical model of the study area was set up, which includes aquifers surrounding the Tiber valley (*far-field*) and Tiber alluvium aquifers (*near-field*); the aim is to better understand the conceptual model and test how the hydrogeological surfaces that have been built in this study and the k values collected can represent the general groundwater system, by the comparison between observed and simulated “targets”.

The model is set up with BCs averaged over 10 years: that means that the observed head used for inserting General head BCs and recharge are calculated over a range of about 10 years. Also head target used to calibrate the model are head data from 90's to 2010.

In an high-urbanized area such as Rome is, other variables should be considered when modeling groundwater: withdrawals, leakage due to sewer and water mains, increased runoff on paved surfaces, overirrigation in municipal gardens; all those “anthropic” issues increase the uncertainty of the model solution.

Moreover, underground infrastructures can divert or canalize groundwater; that's what happens with hydraulic works as *cloache*, channels bringing water from streams towards Tiber River, that were built in ancient Rome to dry the wet areas surrounding the Seven Hills. In the numerical model, well known atrophic channels are simulated as drains, having stage properties coincident with the top surface.

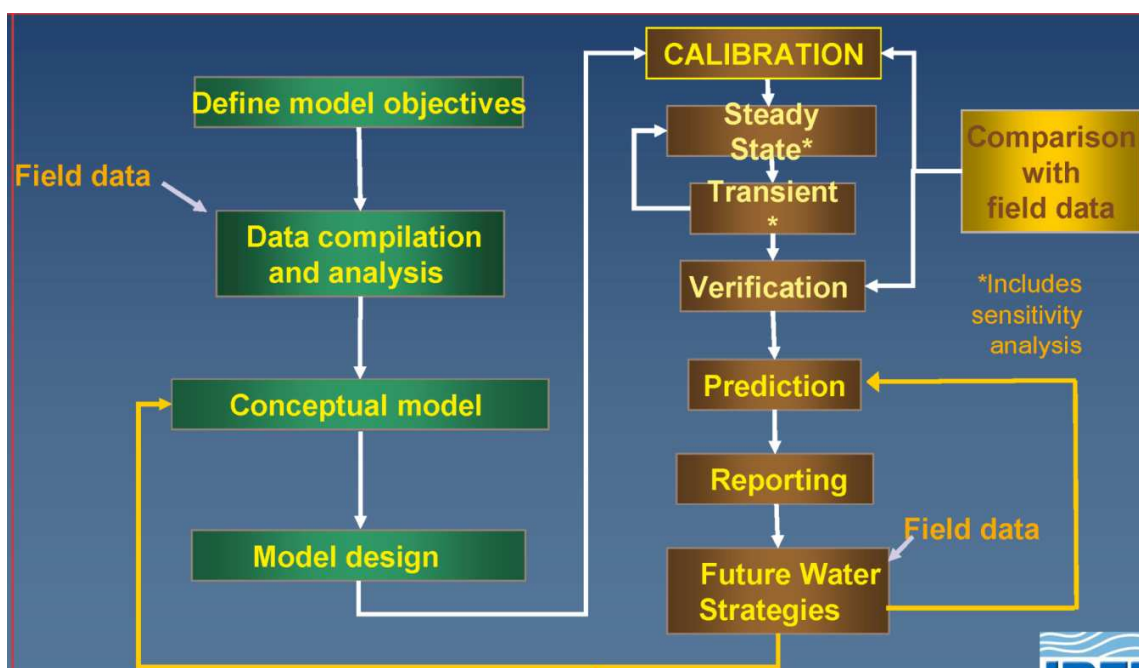


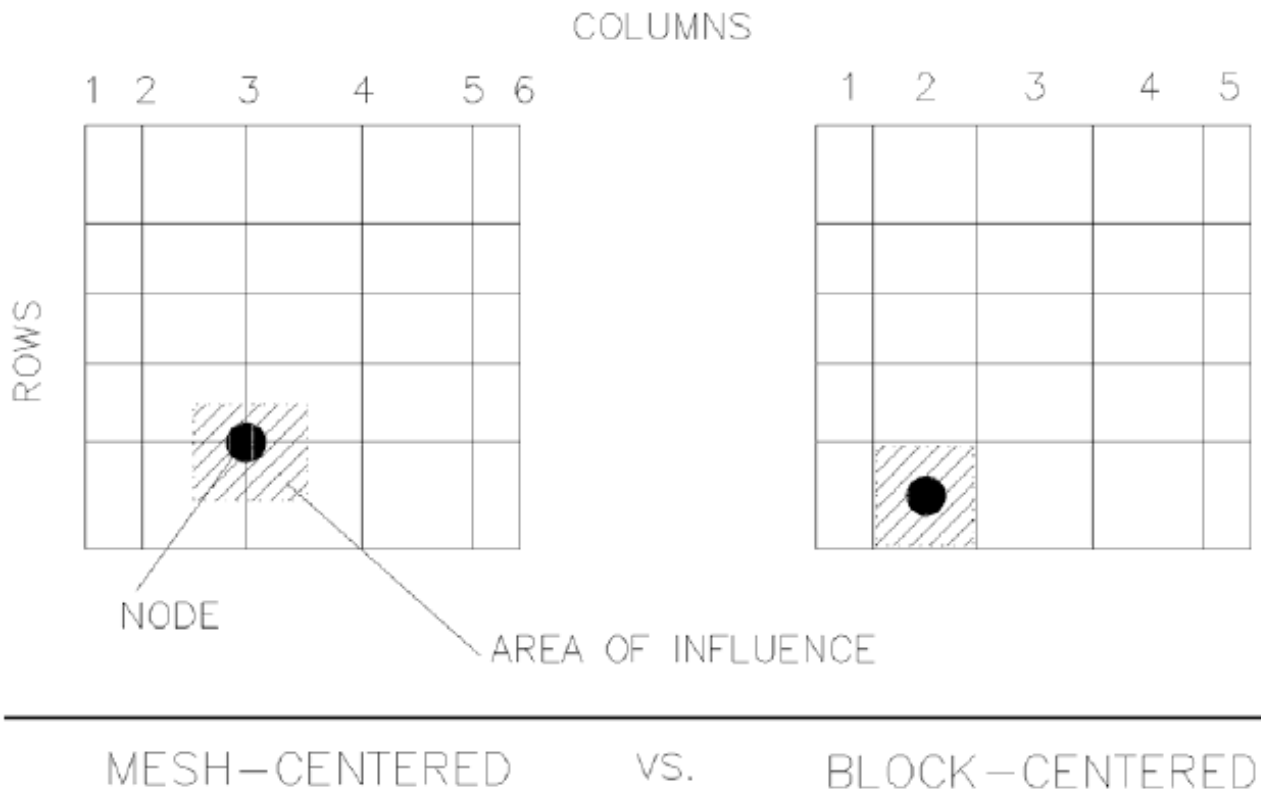
Fig 3.1: schematic representation of the general protocol for numerical hydrogeology modelling

The overall modelling methodology followed the flux diagram presented in figure 6.2.1, which is the protocol adapted from Anderson and Woessner (1992) with some modifications. Model validation is defined as the process of demonstrating that a given model is capable of making sufficiently accurate predictions. This implies the application of the calibrated model without changing the parameter values that were set during the calibration, when simulating the response for a period and/or an area different from the calibration period/area. In the case of this study, the modelling process stops at the steady-state calibration phase; the lacking of a good, “transient” dataset to perform validation makes too high the uncertainty of the results. However, a steady-state, calibrated model is set up, and a working protocol for future improvement has been built.

3.2 Code selection

In this study the codes MODFLOW 96-98 and MODFLOW 2000 (Harbaugh and McDonald, 1996) were used. MODFLOW is a three-dimensional finite-difference ground- water model that was first published in 1984; it simulates steady and non-steady flow in an irregularly shaped flow system in which aquifer layers can be confined, unconfined, or a combination of confined and unconfined. Flow from external stresses, such as flow to wells, areal recharge, evapotranspiration, flow to drains, and flow through river beds, can be simulated. Hydraulic conductivities or transmissivities for any layer may differ spatially and be anisotropic (restricted to having the principal directions aligned with the grid axes), and the storage coefficient may be heterogeneous.

The ground-water flow equation is solved using the finite-difference approximation. The flow region is subdivided into blocks in which the medium properties are assumed to be uniform. In plain view the blocks are made from a grid of mutually perpendicular lines that may be variably spaced. Model layers can have varying thickness. A flow equation is written for each block, called cell. Several solvers are provided for solving the resulting matrix problem; the user can choose the best solver for the particular problem. Flow-rate and cumulative-volume balances from each type of inflow and outflow are computed for each time step. There are two main types of finite-difference techniques, known as block-centered and mesh-centered. The name of the technique refers to the relationship of the node to the grid lines- Head is computed at the center of the rectangular cell in the block- centered approach. Conversely, head is computed at the intersection of grid lines (the mesh) in the mesh-centered technique. Figure 6.3.1 illustrates this concept graphically (GvVistas® Manual reference).



FINITE-DIFFERENCE MODES

Fig.3.2: mesh-centered vs block-centered finite-difference modes in MODFLOW.

In each technique, the head and all physical properties are assumed to be constant throughout the cell region surrounding the node. The finite-difference grid is designed by manipulating rows, columns, and layers of cells. A series of cells oriented parallel to the x-direction is called a row. A series of cells along the y-direction is called a column. A horizontal two-dimensional network of cells is called a layer.

In order to use MODFLOW, initial conditions, hydraulic properties, and stresses must be specified for every model cell in the finite-difference grid.

Primary output is head, which can be written to the listing file or into a separate file; other output include the complete listing of all input data, drawdown, and budget data.

The governing equation is the one below:

$$\frac{\partial}{\partial x} \left(K_{xx} \frac{\partial h}{\partial x} \right) + \frac{\partial}{\partial y} \left(K_{yy} \frac{\partial h}{\partial y} \right) + \frac{\partial}{\partial z} \left(K_{zz} \frac{\partial h}{\partial z} \right) + W = S_s \frac{\partial h}{\partial t} \quad (1)$$

where

K_{xx} , K_{yy} , and K_{zz} are values of hydraulic conductivity along the x, y, and z coordinate axes, which are assumed to be parallel to the major axes of hydraulic conductivity (L/T);

h is the potentiometric head (L);

W is a volumetric flux per unit volume representing sources and/or sinks of water, with $W < 0.0$ for flow out of the ground-water system, and $W > 0.0$ for flow in (T^{-1});

S_s is the specific storage of the porous material (L^{-1}); and

t is time (T).

MODFLOW is designed to simulate steady state or transient conditions. For steady state, the specific storage term in the ground-water flow equation is set equal to zero. In this study, the code MODFLOW 96 was used as first prove; then, in order to use advanced packages, the model has been converted into MODFLOW2000; the graphical interface is the software Groundwater Vistas® version 5.41 developed by ESI®.

The solver chosen to run MODFLOW is the Preconditioned Coniugate Gradient 2 package (PCG2), with a head change criterion of 0.001 and a Residual Criterion for Convergence=10

MODFLOW Solver Packages	
PCG2	GMG SIP SOR PCG4/PCG5
Maximum Outer Iterations	500
Maximum Inner Iterations	10
Head Change Criterion	0.001
Residual Criterion for Convergence	10
Relaxation Parameter	0.98
Matrix Preconditioning Method	Cholesky
Maximum Bound on Eigenvalue	Set Equal to 2
Solver Printing Option	Print All
PCG2 Summary Data Printed Every	5 Iteration
Damping Factor (0.0 to 1.0)	0.5
Converge if Criteria Met for	1 Outer Iterations

Fig 3.3: Gwistas® screen capture for MODFLOW2000 solver options

3.3 Model grid

A finite-difference grid was designed so that the model columns have a NS direction. The model domain is a rectangle of 237402 m². In **table 3.1** grid limits are shown.

Tab 3.1: spatial extent of model grid

Center cell reference	Value (ED50 f33N)
Top	4658997.013346
Bottom	4638816.403181
Left	287265.816474
right	299033.699179

Horizontal discretization

the model discretization was set to a uniform grid 20200 x 11750 meters, for a total area of 237,350 km²; the total number of cells is 759520. In order to represent with acceptable accuracy all the features of the considered hydrogeological system, the spatial discretization was set to a uniform grid of 50 x 50 m cells; the cell dimension was chosen in order to reproduce with accuracy the main model features, as the Tiber River and tributary streams (which width ranges from 80 to 20 meters), or as the hydraulic conductivity zones inside the Tiber River valley.

Model Summary

Grid Rows: 404 Columns: 235 Layers: 8 Total Cells: 759520 Active Cells: 755176		Boundary Conditions Constant Heads: 2704 Wells: 0 Rivers: 1524 Drains: 3072 GHBs: 1216 Streams: 0 Walls: 0 Lakes: 0 Wetlands: 0 No Flow: 4344 FHB: 0		Target Types Head: 368 Head Difference: 0 Drawdown: 0 Concentration: 0 Flux (node): 0 Flux (reach): 0 Prior Information: 0 Constraints: 0 Kx Pilot Point: 0 Kz Pilot Point: 0										
Coordinate Transformation X Offset: 287265.81 Y Offset: 4638816.4 Rotation: 0														
Grid Spacings <table border="1"> <thead> <tr> <th></th> <th>Minimum</th> <th>Maximum</th> </tr> </thead> <tbody> <tr> <td>Rows (Delta-Y)</td> <td>50</td> <td>50</td> </tr> <tr> <td>Columns (Delta-X)</td> <td>50</td> <td>50</td> </tr> </tbody> </table>							Minimum	Maximum	Rows (Delta-Y)	50	50	Columns (Delta-X)	50	50
	Minimum	Maximum												
Rows (Delta-Y)	50	50												
Columns (Delta-X)	50	50												
Original File from GV Version 5: gv548														
<input type="button" value="OK"/>														

Fig 3.4: input data summary

Vertical discretization

The model grid consists in 8 layers defining the aquifer systems; hydrogeological complexes as recognized in Capelli et alii, 2008 (see complexes description, **chapter 2.2.2**) were grouped and modeled initially as 4 hydrostratigraphic units : clayey and sandy clayey units , prevolcanic sandy-gravelly sedimentary units, volcanic units, alluvium units (**Tab 3.2**).

Tab 3.2: hydrogeological complexes grouped in 4 hydrostratigraphic units

<u>Hydrogeological Complex (Capelli et alii, 2008)</u>	<u>Numerical model's initial hydrostratigraphic units</u>
Complex of <i>Monte Vaticano</i> Formation	1
Complex of the alternance of sandy clay, sandy silt and sands of <i>Monte Mario</i> and <i>Ponte Galeria</i> Formations	1
Complex of coarse sands of <i>Ponte Galeria</i> e <i>Fosso Crescenza</i> Formations	2
Complex of gravels and sands of <i>Ponte Galeria</i> e <i>Fosso Crescenza</i> Formations	2
Complex of gravels of <i>Ponte Galeria</i> and <i>Fosso Crescenza</i> Formation	2
Fluvial-palustrine complex of <i>Santa Cecilia</i> Formation	2
Alban Hills Volcanic complex	3
Sabatini Mts. Volcanic complex	3
Holocene alluvium and landfill	4

The number of total layer is 8; the valley is represented by a portion of 6 of those layers. The following procedure has been used for assigning layers tops and bottoms (**figg 3.6 and tabs 3.4 and 3.5**):

- Top of Layer 1, representing volcanic complexes, is the Digital terrain Model with 20 m resolution;
- Bottom of Layer 1 (and top of layer2) is the surface built in this study "Bottom of volcanic complexes";
- Bottom of Layer 2 (and top of layer3) is the surface built in this study "Bottom of PGT complex";
- Bottom of Layer 3 is set uniformly to -15 m asl;
- Bottom of Layer 4 is set uniformly to -30 m asl;
- Bottom of Layer 5 is set uniformly to -40 m asl;
- Bottom of Layer 6 is set uniformly to -50 m asl;

- Bottom of Layer 7 is set uniformly to -100 m asl;
- Bottom of Layer 8 is set uniformly to -120 m asl;

Then, top and bottom of layers **inside the valley** were set up as below:

- Bottom of Layer1 is set uniformly to +5 m a.s.l.;
- Bottom of Layer2 is set uniformly to -5 m a.s.l.;
- Bottom of Layer3 is set uniformly to -15 m a.s.l.;
- Bottom of Layer4 is set uniformly to -30 m a.s.l.;
- Bottom of Layer5 is set uniformly to -40 m a.s.l.;
- Bottom of Layer6 is set equal to the bottom of the alluvial valley (as interpolated in this study);

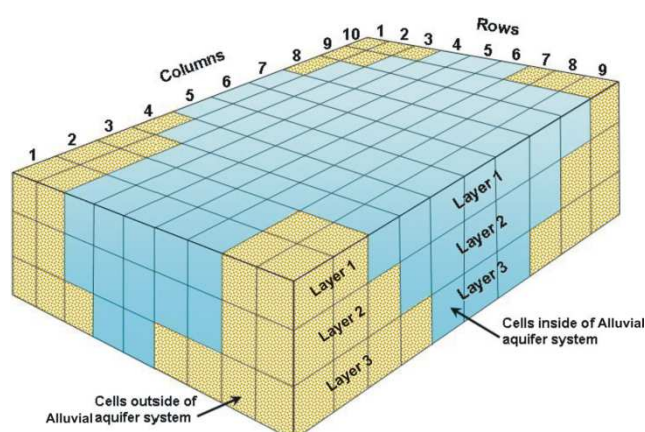


Fig 3.5: simplified schematization of model layering: cells inside and outside the Tiber alluvial valley.

Tab 3.4: schematization of top and bottom of layers OUTSIDE the Tiber Valley

LAYER	TOP SURFACE	BOTTOM SURFACE
L1	DTM	BOTTOM VOLCANIC COMPLEX
L2	BOTTOM VOLCANIC COMPLEX	BOTTOM PGT FLUVIO-DELTAIC COMPLEX
L3	BOTTOM PGT FLUVIO-DELTAIC COMPLEX	UNIFORM ELEVATION -15 m a.s.l.
L4	UNIFORM ELEVATION -15 m a.s.l.	UNIFORM ELEVATION -30 m a.s.l.

L5	UNIFORM ELEVATION -30 m a.s.l.	UNIFORM ELEVATION -40 m a.s.l.
L6	UNIFORM ELEVATION -40 m a.s.l.	UNIFORM ELEVATION -50 m a.s.l.
L7	UNIFORM ELEVATION -50 m a.s.l.	UNIFORM ELEVATION -100 m a.s.l.
L8	UNIFORM ELEVATION -100 m a.s.l.	UNIFORM ELEVATION -120 m a.s.l.

Tab 3.5: schematization of top and bottom of layers INSIDE the Tiber Valley.

LAYER	TOP SURFACE	BOTTOM SURFACE
L1	DTM	UNIFORM ELEVATION +5 m a.s.l.
L2	UNIFORM ELEVATION +5 m a.s.l.	UNIFORM ELEVATION -5 m a.s.l.
L3	UNIFORM ELEVATION -5 m a.s.l.	UNIFORM ELEVATION -15 m a.s.l.
L4	UNIFORM ELEVATION -15 m a.s.l.	UNIFORM ELEVATION -30 m a.s.l.
L5	UNIFORM ELEVATION -30 m a.s.l.	UNIFORM ELEVATION -40 m a.s.l.
L6	UNIFORM ELEVATION -40 m a.s.l.	ELEVATION -50 m a.s.l. (only where valley is deeper than -40 m a.s.l.)

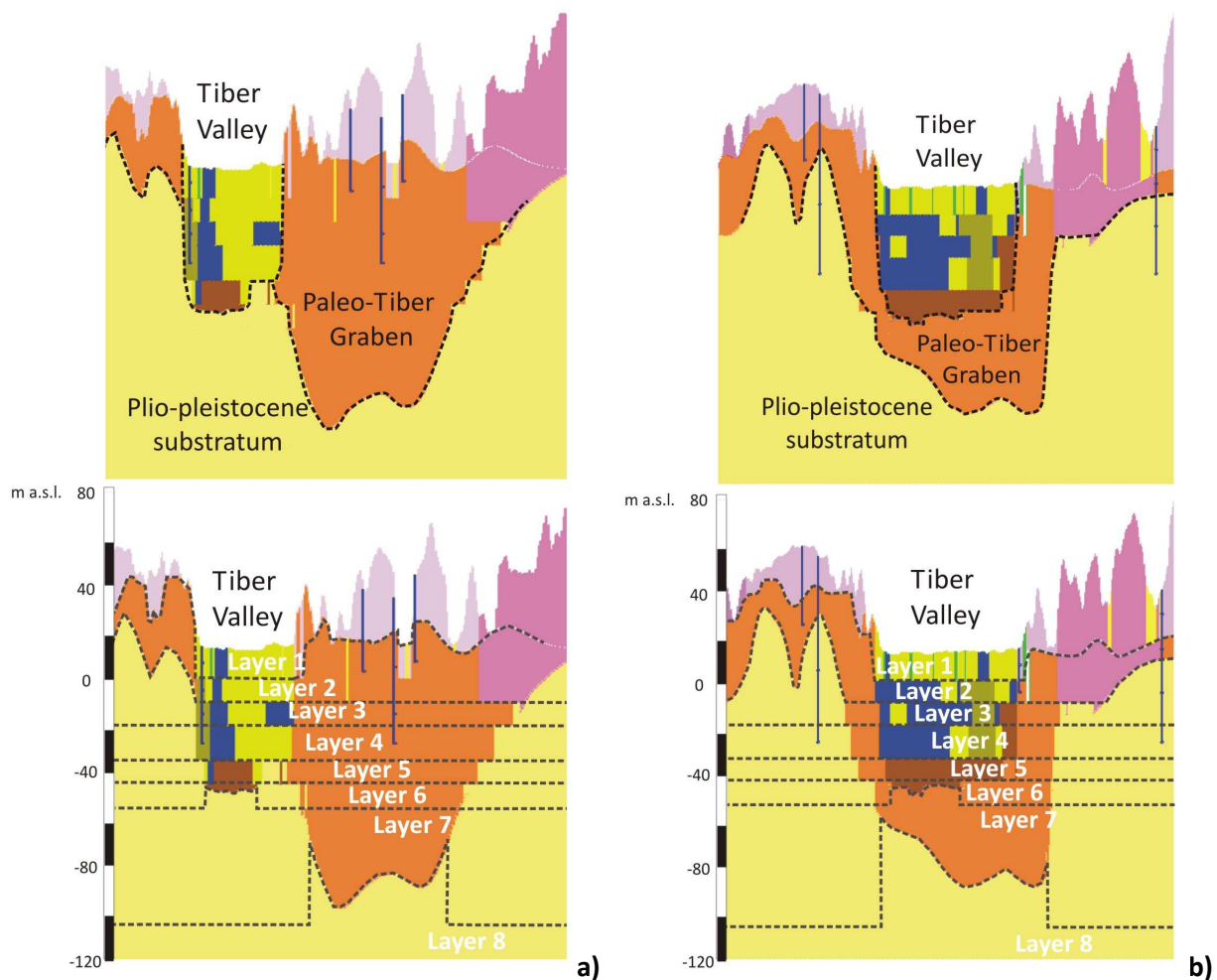


Fig 3.6: a) Vertical discretization along model column 88; the Tiber Valley is mostly excavated into the Plio-Pleistocene clayey substratum; b) vertical discretization along model column 106; the Tiber Valley is excavated inside the sedimentary filling of the Paleo-Tiber Graben.

3.4 Hydraulic parameters

In order to insert the 5 alluvium units in the model, slices with areal distribution of lithotypes at different depths were used according with elaborations made by IGAG-CNR (Roma project 2007). In this cited study, a mapping of different lithotypes recognized in several boreholes drilled inside the Tiber alluvium was built; the lack of data in some areas was overpast taking into account the fluvial-depositional mechanisms. The result is an almost complete coverage of alluvium surface by different k zones for different intervals of depth. The procedure that has been followed is below:

- Analysis of boreholes in database: recognizing of 6 bottom elevations as levels for main changing of alluvial facies. These elevation are: 10, 5, -5, -15, -30, -40 meters a.s.l.: these will be the bottom elevation of 5 different model layers inside the alluvium.

- Creation of Arc Gis® polygon shape files, one for bottom surface recognized, covering the whole extent of alluvium valley.
- Assigning to each polygon a zones corresponding to one of the 5 unit, as recognized from stratigraphies of drillings inside the valley for the considered elevation.

As result, 6 multipolygon-shape files were built, representing the k zones distribution at different depth. (**Figure 3.7**). **Tab 3.6** lists the initial k values chosen alluvium. Since Roma model doesn't take into account small scale heterogeneities, the chosen K value should reproduce the hydraulic conductivity of each hydrogeological unit at the model's scale.

Tab 3.6: Initial k values chosen for the model

K zone	lithotype	Kx, Ky (m/d)	Kz
1	Volcanic complex- Alban Hills	6.04	2.5
2	Volcanic complex- Sabatini Hills	2.13	0.0864
3	PGT complex (Paleo-Tiber)	0.14	0.014
4	Alluvium- clay and silty clay (A)	0.1	0.01
5	Alluvium- sand (B1,B2,D1,D2)	2	0.2
6	Alluvium- clay with peat (C)	0.1	0.01
7	Alluvium- gravel (G)	4.2	0.42
8	Alluvium- clay, also bedrock	0.01	0.001
9	Alluvium- landfill (RP)	0.1	0.01

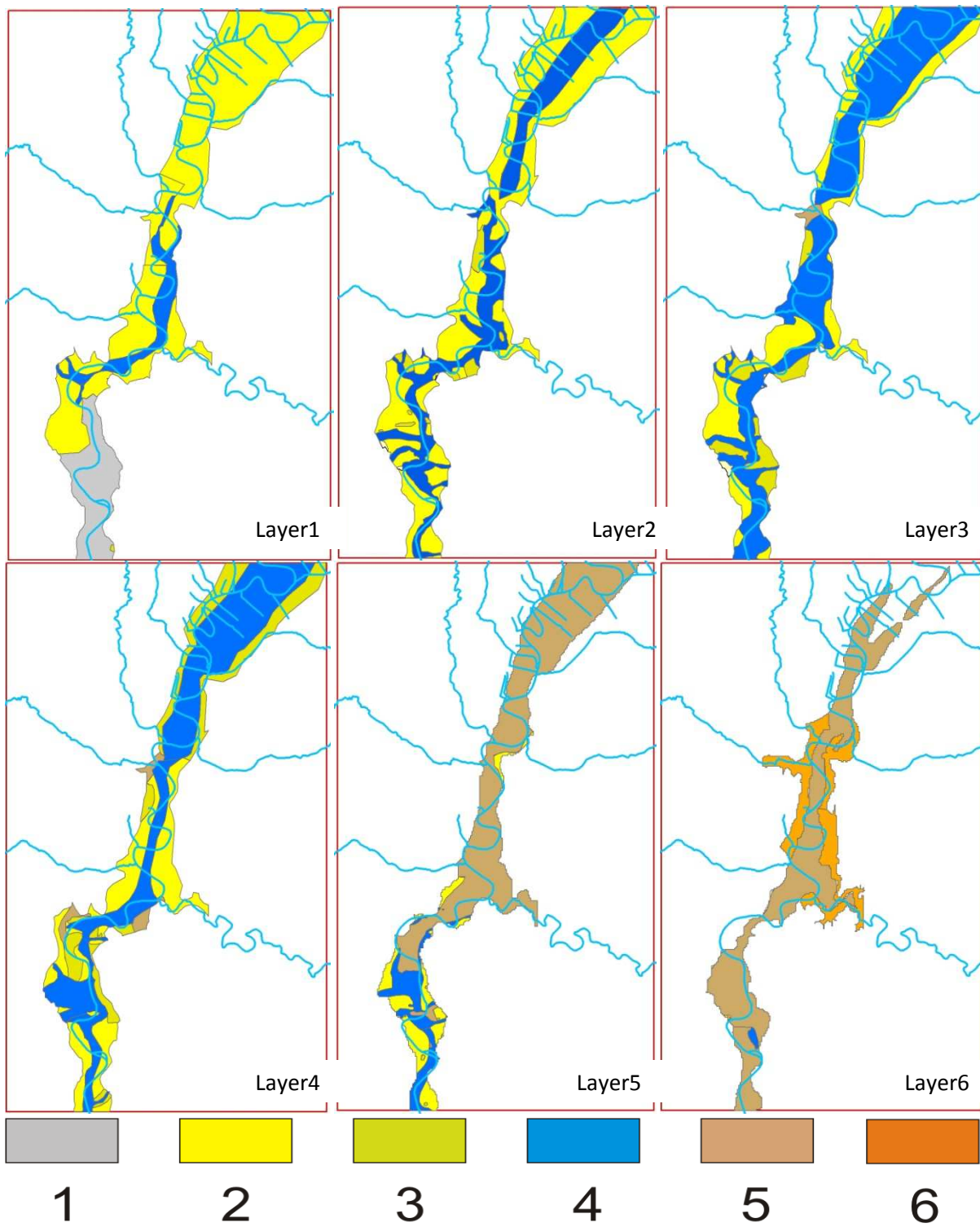


Fig 3.7: areal distribution of hydraulic conductivities assigned to each model's layer INSIDE the Tiber River valley;1=landfill; 2= clay and silty clay; 3=clay with peat; 4=sand; 5=gravel; 6="PGT" complex complex.

3.5 Boundary conditions

3.5.1 Recharge

Not urbanized areas

The recharge assigned to the model comes from a raster with 255x255 m cells, as described in **chapter 2.4.1**; the value of each cell is the 1997-2007 years averaged recharge in the cell. The recharge, was imported in GwVistas® as a shape point file to the first layer. Higher recharge values are distributed in the northern sector, while lower values are in the southern sector (**fig. 3.8**). This is due to the surface sealing in urbanized area which are concentrated in the south; the mostly agricultural character of the northern sector of the model permits higher values of rainfall infiltration.

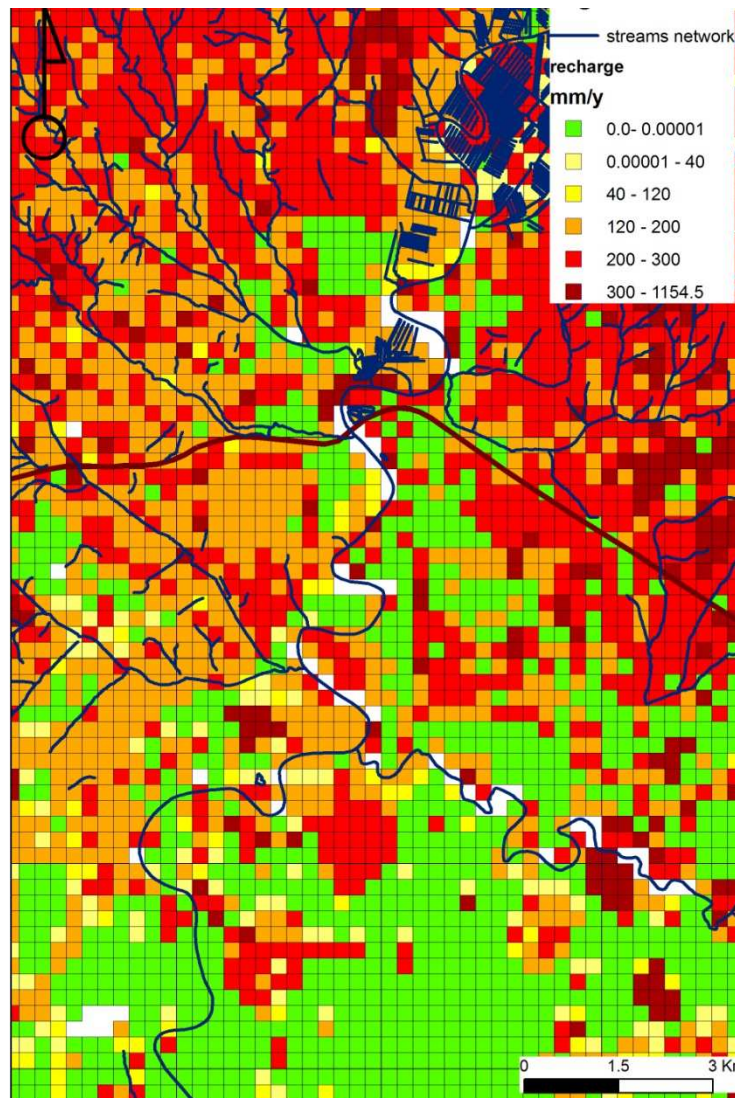


Fig 3.8: shape point file assigned as initial recharge in non-urban areas; green cells, corresponding to urban areas, have zero value, assuming that those areas are covered by impermeable surface.

In order to test the accuracy of the assigned recharge in **non-urban areas**, five model runs were performed: one with the initial calculated values, two with a 10% and 20% decreased recharge, and two with a 10% and 20% increased recharge; the statistic for head target is more satisfying in the case of 20% decreased recharge, so that this was chosen as final recharge rate for non-urban areas (see chapter 4, Calibration).

Urbanized areas

Since the study we refer to (Capelli et alii, 2005) was developed for purposes of regional water balances and regional numerical modeling, a simplified assumption was used for the recharge in high urbanized areas; it is considered that this areas are sealed by paving, and the entire amount of precipitation is assumed to be lost as run-off on the streets and then is wholly conveyed in the artificial drainage network; thus, recharge is set equal to zero. Actually is well known from literature that this assumption is not right, and several sources of recharge are present in urbanized areas; in some case it has been demonstrated that in urban areas recharge can be increased respect to the “natural” values, due to overirrigation and main leakage (Lerner, 1990; Grimmond and Oke, 1991; Ragab et alii, 2003; Berthier et alii, 2006). Most studies have been analyzed in order to quantify the recharge in Rome urban areas; we report in this chapter what we think are the most significative reasonings from Lerner (2002). Since no field data for recharge are available, we tried to estimate the recharge sources and to compare those to the model balance.

“ In an urban setting, different land uses and plant types exist. Extensive parks often exist; heavy usage (sports, car parks) acts to overcompact the soils, whereas extensive cultivation (gardens) increases infiltration rates. Irrigation is often an important part of the urban recharge. Irrigation protocols are very different in urban settings compared to agricultural areas, with significantly higher application rates for amenity land uses such as golf courses and gardens.

No research is known on the significance of localized recharge in urban areas. Most cities have many paths, car parks, compacted soils, driveways, and other low permeability surfaces that do not have any storm drainage associated with them. Very likely significant localized recharge occurs, but little or no evidence exists for this, and no data are available to quantify the amounts.

When studying urban recharge at a regional scale, the interest is no longer in identifying individual points of recharge. Rather, the objective is to show that sufficient individual sources have an impact on overall urban recharge” (Lerner, 2002).

The recharge in urban areas has been estimated starting from the ACEA (Municipal Water Agency) annual statistic report for year 1996; the cited report gives a quantity of main water loss respect to the initial aqueduct discharge; the main leakage from the water net distribution is estimated to be around 31.71% (**tab 3.7**)

Tab 3.7: water supply in 1996 in Rome's hydric network

Water supply in 1996 in the hydric network of Rome (*) from "Annuario statistico dell'Acea" - year 1996)			
	VOLUME (Mm3/d)	Average discharge (l/s)	% of total gained water
TOTAL GAINED WATER	575.71	18.256	100%
LOSSES (to subtract)			
overflows and drainings	16.88	535	2.93
water main leak	182.53	5.788	31.71
other supplies	44.82	1.421	7.79
TOTAL SUPPLIED WATER	331.48	10.511	57,58%
*included Ciampino and Fiumicino municipality and Vatican City			

The total **leaking water** (182.53 Mm3/y) leaks over a total urbanized surface of 197750000 m²; it was considered as distributed on the model's urbanized areas as 0.92 m/y, that is 0.00252 m/d. The resulting calculated recharge on every single cell is 2.05E-07 m/d.

Another source of recharge is due to the **percolation from the paved surfaces**, which are not perfectly sealed; hence, a proportion of the impermeable area should be treated as permeable (perhaps 50%), particularly in residential areas (Lerner, 2002); personal communication from hydraulic engineers working on Rome's hydrology gives an estimation of this recharge contribute as 5% of the rainfall.

Also the **over-irrigation** of municipal gardens should be included in the recharge; this is estimated to be at least 25 % of the irrigation water applied to the gardens (Lerner, 2002). The water used for garden irrigation in the City of Rome in 1996 was 3.81 Mm3 (ACEA Annual statistic report, 1996); that means that the 25% of this amount (0.762 Mm3/y), contributes to the recharge. This approach should require sample areas and sure irrigation records; actually those data are not available. The first run was performed using the value calculated for water main leakage (2.05E-07 m/d); this small recharge didn't show good model result, since the water table was very low; for this reason, the recharge in urban areas was subjected to calibration as discussed in chapter 4.

3.5.2 Specified flux boundary conditions

Specified flux BCs (Neumann)

No Flux Bcs: this type of specified flux BC was used along model borders where the Plio-Pleistocene substratum, which acts as an aquiclude, is outcropping, to simulate negligible water exchange between the Plio-Pleistocene complex and the Alluvium complex; these cells are termed *inactive cells* in MODFLOW.

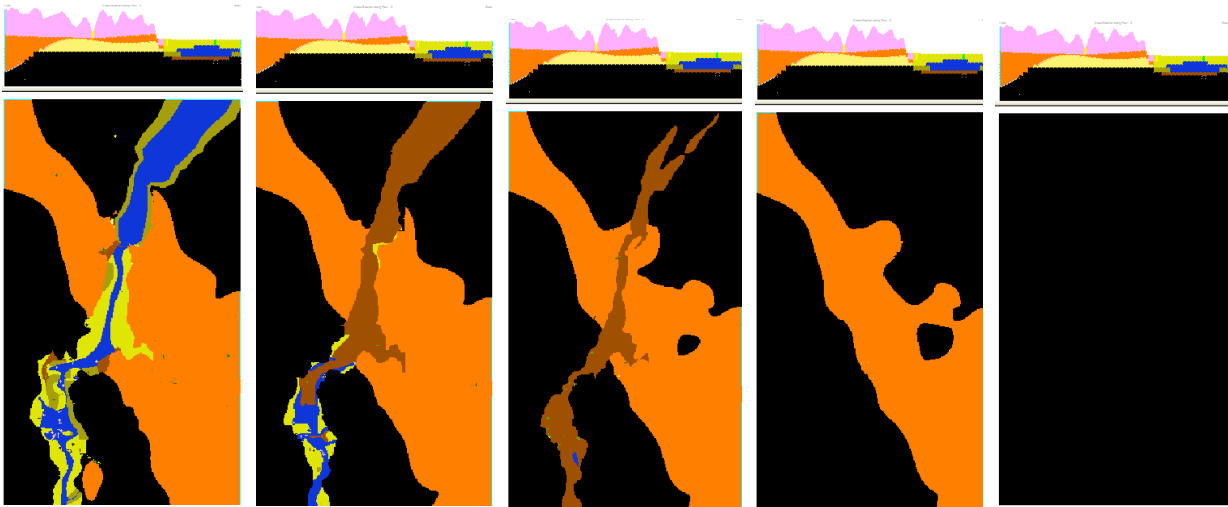


Fig. 3.9: No-Flux BCs (black cells) on model layers 4, 5, 6, 7 and 8 (in sequence).

This type of condition was set on Layers 4, 5, 6, 7 and 8 in each cell representing the Plio-Pleistocene complex. In layers 3, inactive cells are set just along the border of the model, where the Plio-Pleistocene complexes outcrop, so we don't exclude *a priori* a water exchange between the uppermost portion of Plio-Pleistocene complex and the other complexes; the reason is that recently drilled boreholes shown a not negligible amount of sand in this complex, meaning that the hydraulic conductivity value could be not null. Otherwise, we retain that this assumption can be valid within a certain depth, while going deeper in the layers, the lithostatic pressure decreases the permeability, and the water exchange can be considered null; that's why we put No-flow BC on every Plio-Pleistocene cell just in layers from 6 to 8, while in layers from 3 to 5, No-flow BC is set just along the border of the model, where the Plio-Pleistocene complex is present.

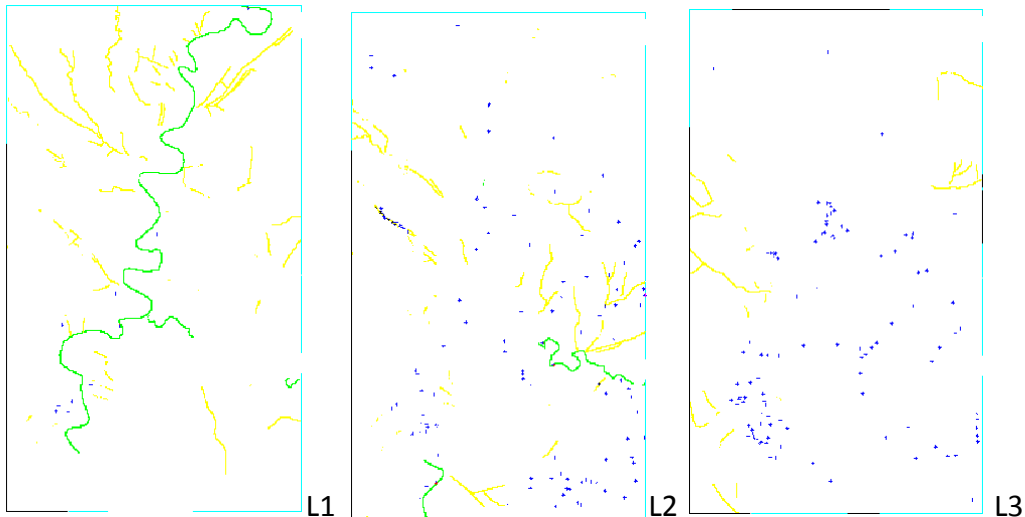


Fig. 3.10: In layers 1, 2 and 3 No-Flux BCs are set along part of the south-west boundaries, in correspondence of the Plio-pleistocene complex outcrop.

Head-dependent flux BCs (Cauchy BCs)

In this type of boundary, MODFLOW computes the difference in head between the boundary and the model cell where the boundary is defined; the head difference is then multiplied by a conductance term to get the amount of water flowing into or out of the aquifer.

Three types of head-dependent BCs were assigned to the model:

- General head
- River
- Drain

Head dependent boundaries always require the input of the conductance term

$$C = kA/L$$

Where:

K =hydraulic conductivity of the boundary material (L/T)

A =area of the boundary (L^2)

L = thickness or width of the boundary

General Head Bcs: In a GHB cell, the flow of water into or out of the aquifer is dependent on the head assigned to the GHB and the conductance term. The head is compared to the computed head in the aquifer for the cell containing the GHB. If the aquifer head is higher than the GHB head, then the GHB removes water from the aquifer. The amount of water removed is based on the conductance term. The conductance is computed from the following equation:

$$C = K \text{ Thick } W/D$$

Where K is the hydraulic conductivity at boundary, $Thick$ is the saturated thickness in the cell, W is the width of the cell, and D is the distance to the GHB head (assumed to be external to the model). This type of BC was chosen along each border of the model domain, where complexes different from the Plio-Pleistocene are present. This type of BC permits an higher water table fluctuation through the boundary, depending on the model result, respect to the Constant Head BC. The GHB head is fixed at the seepage of hydrologic basins; the hydraulic conductivity for GHB cells was set equal to the hydraulic conductivity of the prevalent complexes in the area between the model domain and the General head boundary. The prevalent complexes are the volcanic complexes (both Sabatini Mt.s and Albani Hills volcanic complexes) in the western and south-eastern sectors, and the PGT sedimentary complexes in the north-east sector. As first simulation, the initial complexes k values were chosen for GHB k : 2,13 m/d (Sabatini complex), 6,04 m/d (Alban Hills complex), 0,14 m/d (PGT complex) and 1 (alluvial complex); figure 3.11 shows k values for GHB in layer 1. Then, after the calibration process, the hydraulic conductivity was set equal to the calibrated k values (see chapter 4, calibration). The head value for GH BC was set equal in each layer.

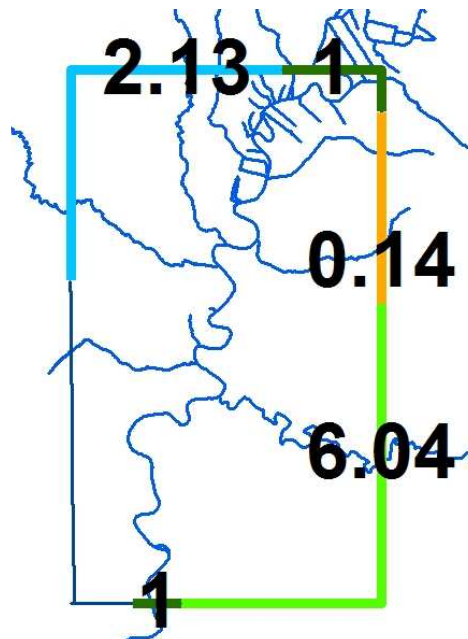


Fig. 3.11: General Head BCs on Layer 1; three “reaches” are shown, each one having the initial k value of the prevalent complex between the model boundary and the General head boundary.

3.5.3 Rivers and drains boundary conditions

River BCs:

River package is used to simulate Tiber and Aniene rivers. In a river boundary, MODFLOW performs an additional check before computing flow rates. If the head in the model cell is below the bottom elevation of the river boundary, the difference in head is computed as the river stage

minus the river bottom elevation. River cells are used where a surface water feature partially penetrate a layer and can both remove water from the aquifer and infiltrate water into the aquifer.

For River BCs MODFLOW requires:

- river stage
- riverbed bottom
- thickness of riverbed
- hydraulic conductivity of riverbed sediments

The volumetric flow rate across the riverbed to the underlying model cell is computed as

$$Q_{rb} = C_{rb} (h_r - h_a)$$

Where:

Q_{rb} is the flow rate across the riverbed,

C_{rb} is the conductance of the riverbed

h_r is the river stage

h_a is the hydraulic head in the cell underlying the riverbed, if the bottom of the riverbed is below the water table in the cell, or the altitude of the bottom of the riverbed is above the water table in the cell.

The conductance of riverbed is computed as below (see fig. 6.4.12):

$$\text{Riverbed Conductance} = (K_v/m) wL$$

Where:

K_v = vertical hydraulic conductivity of riverbed sediments

m = thickness of riverbed sediments

w = width of the river

L = length of the river within the cell

Because of the lacking of data about rivers conductance, it was chosen uniformly as 10 m/d; this value can be reasonable with the supposed hydraulic conductivity, as the riverbed are mainly

made by sandy-clayey sediments. River stages are set as the average stages over the time window 1994-2007 for Tiber and Aniene gauging stations (see table **Tab. 2.8**); this time window is in accord with the period of recharge calculus; river cells distribution is in **fig. 3.13**

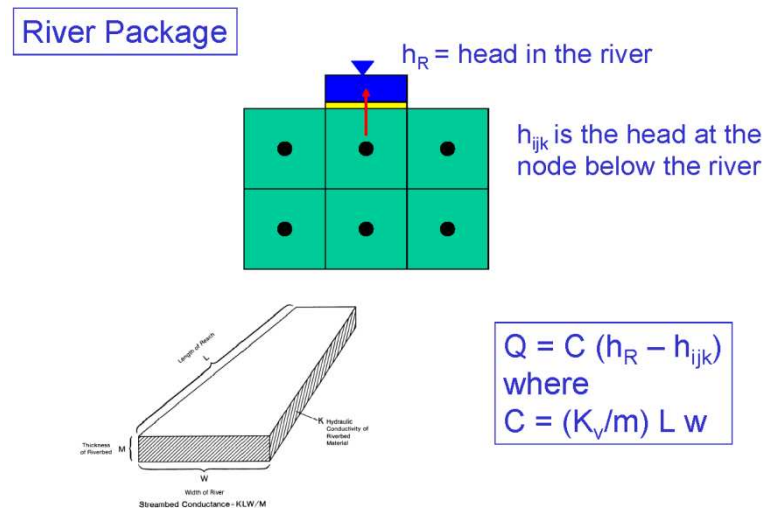


Fig 3.12: meaning of River cells BCs

Drain BCs

Drains are similar to river except that drains will only remove water from the model. If the head in the model cell drops below the drain elevation, the drain will not inject water into the model. Under these conditions, the drains becomes inactive. Drain cells were used in case of streams where flow can go to zero. Drains were used in Roma model to simulate streams and artificial water conduits; drains are the biggest sink for the study area, since they represent the 63 of simulated outflows.

Groundwater Vistas requires the following inputs for setting up drain cells:

- drain stage
- drain width
- drain length
- thickness of drain bed
- hydraulic conductivity of drain bed

Since no detailed information about the minor drainage system is available, the description of drain flow is simplified. Drain width and length are put uniformly as 50 m; the thickness of drain

bed is set uniformly as 1m. The hydraulic conductivity is set equal to the k property of the model cells in which drain BC is set; drain bed k was changed after the calibration process. In the northernmost part of Tiber valley, drains simulates drainage channels in layer 1 with very low hydraulic gradient; outside the Tiber valley, a drain level of 10 m below ground surface is used; were the layer thickness is smaller than 10 meters, the drain cells are set on the lower layer. Following this criteria, drain cells are put on layers 1, 2 and 3 (**fig 3.13a**); depending on the assigned k , 5 different reaches are defined for drain cells (**fig 3.13b and table 3.8**).

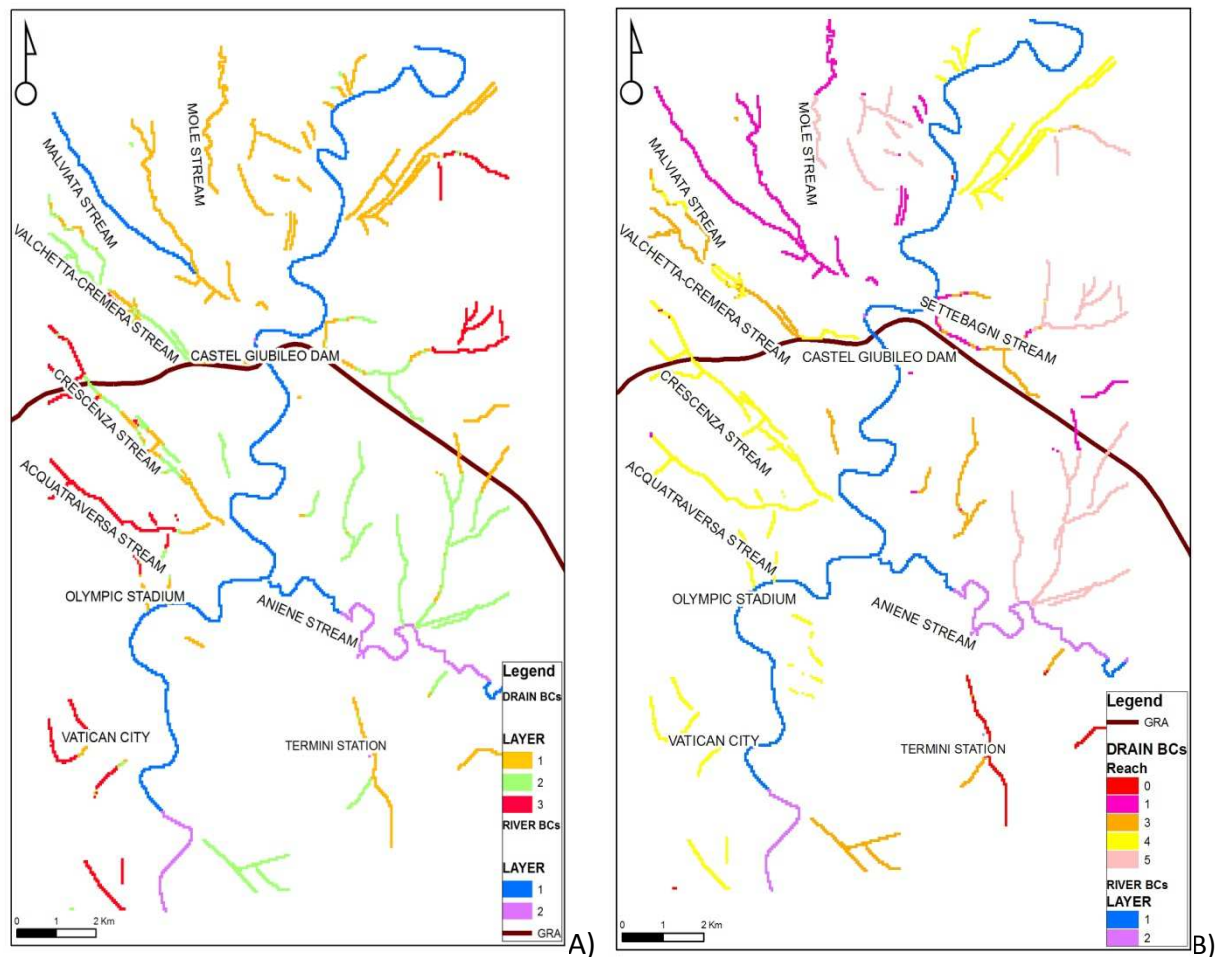


Fig. 3.13: A) distribution of river and drain cells by layers.; B) distribution of drain *reaches*

Tab. 3.8: initial drain bed's hydraulic conductivity

reach	k (m/d)	complex
0	9.12	Alban Hills
1	2.13	Sabatini Mts
3	1.4	PGT (sandy-gravel prevalent)
4	1	clay prevalent complexes
5	0.5	PGT (clay-prevalent)

A sensitivity analysis has been carried out to calibrate drain conductance; results are shown in chapter 4.

3.6 Withdrawals

The calculated total pumping rate is 29097.5 mc/d; 1000 pumping wells were imported in GWVistas, with a total pumping rate of; since no information about screen depth were available, the entire length of the well is considered active, with the top elevation of the screen coincident with the well elevation above sea level, and the screen bottom coincident with the well depth. The distribution of wells in layers is in **table 3.9**.

Tab. 3.9 distribution of pumping wells in layers.

bottom in layer	n of wells
1	347
2	352
3	144
4	87
5	34
6	16
7	17
8	8

total n 1005

Since many wells were not considered in withdrawals calculations for not available data, we retain that the pumping rate is underrated. In order to calculate the uncertainty on pumping rate, 5 model runs were performed, with increased withdrawals of 50, 20, 10 and 5 % respect to the initial estimated values. The best results in terms of model statistic is with an increasing pumping rate of 5% respect to the initial calculated values, which is a total withdrawal of **30552.4 m³/d** on the entire model area which corresponds to a **25% of the recharge rate.**; this pumping rate is considered the final input for the model; the error on withdrawals evaluation is considered to be inside a 10%. Two MODFLOW packages were used to simulate withdrawals: the WELL package and the MULTINODE WELL package.

The **WELL** package simulates a constant flux into or out the aquifer; it can be used for simulate pumping wells of recharging points; in the case of this study, WELL package has been used for simulate pumping wells. Groundwater Vistas allocates pumping rates between the model layers based upon the transmissivity of the layers. The total discharge is automatically divided among the

layers penetrated by the well according to their relative transmissivities. GWV assigns the X,Y location to the proper node (row, column) and assigns the well interval to the proper layers, then creates a MODFLOW *.WEL file according to standard MODFLOW format. The discharge assigned to each layer is withdrawn from the center of the cell according to the standard finite-difference method.

The **Multi-Node Well** (MNW) package provides the MODFLOW user much more control over the behavior of wells than does the WELL package. The increased power of the MNW package to simulate the behavior of pumped and unpumped wells is matched by the additional output it provides with respect to fluxes and water levels both inside and outside the borehole. The effect of this change is that the flux output for the Multi-Node Wells is not written to a binary file that can be read by GWV5, for example, into a mass balance table. Instead, MODFLOW writes all output involving MNW wells to the two special files named “Bynode File Name”=MNW1.NOD and “QSUM File Name”=MNW1.SUM. The amount that enters or exits through each layer is a function not only of the head difference, but also the transmissivity of the layer.

The MNW packages require as input the well radius; the radius of the borehole influences the water level inside a pumped well and the rate of water movement through an unpumped borehole. The influence of the well radius on the drawdown have been tested in two wells (PZ1 and PZ2); as in **table 3.10**, an increasing of well radius produces a decrease in head.

Tab. 3.10: head result for three simulations in two wells, by changing R_w

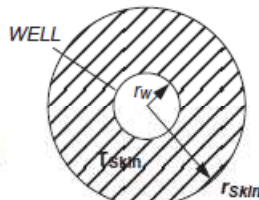
R_w	0.3	0.07	1
Skin	6.2	6.2	6.2
head_PZ1	13.84	11.65	10.69
head_PZ2	14.44	11.36	10.52

Due to the lack of well radius data (r_w), this was set equal to 0.3 meters for each multi-node well, which is considered a reasonable medium value for pumping wells.

The MNW package can simulate the effect of a “skin” around the well on flow to and through the well. It is common for the drilling process to disturb the aquifer in the vicinity of the well and either smear or crush the sediment in such a way as to produce a zone of relative low permeability around the well. This disturbed zone forms a “skin” or “doughnut” around the well with its own radius, r_{skin} . In the picture below (from the MNW manual), the skin is assumed to have a radius twice the length of the well radius, r_w .

Fig. 3.14: Gwvistas well information table; the checked option Use as Multi-Node Well activates the MNW package for the relative well.

The well-loss coefficient collectively defines head loss from flow through formation damaged during well drilling, the gravel pack, and the well screen. The coefficient can be used in terms of a dimensionless “skin” coefficient (S_{kin} in equation below). The skin effect can be pictured as occurring across a cylinder of radius, r_{skin} , around the well with a finite radius, r_w , and a transmissivity, T_{skin} , that differs from the formation transmissivity, T . The skin coefficient can then be described in terms of a transmissivity contrast (T / T_{skin}) over the finite difference between r_w and r_{skin} or by the following equation:

$$Skin = \left(\frac{T}{T_{Skin}} - 1 \right) \ln \left(\frac{r_{Skin}}{r_w} \right) \text{ where,}$$


As written above, the “Friction Loss coefficient” (or “Skin coefficient”) is a function of: 1) the ratio of r_{skin} to r_w and 2) the ratio of T to T_{skin} , where T =transmissivity of the aquifer material outside the well and T_{skin} =the transmissivity of the disturbed zone.

For the magnitude of the “Skin coefficient”, consider this table for an assumed value of $r_{skin}/r_w=2$:

Tab. 3.11: Values of Skin coefficient for changing T/T_{skin} rates

r_{skin}/r_w	T/T_{skin}	Friction Loss (Skin) coefficient
2	≤ 1	0
2	2	0.69
2	3	1.4
2	5	2.8
2	10	6.2
2	100	69
2	1000	692

In this study, we assume that the T/T_{skin} ratio is 10, so that the initial SKin coefficient is=6.2.

The influence of the skin coefficient results in the head value: by increasing the Skin coef., also the head increases. In fact, for a constant r_{skin}/r_w ratio, the increase of Skin coeff is due to a decrease of T_{skin} that, in other words, means a decrease of the damage well zone and, thus, an increase of the skin permeability, so that the head results higher. This relationship was proved by changing the Skin Coef. in two pumping wells (Pz1 and Pz2), as in **table 3.12**:

Tab 3.12: head result for three simulations in two wells, by changing Skin coefficient

Rw	0.3	0.3	0.3
Skin	0.62	6.2	62
head_PZ1	8.77	11.22	13.85
head_PZ2	7.83	10.77	14.44

The ordinary WEL package does not calculate the water level (i.e., drawdown) inside the well. It does not calculate the pumping discharge as a function of the well water level, aquifer water level, well radius, and well skin. Nor does it simulate flow through an unpumped borehole. The MNW does all these things with very little additional input.

A model using MNW for many wells has the ability to more accurately simulate drawdown inside these wells. Perhaps more important, it has the ability to simulate the appreciable leakage that can occur between a shallow, unconfined aquifer and a deep, confined aquifer when there exist many boreholes that are unpumped but still open to multiple aquifers.

The final Multi-node well pumping rate is 1888.88 mc/d; this amount is lower than the initial-calculated pumping rate, because of, despite the MNW package, in some case cells go dry; in that cases, it is assumed that the calculated pumping rate was wrong (too high) and the right pumping

rate is assumed to be the simulated one. The total simulated pumping rate by WELL and Multi-node Well is 18206 m³/d.

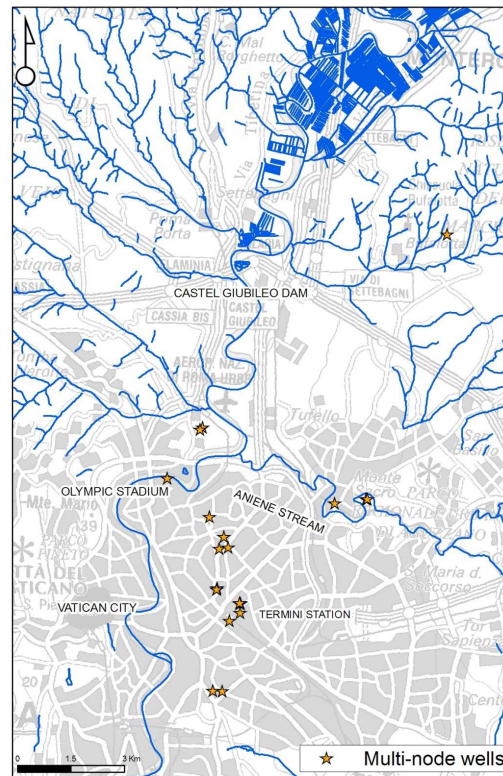


Fig 3.15: distribution of Multi-node wells in the model's area

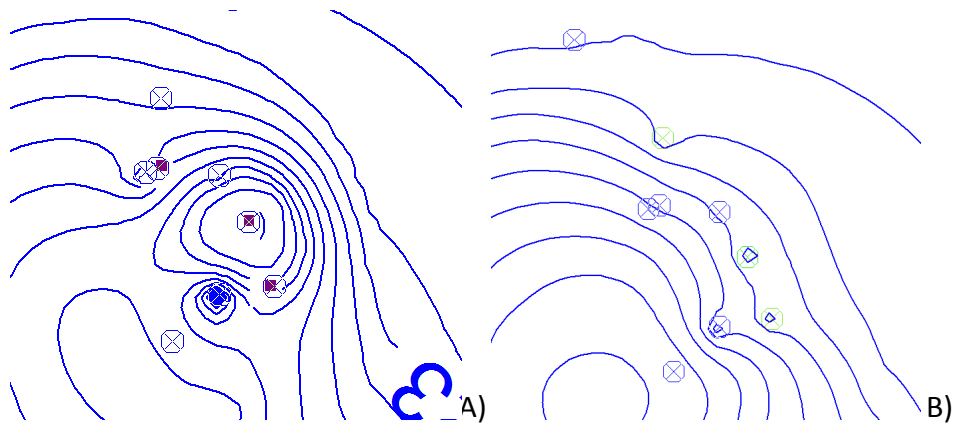


Fig 3.16: effects of MNW package on model's results, in the area of Termini station: A) all wells simulated by WELL package: cells go dry and the total pumping rate is reduced. B) green wells are simulated by MNW package; cells do not go dry and the entire pumping rate is distributed along the multi-node well.

4 Model calibration

4.1 Calibration strategy

Calibration is the process of refining the model representation of the hydrogeological framework, hydraulic properties, and boundary conditions to achieve a desired degree of correspondence between the model simulation and observations of the ground-flow system.

As assessed in the ASTM *Standard Guide for Application of a Ground-Water Flow Model to a Site-Specific Problem* (2004), “the calibration process consists in adjusting hydraulic parameters, boundary conditions and initial conditions within reasonable ranges to obtain a match between observed and simulated potential, flow rates or other calibration targets. The range over which model parameters and boundary conditions may be varied is determined by data presented in the conceptual model [...]. In practice, model calibration is frequently accomplished through trial-and-error adjustment of the model’s input data to match the field observations.[...] The calibration process continues until the degree of correspondence between the simulation and the physical hydrogeologic system is consistent with the objectives of the project. “

The calibration strategy has been performed in this study in a trial-and-error method through three steps:

- Looking at model’s result statistics and check the discrepancy between observed and simulated “target” values;
- Run a sensitivity analysis to find which are the most sensitive parameters;
- Adjusting parameters, repeating model runs and looking at statistic table; then repeating the sensitivity analysis until an adequate fitting between observed and calculated values has been reached.

*“The calibration is evaluated through analysis of **residuals**. A residual is the difference between the observed and the simulated variable. Calibration can be viewed as a regression analysis designed to bring the mean of the residuals close to zero and to minimize the standard deviation of the residuals.[...] calibration often necessitates reconstruction of portion of model, resulting in changes or refinements in the conceptual model. [...]*

Sensitivity analysis plays a key role in calibration process identifying those parameters that are most important to model reliability. [...]Sensitivity analysis is a quantitative method of determining the effect of parameter variation on model results. The purpose of a sensitivity analysis is to quantify the uncertainty in the calibrated model caused by uncertainty in the estimates of aquifer parameters, stresses and boundary conditions. It is a means to identify the model inputs that have the most influence on model calibration and predictions. [...]”(ASTM, 2004). In this study, the automated sensitivity analysis available in GwVistas® has been used.

4.2 Selection of calibration targets

Data available for calibration of ROMA model are only head measurements. As assessed in **chapter 2.4.3**, minor streams flow into water mains when reaching the most urbanized areas; water mains collect also civil uses waste water and leads water to the wastewater treatment plants; for this reason, surface stream flux is not quantified; moreover, the Tiber flux is controlled by dams, and no river discharge target value can be estimated.

Head target data used for calibration are measurements from 1969 to 2010; data can be grouped in three main clusters, referred to the ranges of dates:

WELLS FROM THE LINQ* DATABASE

Wells Mxxx: 1992-1996-2002

Wells Qxx:2003-2004

Wells Rxx:2002

Wells STxx:1999

WELLS FROM THE CNR-IGAG DATABASE

Wells Vxx (Ventriglia): no measure date available

Wells Vitrone: 1983-2003

WELLS BY PRIVATE COMPANIES N1

1999-2001

WELLS BY PRIVATE COMPANIES N2

2008-2009

LINQ FIELD MEASUREMENT DATA 2010

2010

**LINQ:Laboratorio di idrogeologia Numerica e Quantitativa, università Roma Tre*

Head data were selected from the list of observation by removing data retained not sure; in the case of more than one head data measured in different years for a single well, the most recent one was selected. In the case of more than one measure in one single year, a mean of head level was chosen. The total number of control wells to used for model calibration is 368. The most old data, belonging to the range from 1969-1990 were used only in areas with lacking of more recent head data. Based on the mid-point screen elevation of the well screen the observations are distributed into the computational layers (Tab 4.1).

Tab 4.1: distribution of observations into the computational layers

<i>N layer</i>	<i>N of targets</i>
1	15
2	132
3	115
4	70
5	17
6	19
<i>total</i>	<i>368</i>

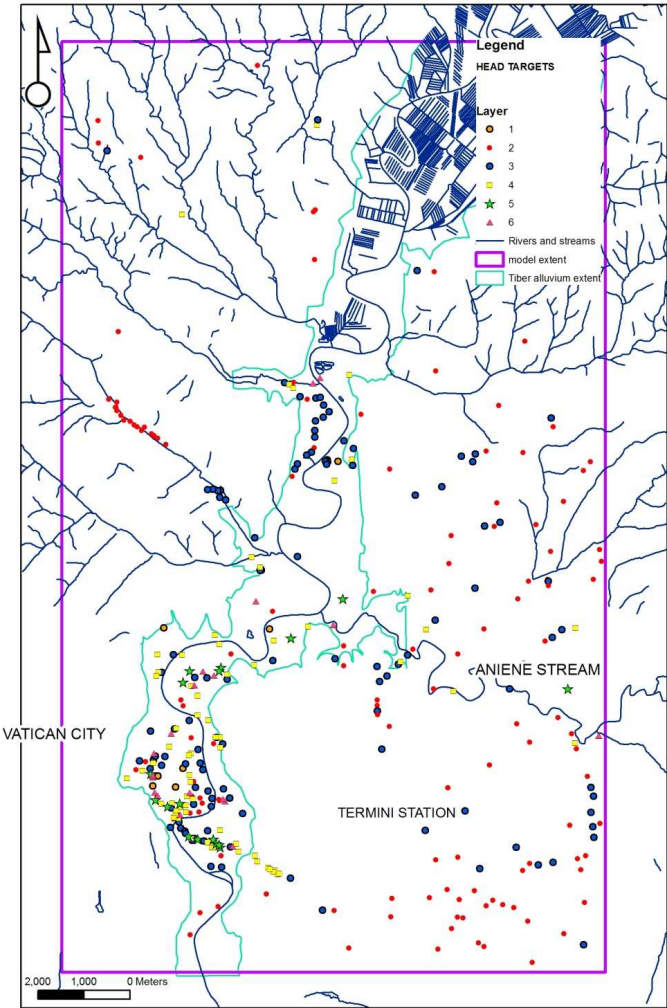


Fig 4.1: distribution of head targets

In analyzing head target, the “calibration rules” by H.M Haitjema (1995) were considered: *“When comparing modeled heads with observed (measured) heads, the modeler should look for trends rather than an exact match. Available field data often consists of heads that are measured at different times at different depths, with uncertain accuracy. [...] Clusters of modeled heads that are too high or too low may indicate (local) errors in the conceptual model”*.

4.3 Nature and sources of uncertainty

According to Sonnenborg et alii (2003) and Seifert et alii (2008), a quantitative estimation of uncertainty on head measurement was carried out. The following types of errors were considered:

- Measurement errors associated with the accuracy of the device used for measuring the water level, and the precision by which the location of the well and the ground level reference have been determined; also, local pumping effects and heterogeneity in the geological complexes can introduce an error. The effect of these errors are assumed to result in a standard deviation of the head measurement of **0.2<E1<2 m**.
- Heads measurements are carried out at random times of the year, so this “transient” effect is estimated to result in a standard deviation of the head value in the order of $E2=\Delta h/2$, where Δh is the average seasonal variation in hydraulic head. The average seasonal variation is 5 meters for head outside the valley, while it is 2 meters for head inside the valley; that is, **E2=2.5 meters** (outside the valley) and **E2=1 m** (inside the valley).
- Interpolation errors are caused by estimation of simulation values at the point of measurement. This is assumed to result in a standard deviation of $E3=0.5 \Delta x J$, where Δx is the grid size (which was used both as raster resolution of bottom and top surfaces and as model cell), and J is the hydraulic gradient in the vicinity of the measurement point. In our case, $\Delta x = 50$ m, and $0.002 < J < 0.06$; that is, **0.05 < E3 < 1.5 meters**.

Using this principles (Sonnenborg et alii, 2003), the head data are estimated to have a total standard deviation in the range from 1.25 to 6 meters.

In this study’s approach, the error is smaller for targets in the Tiber Valley and bigger for target outside the valley. That is because in the Tiber alluvial plain the small seasonal variations, the low hydraulic gradient, and the flat topography significantly reduce the error. The resulting average error estimation is 3 m for targets outside the alluvial aquifer (*target group n° 1*), while it is 1.5 m for targets in the alluvial valley (*target group n° 2*). This numbers are comparable with the Residual Standard Deviation of the calibrated model, as discussed in **chapter 4.4**

4.4 Performing calibration

Aim of calibration is lower the statistical parameters respect to the uncalibrated model (**Tab. 4.2**). Here is a brief description of the cited statistical indicators.

-**RMS Error**: the root mean square error is a frequently-used measure of the differences (residuals) between values predicted by a model or an estimator and the values actually observed from the thing being modeled or estimated. RMS is a measure of precision.

$$\text{RMS error} = \sqrt{\frac{1}{N_h} \sum_{i=1}^{N_h} (H_{\text{obs},i} - H_i(b))^2}$$

Where

b is the calculated value

N is the number of target residuals

$H_{\text{obs},i}$ is the i^{th} head observed value.

-**Residual Sum of Squares** (RSS): the sum of squared residual is computed by squaring all residuals and adding them together. This statistic, meaningless by itself, is useful when judging several different simulations.

$$\text{RSS} = \sum_{i=1}^n (H_{\text{obs},i} - H(b_i))^2$$

Where:

$H_{\text{obs},i}$ is the i^{th} observed head value

$H(b_i)$ is the i^{th} calculated head value

-**Absolute Residual Mean** (AM): the absolute residual mean error is computed by dividing the sum of residuals by the number of residuals. Because both positive and negative residuals are used in the calculation, this value should be close to zero in a good calibration.

$$\text{AM} = \frac{1}{n} \sum_{i=1}^n |H_{\text{obs},i} - H(b_i)|$$

-Residual Standard Deviation (RSD): this is a measure of the overall spread of residual and it can be compared to the overall range in target value. For head value, as in this case, this value shows how the errors relate to the overall gradient across the model.

$$RSD = \sqrt{\frac{\sum H_{obs,i} - H(b_i)}{n-2}}$$

Tab. 4.2: Statistic table for uncalibrated model

uncalibrated	
RMS	3.13
RSS	3840
AM	2.52

Three types of plots are useful in assessing the quality of calibration simulations.

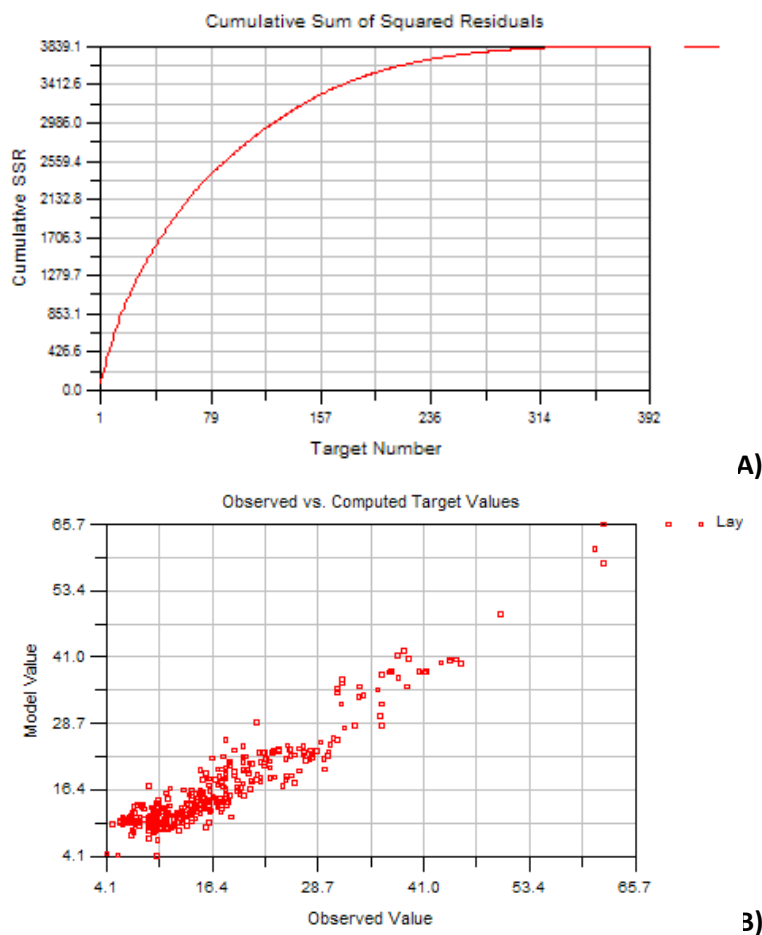


Fig. 4.2: calibration plots available in GwVistas®, referred to the uncalibrated model; A) Observed vs computed head plot; B) Cumulative sum of squared residuals plot.

One (**Fig 4.2A**) is the scattered plot where the observed target values (measurements) are plotted versus the values computed by the software for the uncalibrated model. For an ideal calibrated model, the points should fall on a straight line with a 45° slope; the degree of scatter about this theoretical line is a measure of overall calibration quality. Another plot is a cumulative sum of squared residuals curve (**Fig 4.2B**). The plot resulting from the calibration step shows that around 79 targets (having high residuals) account for about two-thirds of the sum of squares, that is 1/5 of the total number of targets. For some of them, the reason can be a quality data problem, but, being the number of 79 quite high (22%), there can be a problem of aquifer property value, or the conceptual model has to be revisited. Plots for the uncalibrated model will be compared with graphs at the end of calibration. The calibration was performed on layers hydraulic conductivity, General Head boundary hydraulic conductivity, Drain bed hydraulic conductivity and recharge.

Hydraulic conductivity

In the case of model ROMA, the parameter which is more affected by uncertainty is hydraulic conductivity, so this was the first calibrated parameter.

Table 3.15 resumes the seven steps for calibrating hydraulic conductivity; calibration was performed by a manual trial-and-error procedure based on dynamic runs for assessment of parameter values, by plotting targets and looking at model statistics (available in GwVistas menu **plot>calibration>statistics**) and by three sensitivity analysis; goal of calibration has been reduce the Absolute Residuals Mean, and the Residual Sum of Squares , and obtain a value of Root Mean Squared error comparable with the value for uncertainty on heads estimated in **chapter 4.3**. From the initial number of 9 zones, the final model has 19 zones; k values have been changed for every zone but zone 4, 13 and 14. In tables 4.4, 4.5 and 4.6 there are the statistical indicators for the most significant steps.

The result of the first autosensitivity analysis (step b in **table 4.3**)(**fig. 4.3**)shown that the most sensitive k zones are zones **1, 3, 5, 8** and **10** (corresponding to complexes: Alban hills, PGT, Alluvial sand, Marne Vaticane Formation and Monte Mario Formation). Taking into account residuals for k values from the sensitivity analysis, some changes were made, in order to reduce the residuals statistic. Changes were made only for the most sensitive parameters; the k value has been corrected by the multipliers which lower the residual. However, some sensitive k values, as the k5 (Alluvium-sand), haven't been updated, because from k field measurements the "real" value is retained not to exceed 8.8 m/d.

Tab. 4.3: summary of k (m/d) values that have been changed during the calibration. Letters from A to E indicate the 5 calibration steps; blue cells indicate changing values from one calibration step to another.

k zone	COMPLEX	initial kx,ky (m/d)	initial kz	A) k values after statistic adjustments	B) k values after the I autos.	C) k values after the II autos.	D) k values after the adjustment on zones	E) k values after the III autos. and target weighting	F) k values after target grouping	G) k values after statistic adjustments
k1	Alban Hills volcanic	6.04	2.5	6.04	3.04	6.08	9.12	9.12	9.12	9.12
k2	Sabatini Mts volcanic	2.13	0.0864	2.13	2.13	1.065	2.13	2.13	2.13	2.13
k3	Ponte Galeria sedimentary("PGT")	0.14	0.014	0.14	1.4	1.4	1.4	1.4	1.4	1.4
k4	Alluvium-clay	0.1	0.01	0.1	0.1	0.1	0.1	0.1	0.1	0.1
k5	Alluvium-sand	2	0.2	8.8	8.8	8.8	8.8	8.8	8.8	8.8
k6	Alluvium-clay with peat	0.1	0.01	0.1	0.1	1	0.5	0.5	0.5	0.5
k7	Alluvium-sandy gravel	4.2	0.42	4.2	4.2	4.2	4.2	4.5	4.5	4.5
k8	Monte Vaticano Formation	0.01	0.001	0.01	0.1	0.05	0.1	0.1	0.01	0.01
k9	Alluvium_landfill	0.1	0.01	0.1	0.1	1	0.1	0.1	0.1	0.1
k10	Monte Mario Formation 1			0.5	0.5	0.25	0.5	0.5	0.5	0.5
k11	Monte Vaticano Formation 2			0.1	0.1	0.2	0.4	0.4	0.4	0.4
k12	Monte Mario Formation 2			0.09	0.09	0.09	0.09	0.09	0.09	0.09
k13	Monte Mario Formation 3			0.2	0.2	0.2	0.2	0.2	0.2	0.2
k14	Alban Hills volcanic 2				1	0.5	0.5	0.5	0.5	0.5
k15	Sabatini Mts volcanic 2				0.1	0.05	0.1	0.1	0.1	0.1
k16	Alban Hills volcanic 3					1.5	none	1.5	1.5	1.5
k17	Ponte Galeria sedimentary("PGT")2					0.1	none	4.2	4.2	4.2
k18	Monte Vaticano Formation 3								0.1	0.1
k19	Monte Vaticano Formation 4									1

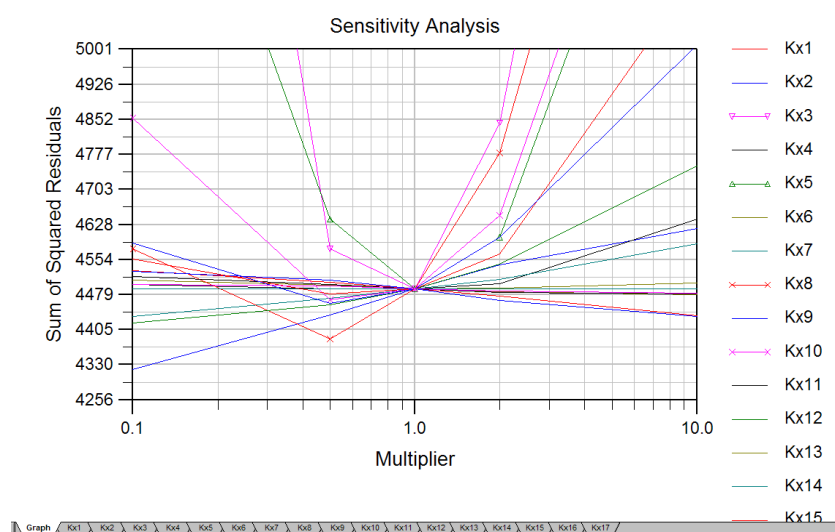


Fig 4.3: Graphic resuming first sensitivity analysis results.

The second Autosensitivity Analysis was carried out on the most sensitive parameters after k value adjustments.

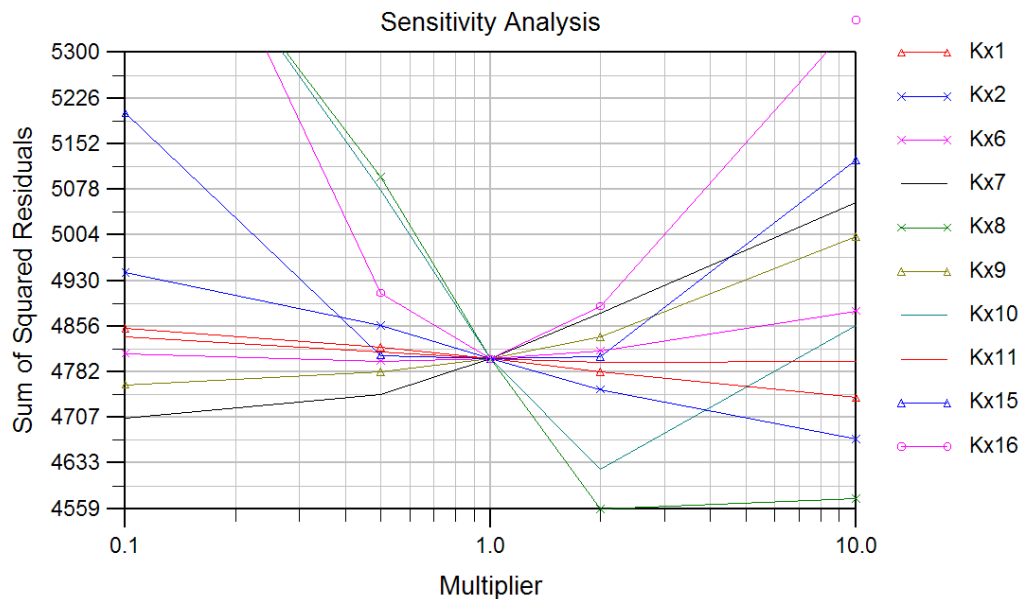


Fig. 4.4: Graph resuming second sensitivity analysis results.

After this second analysis, changes in k values were made for zones **8 - 10 - 16**, which are the most sensitivity parameters for the updated model. Then, also k1, k2, k6, k9, k11 and k15 were changed to test the model with a different set of data. K zones k17 and k18 were added in order to find a better fitting in two areas. The new setting of k zone is in **table 4.3**, step C; resulting statistical indicators are in **table 4.4**.

Tab. 4.4

step C)	
RMS	2.03
RSS	1510
AM	1.74

A fifth run was made after weighting the targets; at first, a weight of 0.5 was assigned to targets which are very close to Tiber and Aniene rivers, and targets which measurement was considered of bad quality. Then, a second weighted-targets calibration was performed, following rules from Hill (1999).

“ the weighting needs to be proportional to the inverse of the variance of the data measurement errors. For a diagonal weight matrix, this means that the weights need to be proportional to one divided by the variance of the measurement errors.[...]”

The statistics used to calculate the weights often can be determined using readily available information and a simple statistical framework. For example, consider an observation well which the measure is considered to be accurate within 5m. To estimate the variance of the measurement error, this statements needs to be quantified to, for example, the probability is 95 percent that the true elevation is within 5 meters of the measured elevation. If the measurement errors are assumed to be normally distributed, a table of the cumulative distribution of a standardized normal distribution (Cooley and Naff, 1990) can be used to determine the desired statistics as follows:

1. Use the table to determine that a 95-percent confidence interval for a normally distributed variable is constructed as the measured value plus and minus 1.96 times the standard deviation of the value.
2. As applied to the situation here, the 95-percent confidence interval is thought to be plus and minus 5 m, so that $1.96 \times X = 5.0$ m, or $X = 2.55$, where X is the estimated standard deviation.

The standard deviation (2.55 m) can be specified and the variance will be calculated, or the variance (6.50 m^2) can be specified.

In the case of this study:

- estimated head error: +/- 5 meters
- standard deviation $\sigma = 2.55$
- variance= $\sigma^2 = 6.5$
- $1/\text{variance} = 0.15$:

So, the weights should be proportional to 0.15.

We obtain the same number by calculating the standard deviation of the residuals of targets put to calibrate the model.

In this study 3 different weights are chosen and used for re-calculate statistics for the calibrated model: 1, 0.60, 0.3.

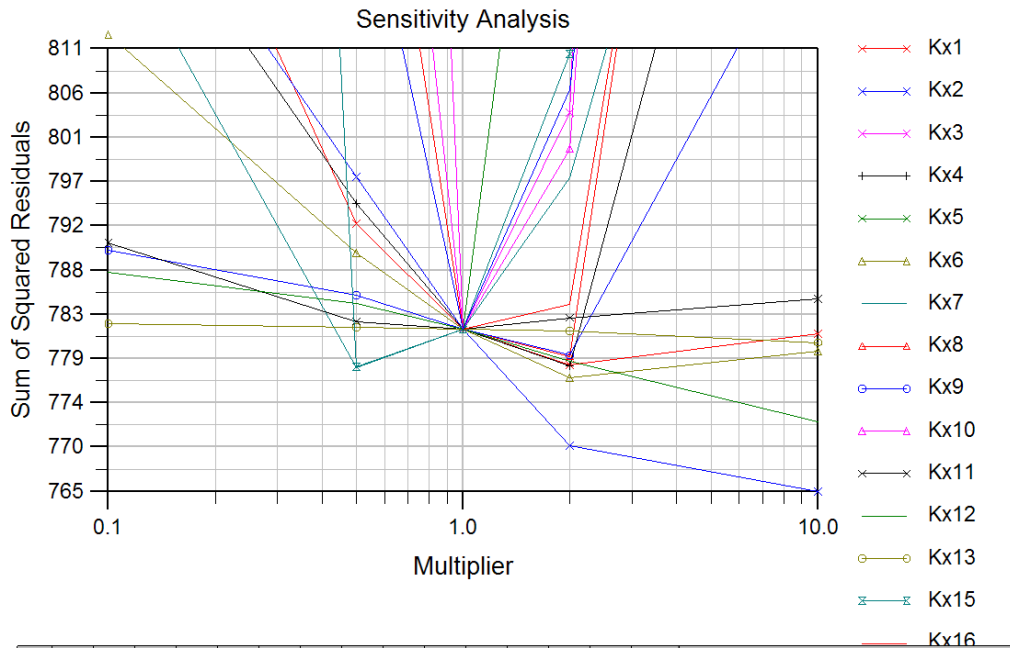


Fig 4.5: result from the third autosensitivity analysis, carried out after the e) calibration step.

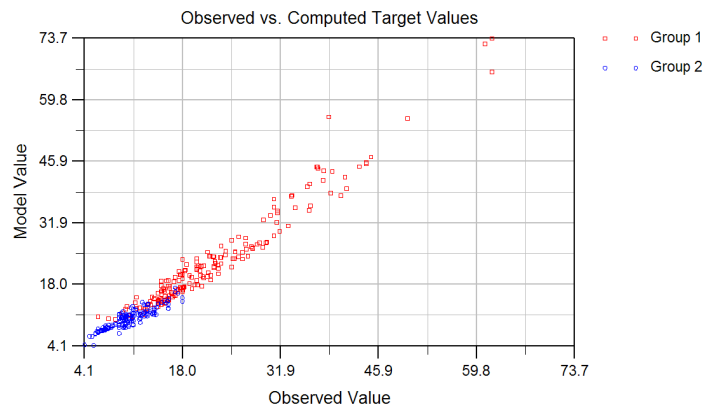
Tab. 4.5: statistic parameters after step E)

step E)	
RMS	1.46
RSS	782
AM	1.25

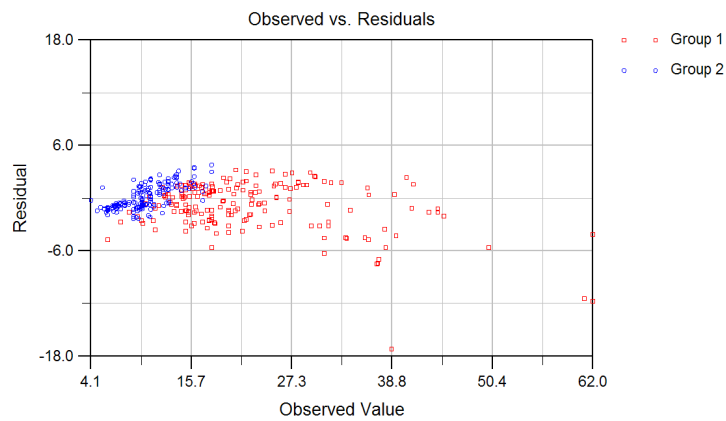
Step F includes the subdivision of head targets in groups :

- Target group n°1: targets located outside the alluvial valley.
- Target group n°2: targets located inside the alluvial valley.

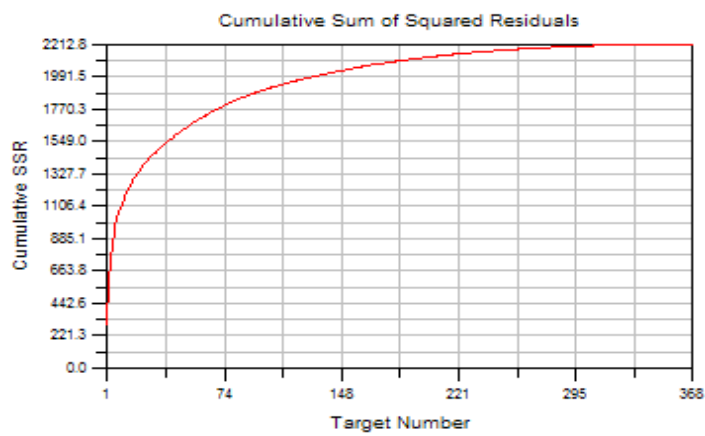
For each group, the value of Residual Standard Deviation, Absolute Residual Mean and RMS error is compatible with the estimation of head error as discussed in chapter 4.3 which is 3 m for *target group 1* and 1.5 m for *target group 2*).



a)



b)



c)

Fig 4.6: updated graphs for k-calibrated model: a) graph observed vs computed heads; b) observed vs residuals; c) cumulative sum of squares.

Tab. 4.6: statistic parameters after steps F) and G)

step G)	target group1	target group2
RMS	3.12	1.36
RSS	1890	324
AM	2.1	1.16

Resuming, k values were updated in the following areas (see **figures 4.7**, and **4.8**):

- area between Prima Porta, S.S. Flaminia and Tiber Valley: the observed piezometric high was simulated by adding the low-permeability zone 16 ($k=0.1$ m/d) in Layers 1 and 2. By this change, the average residuals of targets shows in this area a good lowering, from 10 to 3 m.
- area between Monte Sacro-City Ring Road and Ponte Mammolo: zone 15 was added to layers 1 and 2 in order to obtain a higher head.
- area of Tenuta Boccone, northern than zone 15 ($k=1$ m/d): zone 18 was added in Layer 2 to simulate high permeability facies inside the PGT complex.
- area between Bufalotta-Settebagni-Tiber Valley: the piezometric high was simulated by adding the low permeability zones 11 (in Layer 3) and 19 (Layers 2 and 3). This zones corresponds to a clayey facies recognized in the PGT complex, which is nearly outcropping and influencing the high piezometry.
- area of Trastevere train station: added zone 17 in Layers 1, 2 and 3. This zone has been added to simulate a small outcropping of volcanic complex at the foot of the Monte Mario ridge.
- the area which extends in a NW-SE direction from Parioli neighborhood and the Flaminio stadium, toward Termini Station and Re di Roma square; zone 14 was added in layer 3, to simulate the *Monte Vaticano F.* complex; the value that has been use for this complex ($k=0.01$ m/d) didn't show good results in head simulation, with many dry and flooded cells. The value of 0.1 m/d gave better results.
- area of Monte Mario-Gianicolo ridge; in this area the Plio-Pleistocene structural high is outcropping, constituting the western border of the Tiber Valley. As assessed in the complex description, the ridge is made by an upper part which is the sandy Monte Mario complex until a depth of -10 m a.s.l., and by a lower part, the *Monte Vaticano F.* overconsolidated clay complex. The initial hypothesis was to consider all the ridge with a uniform k , in order to give a very small inflow from the ridge toward the alluvial valley; indeed, sandy Monte Mario ridge was supposed to host a very small aquifer, not connected to the groundwater we are modeling. As the model used to show bad results, a medium permeability was assigned to the uppermost part of the ridge, by adding zones 10, 12 and 13 (respectively $k = 0.2$ m/d, $k= 0.09$ m/d and $k=0.5$ m/d) to layers 1 and 2; in Layers 3, the ridge is simulated wholly by zone 10 (lower permeability). From layer 4 to layer 8, the ridge is only made by the clayey *Monte Vaticano formation* complex.

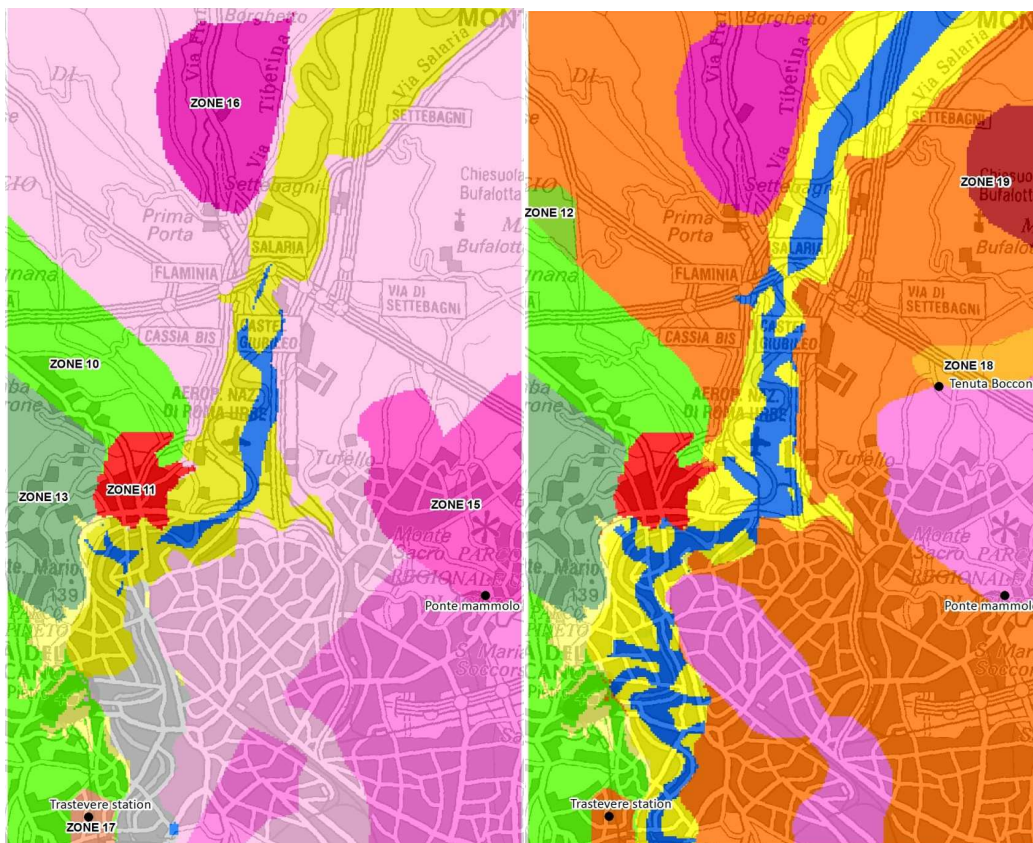


Fig. 4.7: Hydraulic conductivity zones distribution on layer 1 (left) and layer 2 (right).

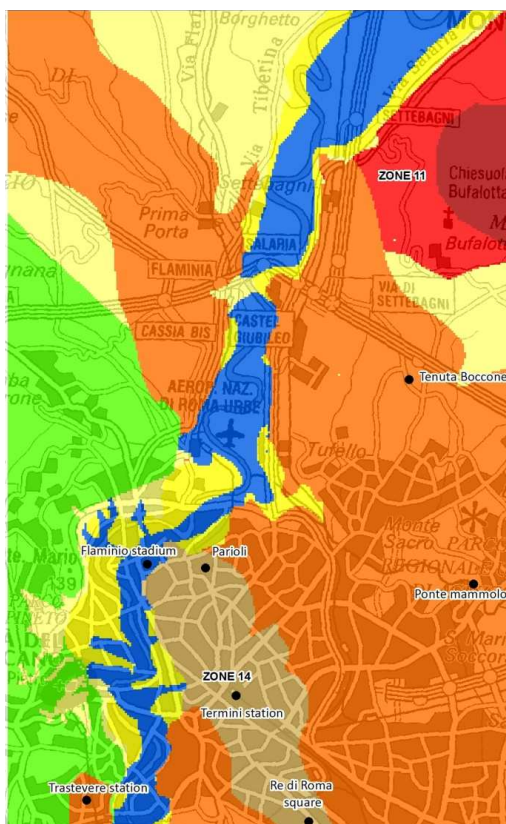


Fig. 4.8: Hydraulic conductivity zones distribution on layer 3

General Head Bc

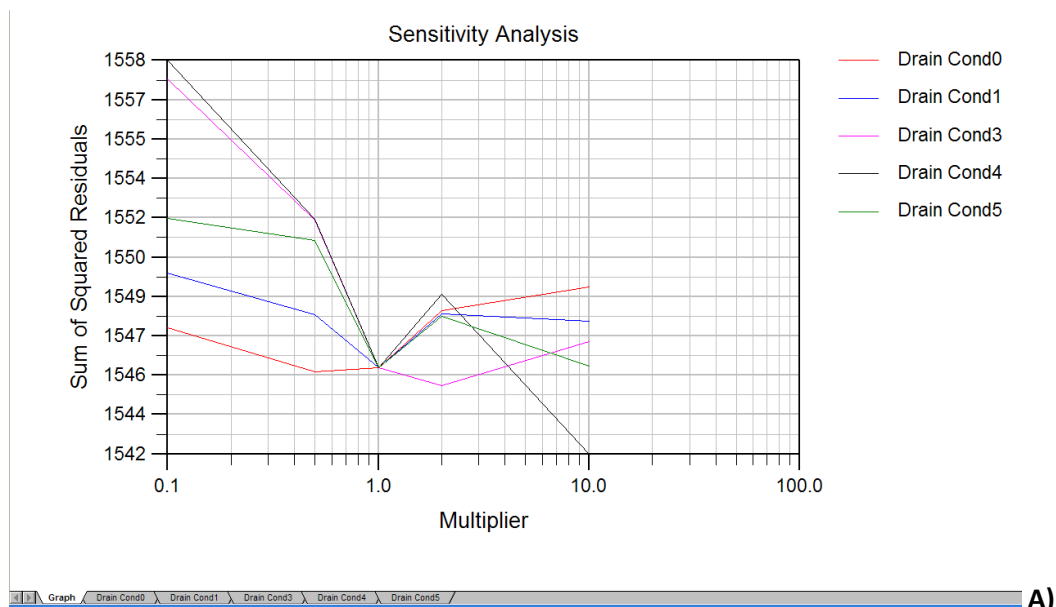
In the calibration phase, also the General Head Boundary's hydraulic conductivity was changed; as explained in **chapter 3.5.2**, k values in GHB were put equal to k assigned for the prevalent complex existing from the model border and the General Head. **Table 4.7** shows initial (k1) and final (k2) values; changes were made after calibration of layer k properties. Because of the negligible differences in target statistic due to this change, GHB conductivity is considered a non-sensitive parameter for the model.

Tab. 4.7: Initial (k1) and final (k2) values chosen for General head Boundary

GHB REACH	k 1(m/d)	k2 (m/d)	complex
1	6.04	9.12	Alban Hills
2	2.13	2.13	Sabatini Mts
3	0.14	1.14	PGT (sandy-gravel prevalent)

Drain Bc

Drain bed hydraulic conductivity was chosen according with the complex on which the drain cell is located; the initial k values were substituted by the calibrated values at the end of the calibration process. A sensitivity analysis has been run, for check drain conductance values; the four reaches used in the model have been multiplied of 0.1, 0.5, 1, 2, 10; results are shown in **figure 4.8** No significant improvements are brought by the analysis; However, a small error reduction is obtained by multiplying the reach n. 3 (drain conductance of streams flowing on "PGT" complex) times 2, that is Conductance=2.8 m/d (**Tab 4.8 and 4.9**).



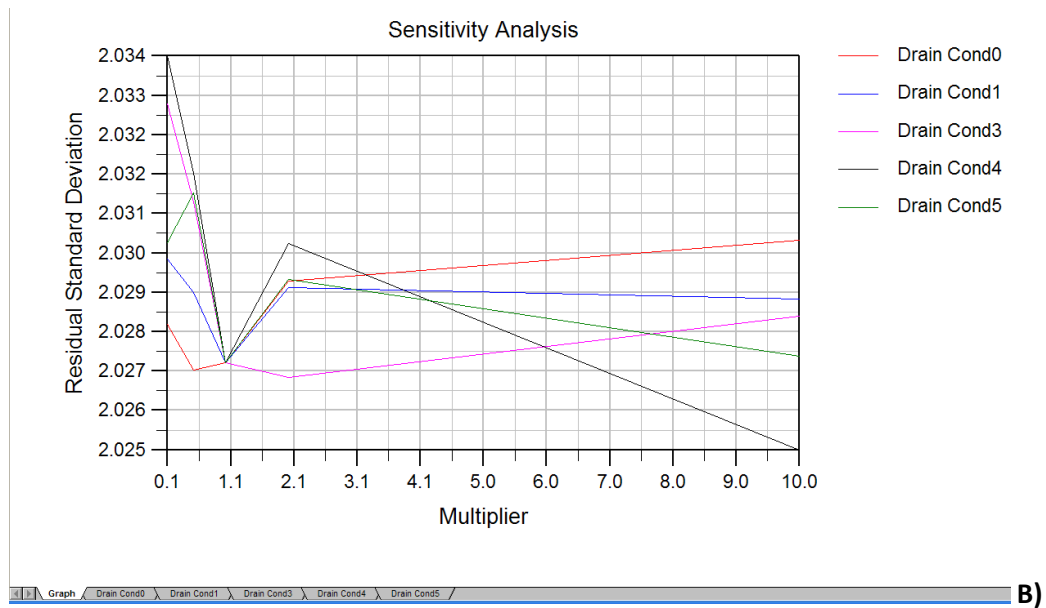


Fig. 4.8: plots of drain bed k autosensitivity analysis results; A) Sum of squared residuals; B) Residual Standard deviation. A small improvement of result is brought by doubling the value of drain conductance in reach n.3.

The last model run, with updated reach n.3 drain conductance, shows a lowering of ARM, RSS and RMS error calculated on target group number 1, while the statistic table remains the same for group target number 2, since no reach n.3 drains are present in the Tiber Valley.

Tab 4.8: drain bed hydraulic conductivity initial (K1) and final (k2) values

reach	K1 (m/d)	K2(m/d)	complex
0	9.12	9.12	Alban Hills
1	2.13	2.13	Sabatini Mts
3	1.4	2.8	PGT (sandy-gravel prevalent)
4	1	1	PGT (clay prevalent)
5	0.5	0.5	alluvium clay

Tab. 4.9: static table for group target number 1 with updated reach n.3 drain conductance value.

DRAIN	Target GROUP 1	Target GROUP 2
RMS	2.55	1.36
RSS	1220	324
AM	1.93	1.16

Recharge

The last step was recharge calibration; this was performed by two actions:

- a) The first assumption of a recharge equal to zero in **urban areas** (see chapter **3.5.1**) gave as a result a too low simulated head (head target residuals around 10 m), with many dry cells on the first layer. By assuming a recharge higher than zero, that in urban areas can be due to several sources (chapter **3.5.1**), a general decrease of residuals can be observed; since no field data are available, recharge on urban areas was assigned by the calibration process listed below (see also **table 4.10**):
- the first run was performed by using the value calculated for water main leakage ($2.05\text{E-}07$ m/d, *simulation n°2*, **tab 4.10**); target residuals shown high negative results, so that the initial value was considered too low.
 - in order to include also the contribute from rainfall infiltration and over-irrigation, the urban area recharge was increased and 3 simulations were performed, with values $2.52\text{E-}05$, $2.52\text{E-}04$ and $2.52\text{E-}03$ m/d; the results are *simulations n°2, 3, 4* in **table 4.10**.
 - The best value was found to be close to $2.52\text{E-}04$ m/d; *simulation n°5* was performed after doubling this value to check its accuracy.
 - The discrepancy between observed and calculated target values shown different best results for head target group 1(outside the valley) and 2(inside the valley); for this reason head target were portioned in two different groups and several runs were made to find the best recharge values.
- b) In order to test the accuracy of the assigned recharge in **non-urban areas**, five model runs were performed: one with the initial calculated values, two with a 10% and 20% decreased recharge, and two with a 10% and 20% increased recharge; the statistic for head target is more satisfying in the case of 20% decreased recharge, so that this was chosen as final recharge rate. (see **table 4.11**).
- c) Other runs were performed to better calibrate the recharge, both in urban and in non-urban areas: in **table 4.12** the most significant four steps are shown; the resulting best values are 0.0008 m/d for recharge in urban areas inside the Tiber Valley, while it is 0.00025 m/d for urban areas outside the Tiber Valley; in the area inside the Valley which extends from the City Ring Road to the north to Tor di Quinto to the South, too high target residuals were simulated; this area is occupied by sport centers, the military airport and the wastewater treatment plant "Roma Nord", and a lower recharge should be due to the less percentage of leaking mains. In order to low the water table, a decreased recharge was set in this area, by adding a zone with $\text{RCG} = 0.00005$ m/d (Zone 3, on **figure 4.9**).

Tab 4.10: The table shows the results of model statistic in the 10 *simulations* of recharge in urban areas calibration. Best results were obtained by grouping the urban areas in 2 zones(1 and 2) with different recharge rate. (RSS= Residual Sum of Squares; RMS= Root Mean Squared; arM= Absolute Residual Mean; maxR= maximum residual, m; minR=minimum residual, m).

n	PARAMETER	RCG urban m/d	RSS_1	RSS_2	rms_1	rms_2	arM_1	arM m_2
1	RCG_e-07	0.000000252	4850	428	5.08	1.57	3.76	1.25
2	RCG_e-05	0.0000252	4400	392	4.84	1.5	3.62	1.22
3	RCG_e-04	0.000252	1390	255	2.73	1.21	2.14	1.07
4	RCG_e-03	0.00252	4840	8980	5.07	7.18	3.62	5.51
5	RCG_5*e-04	0.0005	1220	498	2.56	1.69	1.94	1.46
6	RCG_2 zones	zone 1= 0.0002 zone 2= 0.0001	1360	284	2.71	1.28	2.06	1.12
7	RCG_2 zones	zone 1=0.0003 zone 2=0.0001	1350	335	2.69	1.39	2.06	1.19
8	RCG_2 zones	zone 1=0.0003 zone 2=0.0002	1380	548	2.73	1.78	2.09	1.52
9	RCG_2 zones	zone 1=0.00025 zone 2=0.0001	1080	933	2.41	2.32	1.86	1.88
10	RCG_2 zones	zone 1=0.00025 zone 2=0.0005	1070	1020	2.4	2.42	1.85	1.88

Tab. 4.11: values of Root Mean Squared (RMS), Absolute Mean Error (AM) and Residual Sum of Square (RSS) for different recharge rates; the recharge rate which lowers the discrepancy between simulated and observed heads is the one with a 20% decrease respect to the initial recharge values.

		% of rcg decrease		initail RCG	% of rcg increase	
		10%	20%		10%	20%
group 1	RMS	2.7	2.23	2.4	3.17	2.2
	AM	2.17	1.75	1.85	2.49	1.74
	RSS	1360	923	1070	1870	897
group 2	RMS	2.49	1.57	2.42	2.31	2.57
	AM	1.92	1.3	1.88	1.81	1.98
	RSS	1080	427	1020	927	1150

Tab. 4.12: synthetic table showing the most relevant recharge calibration steps. The four described runs (a,b,c and d), were performed with a decrease of 10 and 20% of non-urban areas initial recharge rate; the zone 1 and 2 represent recharge in urban areas; zone 1 represent recharge inside the Valley, while zone 2 is for urban areas outside the Valley. Zone 1 was maintained constant during the four steps, while the value for zone2 was changed. Zone 3 was added in the last run. The best statistic result is for step d, with zone 2= 0.0008 and zone 3=0.00005 and a decrease of non-urban recharge of 20%.

simulation	zone1 m/d	zone2 m/d	zone3 m/d	RMS	AM	RSS	RCG decrease	target group
a	0.00025	0.00005	-	2.7	2.17	1360	-10%	1
				2.49	1.92	1080	-10%	2
b	0.00025	0.00005	-	2.2	1.74	897	-20%	1
				2.57	1.98	1150	-20%	2
c	0.00025	0.0006	0.00005	2.23	1.75	923	-20%	1
				1.57	1.3	427	-20%	2
d	0.00025	0.0008	0.00005	2.3	1.82	982	-20%	1
				1.43	1.17	357	-20%	2

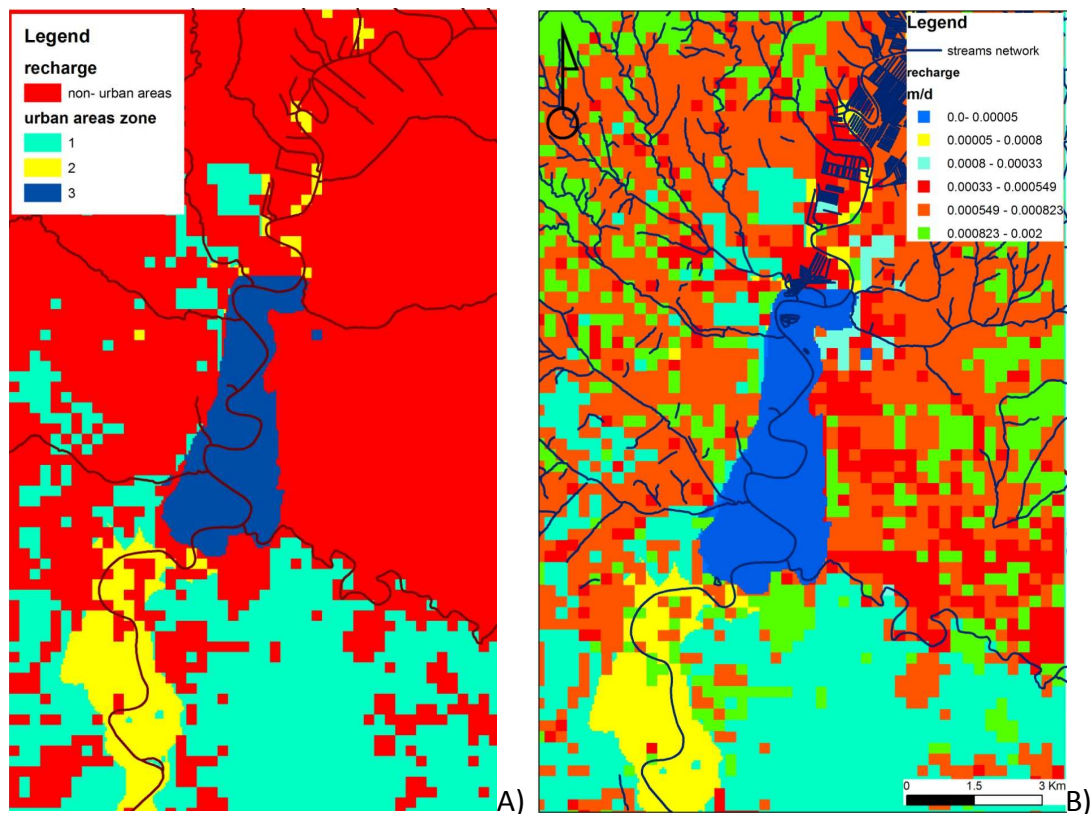


Fig 4.9: A) Zone 1: urban areas located outside the Tiber Valley. Zone 2: urban areas located inside the Tiber Valley Zone 3: Area between the city ring road and Tor di Quinto. Red cells represent not-urbanized cells. Recharge values: zone 1= 0.00025; zone 2=0.0008; zone 3= 0.00005 m/d; B) final assigned recharge (m/d).

The spatial distribution of weighted water-level residuals is in **Fig 4.10**. In an ideal calibrated model, negative and positive should have a random distribution; concentrations of totally positive or negative residuals indicate zone of high difference between simulated and observed head; that's what can be observed in the Tiber valley, between Castel Giubileo and Urbe airport, where a group of negative residuals indicate that in this zone the model doesn't fit the aquifer system .

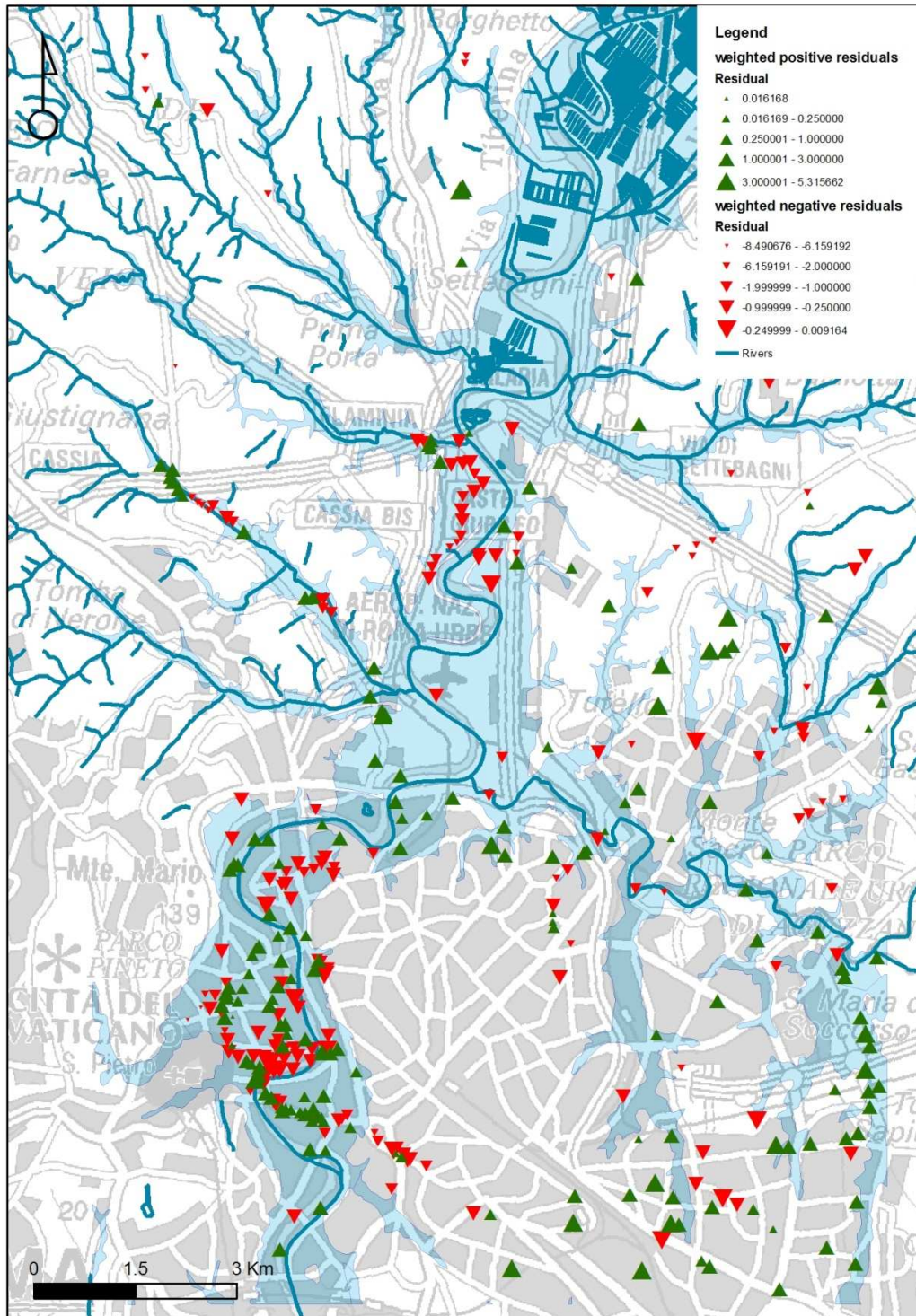


Fig. 4.10: Spatial distribution of weighted water-level residuals.

5 Model results

5.1

Simulated water table

Simulated head contours were compared with contours from Capelli et alii, 2005 (**fig. 5.1**); it must be said that contours from Capelli et alii, 2005, are man-drawn, so that the contours geometries are subjected to interpretation, and no perfect correspondence is expected between observed and simulated. Simulated and observed heads are well-comparable at the model's boundaries, with maximum head in meters a.s.l. on the western boundary; in the northern portion, head reaches 85-90 m a.s.l., while southern, along the Monte Mario-Gianicolo ridge, it reaches 70 m a.s.l..

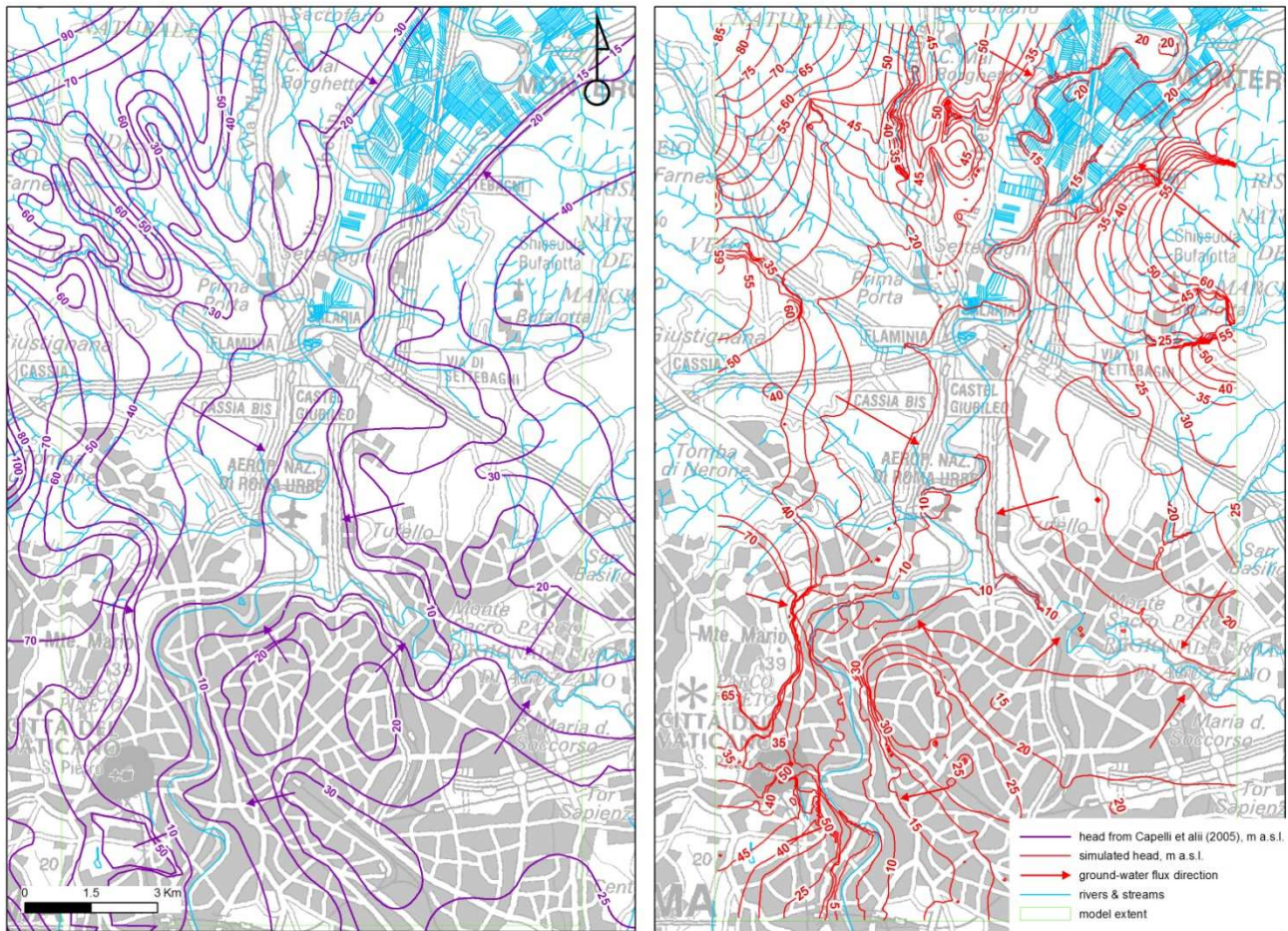


Fig. 5.1: Observed (from Capelli et alii, 2005) vs simulated head, in meters a.s.l.

Going on in a eastern direction, the observed head contour makes complicate convolutions due to the streams incisions, which are only partially reproduced by the simulated head. In both the piezometric contour maps, head reaches the elevation of 20-10 m a.s.l. along the Tiber and Aniene

valleys borders. Head contours are quite different in the north-east area; in the observed one, head decreases from 40 m a.s.l. along the boundary, to 15 m at the Tiber Valley border, while in the simulated head contour map, head is higher on the model's boundary and the hydraulic gradient is higher. Anyway, the simulated head contours conformation is retained to be acceptable, since it has been calibrated with head target. The south-east area is characterized by a piezometric high (20-30 m a.s.l.) in the Termini- Piazza Bologna area; then, the water table decreases towards Tiber and Aniene sinks, reaching the elevation of 10 m a.s.l..

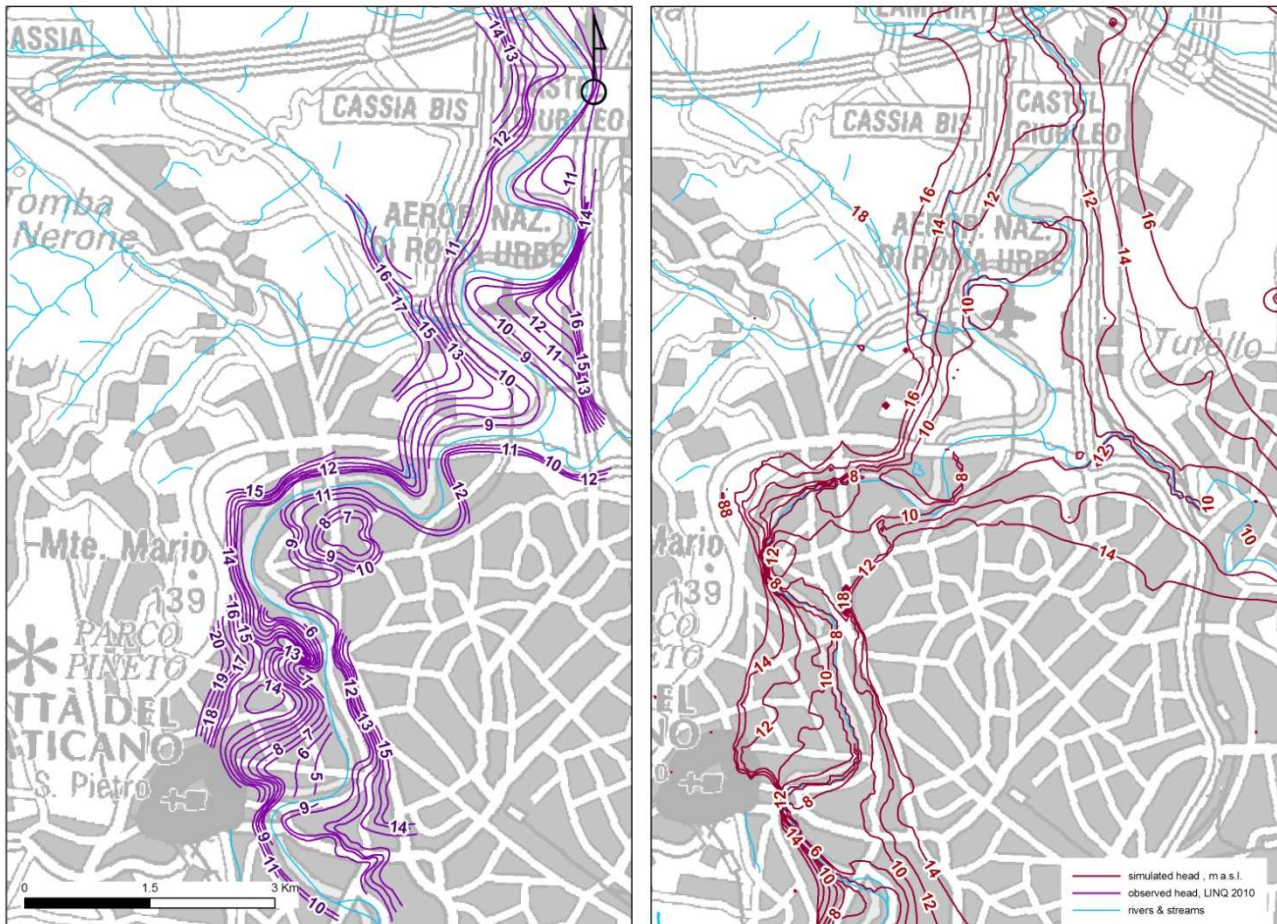


Fig. 5.2 Observed (from LINQ, 2010) vs simulated average head, in meters a.s.l.

Focusing on the Tiber Valley(**Fig 5.2**), simulated head has been compared with the observed head (from LINQ field measurements, 2010); in the southernmost area, between Tor di Quinto and Tiberina Island simulated and observed head are similar, despite of the strong perturbation of the water table; the discrepancy becomes higher close to the Tiber River, where there is the highest head variability due to the strong hydraulic connection between groundwater and the river. In the northernmost portion, between Castel Giubileo and Tor di Quinto, the discrepancy becomes higher; the simulated hydraulic gradient is lower than the observed. This is due to the low number

of data (drilling and head measurements) that increases the uncertainty on the calibrated simulated head.

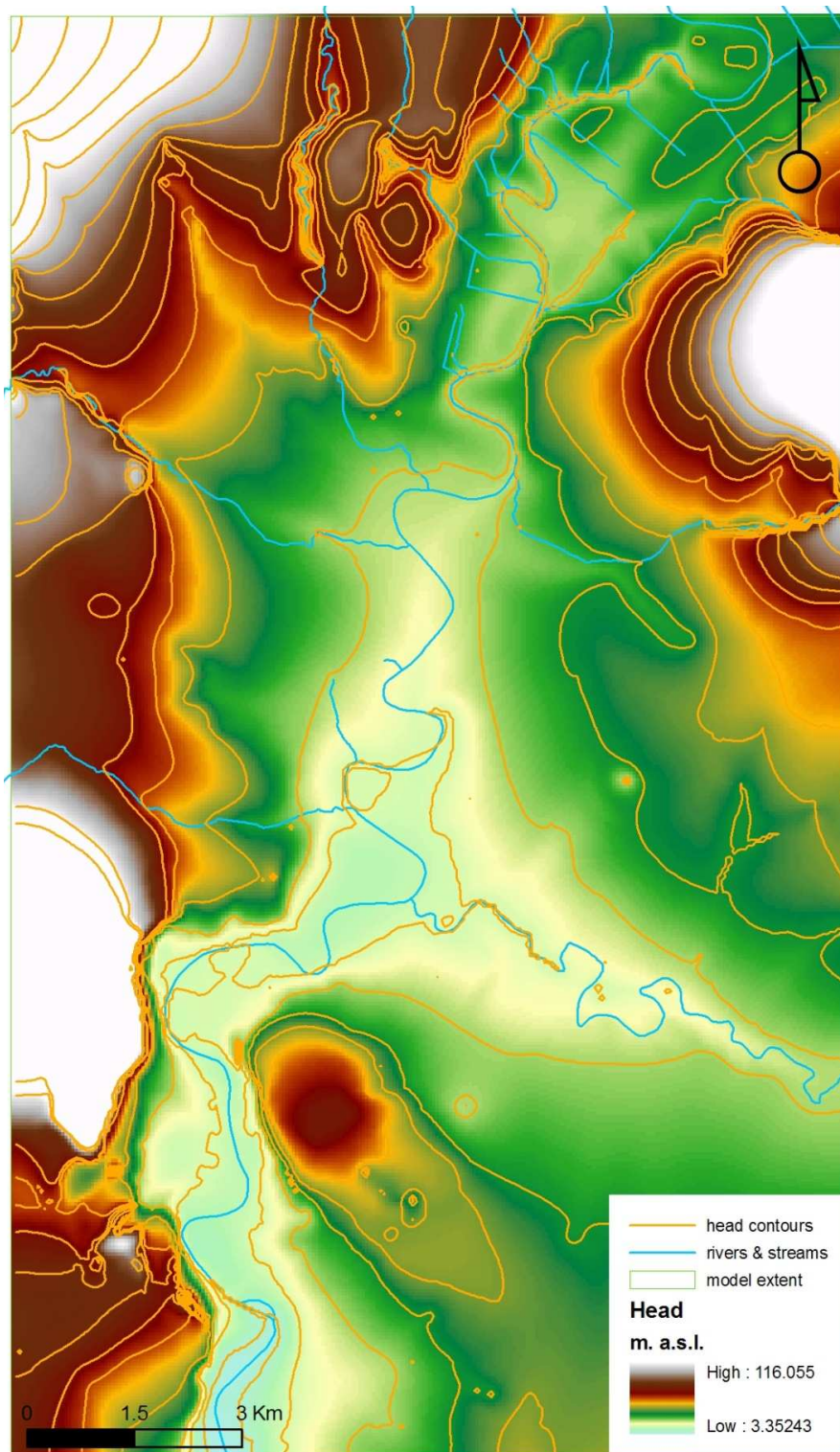


Fig 5.3: color flood representation of simulated head

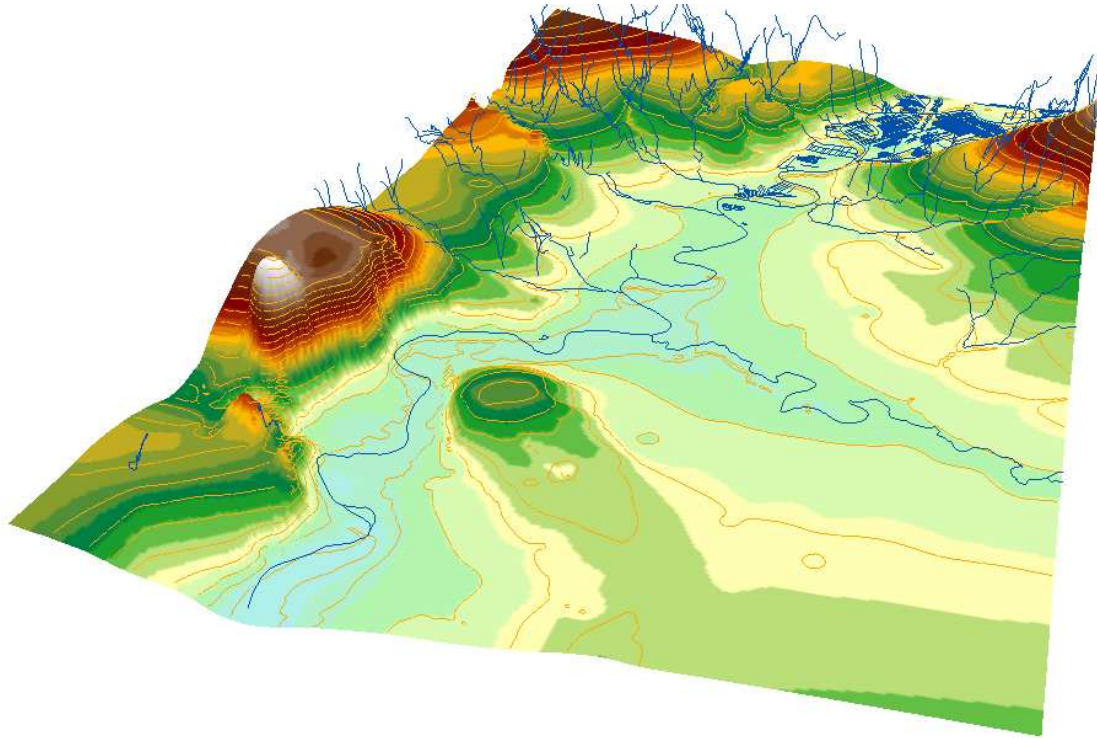


Fig. 5.4: tri-dimensional color flood representation of simulated head; color flood scale is in **Fig. 5.3**

Water budget

Table 5.1 lists the 10-year average water budget for the aquifer system. The total effective infiltration over tributary basins (443808 m/d) corresponds to the groundwater flow from tributary basins to the Tiber Valley basin (see **chapter 2.5**). Tributary basins mostly extend externally to the model area (**chapter 2.4.4**), and part of the ground-water feeds the Tiber and Aniene rivers; outflows from basins to the main rivers (16% of effective infiltration, 270652 m/d) has been quantified by subtracting to the total effective infiltration over basins, the total simulated flow through the model (without accounting the recharge due to anthropic factors, occurring in urban areas). Moreover, the groundwater inflow through boundaries to the model (54615 mc/d) has been evaluated by subtracting to the total groundwater effective infiltration over tributary basins, (net of outflows to main rivers) the recharge (due to precipitation, in non urban areas) occurring just over the model's area (94691 m/d):

basins total effective infiltration - recharge over the model's area - outflows from basins to the main rivers (externally)= groundwater inflow through boundaries

$$443808 - 94691 - 270652 = \underline{54615 \text{ mc/d}}$$

Tab. 5.1: estimated 10-year(1997-2007) average water budget for the study area.

parameter	mc/d
total effective infiltration over tributary basins (not calibrated)	443808
outflow from basins to main rivers (externally to the model)	270652.1286
groundwater inflow through boundaries	54615.87135
recharge in not urban areas (min 20%)	94691
recharge in urban areas	24375.87135
total model recharge	119066.8714
total streams baseflow (*)	89847
withdrawals	28146.5
(*)Tiber and Aniene rivers not accounted.	

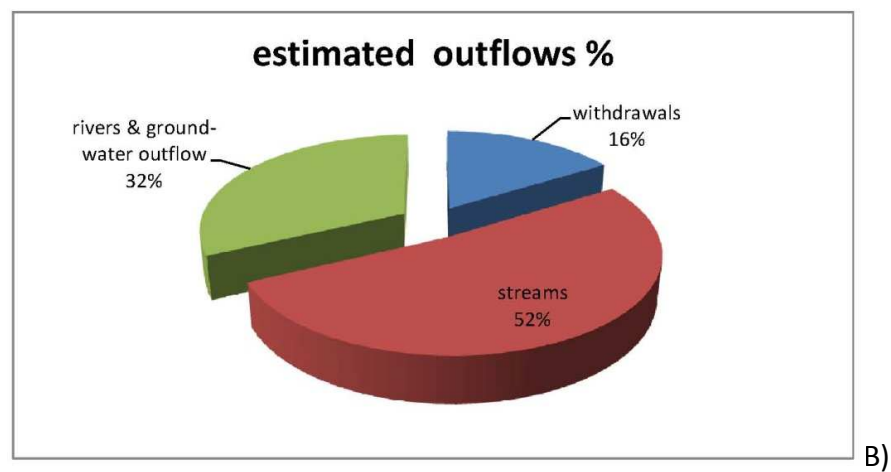
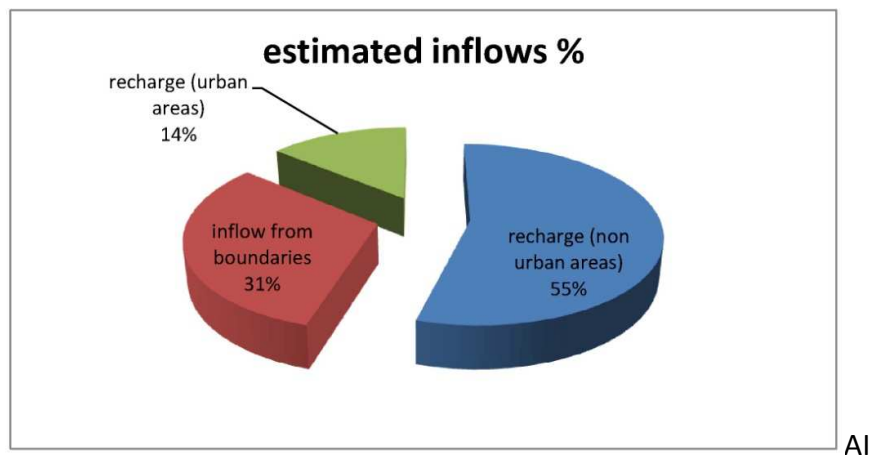


Fig. 5.5: Percentages of estimated flows. A)inflows; B) outflows

The water balance is calculated as:

$$\text{TOTAL RECHARGE} + \text{INFLOW FROM BOUNDARIES} - \text{STREAMS BASE FLOW} - \text{WITHDRAWALS} = 55689 \text{ m}^3/\text{d}$$

55689 m³/d is the amount of water which is calculated to outflow from the system both by surface water and ground water (plus or minus a 20% of error); **Fig 5.4** shows a schematic evaluation of inflow/outflow contributes to the model; inflows are: recharge (natural and due to anthropic factors in urban area), inflows from tributary basins through model's boundaries. Outflows are: outflow to rivers and streams, withdrawals.

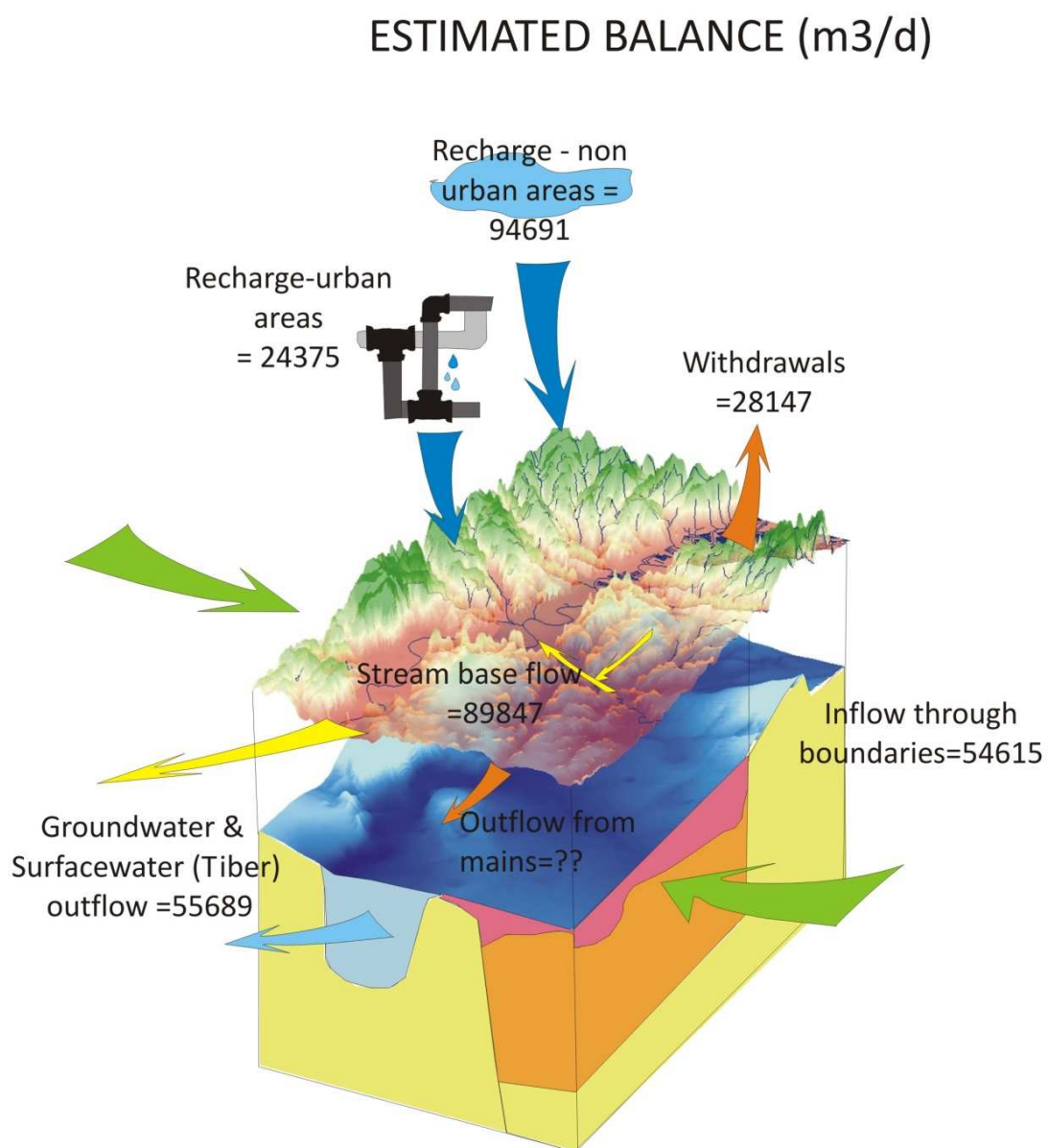


Fig. 5.4; estimated water balance

Comparing aquifer's estimated water budget and model's simulated Mass Balance

The option available in GwVistas ® **Plot>Mass Balance** computes inflow/outflow budget for the entire model, for each single layer, for a chosen polygon or for a given hydrostratigraphic unit. The total simulated flux through the model is 148750 m/d (this amount doesn't include outflow from multi-node wells, which is 1888.88 mc/d); inflows comes from recharge (77%) and General Head Boundary (23%), while outflows are mainly toward drains (63%) and rivers (26%) and then withdrawals from wells (11%). (tab 5.2, fig. 5.6, 5.7a and b)

Tab. 5.2: model simulated inflows/outflows

Category	Flux m/d	Category	Flux m/d
RECHARGE	114076.2421	RECHARGE	0
WELL	0	WELL	-16406.34205
RIVER	52.73271716	RIVER	-39131.63918
DRAIN	0	DRAIN	-93030.09246
GHB	34621.38915	GHB	-212.0975031
ERROR	-29.80723248	ERROR	0
total	148750.36	total	148780.17

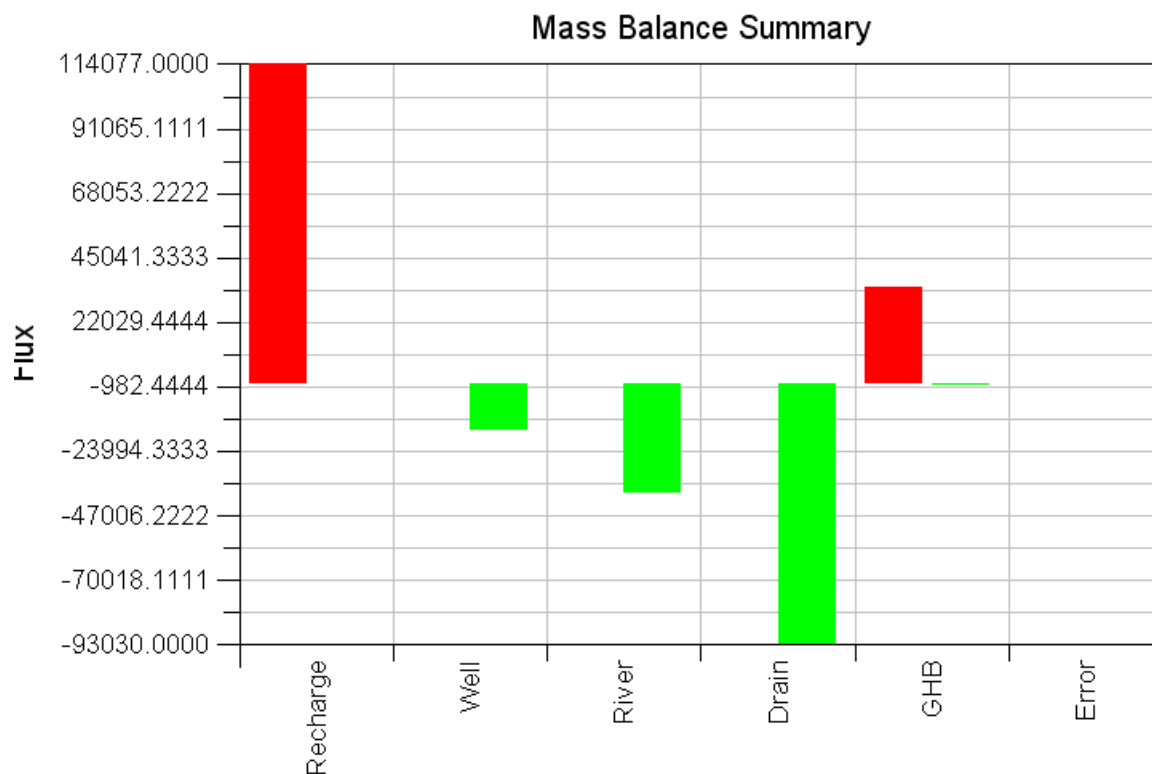


Fig 5.6: model simulated inflows/outflows histogram

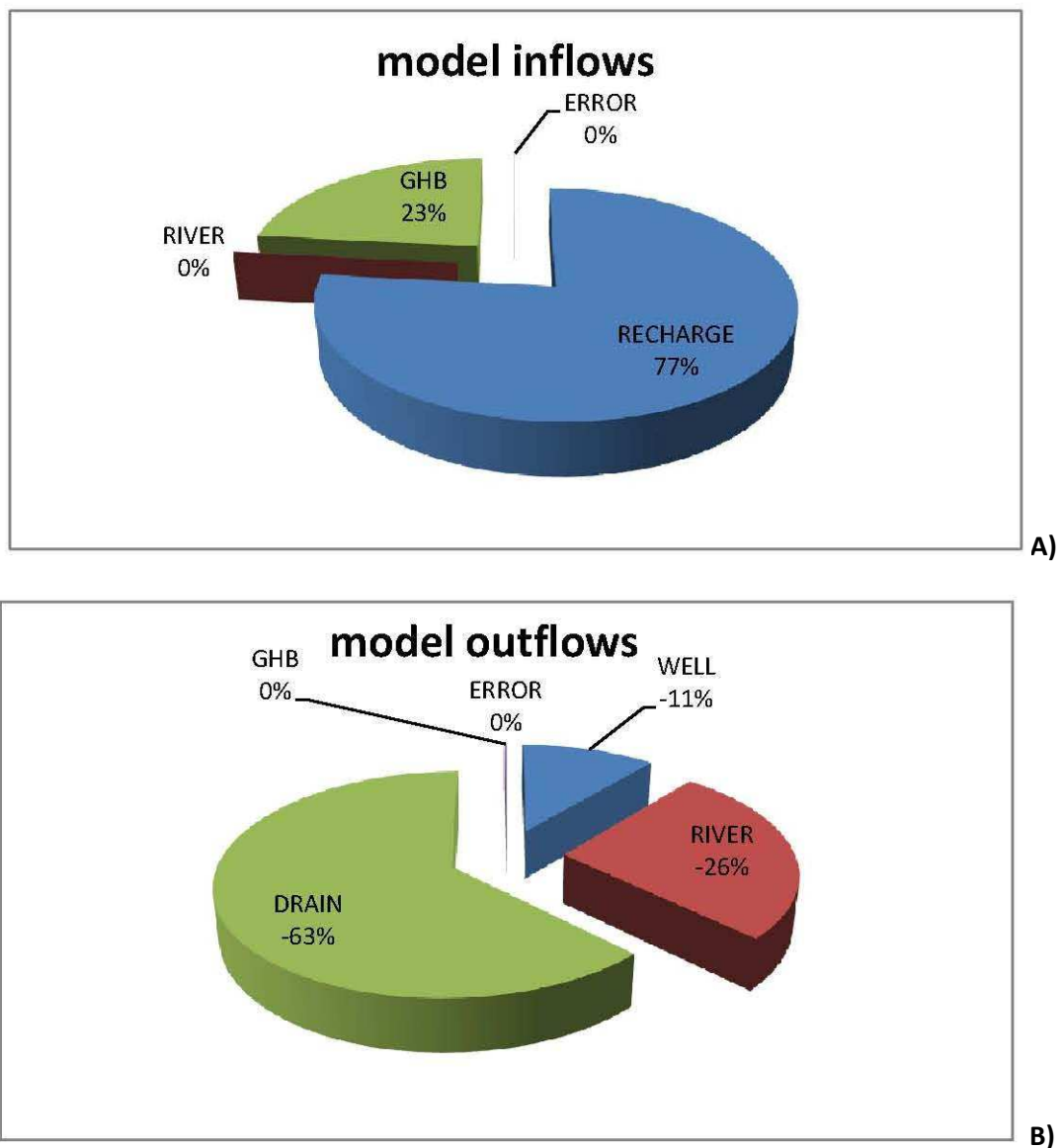


Fig 5.7: Percentages of simulated flows A)inflows; B) outflows

Model's result are listed in table 5.2

The model's simulated water balance is calculated as follows:

**Groundwater inflow trough General Head boundaries + total recharge –withdrawals – drains outflows -
Aniene river outflow = 34621 + 114076 - 16318 – 93471 - 9258 = 29650 m/d**

The result (**29650 m/d**) is the amount of 1997-2007 years averaged outflow from the model both by surface flow (Tiber River) and groundwater flow, plus or minus a calculated error of 20% (that is 8895 m/d).

Table 5.2: summary of model's simulated results

parameter	m3/d
total flow through the model	148780
groundwater inflow through General Head b	34621
<i>recharge in not urban areas (min 20%)</i>	<i>89700.12865</i>
<i>recharge in urban areas</i>	<i>24375.87135</i>
total model recharge	114076
groundwater outflow from General Head b	226
total withdrawals (*)	28146.5
withdrawals (WELL package)(*)	16318
withdrawals (MNW package)(*)	1888.88
drains outflow	93471
Tiber river outflow	29631
Aniene river outflow	9258
total drains + rivers outflow (**)	132161
(*)MODFLOW'S Mass Balance withdrawal doesn't account pumping rate simulated by the Multi-Node Well package (1888.88 m3/d) (**) Tiber and Aniene rivers accounted.	

Simulated water balance contributes are sketched in figure 5.8;

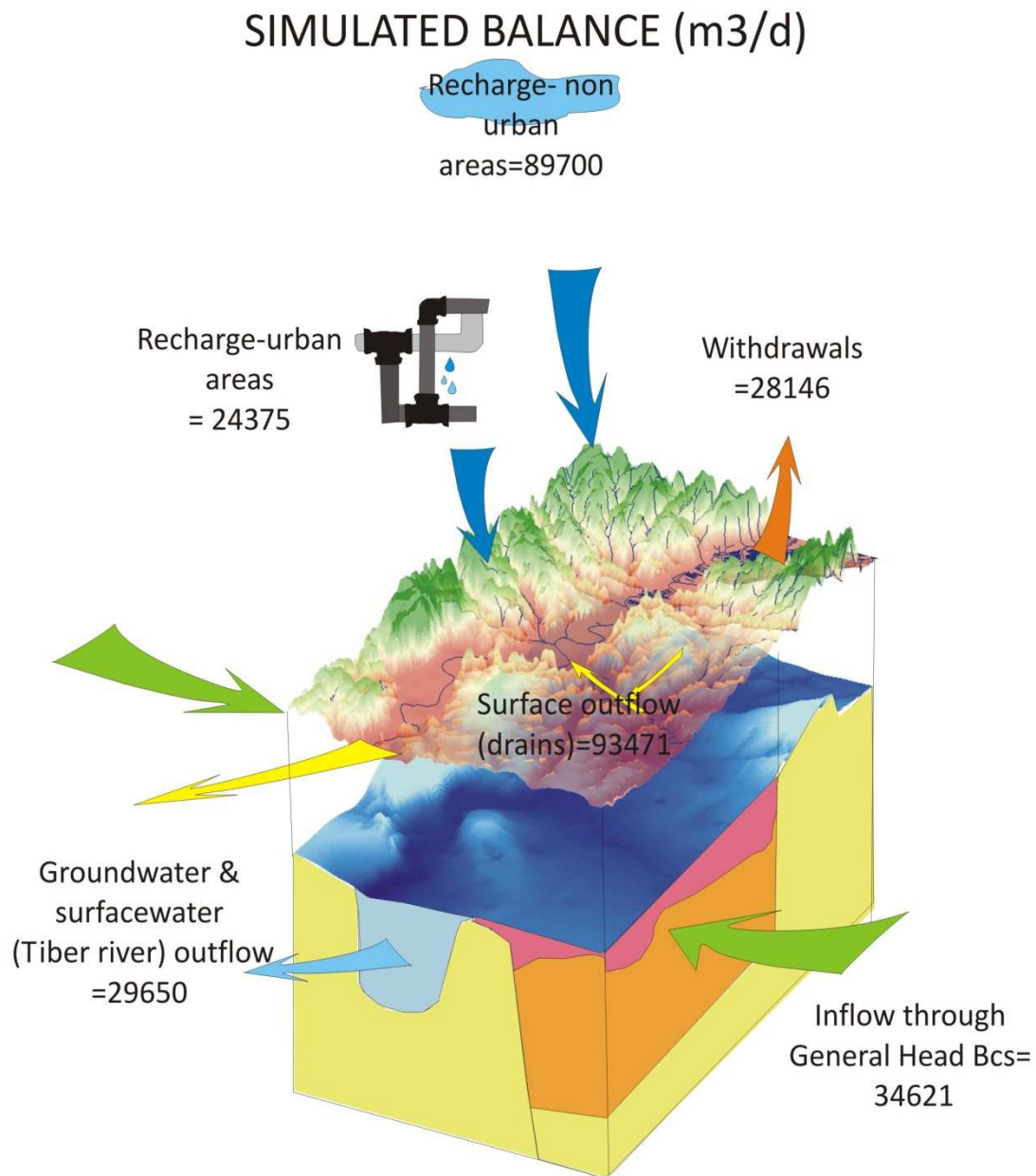


Fig. 5.8: Sketch of simulated inflows/outflows

To examine simulated mass balance for each complex, the model has been subdivided into hydrostratigraphic units (HSU), which were set coincident with the hydrogeological complexes. Then, the Mass Balance function was calculated on the Tiber Valley (**Plot>Mass Balance>Hydrostratigraphic Units**). For each HSU, simulated inflows and outflows averaged on the computational period (1997-2007) are given.

Mass Balance graphs show that inflows to volcanic complexes comes mainly from recharge, and high outflows are from drains; this is because Volcanic complex is set as the topmost layer (layer

1), and its top is coincident with the topography. Simulated results show high water exchange with “PGT” complex, both as inflows (around 30000 m³/d) and outflows (38000 m³/d)(Fig 5.9).

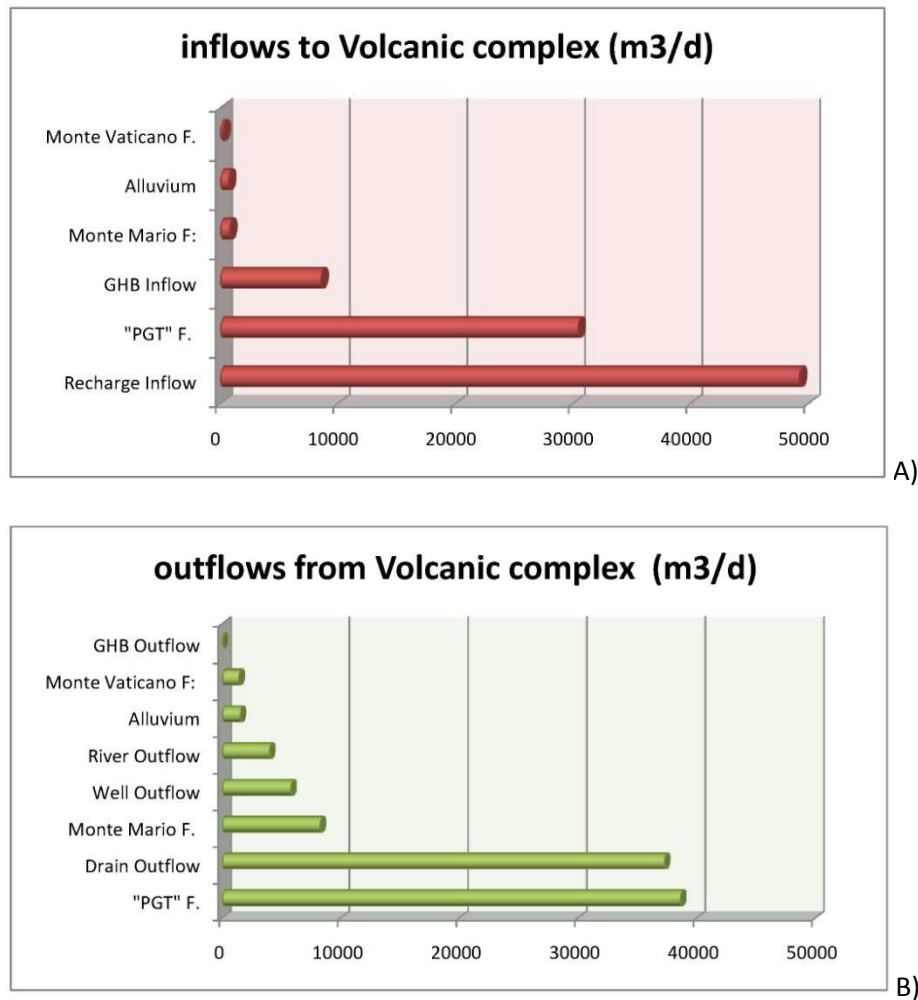


Fig. 5.9: volcanic complex inflows/outflows (m³/d)

The “*Ponte Galeria*” formation complex is mostly fed by volcanic complex, by the model’s recharge and by the General Head boundaries; main outflows from “PGT” complex are toward the volcanic complex and toward drain.

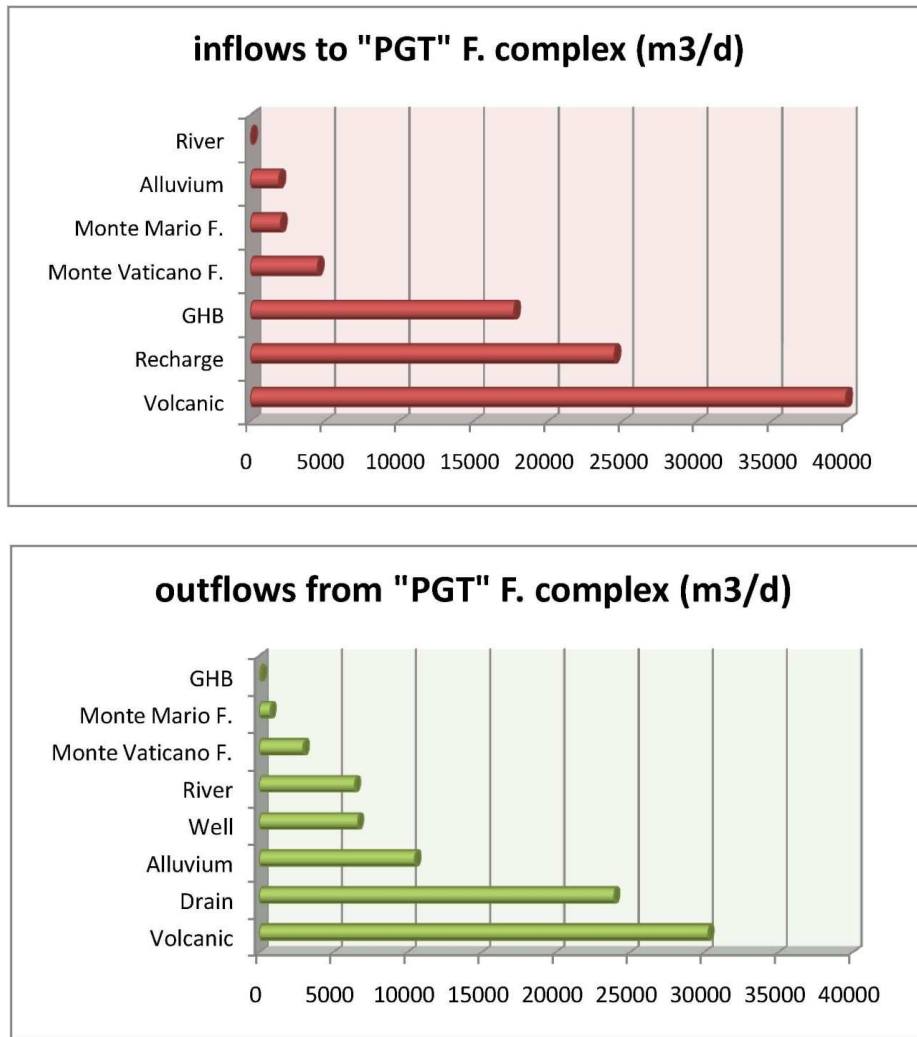


Fig 5.10: "PGT" complex inflows and outflows

In **Fig. 5.11**, Mass Balance for the alluvial complexes is shown; the main groundwater exchange occurs for each HSU with the other alluvial complexes. **Table 5.3** resumes the water balance for the alluvial valley; main inflows comes from aquifers surrounding the valley and mostly from the "*Ponte Galeria*" F. complex, while main outflows are water losses to Tiber River.

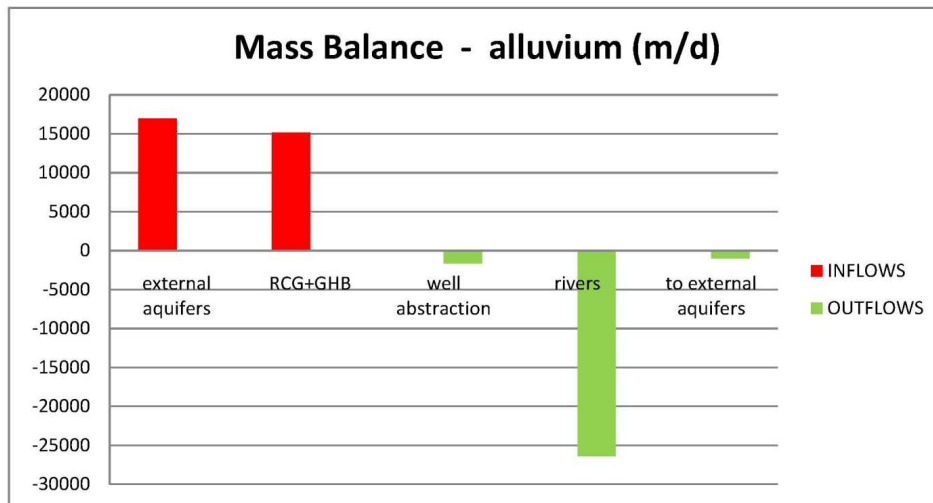


Fig 5.11: Mass balance for alluvium complex

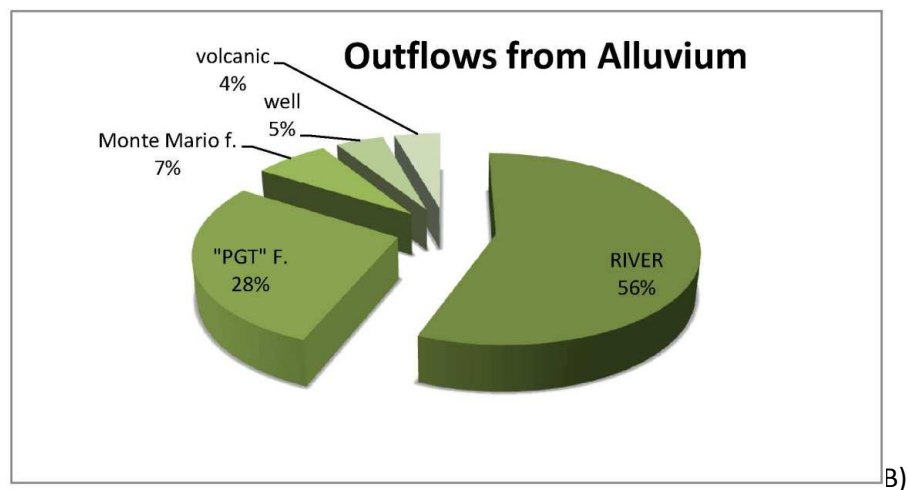
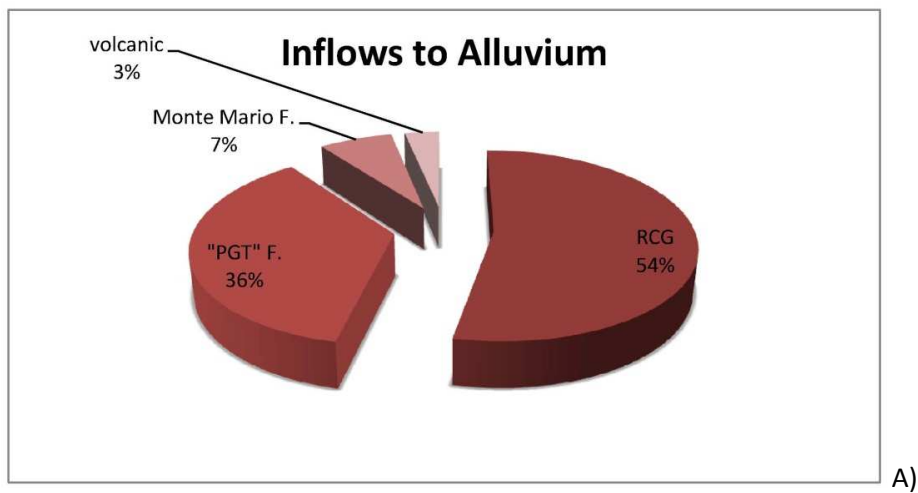


Fig. 5.12: Percentages of simulated flows in Tiber alluvium A)inflows; B) outflows

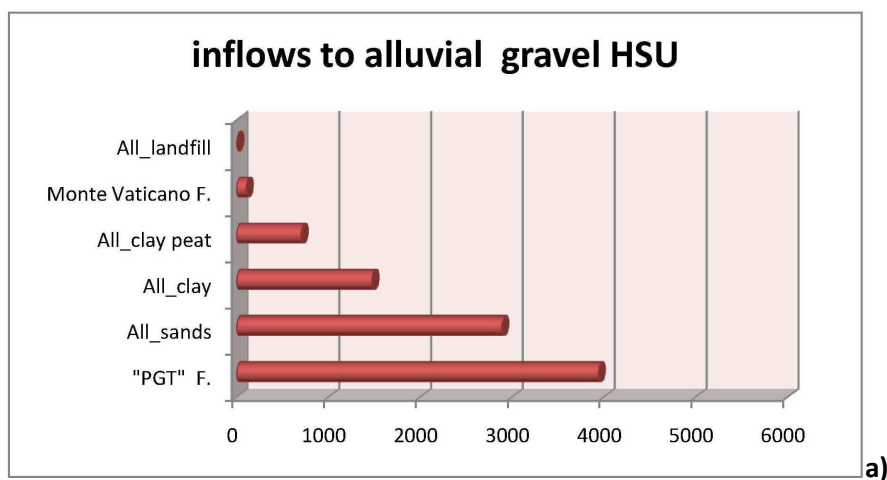
Tab 5.3: Alluvium Mass Balance

water budget for alluvial valley			
inflow contribute		outflow contribute	
external aquifers	16586.09	well abstraction	1634.0319
RCG+GHB	15175.72	rivers	26367.66
		to external aquifers	3300.00
tot inflow	31761.81	tot outflow	31301.69
ERROR=		460.12	mc/d

Regarding the Alluvial Gravel complex, its groundwater budget is simulated as 9142 m³/d (**table 5.4**). Main inflows are from the “PGT” F. complex; main outflows are toward the alluvial sandy complex; this result suggests a prevalence of upward vertical gradient in the alluvium complex, directed to the Tiber river.

Tab. 5.4

water budget for Alluvial Gravel			
inflows		outflows	
from external aquifers	4054.61	to external aquifers	947.27
from other alluvium units	5086.74	to other alluvium units	7921.9731
		well abstraction	275.3948
total inflow	9141.36	total outflow	9144.63
difference=		-3.28	



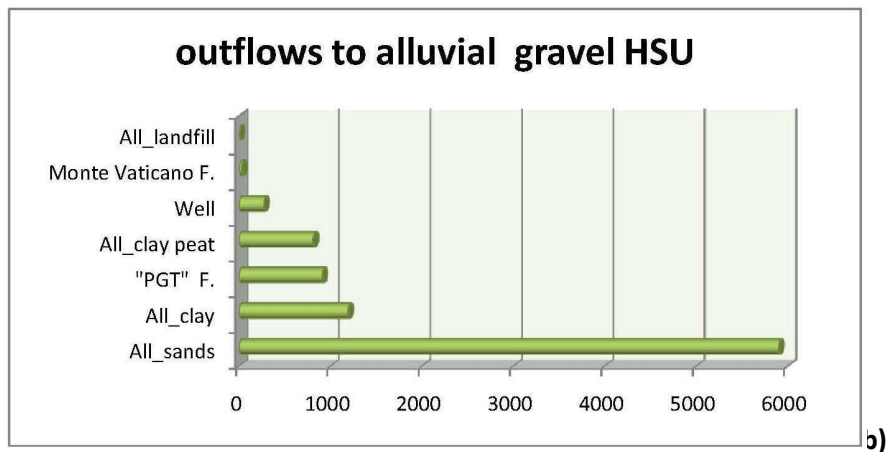


Fig. 5.13: alluvial gravel inflow/outflow histograms (m3/d)

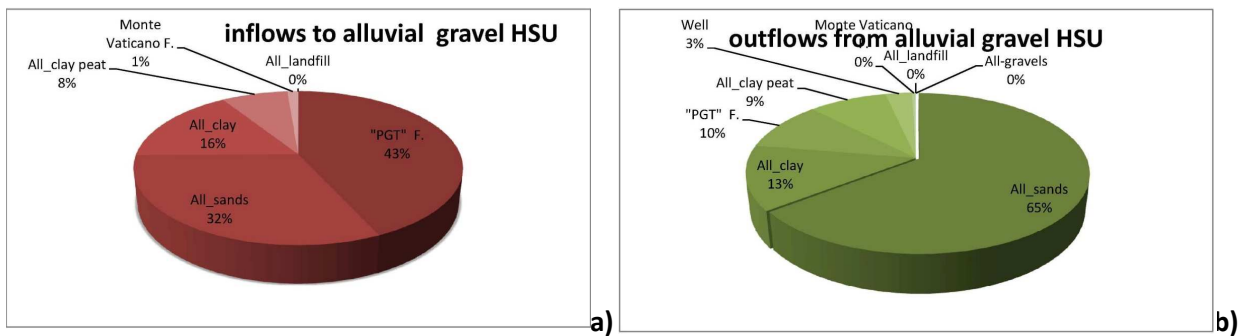


Fig. 5.14: alluvial gravel inflow/outflow percentages

Velocity vectors

The GWVistas® plot option *velocity vectors* allows to understand the flow pattern; vectors are simple arrows that are drawn in the direction of groundwater. The length of the arrow is proportional to the velocity, so that areas of highest inflow/outflow are underlined; vector's color represents flux direction, which is blue for upward velocity and red for downward velocity. Some sample areas are shown below:

- The first screen capture shows the north-east boundary of Layer 2 including the Tiber valley upstream portion; colors indicate hydraulic conductivity zones. High fluxes are concentrated on the sand complex (blue) and on the PGT complex (orange), while in the alluvial clay (yellow) flux is very low (**Fig. 5.15**)

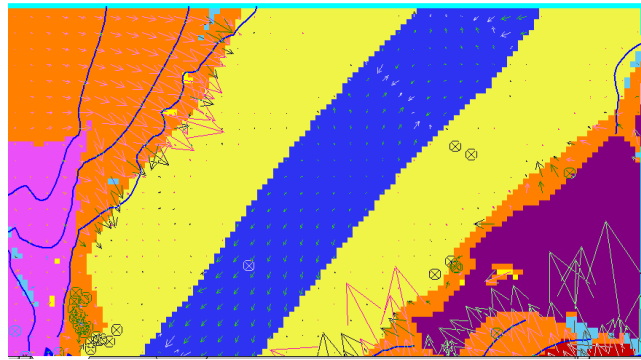
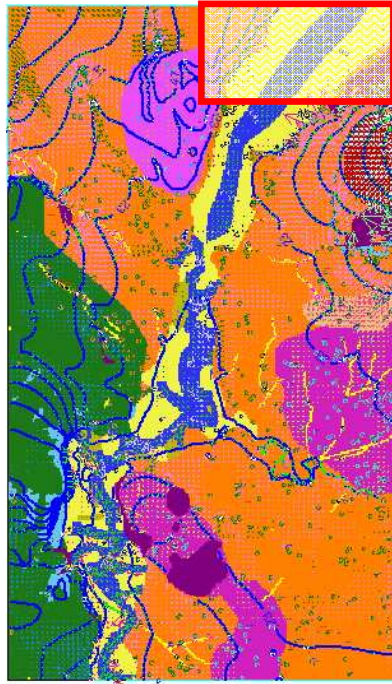


Fig. 5.15: velocity vectors on layer 2

- b) High fluxes due to high hydraulic conductivity are distributed along all the alluvial sand and gravel complexes, acting as conduits of concentrated flow (**Fig. 5.16 and 5.17**: blue= alluvial sandy complex; brown= alluvial gravel complex).

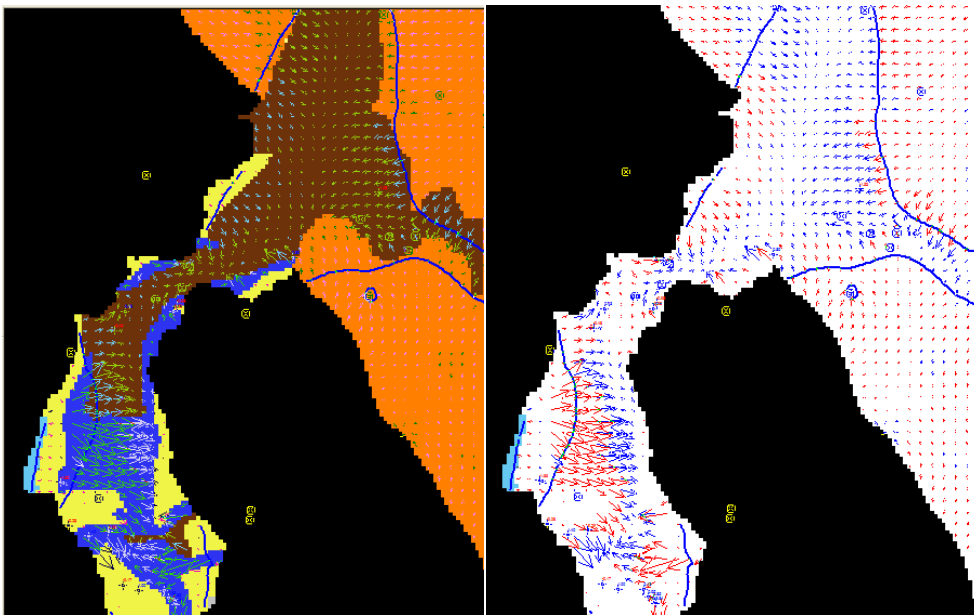
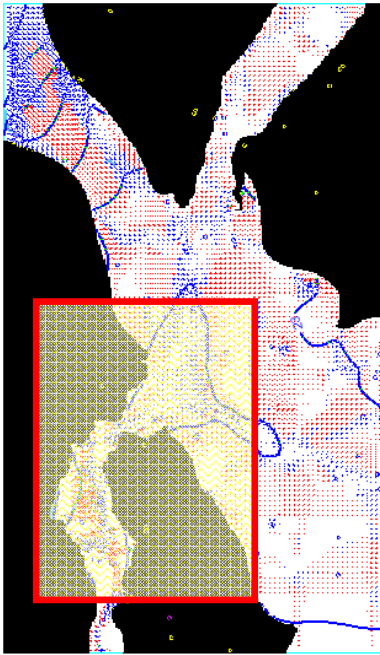


Fig. 5.16: velocity vectors on layer 5

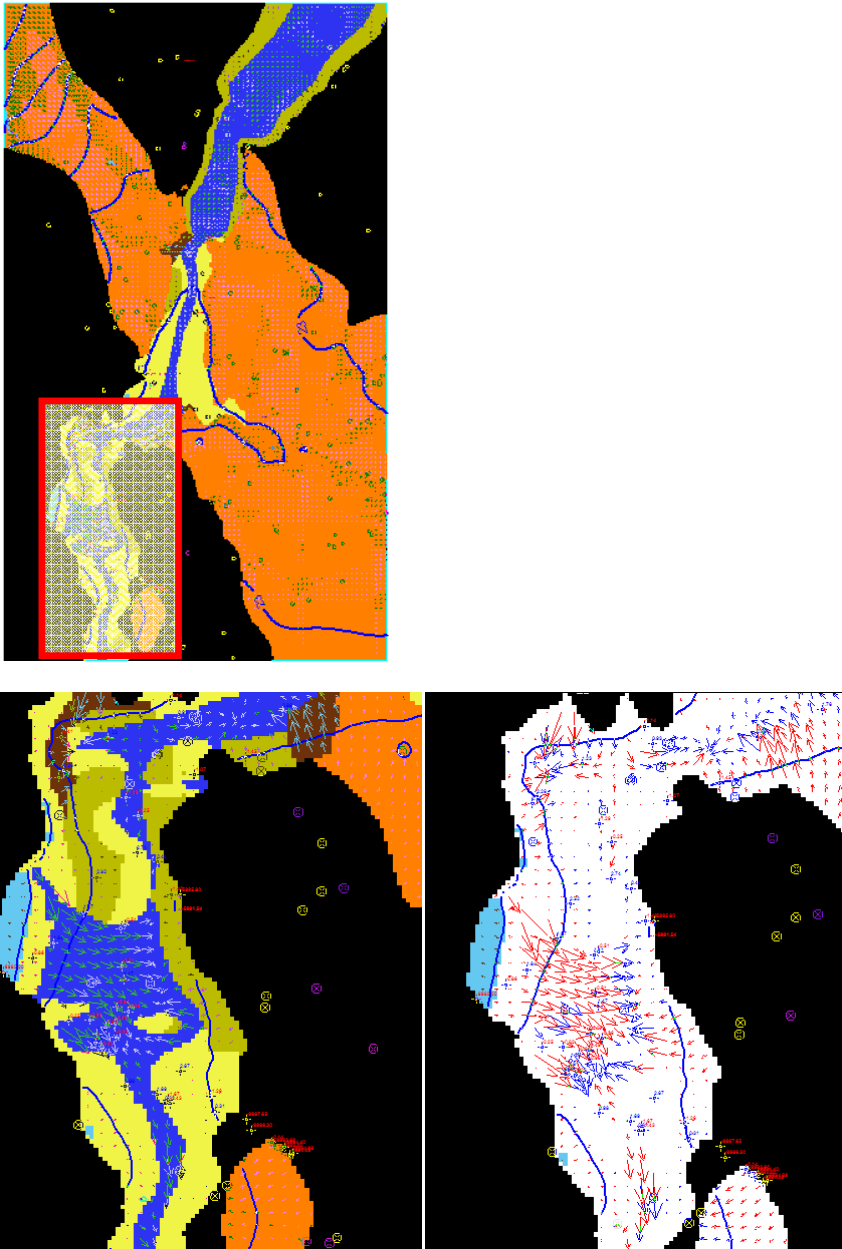


Fig. 5.17: velocity vectors on layer 4

- c) In **Fig. 18** vectors are shown for the north-west area; inflow from General Head boundary occurs with higher velocity when flowing into the PGT complex which fills the Paleo-Tiber Graben (orange, bounded by No-flux bc); velocity decrease moving from boundary toward the alluvial complex.

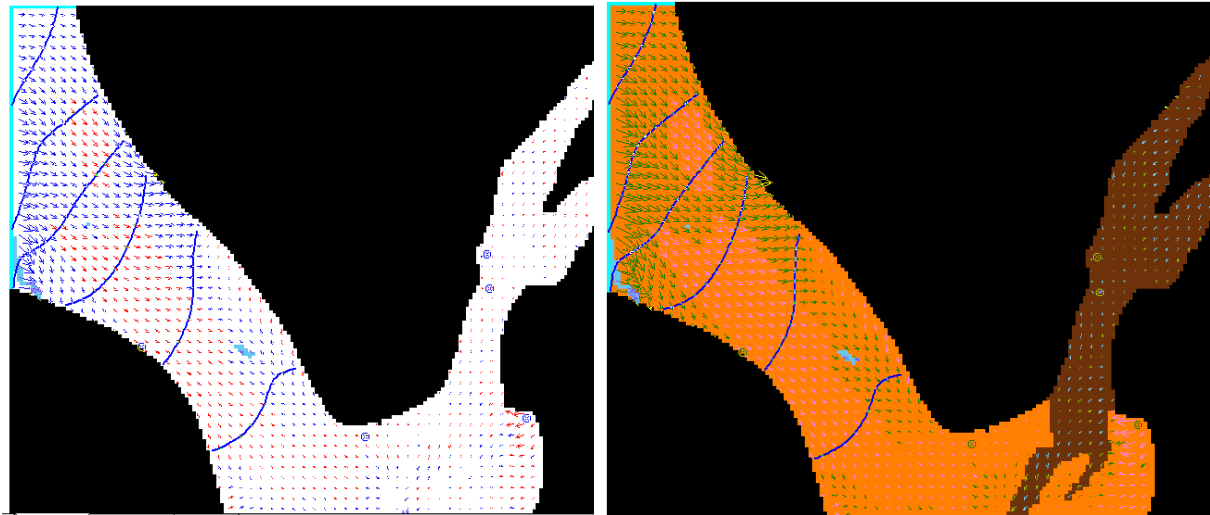
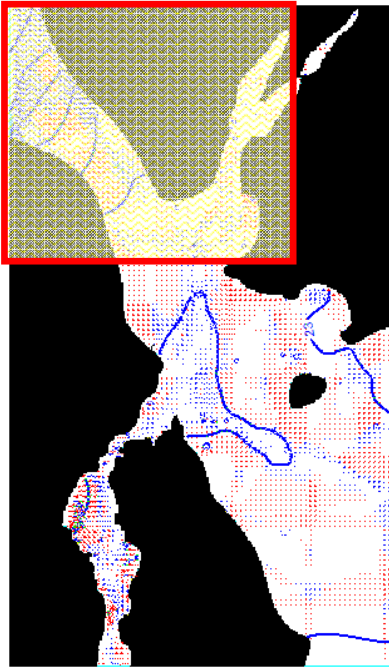


Fig. 5.18: velocity vectors on layer 6

- d) Cross-sections along rows and columns allow to visualize vertical gradients; **Fig. 5.19** shows inflows from PGT complex (orange) to the alluvial valley, occurring with highest velocity to the sandy and gravelly complexes (a), and the vertical gradient directed upward from the basal gravels and sands to the Tiber River (green cells)(b). Very low velocities are drawn in the clayey complex (yellow)

Cross-Section along Row 130

Cross-Section along Row 134

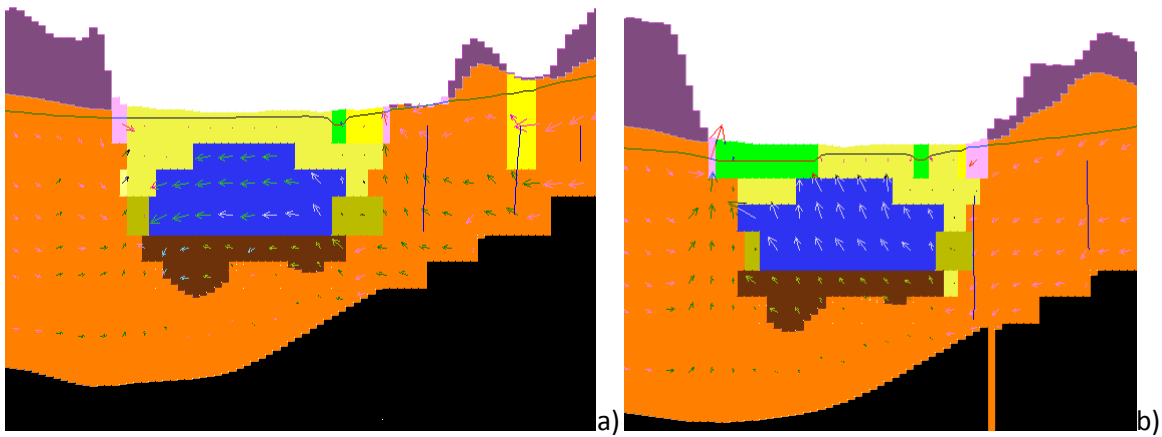


Fig 5.19: velocity vectors in cross sections along Row 130 and 134.

- e) The stratigraphic setting influences vertical gradients; in **Fig 5.20 (a)** the alluvial valley is excavated in the “PGT” *F.* complex, so that the alluvial aquifer can be fed in each direction by the “PGT” *F.* aquifer. In **Fig 5.20(b)**, the valley is partially excavated in the *Monte Vaticano F.* complex (Black; No-flow cells), where velocity is null.

Cross-Section along Row 156

Cross-Section along Row 230

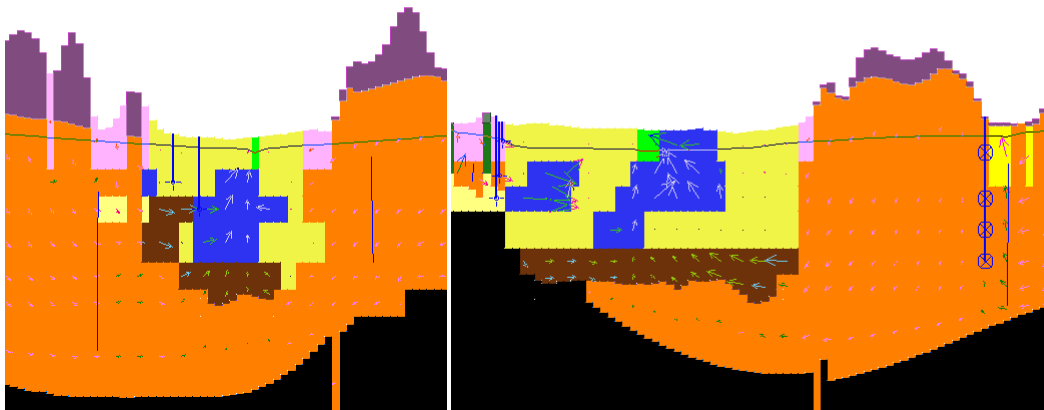


Fig 5.20: velocity vectors in cross sections along Row 156 and 230.

6 Summary and discussion

Summary

The work presented in this thesis is a combined process of conceptual and numerical modeling of Rome's aquifer system; it is carried out by a phase of data collecting and archiving ,and a phase of study in depth of the conceptual geological setting (both phases realized in collaboration with Igag-CNR); then, the geological setting has been translated into a hydrogeological framework, starting from hydrologic and hydrogeologic data and previous regional studies; this phase included extraction of information from the database and the data elaboration into cross sections and modeled surfaces. Finally, the conceptual hydrogeological model has been used to build a numerical model by the finite-difference code MODFLOW2000® and the graphical interface GroundwaterVistas® 5.41(ESI).

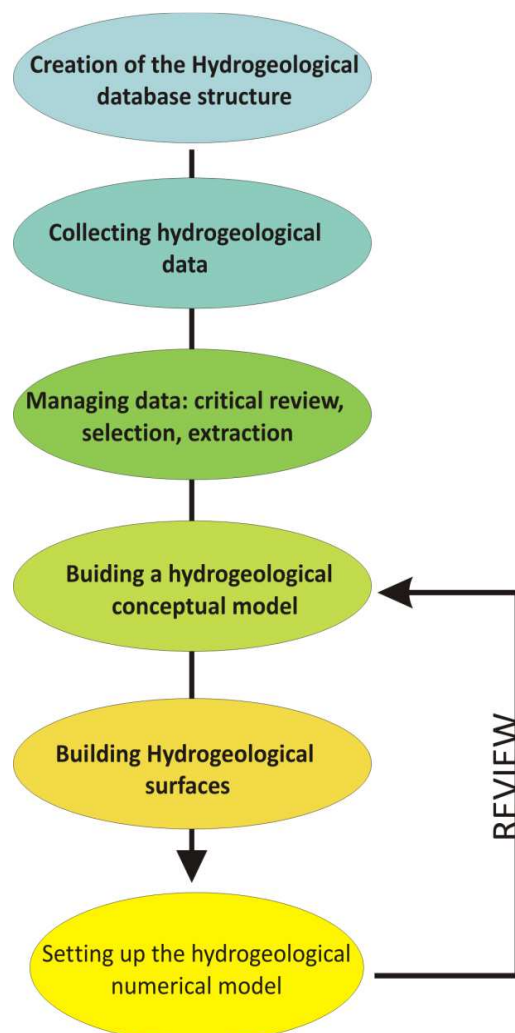


Fig. 6.1= flux diagram for the work presented in this thesis

Modeled area extends on a basin-scale in a rectangle of 237402 m² including high urbanization zones, as the hystorical center of the City; the complexity of the roman sector's geological setting, the complications in groundwater and surface water flux due to the modification of the natural hydrologic setting and the lack of valid series of head data, river flux and k measurements, strongly increase the uncertainty on model results.

As assessed in chapter 1 - Introduction, the work has been developed by those steps (see flux-diagram in **fig 6.1**):

- Creation of database capable to collect hydrogeological data as: well logs, head measurements, spring discharge, pumping tests;
- collecting 2950 well data ; 326 have been used to construct cross sections and top surfaces;

- building top surfaces of: Plio-pleistocene complexes (including *Monte Vaticano* and *Monte Mario Formation*), “*Ponte Galeria*” *Formatio* and Tiber alluvial basal gravel; moreover, the Holocene maximum erosional surface of Tiber alluvial valley has been built
- implementation of a quasi-3D steady state numerical model set up with 8 layers, a horizontal cell discretization of 50 x 50 meters, for a total area of 237402 m².
- model calibration, performed by a trial-and-error method based on head target residuals statistics and by 5 autosensitivity analysis. Calibration has been carried out on following parameters: recharge in urban and non urban areas, complexes hydraulic conductivities, General Head boundaries hydraulic conductivity, drain and river bed hydraulic conductivity;
- Computation of inflows and outflows both for the whole model and for each hydrostratigraphic unit.
- Comparison between the 10-years averaged aquifer system’s water balance (Capelli et alii, 2005) and the model’s water budget

Following tables and graphs resume calibrated model’s results:

Tab. 6.1: hydraulic conductivity values for calibrated model

K zone	COMPLEX	m/d
k1	Alban Hills volcanic (1)	9.12
k2	Sabatini Mts volcanic (1)	2.13
k3	Ponte Galeria F. (“PGT”) (1)	1.4
k4	Alluvium-clay	0.1
k5	Alluvium-sand	8.8
k6	Alluvium-clay with peat	0.5
k7	Alluvium-sandy gravel	4.5
k8	Monte Vaticano Formation	0.01
k9	Alluvium_landfill	0.1
k10	Monte Mario F. (1)	0.5
k11	Monte Vaticano F. (2)	0.4
k12	Monte Mario Formation (2)	0.09
k13	Monte Mario Formation (3)	0.2
k14	Alban Hills volcanic (2)	0.5
k15	Sabatini Mts volcanic (2)	0.1
k16	Alban Hills volcanic (3)	1.5
k17	Ponte Galeria (“PGT”) (2)	4.2
k18	Ponte Galeria F. (“PGT”) (3)	0.1
k19	Ponte Galeria F. (“PGT”) (4)	1

Tab 6.2: input data and simulated values for model ROMA

parameter	mc/d
total flow through the model	148780
groundwater inflow through General Head b	34621
<i>recharge in not urban areas (min 20%)</i>	89700.12865
<i>recharge in urban areas</i>	24375.87135
total model recharge	114076
groundwater outflow from General Head b	226
Withdrawals (*)	28146.5
drains & rivers outflow	132161
drains outflow	93471
Tiber River outflow	29631
Aniene river outflow	9258
total drains + rivers outflow (**)	132161
(*) sum of WELL and MNW simulated withdrawal	
(**)Tiber and Aniene rivers accounted	

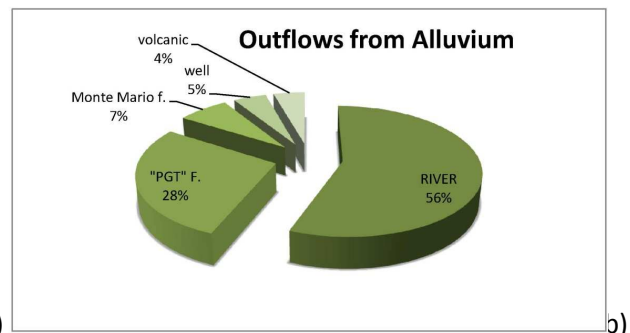
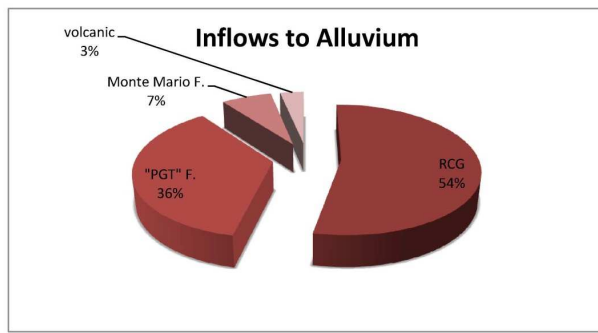


Fig. 6.2: Percentages of simulated flows in Tiber alluvium A)inflows; B) outflows

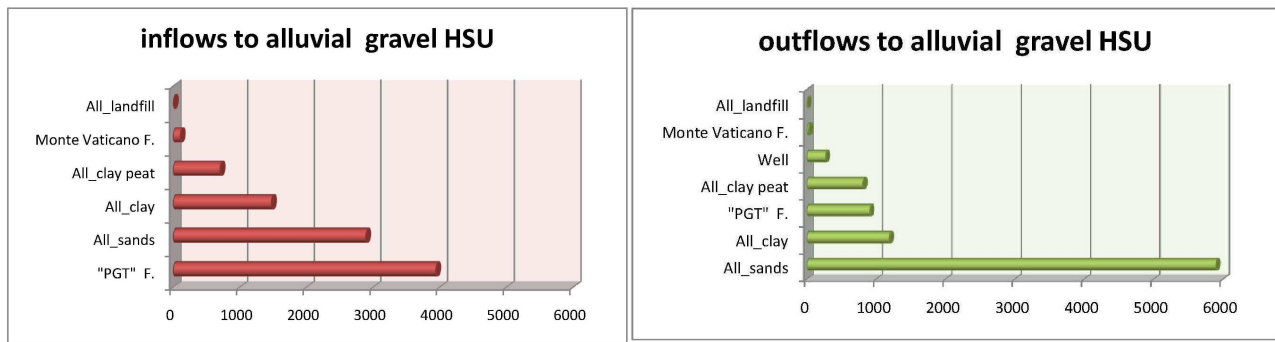


Fig 6.3: simulated alluvial gravels inflows and outflows (m3/d)

Results of model ROMA show that the alluvium complex is mostly fed by recharge and by the “PGT” F. complex; main alluvium complex outflows are from Tiber river. The basal gravel alluvium unit is recharged mainly by the “PGT” complex, and its outflows are for 65% toward the sand complex, generating an upward vertical gradient toward the Tiber river.

Rome model's critical review

This is the first attempt to modeling the groundwater system of Rome at a basin scale; at the actual step the model is not suitable for detailed predictions and groundwater management. Otherwise, it can be useful to better understand the conceptual model and for verification of hypothesis on the aquifer system. As critical review of Rome model, strong and weak points are listed:

Strong points:

- The model can be useful to check, at the basin's scale, the hydraulic relationships between complexes, by comparing mass balance of the calibrated model and initial conceptual hypothesis, ROMA model structure's allows to focus on the hydric exchanges between alluvial valley and surrounding aquifers;
- ROMA model allows to verify the accuracy of alluvial facies spatial distribution, that was developed in the first phase of this study, by the comparison between observed and simulated head in the alluvial valley;
- A set of calibrated k values has been found; focusing on sandy and gravelly alluvium complexes, best results are obtained with $k_{sand} = 8.8$ m/d and $k_{gravel} = 4.5$ m/d, so that the sand is the more permeable facies in the alluvium. Otherwise, in a local-site model this result could be inverted, both for a “scale” effect and for the large heterogeneity of alluvium facies.
- During the calibration, the accuracy of distributed method balance for recharge was verified:

- In non urban areas, the 1997-2007 averaged recharge as calculated in Capelli et alii (2005) was decreased of 20% after the model calibration phase;
- according with model results, the value of zero for recharge in urban areas is retained to be wrong; recharge has been calculated starting from data on water main leakage (by ACEA - Municipal Water Agency) and general estimation methods for percolation through paved surfaces and overirrigation through methods (Lerner, 1990 and 2002) .
- Quantifying and calibrate the total pumping rate over the study area, by using two packages (WELL and MULTI-NODE WELL);
- Quantifying inflows and outflows for each hydrostratigraphic unit and locate areas of main recharge/discharge;
- First approach to modeling gives an overview on the most important lacks of data and makes easier to understand how to plan a new data collecting, focused on the model resolution improvement and reduction of the uncertainty.
- The model can be used to establish boundary conditions for local-scale models.

Weak point:

Weakness of model ROMA are mainly due to the lack of temporal-continuable series of head data (that is, monthly or daily head measurements for a time window extended over several years). Moreover, data sets used for calibration are not completely adequate to the complexity of Rome model's structure; head measurements should affect each aquifer and also the same aquifer at different depth;

- The model is in steady-state; for a predictive analysis and for water management model should be in transient-state.
- The lack of pumping tests for alluvial sands and gravel adds uncertainty in k values calibration.
- Also the lack of flux targets adds uncertainty to the solution; the Tiber River's discharge increase over the urban sector of the City cannot be computed; moreover, tributary streams enter in water mains when reaching high-urbanized areas, and their natural discharge is not monitored at all.
- The model can't be validated; validation requires a set of data different from the target set used for calibration. Aquifers vertical gradient cannot be calculated with high confidence.

Perspectives for future work in modeling Rome's groundwater system should be:

- Installation of a network of piezometers spread along the valley from north to south; installing hydrometric measurement stations along the Tiber and Aniene rivers and main streams (Crescenza and Valchetta), for better understand local hydric relationships between hydrostratigraphic units, and between units and rivers.
- Implementation of models in test-areas at site-specific scale, with wells and rivers stage monitoring stations; available testing areas (in LINQ and Igag-CNR developing research projects) are: the Valco San Paolo area and the Castel S. Angelo area, in the hystorical center (fig. 6.4).

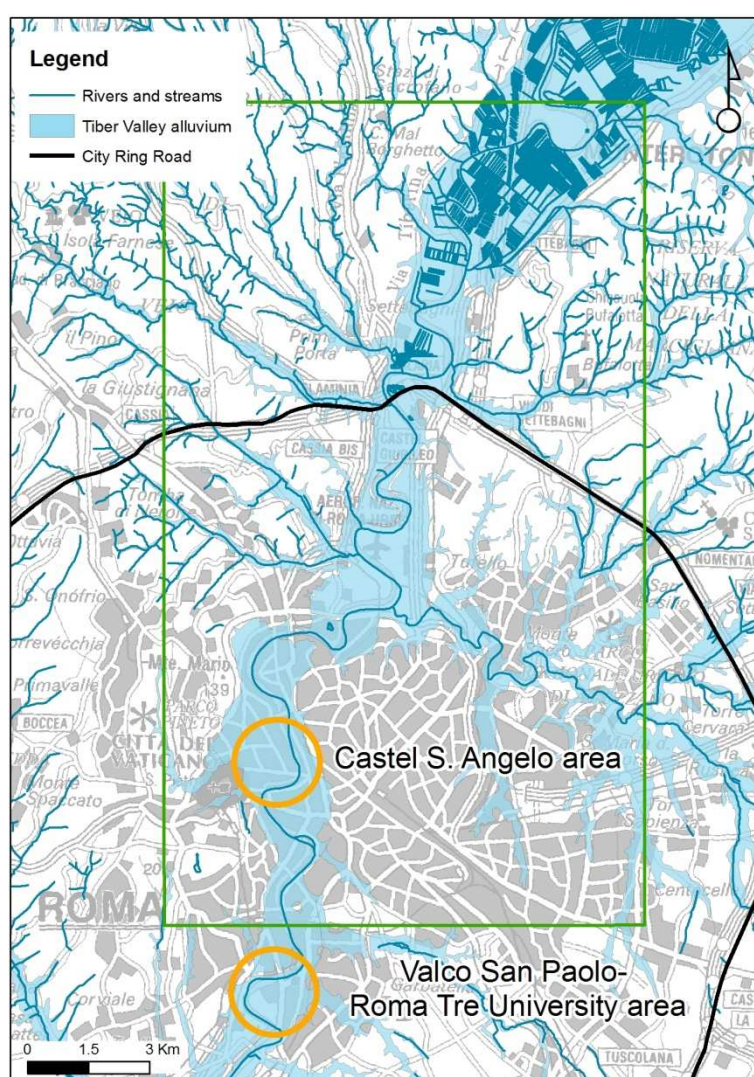


Fig 6.4: possible future test areas for local-scale numerical models

7 References

- Anderson, M. P. and Woessner, W. W. (1992), *Applied Groundwater Modeling*. Academic Press, San Diego.
- ASTM International (2004), *Standard Guide for Application of a Ground-Water Flow Model to a Site-Specific Problem*, D 5718-95
- Autorità di Bacino del Fiume Tevere, (Regione Lazio) (2003), *“Piano stralcio per il tratto metropolitano del Tevere (Castel Giubileo - foce)”*, <http://www.abtevere.it>
- Barberi F., Buonasorte G., Cioni R., Fiordelisi A., Foresi L., Iaccarino S., Laurenzi M.A., Sbrana., Vernia A., Villa I.M. (1994), *Plio-Pleistocene geological evolution of the geothermal area of Tuscany and Latium*. Mem. Descr. Della Carta geol. D'It., 49, Roma.
- E. Berthier a,*, S. Dupont b, P.G. Mestayer d, H. Andrieu c (2006), *Comparison of two evapotranspiration schemes on a sub-urban site*, Journal of Hydrology 328, 635– 646.
- Bonomi T. (2009), *Database development and 3D modelling of textural variations in heterogeneous, unconsolidates aquifer madia: application to the Milan plain*, Computers & Geosciences,35, pp 134-145
- Bozzano F., Andreucci A., Gaeta M., Salucci R. (2000), *A geological model of the buried Tiber River valley beneath the historical center of Rome*, Bull. Eng. Geol. Env , 59, pp 1-21
- Bozzano F., Caserta A., Govoni A., Marra F., Martino S. (2008), *Static and Dynamic characterization of alluvial deposit in the Tiber River Valley: new data for assessing potential ground motion in the City of Rome*, Journal of Geophysical research, 113.
- Bruno R. & Raspa G. (1994), *La pratica della Geostatistica non Lineare. Il trattamento dei dati spaziali*. Ed. Guerini.
- Campolunghi M.P., Lanzini M., Capelli G. (2007), *Geotechnical studies for foundation settlements in Holocenic deposits in the city of Rome (Italy)*, Engineering geology 89, p. 9-35.
- Capelli G., Mazza R., Taviani S. (2008), *La cartografia idrogeologica alla scala 1:50.000 dell'area di Roma (1 TAVOLA)*, in *La geologia di Roma dal centro storico alla periferia*, Mem. Desc. Carta Geol. D'It., 80.
- Capelli G., Mazza R., Taviani S. (2008), *Acque sotterranee nella Città di Roma*. In: *La geologia di Roma: dal centro storico alla periferia*, Mem. Desc. Carta Geologica d'Italia, 80, parte prima, APAT, Roma, 221-245.
- Capelli G., Mazza R., Gazzetti C. (a cura di) (2005), *Strumenti e strategie per la tutela e l'uso compatibile della risorsa idrica nel Lazio – Gli acquiferi vulcanici*. Quaderni di Tecniche di Protezione Ambientale n.78. Pitagora Editrice, 216 pp., 4 tavv. f.t., 21 tavv. f.t. su CD-ROM allegato.

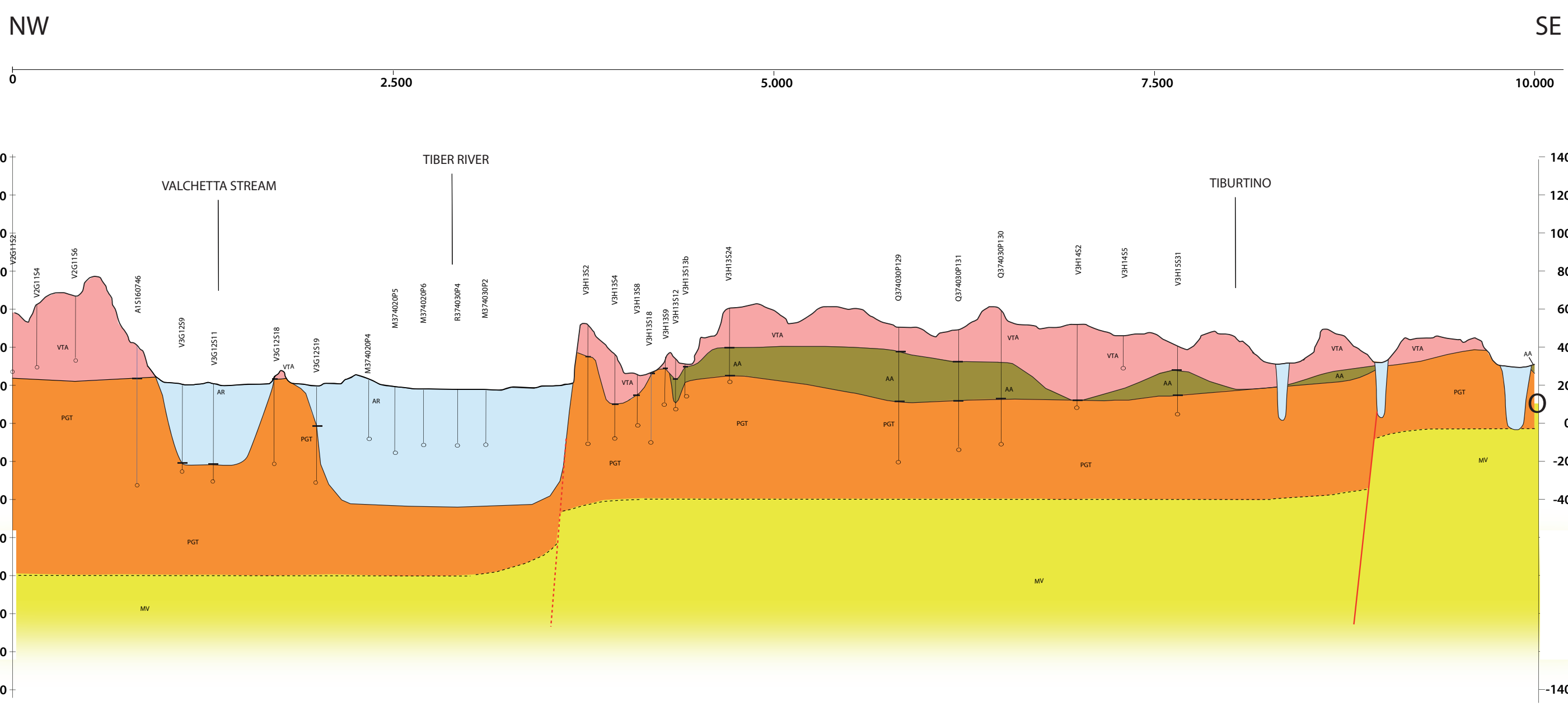
- Cavarretta G., Cavinato G.P., Mancini M., Moscatelli M., Patera A., Raspa G., Stigliano F.P., Vallone R., Folle D., Garbin F., Milli S., Storoni Ridolfi S. (2005), *I terreni di Roma sotto l'aspetto della Geologia tecnica*. In "La IV dimensione, lo spazio sotterraneo di Roma" (Gisotti G., Pazzagli G., Garbin F., Eds.), Supplemento di Geologia dell'Ambiente 4/2005, ISSN 1591-5352, 33-46.
- Chiles J.P. & Delfiner P. (1999), *Geostatistics. Modelling Spatial Uncertainty*. Wiley Series in Probability and Statistics.
- Corazza, A., & Lombardi, L. (1995), *Idrogeologia dell'area del centro storico di Roma*. In R. Funicello (Ed.), *Memorie descrittive della carta geologica d'Italia, la geologia di Roma* (pp. 179–211). Rome: Istituto Poligrafico e Zecca dello Stato.
- Corazza A., Giordano G., De Rita D. (2006), *Hydrogeology of the city of Rome*, in Heiken G. ed., *Tuffs-their properties, uses, hydrology and resources*: Geological Society of America, Special Paper 408, p. 113-118
- Corazza A., Lanzini M., Rosa C., Salucci R. (1999) Caratteri stratigrafici, idrogeologici e geotecnici delle alluvioni tiberine nel settore del centro storico di Roma, *Italian Journal of Quaternary sciences*, 12 (2), 215-235
- Alper Elc,ja, Gregory P. Flachb, Fred J. Molza (2003), *Detrimental effects of natural vertical head gradients on chemical and water level measurements in observation wells: identification and control*, *Journal of Hydrology* 281 (2003) 70–81
- Faccenna C., Funicello R., Marra F. (1995), *Inquadramento geologico-strutturale dell'area romana*, in: *La geologia di Roma. Il centro storico*. Mem. Descr. Carta Geol. d'It., 50, Roma, pp 32 – 47.
- Florindo F., Karner D. B., Marra F., Renne P. R., Roberts A. P., Weaver R. (2007) *Radioisotopic age constraints for Glacial Terminations IX and VII from aggradational sections of Tiber River delta in Roma, Italy*, *Earth and Planetary Science Letters* 256, 61-80
- Funicello R., Giordano G. (2008). *Foglio n. 347 "Roma" della Carta Geologica d'Italia, scala 1:50.000*, APAT, Poligrafico dello Stato.
- Funicello, R., Praturlon, A., Giordano, G. (2008), *La Geologia di Roma, dal centro storico alla periferia*, Part I-II, *Memorie Descrittive della Carta Geol. d'Italia*, Vol LXXX, S.E.L.C.A, Firenze
- Geostudi per Metro C, S.p.a. (2007-2009), *Technical reports, works for "C" subway line*.
- Giordano G., De Benedetti A.A., Diana A., Diano G., Gaudio F., Marasco F., Miceli M., Mollo S., Cas R.A:F., Funicello R. (2006), *The Colli Albani mafic caldera (Roma, Italy): stratigraphy, structure and petrology*, *Journal of Volcanology and Geothermal research*, 155, pp 49-80
- C. S. B. Grimmond and T. R. Oke (1991), *An Evapotranspiration-Interception Model for Urban Areas*, *Water Resources Research*, Vol. 27, No. 7, pp. 1739-1755

- Haitjema, H. M. (1995). *Analytic Element Modeling of Groundwater Flow*. Academic Press, San Diego, CA. , ISBN 0-12-316550-4
- Harbaugh, A.W., McDonald, M.G. (1996), *User's documentation for MODFLOW-96, an update to the US Geological Survey modular finite-difference ground-water flow model: US Geological Survey Open-File Report*, 96-485, 56 p
- Halford K.J. and Hanson R.T.(2002) *User guide for drawdown-limited, Multi-Node Well (MNW) Package for the U.S. Geological Survey's Modular Three-Dimensional Finite-Difference Ground-Water flow Model, Versions MODFLOW-96 and MODFLOW-2000*, U.S. Geological Survey, Open-File Report 02-293
- Mary C. Hill (1999), *Methods and guidelines for effective model calibration*, U.S. Geological Survey, water-resources investigations report 98-4005.
- Lanzini M. (1995-2000°), *Indagine geognostica per il progetto della linea C della Metropolitana di Roma-Tratta da S. Giovanni a Alessandrino, 1995-1996* technical report.
- Lanzini M. (1995-2000b), *Indagine geognostica per il progetto della linea C della Metropolitana di Roma-Tratta in variante da Piazza Risorgimento a Piazza Venezia*, technical report
- Martini P., Albani R., Mouton J., Curli G. (1961), *Contribution à la connaissance de l'hydrogéologie de la région de Rome* – ACEA, Mem SIH, Napoli.
- Lerner D. N. (1990), *Groundwater Recharge In Urban Areas*, Hydrological Processes and Water Management in Urban Areas (Proceedings of the Duisberg Symposium, April 1988). IAHS Publ. no. 198, 1990.
- Lerner D. N (2002), *Identifying and quantifying urban recharge: a review*, *Hydrogeology journal*, 10: 143-152
- LINQ, Laboratorio di Idrogeologia Numerica e Quantitativa, (2010), *Hydrogeological numerical model of the Bracciano lake aquifer*, inedited Ph-D thesis by Sara Taviani
- LINQ, Laboratorio di Idrogeologia Numerica e Quantitativa (2003), *Studio geologico e geotecnico dei depositi alluvionali del F. Tevere nel settore di Roma Nord compreso tra Castel Giubileo e Piazza Mazzini*. Laboratorio di Idrogeologia Numerica e Quantitativa, Dipartimento Scienze Geologiche, Università Roma Tre, Inedited Master Thesis Vitrone C.
- Mancini M., Girotti O., Cavinato G.P. (2004), *Il Pliocene e il Quaternario della Media Valle del Tevere (Appennino centrale)*. *Geologica Romana* (2003-2004), 37, 175-236, two attached tables.
- Marra F. (1993), *Stratigrafia ed assetto geologico-strutturale dell'area romana compresa tra il Tevere e il Rio Galeria*. *Geol. Rom.*, 29, pp 515-535
- Marra F. & Rosa C. (1995), *Stratigrafia e assetto geologico dell'area romana*, in: *La geologia di Roma. Il centro storico*. Mem. Descr. Carta Geol. d'It., 50, Roma, pp 50-112

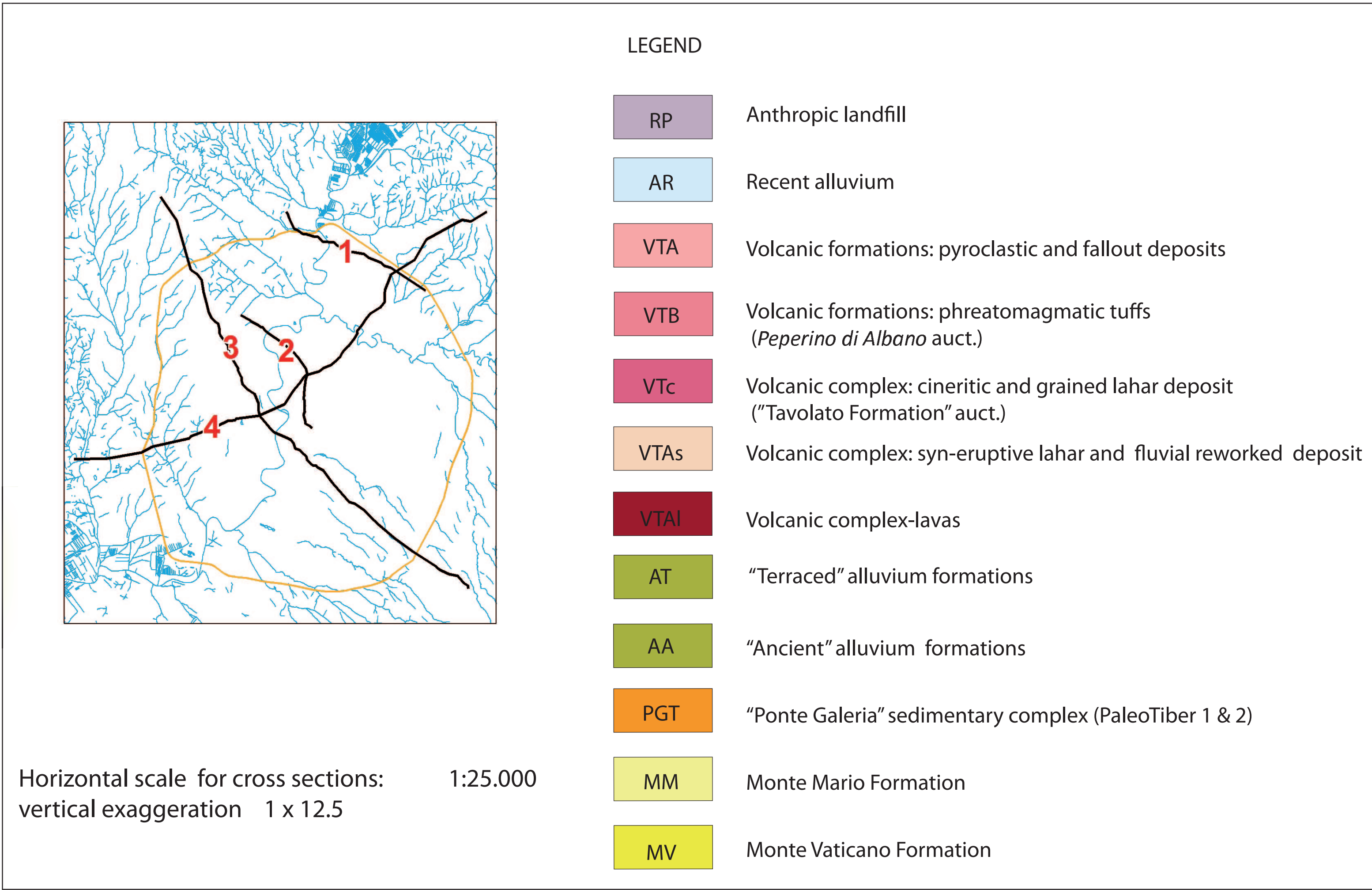
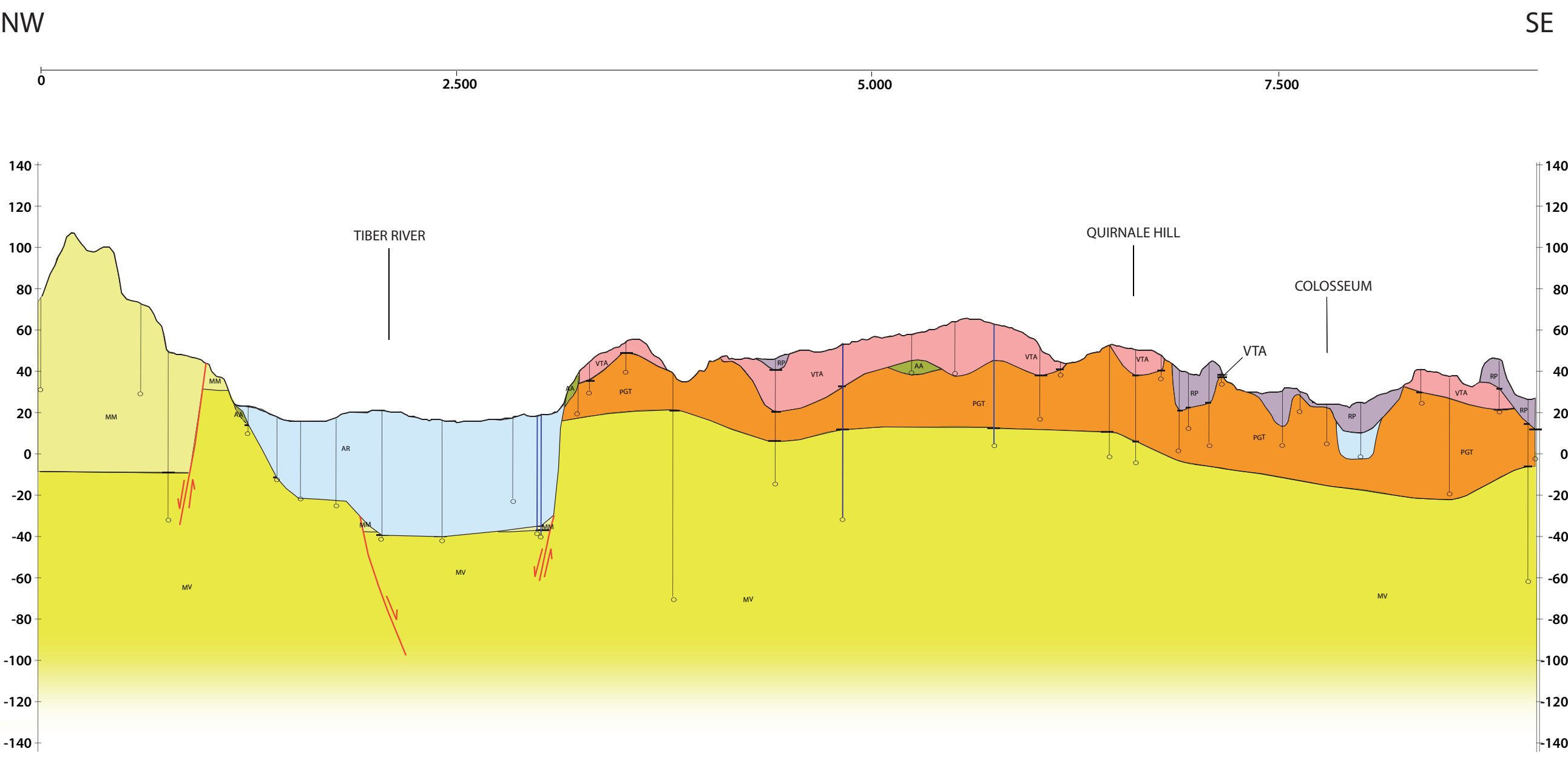
- Matheron G. (1973), The intrinsic random functions and their applications. *Advances in Applied Probability*, 5, 439-468.
- Mattias P.P., Ventriglia U. (1970), *La regione vulcanica dei Monti Sabatini e Cimini*. Mem. Soc. Geol. It., 9/1970, p. 360.
- R. Ragab,* P. Rosier, A. Dixon, J. Bromley and J. D. Cooper (2003), *Experimental study of water fluxes in a residential area: 2. Road infiltration, runoff and evaporation*, *Hydrological Processes*, Volume 17, Issue 12, pp. 2423-2437, 30, Published online in Wiley InterScience (www.interscience.wiley.com). DOI: 10.1002/hyp.125
- Raspa G., Moscatelli M., Stigliano F., Patera A., Marconi F., Folle D., Vallone R., Mancini M., Cavinato G.P., Milli S., Coimbra Leite Costa J.F. (2008) - Geotechnical characterization of the upper Pleistocene-Holocene alluvial deposits of Roma (Italy) by means of multivariate geostatistics: Cross-validation results. *Engineering Geology*, 101, 251-268, doi: 10.1016/j.enggeo.2008.06.007.
- Regione Lazio (2009), *Carta Idrogeologica del Territorio della Regione Lazio, scala 1:100.000*, a cura di: Capelli G., Mazza R., Petitta M., Boni C., autori: Baldoni T., Banzato F., Capelli G., Cascone D., Di Salvo C., La Vigna F., Mastroiillo L., Mazza R., Petitta M., Taviani S., Teoli P., inedited.
- Schulze-Makuch D. & Cherkauer D. S. (1995), *Scale behavior of hydraulic conductivity during a pumping test*, Effects of Scale on Interpretation and Management of Sediment and Water Quality (Proceedings of Boulder Symposium, July 1995). IAHS Publ. no. 226, 1995.
- Dorte Seifert & Torben O. Sonnenborg & Peter Scharling & Klaus Hinsby (2008), *Use of alternative conceptual models to assess the impact of a buried valley on groundwater vulnerability* - *Hydrogeology Journal* , volume 16, n 4, pp. 659-674.
- SIMN (1980-2004), *Dati delle stazioni termo-pluviometriche del Servizio Idrografico e mareografico Nazionale*, compartimento di Roma.
- Sonnenborg TO, Christensen BSB, Nygaard P, Henriksen HJ, Refsgaard JC, (2003) *Transient modeling of regional groundwater flow using parameter estimates from steady-state automatic calibration*. *J Hydrol* 273:188–204
- Wakernagel (1995), *Multivariate geostatistic*. Springer.
- Weissmann, G.S., Yong, Z., Fogg, G.E., Blake, R.G., Noyes, C.D., and Maley, M. (2002), *Modeling alluvial fan aquifer heterogeneity at multiple scales through stratigraphic assessment* , in Findikakis, A.N. (ed.), *Bridging the gap between measurement and modeling in heterogeneous media*, Proceedings of the International Groundwater Symposium, Lawrence Brekeley National Laboratory, Berkeley, California, March 25-28, p. 184-186 (and electronic).
- Ventriglia U. (1971), *Geologia della città di Roma*. Amministrazione Provinciale di Roma.
- Ventriglia U. (2002), *Geologia del territorio del Comune di Roma*. Amministrazione Provinciale di Roma, Servizio Geologico, Difesa del Suolo.

ATTACHED N2a- CROSS SECTIONS TABLE (a)

CROSS SECTION 1

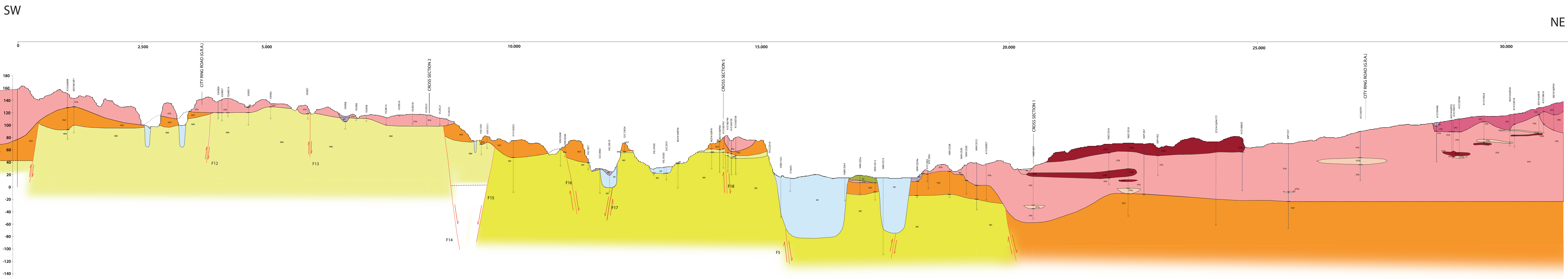


CROSS SECTION 2



Horizontal scale for cross sections: 1:25,000
vertical exaggeration 1 x 12.5

CROSS SECTION 3



CROSS SECTION 4

